Neutrinos and Loops: Studying Neutrino Mass Models Through Their Quantum Effects

Author:
Lackner, Adam

Publication Date:
2025

DOI:
https://doi.org/10.26190/unsworks/31003

Neutrinos and Loops: Studying Neutrino Mass Models Through Their Quantum Effects

Adam Lackner

A thesis in fulfilment of the requirements for the degree of

Doctor of Philosophy

School of Physics

Faculty of Science

The University of New South Wales

April 2025

Declarations

ORIGINALITY STATEMENT

☑ I hereby declare that this submission is my own work and to the best of my knowledge it contains no materials previously published or written by another person, or substantial proportions of material which have been accepted for the award of any other degree or diploma at UNSW or any other educational institution, except where due acknowledgement is made in the thesis. Any contribution made to the research by others, with whom I have worked at UNSW or elsewhere, is explicitly acknowledged in the thesis. I also declare that the intellectual content of this thesis is the product of my own work, except to the extent that assistance from others in the project's design and conception or in style, presentation and linguistic expression is acknowledged.

COPYRIGHT STATEMENT

☑ I hereby grant the University of New South Wales or its agents a non-exclusive licence to archive and to make available (including to members of the public) my thesis or dissertation in whole or part in the University libraries in all forms of media, now or here after known. I acknowledge that I retain all intellectual property rights which subsist in my thesis or dissertation, such as copyright and patent rights, subject to applicable law. I also retain the right to use all or part of my thesis or dissertation in future works (such as articles or books).

For any substantial portions of copyright material used in this thesis, written permission for use has been obtained, or the copyright material is removed from the final public version of the thesis.

AUTHENTICITY STATEMENT

☑ I certify that the Library deposit digital copy is a direct equivalent of the final officially approved version of my thesis.

Publications Statement

UNSW is supportive of candidates publishing their research results during their candidature as detailed in the UNSW Thesis Examination Procedure.

Publications can be used in the candidate's thesis in lieu of a Chapter provided:

- The candidate contributed **greater than 50%** of the content in the publication and are the "primary author", i.e. they were responsible primarily for the planning, execution and preparation of the work for publication.
- The candidate has obtained approval to include the publication in their thesis in lieu of a Chapter from their Supervisor and Postgraduate Coordinator.
- The publication is not subject to any obligations or contractual agreements with a third party that would constrain its inclusion in the thesis.

☑ The candidate has declared that **some of the work described in their thesis has been published and has been documented in the relevant Chapters with acknowledgement**.

A short statement on where this work appears in the thesis and how this work is acknowledged within chapter/s:

> Chapter 4 (Riding the Seesaw: What Higgsstrahlung May Reveal about Massive Neutrinos) is derived from a publication of the same name, and my contribution to it includes the derivation of some relevant formulas, the generation of all results and plots, and much of the discussion. The is acknowledged at the beginning of the chapter.
>
> A section of the same publication, for which I was solely responsible, was also incorporated into Chapter 3; this is acknowledged in a footnote at the beginning of the chapter.

Candidate's Declaration

I declare that I have complied with the Thesis Examination Procedure.

Abstract

The neutrino mass problem, which refers to the unknown origin of neutrino masses, strongly motivates the need for new physics beyond that of the Standard Model (SM). A given mass model, through quantum effects, generates a rich network of predictions deviating from those of the SM. The enterprising physicist can use these to constrain the model, and—in some cases—resolve experimental anomalies and offer solutions to other unsolved problems.

This thesis is divided into two parts. In the first, I investigate whether high-precision measurements of the cross section of the Higgsstrahlung process $e^+e^- \to Zh$ at a next-generation electron-positron collider can be utilised to probe the Type-I and Type-III Seesaw models. By employing an effective field theory approach, I compare the collider reaches to constraints from electroweak observables, probes of lepton flavour universality, and the existing and prospective bounds from searches for lepton flavour violation. I find that while any appreciable correction to the Higgsstrahlung cross section is already strictly constrained in the Type-I Seesaw model, effects of up to $\mathcal{O}(10\%)$ are possible within Type-III Seesaw.

In the second part of this thesis I investigate whether a high-scale realisation of the Zee model of neutrino mass can be used to explain the observed baryon abundance of the universe. In this realisation the baryon asymmetry is generated through the CP-violating decay of a new singly-charged scalar with a mass of $\mathcal{O}(10^{12}\,\mathrm{GeV})$. I find that the flavour structure of the Zee model forces the scenario to be one of flavoured leptogenesis, which turns out to be too restrictive to produce a sufficient asymmetry. This work is followed up with a discussion of infrared divergences in the Zee model, where I demonstrate how to achieve infrared-finiteness at zero temperature and discuss how this cancellation might be extended to finite temperature.

We're gonna go paint your quarks a colour that's not stupid, and then we're gonna throw your Feynman diagrams in the trash!

Frank Reynolds,
in *It's Always Sunny in Philadelphia*,
reimagined by Ryan Seelig

Acknowledgements

I hope you'll forgive the above epigraph and its comparably juvenile brethren decorating this thesis. If you must, consider them as my personality leaking through in a way that stoic academic prose would not otherwise allow. But I digress.

When I penned the acknowledgements of my honours thesis, in what feels like a lifetime ago, I wrote that "I'm not one for long, sappy speeches, so I'll keep this brief," and keep it brief I did. Here I shall instead swing in the opposite direction and offer my thanks to anyone and everyone I can think of. It appears my inclinations are not conserved.

* * *

Though I wish I could say I've been an aspiring physicist since the age of two, my journey into the field began with my high school physics teacher, Dr. Mark Butler. Perhaps it was his limitless enthusiasm and masterful command of the content, or perhaps it was because he happened to be teaching The Interesting Stuff™ (read: relativity and historical quantum theory), or perhaps it's because his teaching coincided with a phase transition in my academic drive—most likely it was some nonlinear combination of the above—but in any case, the result was that I left his classroom with a desire to do more physics. I recall when once asked why he chose to become a high school teacher, he replied that teaching at the tertiary level would be "preaching to the converted," and I thank him for making the choice that he did, for he converted me.

In the present day, the lion's share of my gratitude must of course be directed towards my supervisor Michael Schmidt, without whom I certainly wouldn't be here writing this. Michael exemplifies all conceivable positive qualities one might look for in a supervisor, or even an individual – he is endlessly knowledgeable, friendly, helpful, patient, organised, encouraging, and more. I am half convinced that he must be untethered from the stresses that beset us regular mortals, for to this day I cannot comprehend how, despite all his manyfold commitments, he has always managed to find time to help with any frivolous problem brought to him by myself or his other students. Needless to say, I am heavily indebted to Michael for all the guidance and support he's provided over the years.

Secondarily comes my mentor, collaborator, and friend, Tobias Felkl. Since his arrival in Australia in 2019, Tobias has been a core source of company and fruitful discussion. He is a very influential figure in the formation of this thesis, for without him Chapter 4 would

not exist, and I would likely have instead floundered around haplessly for another year on my first project (which did not end up making the final cut). By pure coincidence I happen to be writing this on his birthday, and I hope to be party to many more in the future.

Thirdly, I should like to thank my second collaborator, Chee Sheng Fong, whose expertise in all things leptogenesis-related helped steer the latter half of this thesis in the right direction. Collaborating with Sheng has proven to be a most enjoyable experience, as he took genuine interest in each problem-of-the-week, offering useful suggestions and valuable insights. I suspect he was equally disappointed as I was when we decided to abandon our quixotic dream of cancelling the IR divergences in favour of the more practical thermal mass treatment.

My next-innermost circle of thankees consists of the members of the UNSW CPPC[1] group, with whom I've shared many lunch outings, friendly chats, productive discussions, and more. Past and present members include Ameek Malhotra, Amrita Mukherjee, Charlie Weihang Zhang, Cosmin Dumitrescu, Dipan Sengupta, Felix Lempriere, Gabi Lichtenstein[2], Giovanni Pierobon (my man!), Jack Bennett, James Vandeleur, Jan Hamann, Joe Zhiyu Chen, Julius Wons, Michael Schmidt, Nathan Cohen, Tobias Felkl, Yeray Garcia Del Castillo, Yuqi Kang, Yvonne Wong, and my nemesis Freya, who, amongst other crimes, changed the label on my desk from *Coolest particle physics people* to *Lamest particle physics people* (hrmph). Thanks are also owed to the USyd branch of the CPPC for their hospitality during our many joint journal clubs and workshops, as well as their general camaraderie.

Beyond our tiny particle physics corner, there are countless other friendly faces from within the UNSW School of Physics who have contributed to a pleasant PhD experience. Foremost among them are my review committee, Oleg Tretiakov and Sarah Brough, who have kept me honest and on track throughout my candidature, and offered many helpful pieces of advice along the way. During my tenure as the Electrodynamics tutor I was taken under the wing of Peter Reece, to whom I owe many thanks for his extreme affability and continued tolerance of my presence (particularly during Friday Morning Teas, in which I'm certain there are more interesting people than myself to talk to). For keeping the gears turning, organising many social events, and ensuring the School of Physics continues to be a welcoming place for everybody, I should also like to thank the various administrative and support staff within the School, including but not limited to: Cecilia Bloise, Jonny Rebolledo Moya, Katie McBean, Seda Cokcetin, Sue Hagon, Tom Dixon, and Zofia Krawczyk. Finally, I must acknowledge the rest of the postgraduate cohort for being a friendly and sociable bunch, with special mention to the first floor astronomers and condensed matter people for pleasant office and lunchtime interactions, and Abhay

[1]Caffeinated Physics People Club / Clan of Particle Phenomena Chasers / Conglomerate of Poorly-Paid sCientists

[2]Special thanks goes to Gabi, who—in possessing a worldliness that I so sorely lack—kept me alive during our trip to Poland and France for the Planck and FPCP conferences.

Gupta for his relentless interest in being friends with everyone (including me).

Outside of physics, and with some overlap in membership, I'd also like to give thanks to a handful of social groups: the *n-dimensional p-algebra* (Dani, Rumi, and Ryan, with special mention to Ryan for instigating thesis writing sessions with me in the UNSW Main Library); the *Monday trivia team* (Alan, Michi, Shannon, Sloan, and Tim); the *game jam gang* (Alan, Dane, Felix, and Tom R); the *corporate sellouts* (Daniel, Kavan, and Vamsi); the *Bitter Phew few* (Alan, Dani, Joe, Nathaniel, Nicola, and Stuart); my *bouldering buddies* (Ameek, Ave, Hunter and Tobias); the *skate club* (Abi, Alejandra, Eva, Gen, and Gwen); and *the maths people* (including Abhinav, Abi, Alan, Dani, David, Eva, Mareike, Michi, Radek, Ryan, Susannah, Tasman, Thomas S, Tom S, and many more). My affiliation with each of these groups has had a marked positive effect on my life during the last few years, and I'm sincerely grateful for the friendships and good times we've all shared. It has been a true pleasure.

In the miscellaneous category, I'd like to thank Matthew Schwartz for signing my copy of his textbook at Planck 2023, and Frederic Schuller (who I've never met and probably never will, despite the fact we are Facebook friends) for his exceptional online lectures. An additional shoutout goes to Brandon Sanderson, who quite inconsiderately released *Wind and Truth* during my thesis writing crunch time. (Responsibly, I allocated only a day to skimming the book and devouring the ending, and now that this thesis has been relinquished unto the world I can begin to read it properly.)

Leaving some of the most important for last, I'd like to give thanks to my parents, David and Ksenija, for everything. I am extraordinarily privileged to have always had their support: they have continually backed and believed in me, and selflessly offered their help whenever I have needed it. In both the literal and figurative sense, I would not be here without them. On the topic of family, I must also thank my brothers, Daniel and Michael, for being pretty cool, and of course Mimi—the fluffiest and most adorable member of the family—for being fluffy and adorable.

Finally, I am grateful for my partner, Isabel. I count myself as very fortunate to have her; she is a wonderful individual, our time together has been fond, and her influence has turned me, I think, into a much better person. I daresay she is nearly as invested in the completion of this thesis as I am, and I am thankful for the many opportunities to discuss my research with her outside of working hours. The support she has provided during these most recent months of dedicated writing has in particular been truly invaluable.

Oh, and it would be remiss of me not to acknowledge the support from the Australian Government Research Training Program Scholarship (RTP), without which I would almost certainly be homeless and destitute. Similar gratitude is owed to the UNSW HDR Completion Scholarship and to my limitlessly benevolent supervisor Michael for magically unearthing funding for me during these final months.

To anybody I've neglected to mention, I offer my sincere apologies. Your omission speaks not to the quality of our time together, but to my competence at writing acknowledgements.

Publications and Presentations

List of Publications

- [1] T. Felkl, A. Lackner, and M. A. Schmidt, *Riding the Seesaw: What Higgsstrahlung May Reveal about Massive Neutrinos*, Eur. Phys. J. C 83, 342 (2023), arXiv:2211.15954 [hep-ph].
- [2] C. S. Fong, A. Lackner, and M. A. Schmidt, *Leptogenesis in the Zee Model*, in preparation.

List of Presentations

Oral presentations:

- *Riding the (Type-I) Seesaw: Neutrinos and New Physics*, at the 16th International Workshop on the Dark Side of the Universe (DSU 2022) & 2nd Gordon Godfrey Workshop on Astroparticle Physics, December 2022.
- *A Physics Murder Mystery: An Investigation of Neutrinos*, at the Fifth CPPC Meeting, February 2023.
- *Riding the Seesaw: What Higgsstrahlung May Reveal about Massive Neutrinos*, at the 25th International Conference From the Planck Scale to the Electroweak Scale (Planck 2023), May 2023.
- *Riding the Seesaw: What Higgsstrahlung May Reveal about Massive Neutrinos*, at the 21st Conference on Flavor Physics and CP Violation (FPCP 2023), May 2023.
- *Cooking up a Baryon Asymmetry: Leptogenesis in the Zee Model*, at the Seventh CPPC Meeting, February 2024.
- *Leptogenesis in the Zee Model*, at the International Joint Workshop on the Standard Model and Beyond 2024 & 3rd Gordon Godfrey Workshop on Astroparticle Physics, December 2024.

Poster presentations:

- *Riding the Seesaw: Neutrinos and New Physics*, at the UNSW School of Physics Research Expo, October 2022.

Abbreviations

BE	Boltzmann equation
BR	branching ratio
BSM	beyond Standard Model / physics beyond the Standard Model
c.c.	complex conjugate
C.L.	confidence level
CKM	Cabibbo–Kobayashi–Maskawa
CP	charge-parity
CTP	closed time path
EFT	effective field theory
eV	electronvolt
EW	electroweak
EWPT	electroweak phase transition
FLRW	Friedmann–Lemaître–Robertson–Walker
GeV	giga-electronvolt
h.c.	Hermitian conjugate
IO	inverted ordering
IR	infrared
JMS	Jenkins–Manohar–Stoffer
KLN	Kinoshita–Lee–Nauenberg
LEFT	Low-energy Effective Field Theory
LFU	lepton flavour universality
LFV	lepton flavour violation

LHC	Large Hadron Collider
LN	lepton number
NO	normal ordering
NP	new physics
PMNS	Pontecorvo–Maki–Nakagawa–Sakata
QCD	quantum chromodynamics
QED	quantum electrodynamics
RG	renormalization group
RGE	renormalization group equation
RHN	right-handed neutrino
RIS	real intermediate state
SM	Standard Model
SMEFT	Standard Model Effective Field Theory
UV	ultraviolet
VEV	vacuum expectation value

Contents

Abstract iii

Acknowledgements v

Publications and Presentations ix

Abbreviations xi

Contents xiii

1 Introduction 1
- 1.1 Conventions and Notation . . . 6

2 The Standard Model and Neutrinos 9
- 2.1 The Standard Model . . . 10
  - 2.1.1 The Gauge Fields . . . 11
  - 2.1.2 The Fermions . . . 13
  - 2.1.3 The Higgs Field . . . 15
  - 2.1.4 The Yukawa Sector . . . 16
- 2.2 Neutrino Masses . . . 20
  - 2.2.1 Mass Models . . . 25

3 Theory: Effective Field Theories 31
- 3.1 Constructing an EFT . . . 32
- 3.2 SMEFT . . . 37
  - 3.2.1 Parameter Shifts in SMEFT . . . 39
- 3.3 LEFT . . . 46

4 Riding the Seesaw: What Higgsstrahlung May Reveal about Massive Neutrinos 49
- 4.1 Introduction . . . 50
- 4.2 Theory Framework . . . 53
  - 4.2.1 Effective Field Theory . . . 53
  - 4.2.2 Seesaw Models . . . 55
  - 4.2.3 Conserved Lepton Number Symmetry . . . 56

4.3 Phenomenology . . . 58
4.3.1 Higgsstrahlung . . . 60
4.3.2 Electroweak Sector . . . 66
4.3.3 Lepton Flavour Universality . . . 70
4.3.4 Lepton Flavour Violation . . . 76
4.3.5 Larger Seesaw Scale . . . 83
4.4 Summary . . . 84
Appendices
4.A Approximate Matching Conditions . . . 89

5 Theory: Leptogenesis **91**
5.1 Ingredients . . . 92
5.2 CP Violation and the Cutting Rules . . . 95
5.3 A Detour: Results from Unitarity . . . 102
5.3.1 The Total CP Asymmetry is Zero . . . 103
5.3.2 Holomorphic Cutting Rules . . . 104
5.4 Modelling Leptogenesis . . . 109
5.4.1 The Expanding Universe . . . 110
5.4.2 Equilibrium Thermodynamics . . . 111
5.4.3 The Boltzmann Equation . . . 116
5.4.4 Evaluating the Equilibrium Rates . . . 124
5.4.5 Spectator Processes and Conserved Charges . . . 128
5.4.6 Summary . . . 137
Appendices
5.A Further Details on Real Intermediate State Subtraction . . . 139

6 Leptogenesis in the Zee Model **143**
6.1 Introduction . . . 144
6.2 The Zee Model . . . 146
6.2.1 CP-Violating Decays . . . 147
6.2.2 Flavour Covariance . . . 153
6.2.3 Boltzmann Equations . . . 154
6.2.4 Qualitative Discussion . . . 156
6.3 A Benchmark Scenario . . . 157
6.4 Minimal Extensions . . . 160
6.4.1 A Third Higgs Doublet . . . 160
6.4.2 A Second Singly-Charged Scalar . . . 162
6.5 Summary . . . 163
Appendices
6.A Feynman Rules . . . 165
6.B The Cutkosky Cuts in Detail . . . 165
6.B.1 $h^- \to LL$ . . . 167

6.B.2 $h^- \to e\bar{L}\bar{H}$ . . . 170
6.C The Explicit Boltzmann Equations . . . 174

7 IR Divergences in the Zee Model **177**
7.1 What is an IR Divergence? . . . 178
7.2 Zero Temperature Cancellation . . . 185
7.2.1 Final State Sum . . . 185
7.2.2 Initial State Sum . . . 188
7.3 Finite Temperature Cancellation – a Discussion . . . 194

Appendices
7.A Regulator Independence of the Final State Sum . . . 199

8 Conclusion **203**

References **207**

The Standard Model is more what you'd call guidelines than actual rules.

Hector Barbossa,
in *Pirates of the Caribbean*,
reimagined by Felix Lempriere

1

Introduction

The field of high-energy physics has come a long way in the last hundred or so years, with the establishment of the dual pillars of relativity and quantum mechanics heralding great advances in our understanding of nature, and culminating in the 1970s with the development of the Standard Model of particle physics (SM). Capstoned with the discovery of the Higgs boson in 2012 [3; 4], the SM beautifully categorises all known fundamental particles and forces (sans gravity) and describes an extraordinarily broad class of phenomena with equally extraordinary precision. It is not an exaggeration to call it a triumph of human accomplishment.

But physics is not a finished science, for in spite of the SM's myriad successes there remains a stubborn enclave of unsolved problems hinting at the need for 'beyond Standard

Model' (BSM) physics [5]. The mystery of dark matter, the unknown origin of the matter-antimatter asymmetry of the universe, and of course, the eternal quest for a quantum theory of gravity are among the most captivating of these problems, and for good reason. Receiving less fanfare in the sphere of popular science, though arguably no less important, are the hierarchy [6; 7] and strong CP problems [8; 9], which are of a more theoretical nature. The problem pertaining to this thesis is that of neutrinos: treated as massless by the SM, these weakly-interacting particles are now known to have a small but finite mass, thanks most famously to the experimental efforts of the Super-Kamiokande [10] and SNO collaborations [11; 12], who observed the flavour oscillation of atmospheric and solar neutrinos, respectively. The importance of this feat was recognised with the 2015 Nobel Prize in Physics, awarded to Takaaki Kajita and Arthur B. McDonald [13].

To be concrete, the neutrino mass problem refers to the unknown nature of neutrino masses and the problem of accommodating them within the framework of the SM. In looking to accomplish this the mainstream approach is to postulate the existence of so-called 'new physics' (NP): a new set of particles (and sometimes symmetries) whose interactions with the SM furnish the appearance of neutrino masses. From Seesaw to Supersymmetric to Scotogenic, there are—for better or for worse—dozens of ways of going about this, and so dozens of mass models (if not more) [14–43]. To distinguish these models and ascertain which, if any, are realised in nature, it is necessary to investigate their predictions beyond that of neutrino mass. Sometimes these predictions are smoking-gun signals – for example, the direct detection of a new particle at the LHC or by a dark matter detector such as LUX-ZEPLIN [44], XENONnT [45], PandaX [46], or ADMX [47] would offer spectacular confirmation of new physics. Unfortunately, such detections have so far been absent [48–67], meaning that any new particles must either be very heavy—too heavy to be produced in terrestrial experiments—or interact very weakly with the SM. As such, we must look towards more indirect probes of NP – experiments where deviations from the SM's predictions have (or have not) been observed, in which hints about the nature of NP can be found. By systematically investigating each model's predictions and comparing to available experimental data, we can methodically set constraints on their respective parameter spaces. When a measurement reports a value consistent with the SM,

it can act as a strong constraint against new physics; conversely, a measurement deviating significantly from the SM's prediction can present an opportunity for an NP model to explain the discrepancy.

This theoretical program extends to proposed experiments in addition to present-day ones. Of particular interest to this thesis, there are five proposals for next-generation electron-positron colliders: CEPC [68–70], ILC [71–74], FCC-ee [75–78], CLIC [79–81], and C^3 [82–84], which—if approved—are optimistically anticipated to become operational within two decades. Part of their proposed purpose is to function as 'Higgs factories' [85], meaning they are to be run at centre-of-mass energies where Higgs bosons are copiously produced via the Higgsstrahlung ('*Higgs radiation*') process, $e^+e^- \to Zh$, in order to study their properties. As this process centrally features both the Z boson—a carrier of the weak force—and the Higgs, which commonly acquires couplings to neutrinos in mass models, it has the potential to be particularly sensitive to BSM neutrino physics. The Higgsstrahlung cross section is forecast to be measured with sub-percent precision at these next-generation colliders, and therefore promises to function as a 'uniquely powerful' precision observable [86] which could be used to constrain corners of mass model parameter space that have been left open by other probes.

This motivates the first part of this thesis, where in Chapter 4 I will investigate the extent to which future measurements of the Higgsstrahlung cross section may be used to probe the Type-I [14–18] and Type-III Seesaw [28] models of neutrino mass. By comparing the collider reaches against present-day constraints from lepton flavour universality and electroweak precision tests, as well as the existing and prospective bounds from the non-observation of lepton flavour violation, we will see that Higgsstrahlung is indeed able to cast new light on the nature of neutrino masses. In doing so, this work therefore adds to the new physics discovery potential of next generation colliders, which may (in some small capacity) contribute to the case for their construction.

In the second half of this thesis I will change gears and attempt to address a different question: could the resolution to the neutrino mass problem be tied to that of other outstanding problems? This is a familiar line of questioning to anyone in the field, where a

model purporting to solve multiple problems at once is naturally lent more credence than one that does not. Neutrino mass models are inarguably well-motivated starting points when searching for a sufficiently versatile model, and many indeed offer potential answers to other unsolved problems – for example, the Seesaw [87; 88] and Scotogenic [33; 39] class of models each contain dark matter candidates. The secondary problem I will focus on herein is that of the unexplained origin of the baryon asymmetry of the universe. In order to explain why the universe today is composed entirely of matter [89; 90] as opposed to, say, an equal amount of matter and antimatter, a theory needs to satisfy the *Sakharov conditions* [91]: it must violate baryon number and the discrete charge (C) and charge-parity (CP) symmetries in sufficient amounts, and it must ensure that this violation occurs out of thermal equilibrium during the early universe's development.[1] It is generally accepted that the SM fails to meet these criteria [98–101], and that we therefore require a BSM mechanism of baryogenesis ('*baryon generation*').

A popular approach to baryogenesis is known as *leptogenesis* [102–105], wherein one first generates an excess of leptons over anti-leptons, and then transmutes it into an excess of baryons. Leptogenesis commonly arises in neutrino mass models, where the new leptonic physics introduced to give neutrinos mass often includes new sources of both lepton number violation and CP violation. In Chapter 6 I will study the leptogenesis prospects of the Zee model [23] of neutrino masses. A TeV-scale realisation of the Zee model has previously been ruled out as a viable progenitor of the necessary lepton asymmetry [106; 107], so I will focus on a high-scale realisation of the model, where the newly-introduced particles are heavy enough to decouple almost entirely from the low-energy physics.

Now, it will turn out that the study of Zee model inevitably leads one to encounter infrared (IR) divergences – a theoretical complication that tends to rear its head in calculations

[1] One might be able to circumvent these conditions by calling upon anthropic arguments or supposing that the initial conditions of the universe contained an imbalance of matter and antimatter; however, these explanations are disfavoured on account of their untestability. Additionally, the hypothesised period of cosmic inflation would exponentially dampen any initial baryon asymmetry [92–94]. The out-of-equilibrium condition may however be circumvented if CPT is violated; see for example Refs. [95–97].

involving massless particles. IR divergences in zero temperature quantum field theory are well-studied, and the famous Bloch–Nordsieck [108] and Kinoshita–Lee–Nauenberg (KLN) [109; 110] theorems are known to give conditions under which one may expect a computation to produce a finite result. Recently, the work of Ref. [111] has strengthened the KLN theorem and provided a practical algorithm for obtaining IR finiteness at any fixed perturbative order. Unfortunately, no such theorem exists for finite-temperature calculations (as are required for leptogenesis), though there are nevertheless a handful of works, such as Refs. [112–121], that have demonstrated IR finiteness in specific situations through explicit calculation. In Chapter 7 I will demonstrate the cancellation of IR divergences in the Zee model at zero temperature and discuss the extension of the cancellation to finite temperatures. The cancellation even at zero temperature is somewhat involved, and requires the use of techniques that—despite their popularisation by Ref. [111]—are not widely known.

This thesis follows in broad strokes a *theory, original work, theory, original work* structure. I will begin in Chapter 2 by reviewing the Standard Model and the anatomy of neutrino masses, and introduce the three mass models that will become the focus of this thesis. Next, Chapter 3 contains a short overview of the topic of effective field theories (EFTs), as well as an introduction to the two EFTs (namely SMEFT and LEFT) that will underlie the study of Higgsstrahlung and the Seesaw models. Said study takes form as Chapter 4, and is adapted (with edits) from the publication of Ref. [1]. Chapter 5 is another theory chapter, containing an introduction to the topic of leptogenesis, the calculation of CP asymmetries, and the construction of the relevant Boltzmann equations. Chapter 6 then features the study of the leptogenesis scenario in the Zee model, and it is followed up by Chapter 7, where I will discuss the problem of infrared divergences in the Zee model. Finally, I will summarise and conclude in Chapter 8.

1.1 Conventions and Notation

Throughout this thesis I will work exclusively with natural units, with $c = \hbar = k_B = 1$. Dimensionful quantities will be given in units of electronvolts (eV).

For the metric of spacetime I will use the mostly-minus signature, so that

$$g_{\mu\nu} = g^{\mu\nu} = \begin{pmatrix} 1 & & & \\ & -1 & & \\ & & -1 & \\ & & & -1 \end{pmatrix}. \tag{1.1}$$

Spacetime indices are denoted with Greek letters, which run from 0 to 3. Repeated indices are understood to be implicitly summed over.

For the first part of this thesis I will use the Roman letters i, j, k, l, running from 1 to 3, to index fermion flavours, as in L_i and e_{Ri}. The summation convention applies to these indices unless otherwise noted. Starting in Chapter 5 this notation will be regretfully usurped, where I will switch to using early-alphabet Greek letters $\alpha, \beta, \gamma, \delta$ for the flavour indices.

I will use boldface to denote three-vectors, such as $\mathbf{p}, \mathbf{k}$, and plain lettering for four-vectors, such as p, k. For integrals over the phase space of a single particle I will use the shorthand

$$\int [\mathrm{d}p] \equiv \int \frac{\mathrm{d}^4 p}{(2\pi)^4} 2\pi\delta(p^2 - m^2)\theta(p^0) = \int \frac{\mathrm{d}^3\mathbf{p}}{(2\pi)^3 2E_p}, \qquad E_p = \sqrt{\mathbf{p}^2 + m^2}. \tag{1.2}$$

For an n-body phase space I will write

$$\int \mathrm{d}\Pi_n \equiv \int [\mathrm{d}p_1] \cdots [\mathrm{d}p_n] (2\pi)^4 \delta^{(4)}(Q - p_1 - \ldots - p_n), \tag{1.3}$$

where Q sets the total four-momentum, and it should be clear from context which momenta are being integrated over. When referring to a generic initial or final state with an unspecified number of particles I will use uppercase letters to indicate the sum of their momenta, writing for example

$$\int \mathrm{d}\Pi_f = \int [\mathrm{d}P_f](2\pi)^4 \delta^{(4)}(Q - P_f). \tag{1.4}$$

Lastly, I will use the upright i to denote the imaginary unit in order to distinguish it from i, which I will often use as an index.

Oh pardon me *Right-Handed Neutrino*, if that is your real name.

Comic Book Guy,
in *The Simpsons*,
reimagined

2

The Standard Model and Neutrinos

Contents

2.1 The Standard Model **10**

2.2 Neutrino Masses **20**

In this chapter I'll review some of the basic concepts and theory underpinning this thesis, thereby setting the groundwork for all following chapters. Most, if not all, material presented here can be found in any sufficiently modern text on Quantum Field Theory and/or the Standard Model, such as Refs. [122; 123], and will undoubtedly be familiar to a practitioner in the field. Other excellent references for select topics are Refs. [36; 124–127].

Field	$\mathrm{SU(3)_C}$	$\mathrm{SU(2)_W}$	$\mathrm{U(1)_Y}$
G_μ	Adj. (8)	1	0
W_μ	1	Adj. (3)	0
B_μ	1	1	Adj. (1)
Q_i	3	2	$\frac{1}{6}$
u_{Ri}	3	1	$\frac{2}{3}$
d_{Ri}	3	1	$-\frac{1}{3}$
L_i	1	2	$-\frac{1}{2}$
e_{Ri}	1	1	-1
H	1	2	$\frac{1}{2}$

Table 2.1: The field content of the SM and their transformation properties under the SM gauge group. The number in the $\mathrm{SU(3)_C}$ and $\mathrm{SU(2)_W}$ columns gives the dimension of the representation, while the number in the $\mathrm{U(1)_Y}$ column gives the charge of the representation. Adj. (n) indicates that the gauge field transforms in the adjoint representation of the group, which is n-dimensional.

2.1 The Standard Model

The **Standard Model of particle physics** (SM), though the language of quantum field theory, provides a fully quantum description of all known fundamental particles—or rather, fields—and their interactions through the strong and electroweak forces. It is a gauge theory, meaning that all fields are defined to transform under a particular representation of the SM gauge group,

$$G = \mathrm{SU(3)_C} \times \mathrm{SU(2)_W} \times \mathrm{U(1)}_Y, \tag{2.1}$$

with a field's representation controlling many of its properties. The $\mathrm{SU(3)_C}$ subgroup captures the strong nuclear force, alternatively called the colour force, and the $\mathrm{SU(2)_W}$ and $\mathrm{U(1)}_Y$ subgroups together describe the unified electroweak (EW) force. The SM fields and their transformation properties under G are tabulated in Table 2.1. For a single field, say L_i, it is common to write $L_i \sim (1, 2, -1/2)$, which should be read as "L_i transforms as an $\mathrm{SU(3)_C}$ singlet, an $\mathrm{SU(2)_W}$ doublet, and with charge $-1/2$ under $\mathrm{U(1)}_Y$."

The SM is specified through its Lagrangian, which reads

$$\begin{aligned}\mathcal{L}_{\text{SM}} = &-\frac{1}{4}G^a_{\mu\nu}G^{a\mu\nu} - \frac{1}{4}W^a_{\mu\nu}W^{a\mu\nu} - \frac{1}{4}B_{\mu\nu}B^{\mu\nu} \\ &+ \overline{Q_i}\mathrm{i}\not{D}Q_i + \overline{u_{Ri}}\mathrm{i}\not{D}u_{Ri} + \overline{d_{Ri}}\mathrm{i}\not{D}d_{Ri} + \overline{L_i}\mathrm{i}\not{D}L_i + \overline{e_{Ri}}\mathrm{i}\not{D}e_{Ri} \\ &+ (D_\mu H)^\dagger(D^\mu H) + \mu^2 H^\dagger H - \lambda(H^\dagger H)^2 \\ &- \left(Y^u_{ij}\overline{Q_i}\widetilde{H}u_{Rj} + Y^d_{ij}\overline{Q_i}Hd_{Rj} + Y^e_{ij}\overline{L_i}He_{Rj} + \text{h.c.}\right).\end{aligned} \tag{2.2}$$

In the next four sections I'll briefly outline and discuss the four respective lines of Eq. (2.2) and the physics they represent.

2.1.1 The Gauge Fields

The first line in Eq. (2.2) contains kinetic terms for the gauge bosons G_μ, W_μ, and B_μ of the three respective gauge subgroups. This thesis is primarily concerned with the electroweak part of the SM, so I will not devote any attention to the gluon field G_μ.

The electroweak gauge bosons interact with the rest of the SM through the gauge-covariant derivative

$$D_\mu = \partial_\mu - \mathrm{i}g_2 W^a_\mu T^a - \mathrm{i}g_1 Y B_\mu, \tag{2.3}$$

where the hypercharge Y is read from the $\mathrm{U}(1)_Y$ column of Table 2.1, and the $\mathrm{SU}(2)_\mathrm{W}$ generators are

$$T^a = \begin{cases} \dfrac{\sigma^a}{2} & \text{when acting on an } \mathrm{SU}(2)_\mathrm{W} \text{ doublet} \\ 0 & \text{when acting on an } \mathrm{SU}(2)_\mathrm{W} \text{ singlet} \end{cases}, \tag{2.4}$$

with σ^a, $a = 1, 2, 3$ the familiar Pauli matrices.

Due to the Higgs mechanism, to be elaborated on shortly, some of these fields acquire masses. The mass eigenstates Z_μ and A_μ, identified as the ***Z* boson** and the **photon**, relate to the original gauge fields by the rotation

$$Z_\mu = \cos\theta_w\, W^3_\mu - \sin\theta_w\, B_\mu, \tag{2.5a}$$
$$A_\mu = \sin\theta_w\, W^3_\mu + \cos\theta_w\, B_\mu, \tag{2.5b}$$

where

$$\theta_w = \tan^{-1}(g_2/g_1) \tag{2.6}$$

is known as the **weak mixing angle**. It is furthermore useful to define the combinations

$$W_\mu^\pm = \frac{1}{\sqrt{2}}(W_\mu^1 \mp \mathrm{i}W_\mu^2), \tag{2.7}$$

referred to as the $W^\pm$ bosons, or simply the ***W* boson** for short. In terms of these fields the gauge-covariant derivative takes on the new form

$$D_\mu = \partial_\mu - \mathrm{i}g_2 W_\mu^+ T^+ - \mathrm{i}g_2 W_\mu^- T^- - \mathrm{i}g_Z(T^3 - Q\sin^2\theta_w)Z_\mu - \mathrm{i}QeA_\mu, \tag{2.8}$$

with

$$T^\pm \equiv \frac{1}{\sqrt{2}}(T^1 \pm \mathrm{i}T^2), \qquad g_Z \equiv \sqrt{g_1^2 + g_2^2}, \qquad Q \equiv T^3 + Y, \quad \text{and} \quad e \equiv \frac{g_1 g_2}{\sqrt{g_1^2 + g_2^2}}. \tag{2.9}$$

The massive W and Z bosons together mediate the weak force, and the familiar photon mediates the electromagnetic force.

It it useful to have a sense for the size of the gauge couplings. Like most parameters, these couplings depend on energy, renormalization scheme, and choice of input parameters, but as a benchmark we have that [124]

$$g_1 \approx 0.36 \quad \text{and} \quad g_2 \approx 0.65 \tag{2.10}$$

at the scale $\mu = m_Z$, which translates to $\sin^2\theta_w \approx 0.23$, $g_Z \approx 0.74$ and $e \approx 0.31$. The more conventional value of $e \approx 0.30$ is found at lower energies, $\mu < 1\,\mathrm{GeV}$.

2.1.2 The Fermions

The fermions, consisting of the **leptons** L, e_R and **quarks** Q, u_R, d_R, make up the matter content of the SM. They appear in three copies, called **generations** or **flavours**, which are identical but for their masses.

Of the fermions, the $\mathrm{SU(2)_W}$ doublets are composite objects whose components we identify (in a preferred $\mathrm{SU(2)_W}$ and flavour basis) as

$$L_i = \begin{pmatrix} \nu_{Li} \\ e_{Li} \end{pmatrix} : \qquad L_1 = \begin{pmatrix} \nu_{eL} \\ e_L \end{pmatrix}, \quad L_2 = \begin{pmatrix} \nu_{\mu L} \\ \mu_L \end{pmatrix}, \quad L_3 = \begin{pmatrix} \nu_{\tau L} \\ \tau_L \end{pmatrix}, \tag{2.11}$$

and[1]

$$Q_i = \begin{pmatrix} u_{Li} \\ d_{Li} \end{pmatrix} : \qquad Q_1 = \begin{pmatrix} u_L \\ d_L \end{pmatrix}, \quad Q_2 = \begin{pmatrix} c_L \\ s_L \end{pmatrix}, \quad Q_3 = \begin{pmatrix} t_L \\ b_L \end{pmatrix}. \tag{2.12}$$

The $\mathrm{SU(2)_W}$ singlets contain the right-handed partners to these fields, with

$$e_{Ri} = \{e_R, \mu_R, \tau_R\}, \qquad u_{Ri} = \{u_R, c_R, t_R\}, \quad \text{and} \quad d_{Ri} = \{d_R, s_R, b_R\}. \tag{2.13}$$

The quark fields Q, u_R, d_R are additionally $\mathrm{SU(3)_C}$ triplets, with the components designated as different 'colourings' of the quark flavours.

The distinction between left- and right-handed fermion fields is an important one. Here the handedness—or **chirality**—of a field refers at a technical level to its transformation properties under the Lorentz group. Chirality only admits a simple physical interpretation for relativistic fermions, in which limit a right-handed particle has its momentum and spin vectors parallel, and left-handed one has them antiparallel. At a practical level we treat chirality through use of the projection operators

[1] It is not possible to identify both the u_{Li} and d_{Li} with mass eigenstates; see Section 2.1.4. Instead, it is more correct to write

$$Q_i = \begin{pmatrix} u_{Li} \\ V_{ij} d_{Lj} \end{pmatrix} \quad (\text{'}\textit{up basis}\text{'}) \qquad \text{or} \qquad Q_i = \begin{pmatrix} V^\dagger_{ij} u_{Lj} \\ d_{Li} \end{pmatrix} \quad (\text{'}\textit{down basis}\text{'}),$$

where V is the CKM matrix.

$$P_L = \frac{1-\gamma^5}{2} \quad \text{and} \quad P_R = \frac{1+\gamma^5}{2}, \tag{2.14}$$

where the chirality operator[2]

$$\gamma^5 \equiv \mathrm{i}\gamma^0\gamma^1\gamma^2\gamma^3 \tag{2.15}$$

satisfies

$$\{\gamma^\mu, \gamma^5\} = 0, \qquad (\gamma^5)^2 = 1, \quad \text{and} \quad \gamma^{5\dagger} = \gamma^5. \tag{2.16}$$

In $\mathcal{L}_{\mathrm{SM}}$ the handedness of the fermions can be made overt by making the replacements

$$Q \to P_L Q, \qquad u_R \to P_R u_R, \qquad d_R \to P_R d_R, \qquad L \to P_L L, \quad \text{and} \quad e_R \to P_R e_R, \tag{2.17}$$

(which is a no-op since $Q = P_L Q$, and so on), and the physics of chirality then emerges through the appearance of these projectors in the Feynman rules and subsequently in scattering amplitudes.

Though not intrinsic to the nature of chirality itself, it is of great phenomenological importance that only the left-handed fields Q_i and L_i couple to the $\mathrm{SU(2)_W}$ gauge fields. As the interaction terms

$$\frac{g_2}{\sqrt{2}}\left(\overline{\nu_{eL}}\not{W}^+ e_L + \overline{e_L}\not{W}^- \nu_{eL}\right) \subset \overline{L_i}\mathrm{i}\not{D} L_i \subset \mathcal{L}_{\mathrm{SM}}, \tag{2.18}$$

when treated as operators, permit the W boson to interact with left-handed electrons e_L^- and right-handed positrons e_R^+, but not right-handed electrons e_R^+ or left-handed positrons e_L^+, the weak interaction maximally violates both C-symmetry (which takes $e^\pm_{L/R} \to e^\mp_{L/R}$) and P-symmetry (which takes $e^\pm_{L/R} \to e^\pm_{R/L}$), though not the combined CP-symmetry.

[2]The gamma matrices are defined to satisfy $\{\gamma^\mu, \gamma^\nu\} = 2g^{\mu\nu}$ and $\gamma^{\mu\dagger} = \gamma^0\gamma^\mu\gamma^0$, and they appear in $\mathcal{L}_{\mathrm{SM}}$ through the conjugate fields $\overline{\psi} \equiv \psi^\dagger\gamma^0$ and the 'slashed' derivatives $\not{D} \equiv \gamma^\mu D_\mu$.

(Actually, CP is violated by weak interactions with the quarks, which we will see when introducing the CKM matrix, and later come to understand in great detail in Chapter 5.) Interactions with the Z boson also violate C and P, though not as strongly.

2.1.3 The Higgs Field

The linchpin of the SM is the scalar $\mathrm{SU}(2)_\mathrm{W}$ doublet H, known as the **Higgs field**. Its purpose is to enact the Higgs mechanism, whereby the electroweak $\mathrm{SU}(2)_\mathrm{W} \times \mathrm{U}(1)_Y$ symmetry is spontaneously broken by the vacuum expectation value (VEV)

$$\langle H \rangle = \frac{\mu}{\sqrt{2\lambda}} \equiv \frac{v}{\sqrt{2}}. \tag{2.19}$$

Through a combined $\mathrm{SU}(2)_\mathrm{W} \times \mathrm{U}(1)_Y$ gauge transformation the VEV can be placed in the lower component of H,

$$H = \begin{pmatrix} 0 \\ \dfrac{v+h}{\sqrt{2}} \end{pmatrix}, \tag{2.20}$$

and the remaining real degree of freedom h is called the **Higgs boson**. We refer to this as **unitary gauge**. The surviving symmetry subgroup $\mathrm{U}(1)_\mathrm{EM}$, generated by $Q = T_3 + Y$ and with gauge field A_μ, is the one which preserves the form of Eq. (2.20). We note that the full gauge symmetry remains extant in $\mathcal{L}_\mathrm{SM}$; the only sense in which the symmetry is broken is through our insistence on the use of unitary gauge.

Plugging Eq. (2.20) back into $\mathcal{L}_\mathrm{SM}$, one observes after some algebra the appearance of the mass terms

$$\mathcal{L}_\mathrm{SM} \supset -\frac{1}{2} m_h h^2 + m_W^2 W_\mu^- W^{+\mu} + \frac{1}{2} m_Z^2 Z_\mu Z^\mu, \tag{2.21}$$

where [124]

$$m_h = \sqrt{2}\mu \approx 125.1\,\text{GeV}, \tag{2.22a}$$
$$m_W = \frac{1}{2} g_2 v \approx 80.4\,\text{GeV}, \quad \text{and} \tag{2.22b}$$
$$m_Z = \frac{1}{2}\sqrt{g_1^2 + g_2^2}\, v = \frac{m_W}{\cos\theta_w} \approx 91.2\,\text{GeV}, \tag{2.22c}$$

while the photon field A_μ is of course massless. The VEV itself, as measured through muon decays by proxy of the Fermi constant $G_F \equiv 1/\sqrt{2}v^2$, is $v \approx 246\,\text{GeV}$, and the original parameters of the Higgs' potential are in turn $\lambda \approx 0.13$ and $\mu \approx 88\,\text{GeV}$.

2.1.4 The Yukawa Sector

The final line of $\mathcal{L}_{\text{SM}}$ contains the **Yukawa interactions**

$$\mathcal{L}_{\text{Yuk}} = -\Big(Y^e_{ij}\overline{L_i} H e_{Rj} + Y^u_{ij}\overline{Q_i}\widetilde{H} u_{Rj} + Y^d_{ij}\overline{Q_i} H d_{Rj} + \text{h.c.}\Big), \tag{2.23}$$

where $\widetilde{H} \equiv \epsilon H^*$, with $\epsilon = \text{i}\sigma^2$ the two-index Levi-Civita symbol. When the Higgs acquires its VEV these interactions turn into mass terms for the fermions with residual h interactions,

$$\mathcal{L}_{\text{Yuk}} \to -\left(1 + \frac{h}{v}\right)\Big(m^e_{ij}\overline{e_{Li}} e_{Rj} + m^u_{ij}\overline{u_{Li}} u_{Rj} + m^d_{ij}\overline{d_{Li}} d_{Rj} + \text{h.c.}\Big), \tag{2.24}$$

where the mass matrices are

$$m^e_{ij} \equiv \frac{v}{\sqrt{2}} Y^e_{ij} \quad \text{and so on.} \tag{2.25}$$

With no symmetries forcing them to take particular forms, these are in principle arbitrary complex matrices which we can decompose by means of a singular value decomposition as

$$Y^e = U^e D^e V^{e\dagger} \quad \text{and so on.} \tag{2.26}$$

Here U^e and V^e are both unitary and D^e is diagonal with non-negative real entries. By redefining the fields

$$L_i \to U^e_{ij} L_j \quad \text{and} \quad e_{Ri} \to V^e_{ij} e_{Rj}, \tag{2.27}$$

which is nothing but a change of basis in flavour space, we are left with the diagonal Yukawa interaction

$$\mathcal{L}_{\text{Yuk}} \supset -D^e_{ij} \overline{L_i} H e_{Rj} + \text{h.c.}, \tag{2.28}$$

and in turn a diagonal mass matrix for the charged leptons. It is in this 'mass basis' that we may then identify e_{R1} as the electron, e_{R2} as the muon, and e_{R3} as the tau, as in Eqs. (2.11) or (2.13). We note that the matrices U^e and V^e are unphysical as the rest of $\mathcal{L}_{\text{SM}}$ is invariant under this change of basis:

$$\begin{aligned} \overline{L} \mathrm{i}\not{D} L + \overline{e_R} \mathrm{i}\not{D} e_R &\to \overline{L} U^{e\dagger} \mathrm{i}\not{D} U^e L + \overline{e_R} V^{e\dagger} \mathrm{i}\not{D} V^e e_R && (2.29) \\ &= \overline{L} \mathrm{i}\not{D} L + \overline{e_R} \mathrm{i}\not{D} e_R, && (2.30) \end{aligned}$$

where for readability I've suppressed the flavour indices and switched to a matrix multiplication notation.

The situation is more complicated for quarks, where to diagonalise both Y^u and Y^d we must apply

$$\begin{aligned} u_L \to U^u u_L, \qquad u_R \to V^u u_R \quad \text{and} && (2.31a) \\ d_L \to U^d d_L, \qquad d_R \to V^d d_R. && (2.31b) \end{aligned}$$

Because U^u and U^d are in general different it is not possible to rotate the doublets via

$$Q \to UQ = \begin{pmatrix} U u_L \\ U d_L \end{pmatrix} \tag{2.32}$$

to a basis in which both the up- and down-type quarks are mass eigenstates, and the identifications in Eq. (2.12) should be made with this understanding. Nevertheless, we can perform the separate rotations in Eq. (2.31) *after* electroweak symmetry breaking has occurred and we have expanded out $\mathcal{L}_{\text{SM}}$ in terms of u_L and d_L instead of Q. In doing

this there is one place where, unlike the leptonic case, the matrices U^u and U^d do not disappear: the W boson interactions, which couple the up- and down-type quarks. Indeed, we can observe that

$$\begin{aligned}\overline{Q}\mathrm{i}\not{D}Q &\supset \frac{g_2}{\sqrt{2}}\left(\overline{u_L}\not{W}^+ d_L + \overline{d_L}\not{W}^- u_L\right) && (2.33)\\ &\to \frac{g_2}{\sqrt{2}}\left(\overline{u_L}U^{u\dagger}\not{W}^+ U^d d_L + \overline{d_L}U^{d\dagger}\not{W}^- U^u u_L\right) && (2.34)\\ &= \frac{g_2}{\sqrt{2}}\left(\overline{u_L}V\not{W}^+ d_L + \overline{d_L}V^\dagger\not{W}^- u_L\right), && (2.35)\end{aligned}$$

where

$$V \equiv U^{u\dagger}U^d, \tag{2.36}$$

is called the **Cabibbo–Kobayashi–Maskawa (CKM) matrix** [128; 129]. The CKM matrix captures the misalignment between the mass eigenstates and weak interaction eigenstates, and any attempts to rotate it away will simply juggle it between the Wud interaction and the quark Yukawas. It has four degrees of freedom, which in the so-called *standard parameterisation* [130] take the form of three mixing angles $\theta_{12}, \theta_{13}, \theta_{23} \in [0, \pi/2]$ and one CP-violating phase $\delta \in [0, 2\pi)$, and with the shorthands $c_{ij} \equiv \cos\theta_{ij}$ and $s_{ij} \equiv \sin\theta_{ij}$ it reads

$$\begin{aligned}V &= \begin{pmatrix}1 & 0 & 0\\ 0 & c_{23} & s_{23}\\ 0 & -s_{23} & c_{23}\end{pmatrix}\begin{pmatrix}c_{13} & 0 & s_{13}e^{-\mathrm{i}\delta}\\ 0 & 1 & 0\\ -s_{13}e^{\mathrm{i}\delta} & 0 & c_{13}\end{pmatrix}\begin{pmatrix}c_{12} & s_{12} & 0\\ -s_{12} & c_{12} & 0\\ 0 & 0 & 1\end{pmatrix} && (2.37)\\ &= \begin{pmatrix}c_{12}c_{13} & s_{12}c_{13} & s_{13}e^{-\mathrm{i}\delta}\\ -s_{12}c_{23} - c_{12}s_{23}s_{13}e^{\mathrm{i}\delta} & c_{12}c_{23} - s_{12}s_{23}s_{13}e^{\mathrm{i}\delta} & s_{23}c_{13}\\ s_{12}s_{23} - c_{12}c_{23}s_{13}e^{\mathrm{i}\delta} & -c_{12}s_{23} - s_{12}c_{23}s_{13}e^{\mathrm{i}\delta} & c_{23}c_{13}\end{pmatrix}.\end{aligned}$$

In Chapter 5 we will turn our attention to CP violation, and there the phase δ will be of interest to us. A parameterisation-independent way of capturing the amount of CP violation in the CKM matrix is through the **Jarlskog invariant** J [131], defined via [122; 124]

$$\mathrm{Im}(V_{ij}V_{kl}V_{il}^*V_{kj}^*) = J\sum_{m,n}\epsilon_{ikm}\epsilon_{jln}, \tag{2.38}$$

Charged Leptons		Up-type Quarks		Down-type Quarks	
Particle	Mass [GeV]	Particle	Mass [GeV]	Particle	Mass [GeV]
e	0.511×10^{-3}	u	2.2×10^{-3}	d	4.7×10^{-3}
μ	0.106	c	1.27	s	0.0935
τ	1.78	t	173	b	4.18

Table 2.2: Masses of the SM fermions [124]. For all quarks but the top quark the values given correspond to $\overline{\text{MS}}$ masses, as pole masses are sensitive to non-perturbative infrared effects in QCD.

with no summation over i, j, k, l; for example $\text{Im}(V_{ud}V_{tb}V_{ub}^*V_{td}^*) = J$. In terms of the standard parameterisation it equates to

$$J = c_{12}c_{13}^2c_{23}s_{12}s_{13}s_{23}\sin\delta, \tag{2.39}$$

and we observe that it vanishes when any of the mixing angles are 0 or $\frac{\pi}{2}$. Though it takes more effort to see, the CP violation also vanishes if any of the quarks are massless (which they are not).

From a recent global fit the magnitudes of the CKM matrix elements are [124]

$$|V| = \begin{pmatrix} |V_{ud}| & |V_{us}| & |V_{ub}| \\ |V_{cd}| & |V_{cs}| & |V_{cb}| \\ |V_{td}| & |V_{ts}| & |V_{tb}| \end{pmatrix} \approx \begin{pmatrix} 0.974 & 0.225 & 0.004 \\ 0.225 & 0.973 & 0.042 \\ 0.009 & 0.041 & 0.999 \end{pmatrix}, \tag{2.40}$$

which corresponds to

$$\sin\theta_{12} \approx 0.225, \qquad \sin\theta_{13} \approx 0.004, \qquad \sin\theta_{23} \approx 0.042, \quad \text{and} \quad \delta \approx 1.15, \tag{2.41}$$

and the Jarlskog invariant is in turn

$$J \approx 3.12 \times 10^{-5}. \tag{2.42}$$

I lastly present the fermion masses in Table 2.2. As a final remark, we observe that the Yukawa interactions have the interesting feature that particles couple to the Higgs boson proportionally to their own mass. As the top quark is so much heavier than all other leptons, with $Y_t \equiv D_{33}^u = \sqrt{2}m_t/v \approx 0.94$ in the $\overline{\text{MS}}$ scheme [124], it is therefore common

in many calculations to neglect contributions from all other particles. We will see one such example of this in Chapter 6, where the top quark will provide the dominant contribution to the thermal mass of the Higgs field.

2.2 Neutrino Masses

Owing to the fact that one has never been observed, right-handed neutrinos (RHNs) are notably absent from the SM. Assuming they exist, it is easy to understand their non-observation – neutrinos are electrically neutral and only interact with the rest of the SM through the weak interaction, and the W boson only couples to left-handed particles. With the gauge representation $\nu_R \sim (1, 1, 0)$, an RHN would not even couple to the Z boson. In this way, RHNs are often referred to as **sterile neutrinos** [87; 88; 132].

The exclusion of RHNs from the SM is however a problem, as SM neutrinos are massless in the absence of right-handed partners. This stands in contrast to oscillation experiments which definitively demonstrate that neutrinos are in fact massive [10–13; 133–151]. The premise behind these experiments is straightforward: if neutrinos have mass then there must be a leptonic analogue of the CKM matrix, and therefore a misalignment of the weak interaction eigenstates ν_e, ν_μ, ν_τ and mass eigenstates ν_1, ν_2, ν_3. This then means, for example, that an electron neutrino ν_e—which is a superposition of ν_1, ν_2, ν_3—may oscillate into and be detected as a muon neutrino ν_μ, or vice versa. Neutrino oscillations are then observed by measuring an under- or overabundance of differently-flavoured neutrinos from a known source, such as the sun (*solar neutrinos*) [11; 12; 135; 136], cosmic rays (*atmospheric neutrinos*) [10; 133; 134], accelerator beams (*accelerator neutrinos*) [139–143], or radioactive sources (*reactor neutrinos*) [144–151].

One is tempted to declare the neutrino mass problem solved with the addition of RHNs and suitable Yukawa interactions to the SM. This is however considered to be an unsatisfying solution on two counts. The first is that it offers no explanation for why neutrinos, with masses constrained to be below 1 eV [90; 124; 152; 153], are lighter than all other SM

particles by many orders of magnitude. The second is that it ignores the possibility that neutrinos are Majorana, which is to say their own antiparticle. Moreover, there is actually a wide class of mechanisms for generating neutrino mass [35; 38], and without definitive evidence favouring a particular one it would be irresponsible of us to not afford them due consideration.

Let us therefore devote some time to a discussion on the anatomy of neutrino masses. There are two types of fermion masses: Dirac and Majorana. Dirac masses feature both left- and right-handed fields and take the familiar form

$$-m^{\nu}\overline{\nu_L}\nu_R + \text{h.c.}, \tag{2.43}$$

where for simplicity I elide the flavour indices. With the two fields coupled the physical neutrino field is the **Dirac field** $\nu \equiv \nu_L + \nu_R$, which is described by the free Lagrangian

$$\begin{aligned} \mathcal{L}_{\nu} &= \overline{\nu}(\mathrm{i}\partial\!\!\!/ - m^{\nu})\nu & (2.44)\\ &= \overline{\nu_L}\mathrm{i}\partial\!\!\!/\nu_L + \overline{\nu_R}\mathrm{i}\partial\!\!\!/\nu_R - m^{\nu}(\overline{\nu_L}\nu_R + \overline{\nu_R}\nu_L). & (2.45) \end{aligned}$$

(This is familiar to us, as all other SM fermions combine into Dirac fields after electroweak symmetry breaking, with $e_i = e_{Li} + e_{Ri}$, and so on.) As Dirac masses are not gauge invariant they must be generated either through the Yukawa interaction

$$-Y^{\nu}\overline{L}\widetilde{H}\nu_R + \text{h.c.}, \tag{2.46}$$

or by more complicated means [38; 154].

Majorana masses, on the other hand, take the form

$$-\frac{1}{2}m^{\nu}\overline{\nu_L}\nu_L^c + \text{h.c.}, \tag{2.47}$$

where the conjugate field ν_L^c is defined as [155]

$$\nu_L^c \equiv \gamma^0 C\nu_L^*, \tag{2.48}$$

with C an antisymmetric unitary matrix defined to satisfy

$$C^{-1}\gamma^\mu C = -(\gamma^\mu)^T. \tag{2.49}$$

In this case the physical neutrino field is the **Majorana field** $\nu_M \equiv \nu_L + \nu_L^c$, described by

$$\mathcal{L}_{\nu_M} = \frac{1}{2}\overline{\nu_M}(\mathrm{i}\partial\!\!\!/ - m^\nu)\nu_M \tag{2.50}$$

$$= \overline{\nu_L}\mathrm{i}\partial\!\!\!/\nu_L - \frac{1}{2}m^\nu(\overline{\nu_L}\nu_L^c + \overline{\nu_L^c}\nu_L). \tag{2.51}$$

Much like a Dirac mass, a Majorana mass term for ν_L is similarly not gauge invariant, though in this case it may be generated by the *Weinberg operator* [156]

$$C_5(\overline{L}\widetilde{H})(\widetilde{H}^T L^c) + \text{h.c.}, \tag{2.52}$$

whereupon $m^\nu = -v^2 C_5$. Unfortunately the Weinberg operator is of mass dimension five and is therefore non-renormalizable, which indicates that it should be interpreted as an effective operator for a UV-complete theory. Thus, a Majorana mass for ν_L *requires* BSM physics.

What are the physical implications of Majorana masses? The most direct one is that Majorana neutrinos are their own antiparticles, as $\nu_M = \nu_M^c$ (which follows from $(\nu_L^c)^c = \nu_L$) implies that the particle and antiparticle creation operators in the mode expansion of ν_M are the same [155]. Related to this is the fact that a Majorana mass for ν_L violates **lepton number** $\mathrm{U}(1)_L$, an accidental symmetry of the SM in which

$$L_i \to e^{\mathrm{i}\theta} L_i \quad \text{and} \quad e_{Ri} \to e^{\mathrm{i}\theta} e_{Ri}, \tag{2.53}$$

as

$$\overline{\nu_L}\nu_L^c \to e^{-2\mathrm{i}\theta}\overline{\nu_L}\nu_L^c \neq \overline{\nu_L}\nu_L^c. \tag{2.54}$$

Lepton number symmetry means that the total number of leptons minus anti-leptons

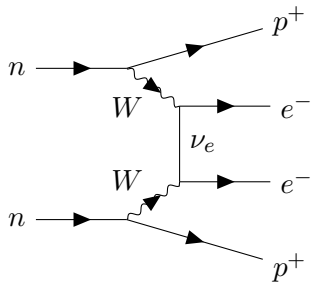

Figure 2.1: Neutrinoless double beta decay with a Majorana ν_e.

is conserved by every Standard Model process.[3] A way to probe whether neutrinos are Majorana is then to search for lepton number-violating processes such as neutrinoless double beta decay [159], pictured in Fig. 2.1. (So far, it has not been observed [66; 160; 161].) One may also leverage lepton number violation to attempt to explain the matter-antimatter asymmetry of the universe through a mechanism called *leptogenesis* [102; 104], which we will explore in Chapters 5 and 6.

Now, to diagonalise m^ν we must rotate

$$\nu_L \to U^\nu \nu_L \quad \text{and} \quad \nu_R \to V^\nu \nu_R \qquad \text{so that} \qquad m^\nu = U^\nu D^\nu V^{\nu\dagger} \tag{2.55}$$

in the Dirac case, and

$$\nu_L \to U^\nu \nu_L \qquad \text{so that} \qquad m^\nu = U^\nu D^\nu U^{\nu T} \tag{2.56}$$

in the Majorana case. The decomposition $m = UDU^T$ in Eq. (2.56), which is possible because a Majorana m^ν is symmetric, is known as a *Takagi factorisation*; see for example Refs. [162; 163]. In exact analogy with the quarks the matrix product

$$V' \equiv U^{\nu\dagger} U^e \tag{2.57}$$

will appear in interactions with the W boson. Here it is conventional to remove the U^e by

[3] Lepton number is actually violated anomalously by quantum effects [122; 157; 158], though the combined baryon-minus-lepton number symmetry $\mathrm{U}(1)_{B-L}$, in which quarks transform with charge $\frac{1}{3}$ and leptons with charge -1, remains a symmetry even at the quantum level if there are three RHNs.

working in a basis in which the charged lepton masses have already been diagonalised via Eq. (2.27);[4] in this way

$$V' = U^{\nu\dagger}, \tag{2.58}$$

and in the mass basis the $We\nu$ interactions take the form

$$\frac{g_2}{\sqrt{2}}\Big(\overline{\nu_L} U^{\nu\dagger} \not{W}^+ e_L + \overline{e_L} U^{\nu} \not{W}^- \nu_L\Big). \tag{2.59}$$

The matrix U^ν, which I will henceforth simply call U, is known as the **Pontecorvo–Maki–Nakagawa–Sakata (PMNS) matrix** [164; 165]. As it fulfils a similar role to the CKM matrix it unsurprisingly admits the near-identical parameterisation

$$\begin{aligned} U &= \begin{pmatrix} 1 & 0 & 0 \\ 0 & c_{23} & s_{23} \\ 0 & -s_{23} & c_{23} \end{pmatrix} \begin{pmatrix} c_{13} & 0 & s_{13}e^{-\mathrm{i}\delta} \\ 0 & 1 & 0 \\ -s_{13}e^{\mathrm{i}\delta} & 0 & c_{13} \end{pmatrix} \begin{pmatrix} c_{12} & s_{12} & 0 \\ -s_{12} & c_{12} & 0 \\ 0 & 0 & 1 \end{pmatrix} \begin{pmatrix} e^{\mathrm{i}\alpha_1} & 0 & 0 \\ 0 & e^{\mathrm{i}\alpha_2} & 0 \\ 0 & 0 & 1 \end{pmatrix} \\ &= \begin{pmatrix} c_{12}c_{13} & s_{12}c_{13} & s_{13}e^{-\mathrm{i}\delta} \\ -s_{12}c_{23} - c_{12}s_{23}s_{13}e^{\mathrm{i}\delta} & c_{12}c_{23} - s_{12}s_{23}s_{13}e^{\mathrm{i}\delta} & s_{23}c_{13} \\ s_{12}s_{23} - c_{12}c_{23}s_{13}e^{\mathrm{i}\delta} & -c_{12}s_{23} - s_{12}c_{23}s_{13}e^{\mathrm{i}\delta} & c_{23}c_{13} \end{pmatrix} \begin{pmatrix} e^{\mathrm{i}\alpha_1} & 0 & 0 \\ 0 & e^{\mathrm{i}\alpha_2} & 0 \\ 0 & 0 & 1 \end{pmatrix}. \end{aligned} \tag{2.60}$$

In addition to the mixing angles $\theta_{12}, \theta_{13}, \theta_{23} \in [0, \pi/2]$ and the CP phase $\delta \in [0, 2\pi)$, the PMNS matrix may also possess two *Majorana phase* degrees of freedom $\alpha_1, \alpha_2 \in [0, 2\pi)$. As the name suggests, these phases are physical only if neutrinos are Majorana, as they can be rotated away in the Dirac case.

The PMNS matrix is measured by oscillation experiments, wherein the oscillation probabilities depend on the mixing angles, the CP phase, and the mass squared differences $\Delta m^2_{ij} \equiv m^2_i - m^2_j$, though not on the Majorana phases [36; 124]. The mass squared differences are important, and are measured to be [152]

$$\Delta m^2_{\text{sol}} = \Delta m^2_{21} \approx 7.5 \times 10^{-5}\,\text{eV}^2 \quad \text{and} \quad |\Delta m^2_{\text{atm}}| \approx 2.5 \times 10^{-3}\,\text{eV}^2. \tag{2.61}$$

The sign of Δm^2_{sol} is known because of the *Mikheyev–Smirnov–Wolfenstein effect* [166; 167]

[4] This is equivalent to replacing $U^\nu \to U^e U^\nu$ and correspondingly redefining $m^\nu \to U^e m^\nu$ (Dirac case) or $m^\nu \to U^e m^\nu U^{eT}$ (Majorana case).

in the sun, which alters the oscillation probabilities as neutrinos travel through the solar matter. The unknown sign of Δm^2_{atm} allows for two possibilities: if it is positive then the neutrino masses follow the **normal ordering** (NO) $m_1 < m_2 < m_3$, and we identify $\Delta m^2_{\text{atm}} > 0$ with Δm^2_{31}. A negative Δm^2_{atm}, on the other hand, implies the **inverted ordering** (IO) $m_3 < m_1 < m_2$, in which case it is identified with Δm^2_{32}. The most recent global fit, NuFit-6.0 [152], reports the values

$$\sin\theta_{12} \approx 0.56, \qquad \sin\theta_{13} \approx 0.15, \quad \text{and} \quad \sin\theta_{23} \approx 0.72, \tag{2.62}$$

with only a slight dependence on the ordering, while the CP phase is consistent with virtually any value at 3σ (though the preferred value is substantially different for NO and IO). This translates roughly to

$$|U| = \begin{pmatrix} |U_{e1}| & |U_{e2}| & |U_{e3}| \\ |U_{\mu 1}| & |U_{\mu 2}| & |U_{\mu 3}| \\ |U_{\tau 1}| & |U_{\tau 2}| & |U_{\tau 3}| \end{pmatrix} \approx \begin{pmatrix} 0.82 & 0.55 & 0.15 \\ 0.4 & 0.6 & 0.71 \\ 0.4 & 0.6 & 0.69 \end{pmatrix}, \tag{2.63}$$

with the understanding that there is considerable variance in the lower-left entries due to the large uncertainty in δ. With the upcoming experiments JUNO [168], DUNE [169], and Hyper-Kamiokande [170] seeking to measure the sign of Δm^2_{atm} and the value of δ with much greater precision, it is expected that we will soon have a much clearer picture of $|U|$.

2.2.1 Mass Models

Now that we have a general understanding of neutrino masses, let us acquaint ourselves with the mass models relevant to this thesis. These are the Type-I and Type-III Seesaw models, to be studied in Chapter 4, and the Zee Model, to be studied in Chapters 6 and 7.

2.2.1.1 Type-I Seesaw

The Type-I Seesaw model [14–18] follows through with the idea of adding RHNs to the SM, extending the SM particle content with n_ν right-handed sterile neutrinos $\nu_{Ri} \sim (1, 1, 0)$.

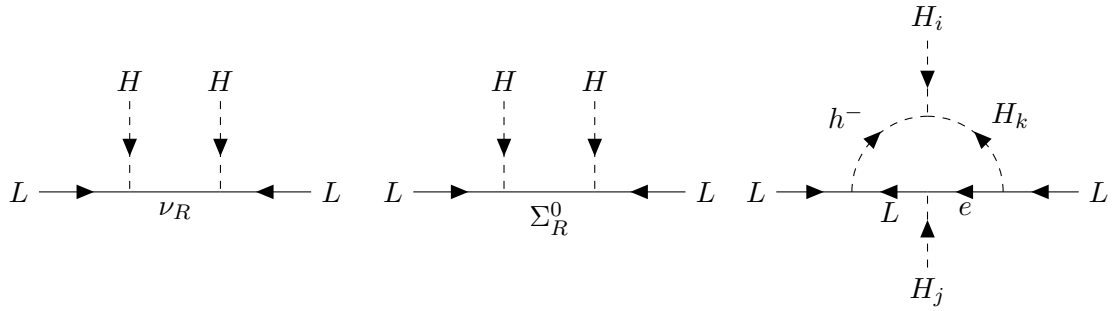

(a) Type-I Seesaw (b) Type-III Seesaw (c) Zee model

Figure 2.2: Neutrino mass diagrams for the three models studied in this thesis.

These sterile neutrinos participate in Yukawa interactions and—as they are not forbidden by any gauge symmetry—additionally possess Majorana masses of their own, with

$$\mathcal{L}_{\nu_R} = \overline{\nu_{Ri}} i\partial\!\!\!/ \nu_{Ri} - \left(Y^\nu_{ij}\overline{L_i}\widetilde{H}\nu_{Rj} + \text{h.c.}\right) - \frac{1}{2}\left(M_{ij}\overline{\nu^c_{Ri}}\nu_{Rj} + \text{h.c.}\right). \tag{2.64}$$

After electroweak symmetry breaking the Dirac and Majorana masses combine into the form

$$\mathcal{L}_{\nu\text{ mass}} = -\frac{1}{2}\begin{pmatrix}\overline{\nu_L} & \overline{\nu^c_R}\end{pmatrix}\begin{pmatrix}0 & m\\ m^T & M\end{pmatrix}\begin{pmatrix}\nu^c_L\\ \nu_R\end{pmatrix} + \text{h.c.}, \tag{2.65}$$

where $m_{ij} \equiv Y^\nu_{ij} v/\sqrt{2}$, and the mass eigenstates are found by diagonalising this combined mass matrix. A $(3+n_\nu)$-by-$(3+n_\nu)$ unitary mixing matrix relates $\begin{pmatrix}\nu^c_L & \nu_R\end{pmatrix}^T$ with the mass eigenstates, which are all generically Majorana, and the PMNS matrix must be identified with the 3-by-3 submatrix connecting ν_{Li} to the first three mass eigenstates. Unitarity of the PMNS matrix is then no longer guaranteed, and PMNS unitarity tests offer a probe of the existence of sterile neutrinos [171; 172].

In the limit that the eigenvalues of M are much larger than the entries of m the mass matrix can be approximately block diagonalised into the form

$$\begin{pmatrix}-mM^{-1}m^T & 0\\ 0 & M\end{pmatrix}, \tag{2.66}$$

resulting in three light neutrinos and n_ν heavy ones. The terminology **seesaw mechanism**

is then ascribed to the observation that as the heavy masses go up, the light masses go down, and vice versa.

2.2.1.2 Type-III Seesaw

The Type-III Seesaw model [28] is very similar to Type-I, with the difference that the fields introduced to fulfil the role of right-handed neutrinos are $\mathrm{SU(2)_W}$ triplets instead of singlets: $\Sigma_{Ri} \sim (1, 3, 0)$. These new fields similarly participate in Yukawa interactions and have Majorana masses of their own, with [173; 174]

$$\mathcal{L}_{\Sigma_R} = \overline{\Sigma_{Ri}} i \not{D} \Sigma_{Ri} - \left(Y^{\Sigma}_{ij} \overline{L_i} \Sigma^a_{Rj} \sigma^a \widetilde{H} + \text{h.c.} \right) - \frac{1}{2} \left(M_{ij} \overline{\Sigma^{ac}_{Ri}} \Sigma^a_{Rj} + \text{h.c.} \right), \tag{2.67}$$

where $a = 1, 2, 3$. For a fixed triplet generation i, the eigenstates of electric charge are given by the combinations

$$\Sigma^{\pm}_{Ri} \equiv \frac{\Sigma^1_{Ri} \mp \mathrm{i}\Sigma^2_{Ri}}{\sqrt{2}} \quad \text{and} \quad \Sigma^0_{Ri} \equiv \Sigma^3_{Ri}. \tag{2.68}$$

The neutral component Σ^0_R couples to neutrinos through the Yukawa interaction, and in a manner completely analogous to Type-I Seesaw we obtain

$$\mathcal{L}_{\nu \text{ mass}} = -\frac{1}{2} \begin{pmatrix} \overline{\nu_L} & \overline{\Sigma^{0c}_R} \end{pmatrix} \begin{pmatrix} 0 & m \\ m^T & M \end{pmatrix} \begin{pmatrix} \nu^c_L \\ \Sigma^0_R \end{pmatrix} + \text{h.c.} \tag{2.69}$$

after electroweak symmetry breaking. The states $\Sigma^{\pm}_{Ri}$ instead mix into the charged leptons, which leads to an enriched phenomenology compared to the Type-I model [173].

2.2.1.3 Zee Model

The Zee Model [23] is an example of a two-Higgs doublet model [175–177], extending the SM with a second Higgs doublet $H_2 \sim (1, 2, 1/2)$ and a charged scalar singlet $h^- \sim (1, 1, -1)$. The new Lagrangian terms relevant to neutrino masses are

$$\mathcal{L} \supset -m_h^2 h^+ h^- + \left(\mu \widetilde{H}_1^\dagger H_2 h^- - \overline{\widetilde{L}} f L h^+ - \overline{L}(Y_1^\dagger H_1 + Y_2^\dagger H_2) e_R + \text{h.c.}\right), \tag{2.70}$$

where I employ a matrix multiplication notation for the coupling matrices Y_1, Y_2 (which are defined with a dagger relative to our SM definition), and f. The second Higgs doublet in principle also couples to the quarks, and the scalar potential is greatly enlarged with interactions such as $|H_1|^2|H_2|^2$, $|H_1^\dagger H_2|^2$, and $|h^-|^2|H_i|^2$.

Though both Higgs doublets can acquire a VEV, it is convenient to rotate to the *Higgs basis* [178; 179] in which $v \approx 246\,\text{GeV}$ is placed in H_1 alone, and Y_1 is real, diagonal, and positive. Due to Fermi statistics the coupling matrix f is necessarily antisymmetric, $f = -f^T$, and moreover it can be taken to be real by simultaneously rephasing L and e_R, so that Y_1 remains unaffected. By rephasing h^- we may also take μ to be real.

Majorana neutrino masses arise in the Zee model at the one-loop level, and in the so-called *decoupling limit* are given by [179; 180]

$$m_{ij}^\nu = -\frac{s_{2\varphi}}{16\pi^2}\frac{v}{\sqrt{2}} \ln\left(\frac{m_{h_2^+}^2}{m_{h_1^+}^2}\right)\left(f Y_1 Y_2 + Y_2^T Y_1^T f^T\right)_{ij}, \tag{2.71}$$

where $h_{1,2}^+$ are mass eigenstates produced by the mixing of h^+ with the charged component of H_2, and

$$s_{2\varphi} = \frac{\sqrt{2} v \mu}{m_{h_2^+}^2 - m_{h_1^+}^2}. \tag{2.72}$$

Here the decoupling limit refers to the limit in which the CP-conserving neutral components of H_1 and H_2 do not mix, resulting in an SM-like Higgs boson h [178; 179].

We note that lepton number is violated in the Zee model by the peculiar $\overline{\widetilde{L}} L h^+$ interaction. One may attempt to enlarge the symmetry by assigning 2 units of lepton number to h^-, in which case it is then violated by the equally peculiar $\widetilde{H}_1^\dagger H_2 h^-$ interaction. It is therefore unsurprising that the Majorana mass matrix is proportional to both μ and f.

The most conservative form of the Zee model is the Zee-Wolfenstein realisation [23; 181], in which a $\mathbb{Z}_2$ symmetry is imposed onto H_2 as to forbid the appearance of the second Yukawa interaction Y_2. Though this realisation has been ruled out [182; 183], the more general Zee model remains viable [179; 184].

What if a particle is heavier than 1 TeV?
We ask it politely, yet firmly, to leave.

Bobby and *Hank Hill*,
in *King of the Hill*,
reimagined

3

Theory: Effective Field Theories

Contents

3.1 Constructing an EFT **32**

3.2 SMEFT **37**

3.3 LEFT **46**

The general success of the Standard Model and the persistent non-observation of clear signals of new physics (for instance, in searches by the ATLAS [55–60] and CMS [61–65] experiments) indicates that new particles, if they exist, must be either very heavy ($M \gtrsim 1\,\text{TeV}$) or very weakly coupled to the SM. If the former is the case then there is a considerable gap between the electroweak scale $v \approx 246\,\text{GeV}$ and the scale $\Lambda = M$ of new physics, and it should be possible to express the effect of such new physics as a well-

defined expansion in powers of v/Λ and p^2/Λ^2. A powerful technique for systematically constructing such an expansion is found in the framework of **effective field theories** (EFTs), which is the topic of this chapter.

What follows is a review of well-known concepts and materials that largely cannot be considered original. A partial exception to this is Section 3.2.1 on parameter shifts,[1] which resulted from considerable toil on my part towards understanding some seemingly-arcane formulas presented in the literature (such as in Ref. [86]). Evidently the material of that section is well-known by the wider community, and indeed a well-presented exposition can be found in Ref. [185, Sec. 4] and references therein, though I regrettably only discovered it while editing this chapter.

Excellent general references for effective field theories are Refs. [186–188], while the recent review of Ref. [189] additionally provides a comprehensive coverage of Standard Model Effective Field Theory (SMEFT). Good supplementary references for SMEFT are Refs. [185; 190–192].

3.1 Constructing an EFT

Suppose we have a theory in which we can separate the field content into 'light' fields ϕ_i and 'heavy' fields Φ_i, and the Lagrangian into

$$\mathcal{L}(\phi_i, \Phi_i) = \mathcal{L}_{\text{IR}}(\phi_i) + \mathcal{L}_{\text{UV}}(\phi_i, \Phi_i). \tag{3.1}$$

An EFT for this theory is one containing only the light fields ϕ_i, with

$$\mathcal{L}_{\text{eff}}(\phi_i) = \mathcal{L}_{\text{IR}}(\phi_i) + \sum_n C_n \mathcal{O}_n, \tag{3.2}$$

where the **effective operators** $\mathcal{O}_n = \mathcal{O}_n(\phi_i)$ and **Wilson coefficients** C_n capture the

[1] This section is adapted from the appendix of the publication *Riding the Seesaw: What Higgsstrahlung May Reveal about Massive Neutrinos* [1], of which the main content forms the next chapter.

influence of the heavy fields. Formally these two theories are related through the path integral representation

$$\int \mathcal{D}\phi_i \, \exp\left(\mathrm{i}\int \mathrm{d}^4x \, \mathcal{L}_{\text{eff}}\right) = \int \mathcal{D}\phi_i \mathcal{D}\Phi_i \, \exp\left(\mathrm{i}\int \mathrm{d}^4x \, \mathcal{L}\right), \tag{3.3}$$

and the heavy fields are therefore said to have been *integrated out*. To compute $\mathcal{L}_{\text{eff}}$ there are two main methods available to us: functional and diagrammatic matching. The functional approach requires carefully carrying out integral in Eq. (3.3) [193–197], while the diagrammatic one involves drawing all possible diagrams in the full and effective theories and insisting they agree, or rather, *match*, when computing physical observables. As it is more readily interpretable and we are not too concerned with the finer details of the procedure, we will restrict our attention to diagrammatic matching.

EXAMPLE

To motivate a discussion of general features of EFTs it is helpful to study a simple matching calculation. Our chosen example is the archetypal *4-Fermi theory*, where the W boson is integrated out from the SM to obtain effective four-fermion interactions. To this end, let us consider the representative scattering process $\mu^-\bar{\nu}_\mu \to e^-\bar{\nu}_e$, which in the SM is due to the interactions

$$\mathcal{L}_{\text{UV}} \supset \frac{g_2}{\sqrt{2}}\left(\overline{\nu_\mu}\not{W}^+ P_L\mu + \bar{e}\not{W}^- P_L\nu_e\right) + \text{h.c.} \tag{3.4}$$

and looks like

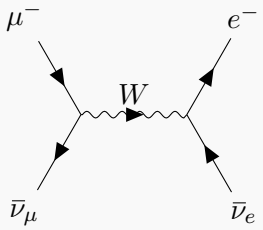

$$= -\frac{g_2^2}{2}(\overline{v_{\nu_\mu}}\gamma^\alpha P_L u_\mu)\frac{-\mathrm{i}g_{\alpha\beta}}{p^2 - m_W^2}(\overline{u_e}\gamma^\beta P_L v_{\nu_e}). \tag{3.5}$$

In an EFT without the W boson this process must instead originate from interactions such as

$$\mathcal{L}_{\text{eff}} \supset C_F(\overline{\nu_\mu}\gamma_\alpha P_L\mu)(\bar{e}\gamma^\alpha P_L\nu_e) + \text{h.c.}, \tag{3.6}$$

where it then takes the form

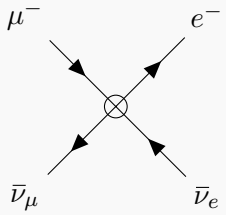

$$= \mathrm{i}C_F(\overline{v_{\nu_\mu}}\gamma^\alpha P_L u_\mu)(\overline{u_e}\gamma_\alpha P_L v_{\nu_e}). \tag{3.7}$$

Here and in the future we use a crossed dot to denote an effective vertex. To match Eq. (3.7) onto Eq. (3.5) we make the important observation that the effective theory can only stand a chance of reproducing the predictions of the full theory at energies below the mass of the W boson, since at higher energies it is possible to create physical W particles, which the EFT is incapable of describing. We must therefore restrict ourselves to $p^2 < m_W^2$, which licenses us to expand the W propagator in the full theory as

$$\frac{1}{p^2 - m_W^2} = -\frac{1}{m_W^2}\left(1 + \frac{p^2}{m_W^2} + \frac{p^4}{m_W^4} + \dots\right). \tag{3.8}$$

The lowest-order term is reproduced by our effective operator if we set its Wilson coefficient to

$$C_F = -\frac{g_2^2}{2m_W^2} \equiv -\frac{4G_F}{\sqrt{2}}, \tag{3.9}$$

where

$$G_F \equiv \frac{\sqrt{2}g_2^2}{8m_W^2} = \frac{1}{\sqrt{2}v^2} \tag{3.10}$$

is the famous **Fermi constant**. The higher-order terms in the expansion match onto the infinite tower of operators

$$\mathcal{O}_{\Box^n} = (\overline{\nu_\mu}\gamma_\alpha P_L \mu)\Box^n(\bar{e}\gamma^\alpha P_L \nu_e), \tag{3.11}$$

and the corresponding Wilson coefficients are evidently suppressed by additional

powers of $1/m_W^2$. Correctly treating the W boson propagator in unitary gauge, which requires replacing $g_{\alpha\beta} \to g_{\alpha\beta} - p_\alpha p_\beta / m_W^2$, similarly leads to the generation of additional subdominant operators.

So far we have considered only tree-level diagrams, and we have therefore performed what is known as *tree-level matching*. A more accurate matching calculation will seek to match the effective theory to the full theory at the loop level in what is called *one-loop matching*, *two-loop matching*, and so on. Though loop-level matching is naturally more involved, the general procedure is in essence identical to the one we just undertook.

One might wonder why we bother with EFTs, as in the above example we appear to have exchanged two interaction terms for infinitely many – an infinite increase in complexity! However, our example also makes clear that in practice we will only need to consider finitely many effective operators to achieve a reasonably accurate result, provided of course that the relevant physical scales are sufficiently separated from the heavy scales. Muon decay $\mu^- \to e^- \bar{\nu}_e \nu_\mu$, for instance, is described rather accurately by the single operator in Eq. (3.6), as there $p^2 < m_\mu^2 \ll m_W^2$.

In a general EFT we can usually assess the importance of an operator by its **mass dimension**. The mass dimension of an object refers to its units as a power of mass (or equivalently energy), and is denoted with square brackets – for example,

$$[E] = [m] = 1, \qquad [x_\mu] = -1, \quad \text{and} \quad [p_\mu] = [\partial_\mu] = 1. \tag{3.12}$$

In d-dimensional spacetime the mass dimension of a Lagrangian is $[\mathcal{L}] = d$, which implies that in four dimensions the mass dimension of bosonic and fermionic fields are respectively

$$[\phi] = [A_\mu] = 1 \quad \text{and} \quad [\psi] = \frac{3}{2}. \tag{3.13}$$

From this we can deduce that our effective operators have dimension

$$[(\overline{\nu_\mu}\gamma_\alpha P_L\mu)(\overline{e}\gamma^\alpha P_L\nu_e)] = 6 \quad \text{and} \tag{3.14a}$$
$$[(\overline{\nu_\mu}\gamma_\alpha P_L\mu)\Box^n(\overline{e}\gamma^\alpha P_L\nu_e)] = 6 + 2n, \tag{3.14b}$$

and to ensure $[\mathcal{L}] = 4$ their respective Wilson coefficients must in turn have

$$[C_F] = -2 \quad \text{and} \quad [C_{\Box^n}] = -2 - 2n; \tag{3.15}$$

indeed,

$$C_F \propto \frac{1}{m_W^2} \quad \text{and} \quad C_{\Box^n} \propto \frac{1}{m_W^{2+2n}}. \tag{3.16}$$

Thus, higher-dimensional operators are generically suppressed by higher powers of a heavy mass scale. It is common in the literature to make this suppression explicit by extracting this scale from the Wilson coefficients and writing

$$\mathcal{L}_{\text{eff}} = \mathcal{L}_{\text{IR}} + \sum_n \frac{C_n}{\Lambda^{[\mathcal{O}_n]-4}}\mathcal{O}_n, \tag{3.17}$$

though we will not adopt this convention. In any case, it is often sufficient in EFT studies to limit one's attention to the lowest-dimensional effective operators.

A noteworthy feature of operators with $[\mathcal{O}] > 4$ is that they are *non-renormalizable*, which means that an infinite number of counterterms—and therefore parameters—are required to remove all divergences in a theory with such operators present. While this would be problematic for a theory that purports to be fundamental, it is of no concern for an EFT, where infinitely-many operators are already expected. In practice, one deals with the non-renormalizability of an EFT by truncating a given computation to a fixed order in $1/\Lambda$, such that higher-order divergences and counterterms are ignored.

Lastly, it is worth remarking that a given collection of operators $\{\mathcal{O}_n\}$ may be *redundant* in the sense that some operators—after possible application of Fierz identities, field redefinitions, or integration by parts—can be realised as linear combinations of others – for example [198],

$$(\overline{L}_i\gamma_\mu\sigma^a L_j)(\overline{L}_k\gamma^\mu\sigma^a L_l) = 2(\overline{L}_i\gamma_\mu L_l)(\overline{L}_k\gamma^\mu\overline{L}_j) - (\overline{L}_i\gamma_\mu L_j)(\overline{L}_k\gamma^\mu L_l). \tag{3.18}$$

To avoid double-counting contributions to physical observables it is desirable to work in terms of a non-redundant operator basis. Fortunately, such a basis is known at dimension-six for the EFTs considered in the next two sections [198; 199], so we will not need to worry about this complication.

3.2 SMEFT

As indicated at the start of this chapter, there is convincing evidence that the SM should be viewed as the low-energy remnant of a more fundamental theory, with a considerable gap between the largest SM scale v and the scale Λ of new physics. This motivates the use of an EFT approach to study such new physics, canonised as **Standard Model Effective Field Theory** (SMEFT):

$$\mathcal{L}_{\text{SMEFT}} = \mathcal{L}_{\text{SM}} + \sum_n C_n\mathcal{O}_n. \tag{3.19}$$

Per our discussion above, we are most interested in the lowest-dimensional effective operators, meaning dimension-five and -six. At dimension-five there is a single unique operator compatible with the SM gauge group (up to a Hermitian conjugate) – the *Weinberg operator* [156]

$$\mathcal{O}_{5,ij} = (\overline{L_i}\widetilde{H})(\widetilde{H}^T L_j^c). \tag{3.20}$$

We encountered this operator in the previous chapter, where we saw that, if present, it generates Majorana masses for neutrinos after electroweak symmetry breaking. At dimension-six there are 63 additional operators (or 59 if we disallow baryon number violation), and the most popular non-redundant basis for them is the so-called *Warsaw Basis* [198]. A handful of Warsaw basis operators are presented in Table 3.1.

$\mathcal{O}_{HW}$	$(H^\dagger H)W^a_{\mu\nu}W^{a\mu\nu}$	$\mathcal{O}_{eH,ij}$	$(H^\dagger H)(\overline{L_i}He_{Rj})$
$\mathcal{O}_{HB}$	$(H^\dagger H)B_{\mu\nu}B^{\mu\nu}$	$\mathcal{O}_{He,ij}$	$(H^\dagger \mathrm{i}\overleftrightarrow{D}_\mu H)(\overline{e_{Ri}}\gamma^\mu e_{Rj})$
$\mathcal{O}_{HWB}$	$(H^\dagger\sigma^a H)W^a_{\mu\nu}B^{\mu\nu}$	$\mathcal{O}^{(1)}_{HL,ij}$	$(H^\dagger \mathrm{i}\overleftrightarrow{D}_\mu H)(\overline{L_i}\gamma^\mu L_j)$
$\mathcal{O}_{eW,ij}$	$(\overline{L_i}\sigma^{\mu\nu}\sigma^a e_{Rj})HW^a_{\mu\nu}$	$\mathcal{O}^{(3)}_{HL,ij}$	$(H^\dagger \mathrm{i}\overleftrightarrow{D}^a_\mu H)(\overline{L_i}\sigma^a\gamma^\mu L_j)$
$\mathcal{O}_{eB,ij}$	$(\overline{L_i}\sigma^{\mu\nu}e_{Rj})HB_{\mu\nu}$	$\mathcal{O}_{LL,ijkl}$	$(\overline{L_i}\gamma_\mu L_j)(\overline{L_k}\gamma^\mu L_l)$

$\mathcal{O}_H$	$(H^\dagger H)^3$
$\mathcal{O}_{H\Box}$	$(H^\dagger H)\Box(H^\dagger H)$
$\mathcal{O}_{HD}$	$(H^\dagger D_\mu H)^*(H^\dagger D^\mu H)$

Table 3.1: The dimension-six SMEFT operators in the Warsaw basis most relevant to this thesis. Here $\sigma^{\mu\nu} \equiv \frac{\mathrm{i}}{2}[\gamma^\mu, \gamma^\nu]$ and $H^\dagger \mathrm{i}\overleftrightarrow{D}^a_\mu H \equiv \mathrm{i}H^\dagger\sigma^a D_\mu H - \mathrm{i}(D_\mu H)^\dagger\sigma^a H$.

The great advantage offered by SMEFT is that it provides a model-agnostic means of performing phenomenological analyses. With it one can work out the physics once and for all as a function of the Wilson coefficients, and then the study of a particular BSM model becomes nearly as simple as matching onto SMEFT. With the advent of software packages such as `DsixTools` [200; 201], `wilson` [202], `SMEFTsim` [185; 203], `SmeftFR` [204–206], `MatchMakerEFT` [207], and `Matchete` [197] automating much of the required work, this procedure is becoming increasingly painless with time. In principle, one could even conceive of a global fit of the SMEFT parameters to all available experimental data, but this is infeasible: at dimension-six there are 3045 such parameters (or 2499 if we restrict to baryon number-conserving operators) [190; 199; 201] – far too many to optimise over. Though this number can be reduced by assuming the SMEFT Wilson coefficients obey certain flavour symmetries, it nonetheless remains prohibitively large [185].

Of course, SMEFT is not a silver bullet for all our BSM needs, as the load-bearing assumption that all new fields are heavy is not borne out by all BSM models. To carry out an EFT analysis in such models it is necessary to work with an expanded operator basis constructed from SM fields and the new light fields, such as in νSMEFT [208; 209] or the *Dark Matter SMEFT* (DSMEFT) of Ref. [210]. We will not pursue this.

3.2.1 Parameter Shifts in SMEFT

An important but oft-overlooked effect of BSM physics is that it alters the relationship between measured quantities and SM parameters, most often due to new loop contributions from new particles. This means that the extraction of SM parameters from such quantities should be modified, resulting in shifts to these parameters which then cascades to shifts in all SM predictions. One might imagine accounting for these shifts in a given BSM model to be a rather laborious task. Fortunately, we can systematically treat this effect in SMEFT.

Such a treatment requires that we distinguish two conceptually different contributions from effective operators. The first type of contribution occurs at the Lagrangian level due to operators featuring the Higgs field H. After electroweak symmetry breaking these operators will contribute to the SM part of the SMEFT Lagrangian – for instance,

$$\mathcal{O}_{eH,ij} = (H^\dagger H)(\overline{L_i} H e_{Rj}) \supset \frac{v^2}{2}(\overline{L_i} H e_{Rj}) \tag{3.21}$$

will directly add to the SM Yukawa interaction $-Y^e_{ij}\overline{L_i} H e_{Rj}$, resulting in an effective Yukawa matrix

$$\bar{Y}^e_{ij} \equiv Y^e_{ij} - \frac{v^2}{2} C_{eH,ij}. \tag{3.22}$$

The second type of contribution concerns the extraction of parameters from data, and is dependent on one's *input scheme*. An input scheme refers to a choice of *input parameters*, and is necessary because many SM parameters are related algebraically. Of particular relevance to us, the electroweak sector admits four independent parameters which we can understand as originating from the gauge couplings g_1, g_2 and the Higgs' self-couplings μ, λ, though we often interface with many derived parameters such as m_W, m_Z, m_h, v, G_F, e, and $\sin^2\theta_w$. In practice the (α, m_Z, G_F, m_h)[2] and (m_W, m_Z, G_F, m_h) schemes are the most commonly used, as these parameters are precisely measured and relatively unaffected in SMEFT [211; 212]. I will opt to use the former scheme, abbreviated as (α, m_Z, G_F), for

[2]Here $\alpha = e^2/4\pi$ is the electromagnetic fine structure constant.

the remainder of this thesis.

Let us now investigate these two contributions to the parameter shifts in detail. Our goal is to obtain an expression for the shift in an observable,

$$\Delta\sigma = \sigma_{\text{SMEFT}} - \sigma_{\text{SM}}, \tag{3.23}$$

due to these parameter shifts. In what follows we will work to leading order in $(v/\Lambda)^2$, where we recall that a factor of $1/\Lambda^2$ is implicit in every dimension-six Wilson coefficient.

Part 1: Effective Parameters The first step in this analysis is to examine how the SM Lagrangian is altered after electroweak symmetry breaking by the presence of operators featuring H. Such an examination can be found for instance in Refs. [185; 189–192]; here I will summarise only the salient points.

To start, the operator $\mathcal{O}_H = (H^\dagger H)^3$ changes the shape of the Higgs' potential, resulting in the VEV taking on the 'true' value

$$v_T = \left(1 + \frac{3v^2}{4\lambda} C_H\right) v. \tag{3.24}$$

Next, the operators $\mathcal{O}_{HW}, \mathcal{O}_{HB}, \mathcal{O}_{H\Box}$, and $\mathcal{O}_{HD}$ contribute to the kinetic terms of the gauge fields and the Higgs boson, which must be redefined to

$$W_\mu^a \to \left(1 + v_T^2 C_{HW}\right) W_\mu^a, \tag{3.25a}$$

$$B_\mu \to \left(1 + v_T^2 C_{HB}\right) B_\mu, \quad \text{and} \tag{3.25b}$$

$$h \to \left(1 + v_T^2 C_{H\Box} - \frac{1}{4} v_T^2 C_{HD}\right) h \tag{3.25c}$$

to ensure they remain correctly normalised. (In these expressions we may interchange v and v_T freely since the difference is second-order in $(v/\Lambda)^2$.) While the factors in the redefinition of h are then carried to every interaction of it with other fields, the gauge boson factors can be absorbed by correspondingly redefining the gauge couplings to

$$g_2 \to \Big(1 - v_T^2 C_{HW}\Big) g_2 \quad \text{and} \quad g_1 \to \Big(1 - v_T^2 C_{HB}\Big) g_1. \tag{3.26}$$

Finally, the operator $\mathcal{O}_{HWB}$ introduces additional mixing between the mass eigenstates Z_μ and A_μ, which must then be re-diagonalised.

Once these redefinitions have been carried out and the dust has settled it is convenient to introduce a barred notation, $\bar{g}$, for effective parameters that appear in place of their unbarred form in the SMEFT Lagrangian. For example, the Z boson part of the gauge-covariant derivative, which in the SM reads

$$D_\mu \supset -i g_Z (T^3 - Q s_w^2) Z_\mu, \tag{3.27}$$

(where we abbreviate $s_w^2 \equiv \sin^2\theta_w$,) becomes in SMEFT

$$D_\mu \supset -i \bar{g}_Z (T^3 - Q \bar{s}_w^2) Z_\mu, \tag{3.28}$$

where

$$\bar{g}_Z = \sqrt{g_1^2 + g_2^2}\left(1 + \frac{g_1 g_2}{g_1^2 + g_2^2} v_T^2 C_{HWB}\right) \quad \text{and} \tag{3.29a}$$

$$\bar{s}_w^2 = \frac{g_1^2}{g_1^2 + g_2^2}\left(1 - \frac{g_2}{g_1}\frac{g_1^2 - g_2^2}{g_1^2 + g_2^2} v_T^2 C_{HWB}\right). \tag{3.29b}$$

To denote the shifts of these parameters from their SM expressions we write

$$\bar{g}_Z = g_Z + \delta\bar{g}_Z \qquad \text{where} \qquad \frac{\delta\bar{g}_Z}{g_Z} = \frac{g_1 g_2}{g_1^2 + g_2^2} v_T^2 C_{HWB}, \quad \text{and} \tag{3.30a}$$

$$\bar{s}_w^2 = s_w^2 + \delta\bar{s}_w^2 \qquad \text{where} \qquad \frac{\delta\bar{s}_w^2}{s_w^2} = -\frac{g_2}{g_1}\frac{g_1^2 - g_2^2}{g_1^2 + g_2^2} v_T^2 C_{HWB}. \tag{3.30b}$$

Note that $\delta\bar{g}_Z/g_Z = \delta\bar{g}_Z/\bar{g}_Z$ at order $(v/\Lambda)^2$ (and similarly so for every other parameter); I will consistently opt to write the former.

To reiterate the notation and have a referenceable equation, the shift for a general parameter g is written

Symbol	Relation	Meaning
g, α	—	Original SM parameter appearing in $\mathcal{L}_{\text{SM}}$
$\bar{g}, \bar{\alpha}$	$\bar{g} = g + \delta\bar{g}$	A 'true' parameter appearing in place of g in $\mathcal{L}_{\text{SMEFT}}$
$\hat{\alpha}$	$\hat{\alpha} = \alpha + \delta\bar{\alpha} + \delta\hat{\alpha}$	Input parameter
$\hat{g}$	$\hat{g} = g + \delta\hat{g}$	Parameter computed from the input parameters

Table 3.2: Summary of notation used for the different types of parameters.

$$\bar{g} = g + \delta\bar{g}. \tag{3.31}$$

There is one exception to this notational rule in v_T, which should be written $\bar{v}$ for consistency, but isn't by convention. In this case we have $v_T = v + \delta\bar{v}$.

Part 2: Input Parameters Let us refer to our chosen input parameters with the symbol α, and use a hat to denote the measured value of these parameters, $\hat{\alpha}$. It is possible for $\hat{\alpha}$ to differ from the Lagrangian value $\bar{\alpha}$ due to the contribution of new diagrams to the process through which α is measured; labelling this additional shift $\delta\hat{\alpha}$, we have

$$\hat{\alpha} = \bar{\alpha} + \delta\hat{\alpha} = \alpha + \delta\bar{\alpha} + \delta\hat{\alpha}. \tag{3.32}$$

Such diagrams typically arise at the loop order or at $\mathcal{O}((v/\Lambda)^4)$, which we neglect, therefore leaving $\delta\hat{\alpha} = 0$. The sole exception to this is the Fermi constant, which acquires tree-level contributions to $\delta\hat{G}_F$ from the diagrams in Fig. 3.1, giving

$$\delta\hat{G}_F = \frac{1}{\sqrt{2}}\left(C^{(3)}_{HL,11} + C^{(3)}_{HL,22}\right) - \frac{1}{2\sqrt{2}}(C_{LL,1221} + C_{LL,2112}). \tag{3.33}$$

For a parameter computed from the input parameters using the tree-level SM relations we will also use a hat: $\hat{g} \equiv g(\hat{\alpha}_i)$. (One simple example would be computing the elementary charge from the measured value of the fine structure constant via $\hat{e} = \sqrt{4\pi\hat{\alpha}}$.) For these parameters we instead have

$$\hat{g} = g + \sum_i \frac{\partial g}{\partial \alpha_i}(\delta\bar{\alpha}_i + \delta\hat{\alpha}_i) \equiv g + \delta\hat{g}. \tag{3.34}$$

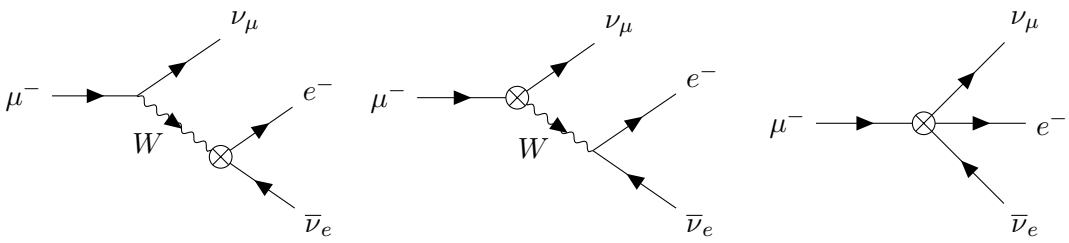

Figure 3.1: The Fermi constant is obtained from measurements of the muon lifetime. Pictured are muon decay diagrams with the effective operators contributing to $\delta\hat{G}_F$.

By combining Eqs. (3.31) and (3.34) we see that

$$\begin{aligned} \bar{g} &= \hat{g} + \delta\bar{g} - \delta\hat{g} \\ &\equiv \hat{g} + \delta g, \end{aligned} \tag{3.35}$$

and as will soon become apparent, we are most interested in this total shift,

$$\delta g \equiv \delta\bar{g} - \delta\hat{g} = \delta\bar{g} - \sum_i \frac{\partial g}{\partial \alpha_i}(\delta\bar{\alpha}_i + \delta\hat{\alpha}_i). \tag{3.36}$$

Example

To make this less abstract, let's work out the shift in g_{ZZh}, which appears in the SM Lagrangian as

$$\mathcal{L}_{\text{SM}} \supset \frac{1}{4} g_Z^2 v Z_\mu Z^\mu h \equiv \frac{1}{2} g_{ZZh} Z_\mu Z^\mu h. \tag{3.37}$$

In SMEFT this becomes

$$\mathcal{L} \supset \frac{1}{4}\bar{g}_Z^2 v_T Z_\mu Z^\mu \left(1 + v_T^2 C_{H\Box} - \frac{1}{4} v_T^2 C_{HD}\right) h + C_{HD} \frac{1}{2} g_Z^2 v_T^3 Z_\mu Z^\mu h \tag{3.38}$$

$$= \frac{1}{4} g_Z^2 v \left(1 + 2\frac{\delta\bar{g}_Z}{g_Z} + \frac{\delta\bar{v}}{v} + v_T^2 C_{H\Box} + \frac{3}{4} v_T^2 C_{HD}\right) Z_\mu Z^\mu h \tag{3.39}$$

$$\equiv \frac{1}{2}\bar{g}_{ZZh} Z_\mu Z^\mu h, \tag{3.40}$$

where $\mathcal{O}_{HD}$ directly contributes a new $Z_\mu Z^\mu h$ term, and we recall from Eq. (3.25c) that h is redefined with a new normalisation. From this we can read off

$$\frac{\delta\bar{g}_{ZZh}}{g_{ZZh}} = 2\frac{\delta\bar{g}_Z}{g_Z} + \frac{\delta\bar{v}}{v} + v_T^2 C_{H\Box} + \frac{3}{4}v_T^2 C_{HD} \tag{3.41}$$

$$= 2c_w s_w v_T^2 C_{HWB} + v_T^2 C_{H\Box} + \frac{3}{4}v_T^2 C_{HD} + \frac{\delta\bar{v}}{v}. \tag{3.42}$$

The $\delta\hat{g}_{ZZh}$ part of the full shift depends on one's choice of input parameters; in the (α, m_Z, G_F) scheme one has

$$\hat{g}_{ZZh} = 2^{5/4}\hat{m}_Z^2\sqrt{\hat{G}_F}, \tag{3.43}$$

which is a tree-level relation valid in the SM. In accordance with Eq. (3.34) we then have

$$\frac{\delta\hat{g}_{ZZh}}{g_{ZZh}} = \left(\frac{\delta\bar{m}_Z^2}{m_Z^2} + \frac{\delta\hat{m}_Z^2}{m_Z^2}\right) + \frac{1}{2}\left(\frac{\delta\bar{G}_F}{G_F} + \frac{\delta\hat{G}_F}{G_F}\right). \tag{3.44}$$

Plugging in the known shifts[3]

$$\frac{\delta\bar{m}_Z^2}{m_Z^2} = \frac{1}{2}v_T^2 C_{HD} + 2c_w s_w v_T^2 C_{HWB} + 2\frac{\delta\bar{v}}{v}, \qquad \frac{\delta\hat{m}_Z^2}{m_Z^2} = 0, \qquad \frac{\delta\bar{G}_F}{G_F} = -2\frac{\delta\bar{v}}{v}, \tag{3.45}$$

and leaving $\delta\hat{G}_F/G_F$ symbolic as it has the cumbersome expression of Eq. (3.33), this evaluates to

$$\frac{\delta\hat{g}_{ZZh}}{g_{ZZh}} = \frac{1}{2}v_T^2 C_{HD} + 2c_w s_w v_T^2 C_{HWB} + \frac{\delta\bar{v}}{v} + \frac{1}{2}\frac{\delta\hat{G}_F}{G_F}. \tag{3.46}$$

Lastly, we bring it all together as per Eq. (3.36) to obtain

[3]One arrives at the shift $\delta\bar{G}_F$ by writing

$$\bar{G}_F = \frac{1}{\sqrt{2}v_T^2} = \frac{1}{\sqrt{2}v^2}\left(1 - 2\frac{\delta\bar{v}}{v}\right).$$

$\delta\bar{m}_Z$ is more involved, as $\bar{m}_Z^2$ additionally receives a direct contribution from $\mathcal{O}_{HD}$ and an indirect contribution from $\mathcal{O}_{HWB}$ due to the rediagonalisation of Z_μ and A_μ. Lastly, $\delta\hat{m}_Z$ is zero as there are no tree-level diagrams at order $(v/\Lambda)^2$ which contribute to the Z boson's self energy.

$$\frac{\delta g_{ZZh}}{g_{ZZh}} = \frac{\delta \bar{g}_{ZZh}}{g_{ZZh}} - \frac{\delta \hat{g}_{ZZh}}{g_{ZZh}} \tag{3.47}$$

$$= v_T^2 C_{H\Box} + \frac{1}{4} v_T^2 C_{HD} - \frac{1}{2} \frac{\delta \hat{G}_F}{G_F}$$

$$= v_T^2 \left(C_{H\Box} + \frac{1}{4} C_{HD} - \frac{1}{\sqrt{2}} \delta \hat{G}_F \right). \tag{3.48}$$

Note that the dependence on $\delta \bar{v}$ completely cancels. This is a general trend for all shifts relevant to this thesis – thus, for our purposes, the replacement $v \to v_T$ is functionally unphysical.

Part 3: Shifts in Observables We now come to the climax of this exposition. Suppose that SMEFT represents the 'true' theory, and that we wish to compute the correction to a quantity such as a cross section which has been calculated under the mistaken assumption that the SM was the correct theory: $\Delta\sigma = \sigma_{\text{SMEFT}} - \sigma_{\text{SM}}$. In addition to direct contributions from new operators, there will be an indirect contribution from the shifts of the SM parameters.

To arrive at this conclusion carefully, convince yourself that the correct cross section should be written in terms of the barred parameters, $\sigma(\bar{\alpha}_i, \bar{g}_j)$, as—after all—these parameters are the ones extant in the 'true' Lagrangian. In the SM, however, the distinction between g, $\bar{g}$, and $\hat{g}$ is meaningless,[4] and one computes the cross section simply as a function of the measured parameters, $\sigma(\hat{\alpha}_i, \hat{g}_j)$. Explicitly,

$$\sigma_{\text{SMEFT}} = \sigma(\bar{\alpha}_i, \bar{g}_j) + \Delta\sigma_{\text{Direct}} \quad \text{and} \quad \sigma_{\text{SM}} = \sigma(\hat{\alpha}_i, \hat{g}_j), \tag{3.49}$$

and so

[4] Actually, it's not strictly true that $\hat{g}_i = g_i$, as there will be loop effects contributing to the screening of g_i even in the SM. This is however a separate shift to the one under consideration and it can be independently dealt with, so we do not treat it here.

$$\Delta\sigma = \Delta\sigma_{\text{Direct}} + \sigma(\bar{\alpha}_i, \bar{g}_j) - \sigma(\hat{\alpha}_i, \hat{g}_j) \tag{3.50}$$

$$= \Delta\sigma_{\text{Direct}} + \sum_i \frac{\partial\sigma}{\partial\alpha_i}(\bar{\alpha}_i - \hat{\alpha}_i) + \sum_j \frac{\partial\sigma}{\partial g_j}(\bar{g}_j - \hat{g}_j), \tag{3.51}$$

or

$$\Delta\sigma = \Delta\sigma_{\text{Direct}} - \sum_i \frac{\partial\sigma}{\partial\alpha_i}\delta\hat{\alpha}_i + \sum_j \frac{\partial\sigma}{\partial g_j}\delta g_j. \tag{3.52}$$

It is worth emphasising that Eq. (3.52) applies only when computing a correction to an SM prediction, which we do in Sections 4.3.1 and 4.3.2 of the next chapter. However, as in Sections 4.3.3 and 4.3.4, it does *not* apply when one is only interested in the SMEFT prediction, σ_{SMEFT}.

3.3 LEFT

To describe processes at energies significantly below the electroweak scale—and more pertinently, new physics contributions to these processes—it is better to use an EFT in which the heavy W, Z, and h bosons, as well as the top quark t, have additionally been integrated out. Such an EFT is known as **Low-energy Effective Field Theory** (LEFT) or **Weak Effective Theory**. The operative symmetry in LEFT is $\text{SU}(3)_\text{C} \times \text{U}(1)_\text{EM}$, and the standard operator basis is the *Jenkins–Manohar–Stoffer* (JMS), or *San Diego basis* [199]. The JMS basis consists of the dimension-three operator

$$\mathcal{O}_{\nu,ij} = \overline{\nu^c_{Li}}\nu_{Lj}, \tag{3.53}$$

which is a Majorana mass for ν_L; six dimension-five operators such as

$$\mathcal{O}_{e\gamma,ij} = (\overline{e_i}\sigma^{\mu\nu}P_R e_j)F_{\mu\nu}, \tag{3.54}$$

known as *dipole operators*; and 89 dimension-six operators such as

$$\mathcal{O}^{V,LL}_{\nu e,ijkl} = (\overline{\nu_i}\gamma_\mu P_L \nu_j)(\overline{e_k}\gamma^\mu P_L e_l), \tag{3.55}$$

which generalises the operator $\mathcal{O}_F$ used in the 4-Fermi example earlier in this chapter.[5]

As the masses of the heavy particles W, Z, h, and t are all proportional to v we generically expect the Wilson coefficients to scale with v, with for instance $C \propto 1/v^2$ for the dimension-six coefficients. When LEFT is matched to SMEFT, however, it will inherit the scaling against the new physics scale Λ from the SMEFT Wilson coefficients. For example, tree-level matching onto $\mathcal{O}^{V,LL}_{\nu e}$ reads [199]

$$C^{V,LL}_{\nu e,ijkl} = -\frac{2}{v_T^2}\left(\delta_{il} + v_T^2 C^{(3)}_{HL,il}\right)\left(\delta_{jk} + v_T^2 C^{(3)*}_{HL,jk}\right) + C_{LL,ijkl} + C_{LL,lkji} + \dots \tag{3.56}$$

$$= -\frac{2}{v_T^2}\delta_{il}\delta_{jk} - 2\delta_{il}C^{(3)*}_{HL,jk} - 2\delta_{jk}C^{(3)}_{HL,il} + C_{LL,ijkl} + C_{LL,lkji} + \dots . \tag{3.57}$$

The first term reproduces the 4-Fermi result, Eq. (3.9), and exhibits the expected $1/v^2$ scaling, while the remaining terms shown all scale instead as $1/\Lambda^2$.

To match a BSM model onto LEFT it is typical to first match the model onto SMEFT and then match SMEFT onto LEFT; in this way we can reuse known matching results without needing to perform additional work. Doing this correctly however requires that we match onto SMEFT at the high scale $\mu \sim \Lambda$ and run the SMEFT parameters down to the scale $\mu \sim m_Z$ before matching to LEFT. Fortunately for the practising researcher, the public codes `DsixTools` [200; 201] and `wilson` [202] provide convenient automatic routines for running and matching between SMEFT and LEFT.

The aforementioned running—short for **renormalization group** (RG) **running**—of a theory's parameters is important enough to warrant a brief word. As the name suggests, it is a consequence of the renormalization procedure, and its origin can be traced to the appearance of logarithms such as

[5] Though the form of $\mathcal{O}^{V,LL}_{\nu e}$ may appear different to that of $\mathcal{O}_F$ in Eq. (3.6), we can apply a Fierz transformation to equivalently write $\mathcal{O}^{V,LL}_{\nu e,ijkl} = (\overline{\nu_i}\gamma_\mu P_L e_l)(\overline{e_k}\gamma^\mu P_L \nu_j)$.

$$\ln \frac{\mu^2}{m^2} \quad \text{or} \quad \ln \frac{\mu^2}{p^2} \tag{3.58}$$

in loop calculations. Here μ is an unphysical scale introduced in *dimensional regularisation*, in which divergent integrals are regulated by evaluating them in $d = 4 - \epsilon$ dimensions. Its unphysicality critically implies that the renormalized couplings and Wilson coefficients must also depend on μ in such a way that μ drops out of all physical observables:

$$\frac{\mathrm{d}}{\mathrm{d}\mu}\sigma(g_i(\mu), C_i(\mu); \mu) = 0. \tag{3.59}$$

Eq. (3.59) leads to the **renormalization group equations** (RGEs), which can be solved to determine $g_i(\mu)$ and $C_i(\mu)$. Though μ is unphysical and $g_i(\mu)$ and $C_i(\mu)$ are therefore in principle meaningless functions, it is conventional to attempt to make contact with physical reality by choosing μ to coincide with the relevant energy scale Q of a process. The rationale behind this choice is that powers of $\ln(\mu^2/Q^2)$ will appear in the perturbative Dyson series, and the convergence—and therefore reliability—of this series is maximised if these log factors were to vanish. Thus, the zeitgeist demands that when one wishes to perform a calculation for a process using parameters measured (or otherwise extracted) at a vastly different energy scale, it is necessary to run the RGEs to ensure the accuracy of the result.

In SMEFT and LEFT the RGEs take the form [190; 213]

$$16\pi^2 \mu \frac{\mathrm{d}C_i}{\mathrm{d}\mu} = \gamma_{ij} C_j, \tag{3.60}$$

and though this expression suggests otherwise, they are nonlinear. An important consequence of the RGEs is that the effective operators *mix* into each other, meaning that operators which do not arise from matching may still be induced by running from the matching scale.

There is much more that can be said about RG running, but here is a good place to stop; for more exposition in the EFT context I refer you to Refs. [186–188].

They've got a lot of colliders, and they've got a lot of chutzpah.

Zapp Brannigan,
in *Futurama*,
reimagined

4

Riding the Seesaw: What Higgsstrahlung May Reveal about Massive Neutrinos

Contents

4.1 Introduction **50**
4.2 Theory Framework **53**
4.3 Phenomenology **58**
4.4 Summary **84**
4.A Approximate Matching Conditions **89**

In this chapter we'll investigate if high-precision measurements of the cross section of the **Higgsstrahlung** process

$$e^+e^- \to Zh$$

at a future electron-positron collider can be used to probe the Type-I and Type-III Seesaw models (together referred to as the *fermionic Seesaw models*). Using an effective field theory approach we'll compare the collider reaches to constraints from electroweak observables and probes of lepton flavour universality, as well as the existing and prospective bounds from searches for lepton flavour violation. At risk of ruining the suspense, it turns out that a measurement of $\sigma(e^+e^- \to Zh)$ in agreement with the SM prediction is necessitated in Type-I Seesaw, whereas a difference of up to $\mathcal{O}(10\%)$ is possible with Type-III Seesaw. In this way, we demonstrate that Higgsstrahlung promises to function as a probe complementary to existing experiments.

This chapter is a taxidermied reproduction of a publication of the same name [1], with slight alterations to the wording and exposition to ensure it flows well from the previous chapters. My contribution to this work was significant, including the derivation of expressions for shifts in SMEFT, the generation of all results and plots, and much of the discussion.[1]

4.1 Introduction

The discovery of the Higgs boson in 2012 [3; 4], while momentous, marked only the first foray into the era of observational Higgs physics. Many of the Higgs' properties remain to this day only imprecisely determined, and rectifying this is a major goal in the proposed program of next-generation lepton colliders. There are five proposals for so-called electron-positron 'Higgs factories' [85]: the Circular Electron Positron Collider (CEPC) [68–70], the International Linear Collider (ILC) [71–74], the Future Circular Collider (FCC-ee) [75–78], the Compact Linear Collider (CLIC) [79–81] and the Cool Copper Collider (C^3) [82–84]. The designation 'Higgs factory' mainly refers to the stage in which a future e^+e^- collider

[1] I also acknowledge the contributions of my coauthors Tobias Felkl and Michael Schmidt, which I feel were equally significant.

is run at a centre-of-mass energy of roughly $\sqrt{s} = 240$–$250\,\text{GeV}$, where the integrated cross section of the Higgsstrahlung process peaks and so dominates over all Higgs production mechanisms. Other stages involve the operation as a 'Z factory' at $\sqrt{s} = m_Z$, close to the W^+W^- production threshold at $\sqrt{s} = 2m_W$, and close to or at the $t\bar{t}$ threshold for $\sqrt{s} = 350$–$370\,\text{GeV}$, as well as potential upgrades for runs at even higher centre-of-mass energies [214].

It should come as no surprise that physicists, being the enterprising lot that they are, have sought to understand the extent to which these colliders can also be used to test various BSM scenarios. Many studies, for instance, focus on the direct production of sterile neutrinos in electroweak and Higgs production processes [215–223], and there are a number of reviews on the observational prospects of heavy neutral leptons [224–227]. Electroweak triplet fermions at colliders have similarly been studied for example in Refs. [228; 229]. The anticipated high precision attainable at future lepton colliders also serves as a motivation to consider virtual corrections [230] – for instance, Refs. [231; 232] study the contribution of sterile neutrinos to the triple-Higgs coupling.

Here we will investigate whether we may exploit measurements of the Higgsstrahlung cross section at a future collider to test the Type-I and -III Seesaw models of neutrino mass. The anticipated sub-percent precision of these measurements is due to the so-called 'recoil method', where Higgsstrahlung events are selected by measuring the four-momenta of the decay products of the Z boson, which *recoils* against the Higgs boson. This method is in principle applicable for any Higgs decay mode, allowing for a model-independent reconstruction of the Higgs boson mass [85]. Moreover, Higgsstrahlung is well-understood in the SM, with two-loop electroweak corrections to the SM cross section recently calculated in Refs. [233; 234]; see also Refs. [235–241].

In what follows we will consider the process at two benchmark centre-of-mass energies, $\sqrt{s} = 240\,\text{GeV}$ and $365\,\text{GeV}$. As argued for in Ref. [242], the smaller cross section at larger s can be partly compensated for by a higher instantaneous luminosity which scales approximately linearly with s. Moreover, the additional boost of the Z and h bosons allows for a better separation of the respective jets and therefore a more precise measurement of

$\sigma_{Zh} \times \mathrm{BR}(h \to X)$. Further advantages mentioned are the immediate access to top-pair production as well as the $e^+e^- \to h\nu_e\bar{\nu}_e$ process via W^+W^- fusion, which enables a precise determination of the Higgs boson width as well as the offering the potential to measure m_h with a precision similar to that of $\sqrt{s} = 240\,\mathrm{GeV}$.

Now, for both models considered here the Seesaw relation

$$m_\nu \simeq \frac{v^2}{M} Y^2 \tag{4.1}$$

suggests that to accommodate sterile states with $M = \mathcal{O}(\mathrm{TeV})$ the neutrino Yukawa couplings must be tiny, meaning lepton number-conserving processes will be suppressed [243–245] and beyond the reach of the proposed lepton colliders. This restriction can however be circumvented in *symmetry-protected Seesaw models* [173; 243; 246–255], where the imposition of an (approximate) symmetry will allow us to entertain relatively light singlets or triplets around the TeV scale without the need to assume tiny Yukawa couplings. This symmetry permits some elements of the Dirac and Majorana mass matrices to be sizeable, whereas the remaining ones must be comparatively suppressed (or zero in the exact limit). The smallness of active neutrino masses is then guaranteed through their proportionality to these small entries, and hence does not rely on overall suppression through a large mass scale M. In addition, no fine-tuned cancellation between (a priori unrelated) elements of the mass matrices are needed.

The remainder of this chapter is laid out as follows. After reviewing the relevant theory in the next section, I will in Section 4.3 discuss the phenomenology of Higgsstrahlung and other processes sensitive to the same parameters. The bulk of our time will be spent there, as there is much that can be said about these processes and the constraints they place on the parameter space of the Seesaw models. Finally, I will summarise the results and draw conclusions in Section 4.4.

4.2 Theory Framework

To save you from needing to flip back to the previous chapters, here I'll offer an abridged presentation of the relevant theory together with some additional contextual discussion. Firstly, we remind ourselves of the SM Lagrangian, of which the electroweak and leptonic parts are

$$\begin{aligned}\mathcal{L}_{\text{SM}} \supset -\frac{1}{4}W^a_{\mu\nu}W^{a\mu\nu} - \frac{1}{4}B_{\mu\nu}B^{\mu\nu} + (D_\mu H)^\dagger(D^\mu H) + \mu^2 H^\dagger H - \lambda(H^\dagger H)^2 \\ + \overline{L_i} i\not{D} L_i + \overline{e_{Ri}} i\not{D} e_{Ri} - Y^e_{ij}(\overline{L_i} e_{Rj} H + H^\dagger \overline{e_{Rj}} L_i).\end{aligned} \tag{4.2}$$

The gauge-covariant derivative post-electroweak symmetry breaking reads

$$D_\mu = \partial_\mu - \mathrm{i}g_2 W^+_\mu T^+ - \mathrm{i}g_2 W^-_\mu T^- - \mathrm{i}g_Z(T^3 - Q\sin^2\theta_w)Z_\mu - \mathrm{i}QeA_\mu, \tag{4.3}$$

and for later use it is convenient to assign the symbols

$$g_L \equiv g_Z\left(-\frac{1}{2} + \sin^2\theta_w\right) \quad \text{and} \quad g_R \equiv g_Z \sin^2\theta_w \tag{4.4}$$

to the Ze_Le_L and Ze_Re_R couplings, respectively.

Since we will want to distinguish electrons, muons, and taus in this chapter, I will for its duration exchange the notation e_i for ℓ_i to avoid accidentally giving the impression that I am only talking about electrons. In this way, $\ell_i = e_{Li} + e_{Ri}$, with $\ell_1 = e$, $\ell_2 = \mu$, and $\ell_3 = \tau$.

4.2.1 Effective Field Theory

4.2.1.1 SMEFT

We will use SMEFT, and later LEFT, as our means of studying the Type-I and -III Seesaw models. The SMEFT operators that these models match onto are found in the subset

$$\begin{aligned}\mathcal{L}_{\text{SMEFT}} \supset \Big[&C_{5,ij}(\overline{L_i}\widetilde{H})(\widetilde{H}^T L_j^c) + C_{eB,ij}(\overline{L_i}\sigma^{\mu\nu}e_{Rj})HB_{\mu\nu} \\ &+ C_{eW,ij}(\overline{L_i}\sigma^{\mu\nu}\sigma^a e_{Rj})HW^a_{\mu\nu} + C_{eH,ij}(H^\dagger H)(\overline{L_i}e_{Rj}H) + \text{h.c.}\Big] \\ &+ C^{(1)}_{HL,ij}(H^\dagger \mathrm{i}\overleftrightarrow{D}_\mu H)(\overline{L_i}\gamma^\mu L_j) + C^{(3)}_{HL,ij}(H^\dagger \mathrm{i}\overleftrightarrow{D}^a_\mu H)(\overline{L_i}\sigma^a\gamma^\mu L_j),\end{aligned} \tag{4.5}$$

and additional operators relevant to Higgsstrahlung, which will pick up non-zero coefficients from RG running, are also listed in Table 4.2. In our convention the Wilson coefficients C_i are dimensional, and so for later convenience let us also define the dimensionless variants

$$\hat{C}_i \equiv C_i \times \text{TeV}^2 \tag{4.6}$$

for the dimension-six coefficients.

4.2.1.2 LEFT

To describe low-energy processes our EFT of choice will naturally be LEFT. The relevant part of the LEFT Lagrangian for purely leptonic transitions is

$$\begin{aligned}\mathcal{L}_{\text{LEFT}} \supset\ &C^{VLL}_{ee,ijkl}(\overline{\ell_i}\gamma^\mu P_L \ell_j)(\overline{\ell_k}\gamma_\mu P_L \ell_l) + C^{VRR}_{ee,ijkl}(\overline{\ell_i}\gamma^\mu P_R \ell_j)(\overline{\ell_k}\gamma_\mu P_R \ell_l) \\ &+ C^{VLR}_{ee,ijkl}(\overline{\ell_i}\gamma^\mu P_L \ell_j)(\overline{\ell_k}\gamma_\mu P_R \ell_l) + \Big[C_{e\gamma,ij}(\overline{\ell_i}\sigma^{\mu\nu}P_R\ell_j)F_{\mu\nu} + \text{h.c.}\Big],\end{aligned} \tag{4.7}$$

while for semi-leptonic neutral current transitions we will need

$$\begin{aligned}\mathcal{L}_{\text{LEFT}} \supset\ &C^{VLL}_{eq,ijkl}(\overline{\ell_i}\gamma^\mu P_L \ell_j)(\overline{q_k}\gamma_\mu P_L q_l) + C^{VRR}_{eq,ijkl}(\overline{\ell_i}\gamma^\mu P_R \ell_j)(\overline{q_k}\gamma_\mu P_R q_l) \\ &+ C^{VLR}_{eq,ijkl}(\overline{\ell_i}\gamma^\mu P_L \ell_j)(\overline{q_k}\gamma_\mu P_R q_l) + C^{VLR}_{qe,ijkl}(\overline{q_i}\gamma^\mu P_L q_j)(\overline{\ell_k}\gamma_\mu P_R \ell_l).\end{aligned} \tag{4.8}$$

To obtain the LEFT Wilson coefficients for the Seesaw models we'll use the software package `DsixTools` [200; 201] to (i) run the SMEFT coefficients between the Seesaw scale and the electroweak scale, $\mu = m_Z$, (ii) match the SMEFT and LEFT coefficients, and (iii) run the LEFT coefficients to the low scale $\mu = 5\,\text{GeV}$, at which point it is unable to run further. Below this scale the running is dominated by QCD effects, and as there are no

Coefficient	Type-I	Type-III
$C_{5,ij}$	$\frac{1}{2}\left(YM^{-1}Y^T\right)_{ij}$	$\frac{1}{2}\left(YM^{-1}Y^T\right)_{ij}$
$C^{(1)}_{HL,ij}$	$\frac{1}{4}\left(Y(M^\dagger M)^{-1}Y^\dagger\right)_{ij}$	$\frac{3}{4}\left(Y(M^\dagger M)^{-1}Y^\dagger\right)_{ij}$
$C^{(3)}_{HL,ij}$	$-\frac{1}{4}\left(Y(M^\dagger M)^{-1}Y^\dagger\right)_{ij}$	$\frac{1}{4}\left(Y(M^\dagger M)^{-1}Y^\dagger\right)_{ij}$
$C_{eH,ij}$	0	$\left(Y(M^\dagger M)^{-1}Y^\dagger Y^e\right)_{ij}$
$C_{eB,ij}$	$\frac{1}{16\pi^2}\frac{g_1}{24}\left(Y(M^\dagger M)^{-1}Y^\dagger Y^e\right)_{ij}$	$\frac{1}{16\pi^2}\frac{g_1}{8}\left(Y(M^\dagger M)^{-1}Y^\dagger Y^e\right)_{ij}$
$C_{eW,ij}$	$\frac{1}{16\pi^2}\frac{5g_2}{24}\left(Y(M^\dagger M)^{-1}Y^\dagger Y^e\right)_{ij}$	$\frac{1}{16\pi^2}\frac{3g_2}{8}\left(Y(M^\dagger M)^{-1}Y^\dagger Y^e\right)_{ij}$

Table 4.1: SMEFT Wilson coefficients obtained from matching the Type-I and Type-III Seesaw models at the scale $\mu = M$ [256–258]. In order to properly account for the stringent bounds from the non-observation of lepton flavour violation, the electroweak dipole operators C_{eB} and C_{eW} are matched to one-loop order, while all other operators are matched at tree level.

sizeable contributions to quark operators in the Seesaw models we may assume that this procedure captures the main contributions from RG running in LEFT, and that further effects at lower scales do not appreciably change the results. A more detailed discussion is provided in the appendix of this chapter, Section 4.A.

4.2.2 Seesaw Models

4.2.2.1 Type-I

The Type-I Seesaw model [14–18] augments the SM with n_ν right-handed sterile neutrinos $\nu_{Ri} \sim (1, 1, 0)$, with

$$\mathcal{L}_{\nu_R} = \overline{\nu_{Ri}} i\not{\partial} \nu_{Ri} - \left(Y_{ij}\overline{L_i}\nu_{Rj}\tilde{H} + \frac{1}{2}M_{ij}\overline{\nu^c_{Ri}}\nu_{Rj} + \text{h.c.}\right). \tag{4.9}$$

After electroweak symmetry breaking the masses combine into the matrix form

$$\mathcal{L}_{\nu\text{ mass}} = -\frac{1}{2}\begin{pmatrix}\overline{\nu_L} & \overline{\nu^c_R}\end{pmatrix}\begin{pmatrix}0 & m\\ m^T & M\end{pmatrix}\begin{pmatrix}\nu^c_L\\ \nu_R\end{pmatrix} + \text{h.c.}, \tag{4.10}$$

where $m_{ij} \equiv Y_{ij}v/\sqrt{2}$ is referred to as the Dirac mass matrix, and M as the Majorana

mass matrix. Matching this theory onto SMEFT at the scale $\mu = M$ yields the effective operators collected on the left side of Table 4.1.

4.2.2.2 Type-III

The Type-III Seesaw model [28] extends the SM Lagrangian with n_Σ right-handed weak fermion triplets $\Sigma_{Ri} \sim (1, 3, 0)$, with

$$\mathcal{L}_{\Sigma_R} = \overline{\Sigma_{Ri}} i \not{D} \Sigma_{Ri} - \left(Y_{ij} \overline{L_i} \Sigma^a_{Rj} \sigma^a \widetilde{H} + \frac{1}{2} M_{ij} \overline{\Sigma^{ac}_{Ri}} \Sigma^a_{Rj} + \text{h.c.} \right), \tag{4.11}$$

and in an identical manner to the Type-I model, neutrino masses take the form

$$\mathcal{L}_{\nu \text{ mass}} = -\frac{1}{2} \begin{pmatrix} \overline{\nu_L} & \overline{\Sigma^{0c}_R} \end{pmatrix} \begin{pmatrix} 0 & m \\ m^T & M \end{pmatrix} \begin{pmatrix} \nu^c_L \\ \Sigma^0_R \end{pmatrix} + \text{h.c.}, \tag{4.12}$$

where $\Sigma^0_{Ri} = \Sigma^3_{Ri}$ is the electrically neutral component of the triplet. The charged eigenstates $\Sigma^\pm_R = (\Sigma^1_R \mp \mathrm{i}\Sigma^2_R)/\sqrt{2}$ instead mix into the charged leptons. Matching this theory onto SMEFT at the scale $\mu = M$ yields the effective operators collected on the right side of Table 4.1.

4.2.3 Conserved Lepton Number Symmetry

In this work we study symmetry-protected versions of the fermionic Seesaw models, wherein a lepton number (LN) symmetry decouples the physics of neutrino masses from the phenomenology associated with the conservation of LN [173; 243; 253–255]. Without loss of generality we may fix $n_\nu = n_\Sigma = 2$, with which we can generate two massive active neutrinos as required to explain the observed mass splittings from oscillation data. The heavy fermion states are assigned 1 and -1 units of LN, respectively. After electroweak symmetry breaking the Dirac and Majorana mass matrices may be respectively parameterised as

$$m_{ij} = \frac{v}{\sqrt{2}} \begin{pmatrix} Y & \epsilon Y' \end{pmatrix}_{ij} = \frac{v}{\sqrt{2}} \begin{pmatrix} Y_e & \epsilon Y'_e \\ Y_\mu & \epsilon Y'_\mu \\ Y_\tau & \epsilon Y'_\tau \end{pmatrix}_{ij}, \tag{4.13}$$

and

$$M_{ij} = \begin{pmatrix} \mu_1 M & M \\ M & \mu_2 M \end{pmatrix}_{ij}, \tag{4.14}$$

where ϵ and $\mu_{1,2}$ are dimensionless parameters. The mixing of the SM neutrino ν_{Li} with ν_{Ri} (in Type-I) or Σ^0_{Ri} (in Type-III) is captured by the dimensionless ratios

$$\theta_i = \frac{m_{i1}}{M} = \frac{Y_i}{\sqrt{2}} \frac{v}{M}, \tag{4.15}$$

which are equal to the active-sterile *mixing angles* in the small-mixing approximation, that is, if $\mathcal{O}((v/M)^3)$ effects are neglected. (Note that these are *not* the mixing angles appearing in the PMNS matrix, as those angles instead parameterise the mixing among the active neutrinos.) For simplicity, I'll refer to θ_e as the 'electron(-flavour) mixing angle', or just 'electron mixing' for short, and so on.

In this parameterisation light neutrino masses are proportional to ϵ and μ_2, which break LN:

$$m_\nu = \frac{v^2}{2} \left[\mu_2 Y M^{-1} Y^T - \epsilon \left(Y' M^{-1} Y^T + Y M^{-1} Y'^T \right) \right]. \tag{4.16}$$

The limit $\mu_2 \neq 0$ and $\mu_1 = \epsilon = 0$ is referred to as *inverse Seesaw* [246; 259; 260], and $\epsilon \neq 0$ and $\mu_{1,2} = 0$ is commonly known as *linear Seesaw* [261; 262].

Here we'll adopt the LN-conserving limit $\epsilon = \mu_{1,2} = 0$ – that is, we'll assume the textures

$$Y_{ij} = \begin{pmatrix} Y_e & 0 \\ Y_\mu & 0 \\ Y_\tau & 0 \end{pmatrix} \quad \text{and} \quad M_{ij} = \begin{pmatrix} 0 & M \\ M & 0 \end{pmatrix} \tag{4.17}$$

for both models. This results in massless active neutrinos and a heavy Dirac neutrino of mass M. In this way, we neglect the phenomenological implications of LN violation, and instead focus on LN-conserving effects.[2] That said, it is possible to relax the requirement

[2]Note that this also means that the parameters θ_i can be treated as independent. If data on lepton mixing and the hierarchy of neutrino masses is to be properly accommodated,

that $\mu_{1,2} = 0$, and with the help of Table 4.1 one can check that—as long as the contribution of the Weinberg operator to the dimension-six operators via RG running can be neglected—the only change compared to the LN-conserving limit is

$$\theta_i^2 \to \frac{1+\mu_2^2}{(1+\mu_1\mu_2)^2}\theta_i^2 \tag{4.18}$$

for each mixing angle in all of our formulae. As this does not meaningfully impact the phenomenology, we will maintain the exact limit.

One may add a further singlet or triplet with vanishing LN such that

$$Y_{ij} = \begin{pmatrix} Y_e & 0 & 0 \\ Y_\mu & 0 & 0 \\ Y_\tau & 0 & 0 \end{pmatrix} \quad \text{and} \quad M_{ij} = \begin{pmatrix} 0 & M & 0 \\ M & 0 & 0 \\ 0 & 0 & M' \end{pmatrix}, \tag{4.19}$$

which supports three massive active neutrinos if one departs from the LN-conserving limit. Still, the additional state trivially decouples from the phenomenology.[3]

4.3 Phenomenology

We shall choose the benchmark value $M = 1\,\text{TeV}$ for the masses of the new interaction states in our analysis. This is consistent with all performed direct searches for heavy neutral leptons at colliders, see for instance Refs. [227; 265] for recent overviews. In Ref. [266], for sterile neutrinos of a mass $M \approx 1\,\text{TeV}$ the constraint $|\theta_e| \sim |\theta_\mu| \lesssim \mathcal{O}(1)$ was derived via a search for the signature of three charged leptons with any combination of electron and muon flavours. Ref. [267] reports the constraint $|\theta_\mu|^2 \lesssim \mathcal{O}(0.1)$ for TeV-scale Majorana neutrinos based on a search for same-sign dimuon final states; see also Refs. [245]. The

the θ_i exhibit non-trivial correlations [174; 263; 264].

[3] As is discussed in Ref. [173], the determinant of the full neutrino mass matrix also vanishes in the (LN-violating) case $\mu_1 \neq 0$ and $\epsilon = \mu_2 = 0$, which however generally guarantees only one massless active neutrino. One could also consider a vanishing Majorana mass matrix and a completely general Dirac mass matrix, but this yields light Dirac neutrinos and is not suitable for a study in SMEFT.

bound $M_{\Sigma_0} \geq 910\,\text{GeV}$ was derived in a recent study [56] which focuses on leptonic final states and takes into account earlier ATLAS results.

In our phenomenological discussion we'll consider the following observables:

- the relative shift $\Delta\sigma/\sigma_0$ in the Higgsstrahlung cross section from its SM prediction,
- the effective leptonic weak mixing angle $\sin^2\theta^{\text{lept}}_{w,\text{eff}}$ and the W boson mass m_W,
- the ratios $g^X_{\mu/e}$ and $g^X_{\tau/\mu}$ of leptonic gauge couplings as probes of lepton flavour universality (LFU), and the ratios $R(K_{\ell 3})$ and $R(V_{us})$, and
- the branching ratios of the lepton flavour-violating (LFV) processes $\mu \to e\gamma$, $\mu \to 3e$, $\tau \to e\gamma$, $\tau \to 3e$, and the ratios of the $\mu - e$ conversion rates over the muon capture rate in different target nuclei.

The theoretical expressions for these observables in the fermionic Seesaw models are listed in Tables 4.4, 4.5, 4.6 and 4.7 as functions of the mixing angles θ_e, θ_μ, θ_τ, as defined in Eq. (4.15), for a matching scale $\mu = M = 1\,\text{TeV}$. While these expressions hold for complex Yukawa couplings, they evidently do not depend on the phases of the mixing angles, and so nothing is lost by treating them as positive real numbers. If effects from RG running in SMEFT above the matching scale are neglected, one may naïvely interpret the results also for a larger mass after appropriately rescaling the couplings. That said, to facilitate a less crude analysis the relevant expressions derived from matching at the scale $\mu = M = 10\,\text{TeV}$ are also provided and discussed in Section 4.3.5.

The following discussions are supported by plots in the θ_e–θ_μ plane, as well as plots in the θ_e–θ_τ plane for the LFU and LFV observables. (As the main objective of this work concerns Higgsstrahlung, we are most interested in phenomenological effects related to electron flavour, and hence have no need to view the θ_μ–θ_τ plane.) The third mixing angle is fixed to the benchmark values $\theta_\tau = 10^{-2}$ and $\theta_\mu = 10^{-6}$; these choices are most transparently justified (at least for Type-III) by Fig. 4.7, which depicts the most competitive constraints for both models. There are no appreciable changes to the resulting

phenomenology if these values are tuned smaller or even zero, apart from the fact that the LFV bounds become weaker and eventually vanish. The exclusion regions in each of these plots either reflect the current bounds at 2σ for the electroweak and LFU observables, or the upper limits on the LFV processes at 90% C.L.

4.3.1 Higgsstrahlung

4.3.1.1 SM Tree-Level Contribution

The tree-level differential cross section in the SM is well-known, and is given by [86; 268]

$$\frac{\mathrm{d}\sigma_0}{\mathrm{d}\cos\theta} = \frac{\sqrt{\lambda}}{32\pi s^2}|\mathcal{M}_0|^2, \tag{4.20}$$

where unpolarised beams are assumed, with

$$|\mathcal{M}_0|^2 = \frac{s}{2}(g_L^2 + g_R^2)\left(\frac{g_{ZZh}}{s - m_Z^2}\right)^2\left(1 + \frac{\lambda \sin^2\theta}{8sm_Z^2}\right) \tag{4.21}$$

the spin-averaged invariant matrix element. Here $g_{ZZh} = g_2 m_Z/\cos\theta_w$, θ is the angle between the incoming electron and outgoing Z boson, and

$$\lambda = (s - m_Z^2 - m_h^2)^2 - 4m_Z^2 m_h^2 \tag{4.22}$$

is the relevant Källèn function. The corresponding integrated cross section is

$$\sigma_0 = \frac{\sqrt{\lambda}}{32\pi s}(g_L^2 + g_R^2)\left(\frac{g_{ZZh}}{s - m_Z^2}\right)^2\left(1 + \frac{\lambda}{12sm_Z^2}\right). \tag{4.23}$$

The dependence of σ_0 on $\sqrt{s}$ is depicted in Fig. 4.1. It peaks around a centre-of-mass energy of $\sqrt{s} \approx 245\,\mathrm{GeV}$.

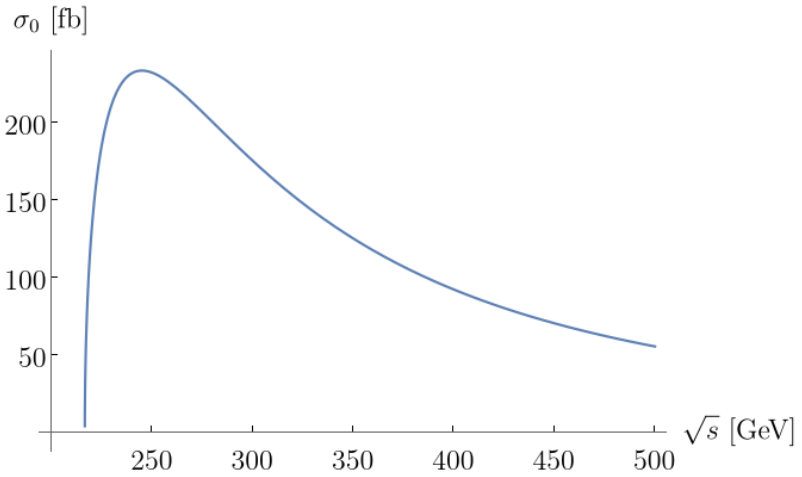

Figure 4.1: The tree-level cross section for the Higgsstrahlung process in the SM as a function of the centre-of-mass energy $\sqrt{s}$.

4.3.1.2 Corrections in SMEFT

Including corrections from new physics gives

$$\frac{\mathrm{d}\sigma}{\mathrm{d}\cos\theta} = \frac{\sqrt{\lambda}}{32\pi s^2}\Big(|\mathcal{M}_0|^2 + \delta|\mathcal{M}_0|^2 + 2\,\mathrm{Re}\,\mathcal{M}_0^*\mathcal{M}_1\Big), \tag{4.24}$$

where $\delta|\mathcal{M}_0|^2$ denotes the effect of parameter shifts in SMEFT to the tree-level cross section, as discussed in Section 3.2.1 of the previous chapter, and $2\,\mathrm{Re}\,\mathcal{M}_0^*\mathcal{M}_1$ is the interference term of the tree-level amplitude with corrections from new operators. The explicit result reads

$$\begin{aligned}\Delta\frac{\mathrm{d}\sigma}{\mathrm{d}\cos\theta} &\equiv \frac{\mathrm{d}\sigma}{\mathrm{d}\cos\theta} - \frac{\mathrm{d}\sigma_0}{\mathrm{d}\cos\theta} \\ &= \frac{\sqrt{\lambda}}{32\pi s^2}\left[2\left(\frac{\delta g_{ZZh}}{g_{ZZh}} + \frac{g_L\delta g_L + g_R\delta g_R}{g_L^2+g_R^2}\right)|\mathcal{M}_0|^2 + \frac{g_{ZZh}v}{2}\sum_{i=2}^{5} d_i F_i\right],\end{aligned} \tag{4.25}$$

where the parameter shifts and coefficients d_i are presented below, and the form factors F_i may be found in Ref. [86].

Integrating over $\cos\theta$, the full resulting fractional shift for the cross section is

$$\frac{\Delta\sigma}{\sigma_0} = 2\left(\frac{\delta g_{ZZh}}{g_{ZZh}} + \frac{g_L\delta g_L + g_R\delta g_R}{g_L^2 + g_R^2}\right) + \frac{v}{g_{ZZh}}\sum_{i=2}^{5} d_i f_i. \tag{4.26}$$

Here the parameter shifts in the (α, m_Z, G_F) input scheme are

$$\frac{\delta g_{ZZh}}{g_{ZZh}} = v_T^2\left(C_{H\Box} + \frac{1}{4}C_{HD} - \frac{1}{\sqrt{2}}\delta\hat{G}_F\right), \tag{4.27a}$$

$$\frac{\delta g_L}{g_Z} = \frac{1}{8(c_w^2 - s_w^2)}v_T^2\left(8s_w c_w C_{HWB} + C_{HD} + 2\sqrt{2}\delta\hat{G}_F\right) - \frac{1}{2}v_T^2\left(C_{HL,11}^{(1)} + C_{HL,11}^{(3)}\right), \tag{4.27b}$$

$$\frac{\delta g_R}{g_Z} = \frac{s_w^2}{4(c_w^2 - s_w^2)}v_T^2\left(4\frac{c_w}{s_w}C_{HWB} + C_{HD} + 2\sqrt{2}\delta\hat{G}_F\right) - \frac{1}{2}v_T^2 C_{He,11}, \tag{4.27c}$$

with the shorthands $s_w \equiv \sin\theta_w$ and $c_w \equiv \cos\theta_w$, and we recall that

$$\delta\hat{G}_F = \frac{1}{\sqrt{2}}\left(C_{HL,11}^{(3)} + C_{HL,22}^{(3)}\right) - \frac{1}{2\sqrt{2}}(C_{LL,1221} + C_{LL,2112}) \tag{4.28}$$

from Chapter 3. The integrated form factors f_i are

$$f_2 = 12m_Z^2\frac{s(s + m_Z^2 - m_h^2)}{12sm_Z^2 + \lambda}, \tag{4.29a}$$

$$f_3 = -12em_Z^2\frac{g_L + g_R}{g_L^2 + g_R^2}\frac{(s - m_Z^2)(s + m_Z^2 - m_h^2)}{12sm_Z^2 + \lambda}, \tag{4.29b}$$

$$f_4 = \frac{2g_L}{g_L^2 + g_R^2}(s - m_Z^2), \quad \text{and} \tag{4.29c}$$

$$f_5 = \frac{2g_R}{g_L^2 + g_R^2}(s - m_Z^2), \tag{4.29d}$$

and their corresponding coefficients d_i are

$$d_2 = 4(s_w^2 C_{HB} + s_w c_w C_{HWB} + c_w^2 C_{HW}), \tag{4.30a}$$

$$d_3 = -4s_w c_w C_{HB} - 2(c_w^2 - s_w^2)C_{HWB} + 4s_w c_w C_{HW}, \tag{4.30b}$$

$$d_4 = -g_Z(C_{HL,11}^{(1)} + C_{HL,11}^{(3)}), \quad \text{and} \tag{4.30c}$$

$$d_5 = -g_Z C_{He,11}. \tag{4.30d}$$

The diagrams giving rise to the d_i's are depicted in Fig. 4.2. Note that d_1 and f_1 are

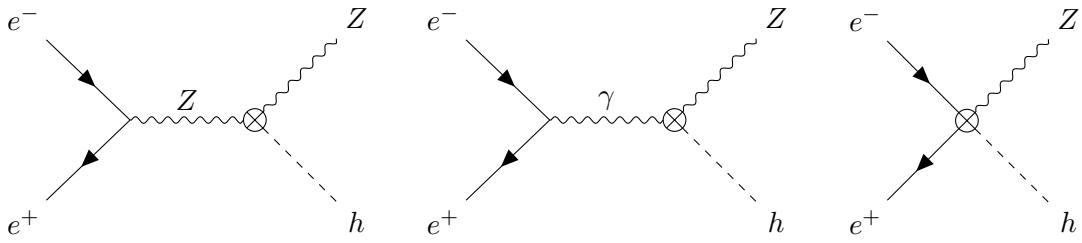

Figure 4.2: Diagrams with effective vertices contributing to Eq. (4.26).

$\mathcal{O}_{HW}$	$H^\dagger H W^a_{\mu\nu} W^{a\mu\nu}$	$\mathcal{O}_{H\Box}$	$(H^\dagger H)\Box(H^\dagger H)$	$\mathcal{O}^{(1)}_{HL,ij}$	$(H^\dagger \mathrm{i}\overleftrightarrow{D}_\mu H)(\overline{L_i}\gamma^\mu L_j)$
$\mathcal{O}_{HB}$	$H^\dagger H B_{\mu\nu} B^{\mu\nu}$	$\mathcal{O}_{HD}$	$(H^\dagger D_\mu H)^*(H^\dagger D^\mu H)$	$\mathcal{O}^{(3)}_{HL,ij}$	$(H^\dagger \mathrm{i}\overleftrightarrow{D}^a_\mu H)(\overline{L_i}\sigma^a\gamma^\mu L_j)$
$\mathcal{O}_{HWB}$	$H^\dagger \sigma^a H W^a_{\mu\nu} B^{\mu\nu}$	$\mathcal{O}_{LL,ijkl}$	$(\overline{L_i}\gamma^\mu L_j)(\overline{L_k}\gamma_\mu L_l)$	$\mathcal{O}_{He,ij}$	$(H^\dagger \mathrm{i}\overleftrightarrow{D}_\mu H)(\overline{e_{Ri}}\gamma^\mu e_{Rj})$

Table 4.2: Dimension-six SMEFT operators in the Warsaw basis [198] which enter the correction to the Higgsstrahlung cross section.

absent here, as unlike Ref. [86] I elect instead to absorb their contribution into δg_{ZZh}. The dimension-six SMEFT operators which constitute these corrections are listed in Table 4.2. We note that the d_i's are zero at tree level in the Seesaw models, apart from d_4 in Type-III.

4.3.1.3 Discussion

The programs of the proposed next-generation lepton colliders include runs as Higgs factories at a centre-of-mass energy of $\sqrt{s} = 240\,\text{GeV}$ (CEPC, FCC-ee) or 250 GeV (ILC), and as scans of the $t\bar{t}$ production threshold in the range $\sqrt{s} = 350$–$380\,\text{GeV}$. Measurements of the Higgsstrahlung cross section are foreseen at both stages for all collider proposals we consider, apart from CLIC which is envisioned to directly run at $\sqrt{s} = 380\,\text{GeV}$ in its initial stage. Therefore, we evaluate the relative shift $\Delta\sigma/\sigma_0$ of the Higgsstrahlung cross section, as given by Eq. (4.26), at $\sqrt{s} = 240\,\text{GeV}$ and 365 GeV. Regarding the precision of the measurement, we take the two benchmark values of 0.5% and 1.0% for $\sqrt{s} = 240\,\text{GeV}$, and 1.0% for $\sqrt{s} = 365\,\text{GeV}$. This is representative of the results of several analyses of the attainable precision, which are collected in Table 4.3.

The shifts in the cross section as functions of the mixing angles are listed for both Seesaw

Collider	L_{int} [ab^{-1}]	Z-decay final states	$\sqrt{s}$ [GeV]	Precision
CEPC	20	$\ell^+\ell^-$, $q\bar{q}$, $\nu\bar{\nu}$	240	0.26% [70]
	1	$\ell^+\ell^-$, $q\bar{q}$, $\nu\bar{\nu}$	360	1.4% [70]
FCC-ee	5	$\ell^+\ell^-$	240	0.5% [78]
	1.5	$\ell^+\ell^-$, $q\bar{q}$, $\nu\bar{\nu}$	365	0.9% [78]
ILC	1.35	$\ell^+\ell^-$	250	1.1% [269]
	0.115 (0.5)	$\ell^+\ell^-$ ($q\bar{q}$)	350	5% (1.63%) [269; 270]
	1.6 (0.5)	$\ell^+\ell^-$ ($q\bar{q}$)	500	2.9% (3.9%) [269; 271]
CLIC	0.5	$\ell^+\ell^-$, $q\bar{q}$	350	1.65% [242]

Table 4.3: Forecast (statistical) precision of measurements of the Higgsstrahlung cross section at different proposed next-generation colliders. The third column gives the Z-decay final states taken into account in the respective analysis; $\ell^+\ell^-$ always implies both $Z \to e^+e^-$ and $Z \to \mu^+\mu^-$. For the results from Ref. [269] a polarisation $(P_{e^-}, P_{e^+}) = (-80\%, +30\%)$ is assumed; still, this changes the expected Higgsstrahlung event rate by at most 50% compared to unpolarised beams [242; 270]. No polarisation is assumed for the ILC precision for $\sqrt{s} = 350\,\text{GeV}$ and hadronic Z boson decays in Ref. [270], wherein an attainable precision of 1.76% for polarised beams and an integrated luminosity of $0.35\,\text{ab}^{-1}$ is reported as well.

	Type-I	Type-III
$\Delta\sigma/\sigma_0$ (240 GeV)	$0.95\,\lvert\theta_e\rvert^2 + 1.10\,\lvert\theta_\mu\rvert^2 + 0.02\,\lvert\theta_\tau\rvert^2$	$27.59\,\lvert\theta_e\rvert^2 - 1.08\,\lvert\theta_\mu\rvert^2 - 0.01\,\lvert\theta_\tau\rvert^2$
$\Delta\sigma/\sigma_0$ (365 GeV)	$0.87\,\lvert\theta_e\rvert^2 + 1.12\,\lvert\theta_\mu\rvert^2 + 0.04\,\lvert\theta_\tau\rvert^2$	$66.15\,\lvert\theta_e\rvert^2 - 1.09\,\lvert\theta_\mu\rvert^2 - 0.01\,\lvert\theta_\tau\rvert^2$
$\Delta\sigma/\sigma_0$ (500 GeV)	$0.80\,\lvert\theta_e\rvert^2 + 1.14\,\lvert\theta_\mu\rvert^2 + 0.05\,\lvert\theta_\tau\rvert^2$	$126.39\,\lvert\theta_e\rvert^2 - 1.10\,\lvert\theta_\mu\rvert^2 - 0.01\,\lvert\theta_\tau\rvert^2$

Table 4.4: Shifts of the Higgsstrahlung cross section at different centre-of-mass energies in terms of the mixing angles, when $M = 1\,\text{TeV}$. For the sake of comparison, the shift for the larger centre-of-mass energy $\sqrt{s} = 500\,\text{GeV}$ is also shown.

models in Table 4.4, and are depicted in Fig. 4.3. The red areas of the plots indicate parameter regions where the shift $\Delta\sigma/\sigma_0$ is smaller than our precision benchmarks. To stand a chance of observing a deviation from the SM prediction at a next-generation collider we therefore require that the mixing angles lie outside these regions. The purpose of the next sections, in which we analyse the constraints imposed by the electroweak observables and probes of LFU and LFV, is to determine how much of these exterior regions are available.

Before this, however, let's take a moment to understand why these regions are the way

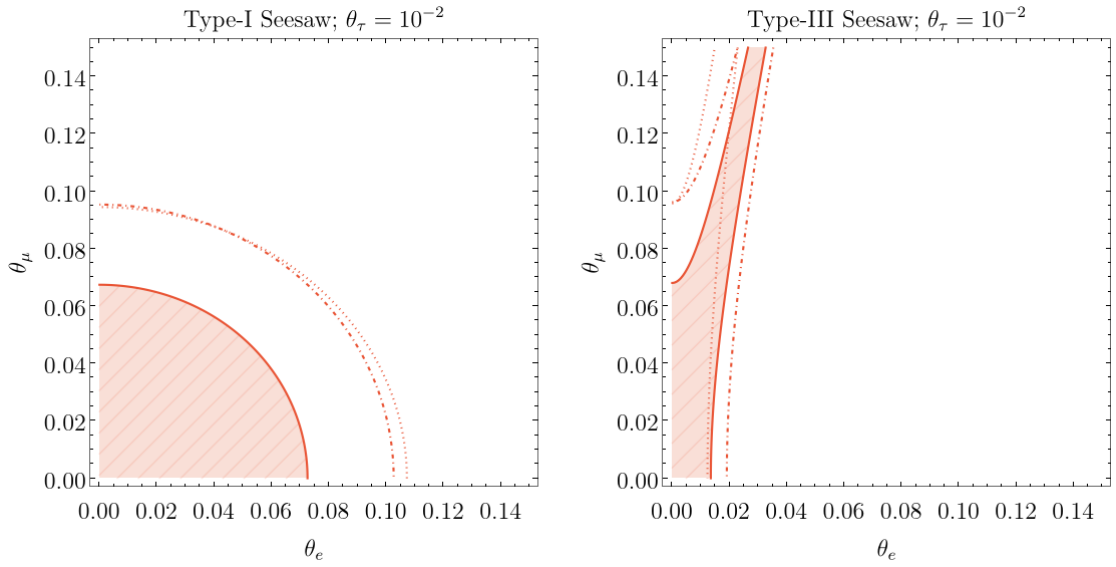

Figure 4.3: Projected sensitivities of precision Higgsstrahlung measurements. The red-ruled regions indicate $|\Delta\sigma/\sigma| < 0.5\%$ at $\sqrt{s} = 240\,\text{GeV}$. The dot-dashed and dotted red lines are the corresponding 1% contours at $\sqrt{s} = 240\,\text{GeV}$ and 365 GeV, respectively.

that they are. To aid in the following discussion, let us write

$$\frac{\Delta\sigma}{\sigma_0} \approx \begin{cases} 0.90\,\hat{C}^{(1)}_{HL,11} + 0.77\,\hat{C}^{(3)}_{HL,11} - 0.13\,\hat{C}^{(3)}_{HL,22} & \text{at } \sqrt{s} = 240\,\text{GeV} \\ 2.09\,\hat{C}^{(1)}_{HL,11} + 1.96\,\hat{C}^{(3)}_{HL,11} - 0.13\,\hat{C}^{(3)}_{HL,22} & \text{at } \sqrt{s} = 365\,\text{GeV} \end{cases}, \tag{4.31}$$

where the Wilson coefficients are evaluated at $\mu = \sqrt{s}$, respectively, and as a reminder, the dimensionless Wilson coefficients are defined by $\hat{C} = C \times \text{TeV}^2$. These approximate expressions deviate from the exact results, presented in Table 4.4, by at most 5% in either model.

As the couplings of the Z boson to charged leptons are not directly altered at tree level in the Type-I Seesaw model, $\sigma(e^+e^- \to Zh)$ is predominantly modified via the shift in the Fermi constant, Eq. (4.28), which enters through the shifts δg_{ZZh}, δg_L, and δg_R in Eq. (4.27). While the contributions of electron and muon mixing are of fairly similar magnitudes, $\Delta\sigma/\sigma_0$ turns out to be slightly more sensitive to the latter. This is due to a partial cancellation of the coefficient d_4 in Eq. (4.30c) (which acquires a non-zero value from RG running) against the dominant contribution from the Fermi constant for electron mixing. As the corresponding form factor f_4 scales with s, the resulting sensitivity to

electron mixing shrinks even further at higher energies. If sterile neutrinos are to be searched for via precision Higgs measurements, we therefore do not expect running a next-generation lepton collider at higher centre-of-mass energies to reveal much for Type-I.

On the other hand, the charged states $\Sigma^{\pm}$ in Type-III Seesaw induce the effective four-point interaction $\bar{\ell}\gamma^{\mu}P_L\ell Z_{\mu}h$ at tree-level through their t-channel exchange, resulting in a sizeable contribution to d_4. This generates a very pronounced sensitivity of the ratio $\Delta\sigma/\sigma_0$ to electron mixing which approximately scales with s. Consequently, if enough luminosity can be attained to compensate for smaller statistics, fermion triplets may well be searched for in Higgsstrahlung measurements at larger centre-of-mass energies. While the contributions from electron mixing could in principle be (partly) cancelled by large muon mixing, we will however find that this scenario is tightly constrained by existing phenomenological bounds. From Table 4.4 one can immediately deduce that if only electron mixing is sizeable, a minimal shift of $\Delta\sigma/\sigma_0 \geq 1\%$ for $\sqrt{s} = 240\,\text{GeV}$ requires $|\theta_e| \gtrsim 0.019$, whereas $|\theta_e| \gtrsim 0.013$ is sufficient for a shift of 0.5%, or if $\sqrt{s} = 365\,\text{GeV}$ is considered instead.

4.3.2 Electroweak Sector

When (α, m_Z, G_F) are used as electroweak inputs, the W boson mass m_W and the (squared sine of the) weak mixing angle $s_w^2 = \sin^2\theta_w$ become predicted quantities, and direct measurements of them function as precision tests of the SM. The fact that m_W and s_w^2 receive shifts in SMEFT means that we may appropriate these measurements to place constraints on the parameter spaces of the Seesaw models.

4.3.2.1 Weak Mixing Angle

In accordance with the parameter shifts recipe outlined in Section 3.2.1 of the previous chapter, the weak mixing angle receives the modification (see e.g. Ref. [191])

$$\delta s_w^2 = \frac{c_w s_w}{c_w^2 - s_w^2} v_T^2 \left(\frac{1}{2} c_w s_w C_{HD} + C_{HWB} + \sqrt{2} c_w s_w \delta \hat{G}_F \right), \tag{4.32}$$

where the shift in the Fermi constant $\delta \hat{G}_F$ is defined in Eq. (4.28). There are numerous ways to extract the weak mixing angle from data; the most precise determination is that of the *effective leptonic weak mixing angle* $s^2_{w,\text{eff}} \equiv \sin^2(\theta^{\text{lept}}_{w,\text{eff}})$ at LEP [272], achieved via measurements of the left-right asymmetry factor

$$\mathcal{A}_f = \frac{g_L^2 - g_R^2}{g_L^2 + g_R^2} = \frac{2(1 - 4s_w^2)}{1 + (1 - 4s_w^2)^2}. \tag{4.33}$$

Apart from the general shift in Eq. (4.32), we must also take into account the fact that a modification of the Z couplings to charged leptons will directly affect the extraction of $s^2_{w,\text{eff}}$ from $\mathcal{A}_f$. Incorporating the 'direct' shifts to these couplings,

$$\delta g^{\text{direct}}_{L,ij} = -\frac{1}{2} g_Z v_T^2 \left(C^{(1)}_{HL,ij} + C^{(3)}_{HL,ij} \right) \quad \text{and} \quad \delta g^{\text{direct}}_{R,ij} = -\frac{1}{2} g_Z v_T^2 C_{He,ij}, \tag{4.34}$$

we find

$$\begin{aligned} s^2_{w,\text{eff}} &= s^2_{w,\text{SM}} + \delta s_w^2 + \frac{1}{3} \frac{\mathrm{d}s_w^2}{\mathrm{d}\mathcal{A}_\ell} \left(\frac{\partial \mathcal{A}_\ell}{\partial g_L} \sum_{i=1}^{3} \delta g^{\text{direct}}_{L,ii} + \frac{\partial \mathcal{A}_\ell}{\partial g_R} \sum_{i=1}^{3} \delta g^{\text{direct}}_{R,ii} \right) \\ &\approx s^2_{w,\text{SM}} + 0.020 \left(\hat{C}^{(3)}_{HL,11} + \hat{C}^{(3)}_{HL,22} \right) - 0.005 \sum_{i=1}^{3} \left(\hat{C}^{(1)}_{HL,ii} + \hat{C}^{(3)}_{HL,ii} \right), \end{aligned} \tag{4.35}$$

where the right-hand side is evaluated at the scale $\mu = m_Z$. Contributions from C_{He} are not sourced at tree level in either Seesaw model, and so the shift is dominated by $C^{(1)}_{HL}$ and $C^{(3)}_{HL}$.

4.3.2.2 *W* Boson Mass

The shift incurred by m_W in SMEFT is [191]

$$\frac{\delta m_W^2}{m_W^2} = -\frac{1}{2(c_w^2 - s_w^2)} v_T^2 \left(4 c_w s_w C_{HWB} + c_w^2 C_{HD} + 2\sqrt{2} s_w^2 \delta \hat{G}_F \right), \tag{4.36}$$

Electroweak Sector				
Observable	SM prediction		Measurement	
$\sin^2(\theta^{\text{lept}}_{w,\text{eff}})$	0.231534 ± 0.000030	[273]	0.23153 ± 0.00026	[272]
m_W [GeV]	80.356 ± 0.006	[274]	80.377 ± 0.012	[274]

Shift	Type-I	Type-III
δs^2_w	$-0.157(\lvert\theta_e\rvert^2 + \lvert\theta_\mu\rvert^2) + 0.003\,\lvert\theta_\tau\rvert^2$	$0.017(\lvert\theta_e\rvert^2 + \lvert\theta_\mu\rvert^2) - 0.143\,\lvert\theta_\tau\rvert^2$
δm_W [GeV]	$8.24(\lvert\theta_e\rvert^2 + \lvert\theta_\mu\rvert^2) - 0.13\,\lvert\theta_\tau\rvert^2$	$-8.51(\lvert\theta_e\rvert^2 + \lvert\theta_\mu\rvert^2) - 0.13\,\lvert\theta_\tau\rvert^2$

Table 4.5: SM predictions for and current measurements of the electroweak observables considered in this work, together with approximate expressions for their shifts in terms of the mixing angles. The W boson mass listed by the Particle Data Group [274] corresponds to the mass parameter in a Breit-Wigner distribution with a mass-dependent width. The SM prediction for the effective leptonic weak mixing angle is taken from Table II in Ref. [273]. The model predictions are obtained from matching onto SMEFT at the Seesaw scale $\mu = M = 1\,\text{TeV}$ and running to the electroweak scale $\mu = m_Z$.

which approximately evaluates to

$$m_W \approx m_{W,\text{SM}} - 1.05\Big(\hat{C}^{(3)}_{HL,11} + \hat{C}^{(3)}_{HL,22}\Big)\,\text{GeV} \tag{4.37}$$

at the scale $\mu = m_Z$. With C_{HWB} and C_{HD} not induced at tree-level in the Seesaw models, the largest correction to m_W is due to the shift in the Fermi constant.

4.3.2.3 Discussion

The expressions obtained for $\delta s^2_{w,\text{eff}}$ and δm_W in terms of the mixing angles are listed in Table 4.5, and the constraints arising from these observables are illustrated in Fig. 4.4.

For Type-I Seesaw we immediately notice that the prospect of an observable shift to the Higgsstrahlung cross section is in direct conflict with the determination of $s^2_{w,\text{eff}}$, with a 0.5% shift at $\sqrt{s} = 240\,\text{GeV}$ suffering from a 2.9σ tension, and a 1% shift excluded at $\sim 6\sigma$. While this tension can be reduced by turning up θ_τ (see the expression in Table 4.5), LFU constraints discussed in Section 4.3.3 below preclude this from occurring. Thus, we can already conclude that the Type-I Seesaw model is unlikely to be a viable minimal

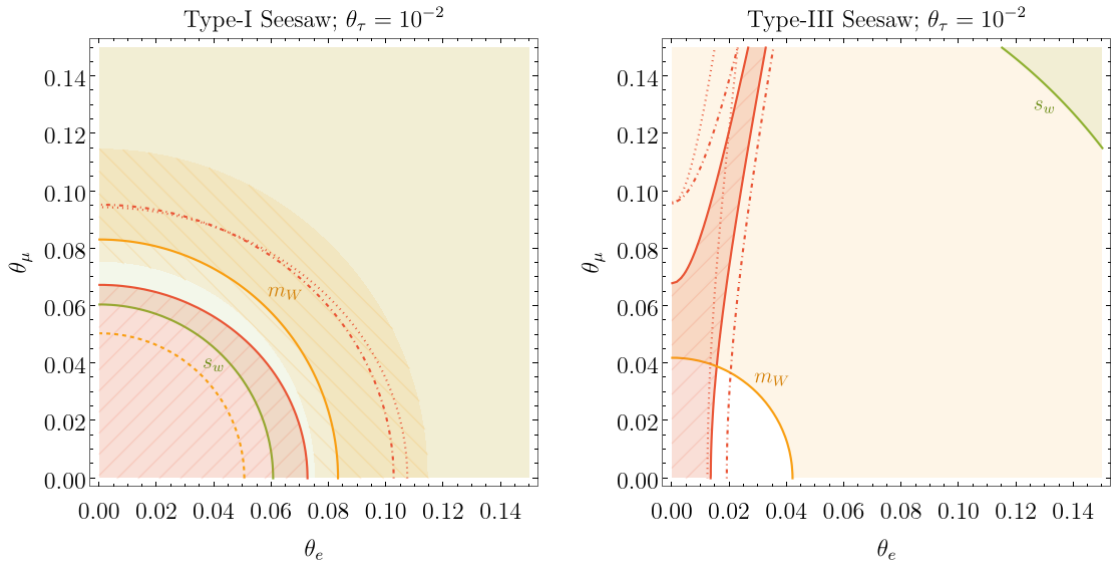

Figure 4.4: Current constraints from electroweak observables at 2σ, in comparison with projected sensitivities of precision Higgsstrahlung measurements. The red-ruled regions indicate $|\Delta\sigma/\sigma| < 0.5\%$ at $\sqrt{s} = 240\,\text{GeV}$. The dot-dashed and dotted red lines are the corresponding 1% contours at $\sqrt{s} = 240\,\text{GeV}$ and $365\,\text{GeV}$, respectively. For Type-I Seesaw, the dashed orange line marks where the current experimental world average for m_W is exactly accommodated, and in the orange-ruled region the CDF measurement [275] is explained at 2σ.

SM extension that can be probed in precision Higgs measurements, unless a significant reduction of the statistical uncertainty of these measurements can be attained.

In Type-III Seesaw, the direct contributions to the leptonic gauge couplings largely cancel against the shift from the Fermi constant in δs_w^2 for both the electron and muon flavour; see Eq. (4.35). As a result, $s^2_{w,\text{eff}}$ acts as a rather weak constraint on the Type-III model, and is in fact most relevant for tau-flavour mixing, implying $|\theta_\tau| \lesssim 0.06$ at 2σ.

The existing tension between the SM prediction for the W boson mass m_W and the larger experimental world average is however exacerbated in Type-III, leading to a much stronger constraint. In contrast, as $C^{(3)}_{HL}$ is induced with equal magnitude but opposite sign in Type-I, it offers to alleviate the existing tension; if uncertainties are ignored, the current world average is reproduced for $\sqrt{|\theta_e|^2 + |\theta_\mu|^2} \approx 0.051$, and the CDF measurement [275] for $\sqrt{|\theta_e|^2 + |\theta_\mu|^2} \approx 0.097$. A detectable shift in $\sigma(e^+e^- \to Zh)$ could in principle only be

induced in the latter case.

Testing the Type-III Seesaw model via Higgsstrahlung measurements is generally compatible with the current constraint arising from m_W, though it disfavours a detectable shift due to muon mixing, and preferring instead contributions from electron mixing. The bound from m_W can be expected to become more competitive when the CDF measurement is included in the experimental average in the future.

4.3.3 Lepton Flavour Universality

In the absence of neutrino masses—and hence the PMNS matrix—in the SM, the W boson couples with equal strength to each charged lepton and neutrino – a feature known as **lepton flavour universality** (LFU). Since we know neutrinos do in fact have mass, probes of LFU offer a fertile testing ground for BSM physics. These probes take the form of ratios of decay rates such as

$$\frac{\Gamma(\pi \to \mu\nu_\mu)}{\Gamma(\pi \to e\nu_e)}, \tag{4.38}$$

which, if kinematical factors and subdominant loop corrections are accounted for and removed, should be exactly equal to 1 unless LFU is violated.

LFU violation manifests in SMEFT through the operator $\mathcal{O}^{(3)}_{HL}$, which modifies the $W\ell\nu$ coupling to

$$\mathcal{L} \supset \frac{g_2}{\sqrt{2}}\left(\delta_{ij} + v_T^2 C^{(3)}_{HL,ij}\right)\overline{\ell_i}\not{W}^- P_L \nu_j + \text{h.c.} \tag{4.39}$$

In leveraging this against measured LFU ratios, we may place our second set of constraints on the parameter spaces of the Seesaw models. The ratios we will consider are those derived from the leptonic decays $\pi \to \ell\nu$, $K \to \ell\nu$, and $\tau \to \ell\nu\overline{\nu}$, and from (semi-)leptonic decays relating to the CKM matrix element V_{us}.

4.3.3.1 Ratios of Leptonic Gauge Couplings

Our first LFU ratios are those of the leptonic gauge couplings [276; 277],

$$g^X_{\mu/e} \equiv \left(\frac{g_\mu}{g_e}\right)^X \approx 1 + v_T^2 C^{(3)}_{HL,22} - v_T^2 C^{(3)}_{HL,11} \approx 1 + 0.06\left(\hat{C}^{(3)}_{HL,22} - \hat{C}^{(3)}_{HL,11}\right), \tag{4.40}$$

as extracted from[4]

$$g^X_{\mu/e} \leftrightarrow \begin{cases} \dfrac{\Gamma(X \to \mu\nu)}{\Gamma(X \to e\nu)} & X = W, \pi, K \\ \dfrac{\Gamma(\tau \to \mu\nu\bar{\nu})}{\Gamma(\tau \to e\nu\bar{\nu})} & X = \ell \end{cases}, \tag{4.41}$$

as well as

$$g^X_{\tau/\mu} \equiv \left(\frac{g_\tau}{g_\mu}\right)^X \approx 1 + 0.06\left(\hat{C}^{(3)}_{HL,33} - \hat{C}^{(3)}_{HL,22}\right), \tag{4.42}$$

extracted from

$$g^X_{\tau/\mu} \leftrightarrow \begin{cases} \dfrac{\Gamma(\tau \to \pi\nu)}{\Gamma(\pi \to \mu\nu)} & X = \pi \\ \dfrac{\Gamma(\tau \to e\nu\bar{\nu})}{\Gamma(\mu \to e\nu\bar{\nu})} & X = \ell \end{cases}. \tag{4.43}$$

The measured values and model predictions for these ratios are presented in Table 4.6, with the exception of $g^W_{\mu/e}$, which is omitted as it leads to weaker constraints than the other $g_{\mu/e}$ ratios.

In our Seesaw models the predicted deviation of these LFU ratios from 1 is at leading order proportional to $\pm(|\theta_i|^2 - |\theta_j|^2)$, with the sign depending on the model, and the derived constraints therefore give rise to hyperbolic contours in the θ_i–θ_j planes. If the data favours a ratio to be, say, smaller than 1, predicting it to be larger than 1 will clearly lead to a tighter constraint. This then translates into one of the mixing angles being slightly more

[4] As the dominant BSM contribution to these decays is due to the interference with the leading SM amplitude, we only need to consider final state neutrinos whose flavour matches that of the charged lepton – that is, we only need the diagonal entries of $C^{(3)}_{HL}$.

Lepton Flavour Universality			
Observable	Measurement		Model prediction
$g^{\pi}_{\mu/e}$	1.0010 ± 0.0009	[278]	$1 \pm 0.48(\lvert\theta_e\rvert^2 - \lvert\theta_\mu\rvert^2)$
$g^{\ell}_{\mu/e}$	1.0017 ± 0.0016	[278]	
$g^{K}_{\mu/e}$	0.9978 ± 0.0018	[278]	
$R(K_{\ell 3})$	1.001295 ± 0.002891	[279]	
$g^{\pi}_{\tau/\mu}$	0.9965 ± 0.0026	[278]	$1 \pm 0.48(\lvert\theta_\mu\rvert^2 - \lvert\theta_\tau\rvert^2)$
$g^{\ell}_{\tau/\mu}$	1.0011 ± 0.0014	[278]	
$R(V_{us})$	0.98898 ± 0.00606	[274]	$1 \pm 0.47\lvert\theta_e\rvert^2 \pm 8.80\lvert\theta_\mu\rvert^2 \mp 0.04\lvert\theta_\tau\rvert^2$

Table 4.6: Current constraints on and model predictions for the LFU ratios taken into account in this work. For $R(V_{us})$, the given experimental value refers to the case of $N_f = 2+1+1$ dynamical quark flavours in the lattice simulations from which the relevant decay constants are extracted. The case of $N_f = 2+1$ quark flavours gives rise to a less competitive bound [274]. The model predictions are obtained from matching onto SMEFT at the Seesaw scale $\mu = M = 1\,\text{TeV}$ and running to the electroweak scale $\mu = m_Z$. In the rightmost column, the upper sign refers to Type-I Seesaw, and the lower sign to Type-III Seesaw.

strongly bounded than the other one, with the roles reversed in the other Seesaw model. As a result, if the contribution from a specific mixing angle accommodates the data well in one model, the other model will necessarily increase the tension with the SM.

4.3.3.2 Light Quark Mixing

Our remaining LFU ratios are those of the CKM matrix element V_{us} extracted from the semi-leptonic kaon decays $K_{\mu 3} \equiv K \to \pi\mu\nu$ and $K_{e3} \equiv K \to \pi e\nu$, the leptonic kaon decay $K_{\mu 2} \equiv K \to \mu\nu$, and nuclear beta decay $\beta \equiv n \to pe\nu$:

$$R(K_{\ell 3}) \equiv \frac{V_{us}^{K_{\mu 3}}}{V_{us}^{K_{e3}}} \quad \text{and} \quad R(V_{us}) \equiv \frac{V_{us}^{K_{\mu 2}}}{V_{us}^{\beta}}. \tag{4.44}$$

The dependence of $R(K_{\ell 3})$ on new physics is identical to that of $g^{\pi}_{\mu/e}$ and $g^{K}_{\mu/e}$, of which both can similarly be viewed as CKM ratios, with $g^{K}_{\mu/e}$ being commonly denoted by $R(K_{\ell 2})$.

The ratio $R(V_{us})$, on the other hand, is a special case deserving of additional attention. To understand it, we note that the decay rate for $K \to \mu\nu$ in the SM is

$$\Gamma(K \to \mu\nu) = A|V_{us}|^2 G_F^2, \tag{4.45}$$

where A contains all other factors; the CKM element V_{us} is then extracted as

$$V_{us} = \sqrt{\frac{\Gamma}{A G_F^2}}. \tag{4.46}$$

In SMEFT, the decay rate is modified to

$$\Gamma(K \to \mu\nu) = A|V_{us}|^2 \bar{G}_F^2 \left(1 + 2v_T^2 C_{HL,22}^{(3)}\right) \tag{4.47}$$

$$= A|V_{us}|^2 \hat{G}_F^2 \left(1 + 2v_T^2 C_{HL,22}^{(3)} - 2\frac{\delta \hat{G}_F}{G_F}\right), \tag{4.48}$$

where the $C_{HL,22}^{(3)}$ is due to the new direct contribution, Eq. (4.39), and in the notation of the previous chapter (see Table 3.2 for a reminder), the Lagrangian parameter $\bar{G}_F$ relates to the measured value of $\hat{G}_F$ by $\bar{G}_F = \hat{G}_F - \delta\hat{G}_F$. This being the case, the extracted value of V_{us} is actually[5]

$$V_{us}^{K_{\mu 2}} = \sqrt{\frac{\Gamma}{A \hat{G}_F^2}} = V_{us}\left(1 + v_T^2 C_{HL,22}^{(3)} - \frac{\delta \hat{G}_F}{G_F}\right). \tag{4.49}$$

Similarly, beta decay results in

$$V_{ud}^{\beta} = V_{ud}\left(1 + v_T^2 C_{HL,11}^{(3)} - \frac{\delta \hat{G}_F}{G_F}\right), \tag{4.50}$$

and through unitarity of the Lagrangian CKM parameters, it translates to

$$V_{us}^{\beta} = \sqrt{1 - |V_{ud}^{\beta}|^2 - |V_{ub}|^2} \approx V_{us}\left[1 - \left(\frac{V_{ud}}{V_{us}}\right)^2 \left(v_T^2 C_{HL,11}^{(3)} - \frac{\delta \hat{G}_F}{G_F}\right)\right]. \tag{4.51}$$

Bringing the two together then gives the ratio

[5] This result is reproduced by the general formula of Eq. (3.52) upon identifying $(V_{us})_{\text{SMEFT}} = V_{us}$ and $(V_{us})_{\text{SM}} = V_{us}^{K_{\mu 2}}$.

$$R(V_{us}) = \frac{V_{us}^{K_{\mu 2}}}{V_{us}^{\beta}} = 1 + v_T^2 C_{HL,22}^{(3)} - \frac{\delta \hat{G}_F}{G_F} + \left(\frac{V_{ud}}{V_{us}}\right)^2 \left(v_T^2 C_{HL,11}^{(3)} - \frac{\delta \hat{G}_F}{G_F}\right) \tag{4.52}$$
$$\approx 1 - v_T^2 \left[\left(\frac{V_{ud}}{V_{us}}\right)^2 C_{HL,22}^{(3)} + C_{HL,11}^{(3)}\right].$$

As is explained in Ref. [276], wherein the ratio was originally proposed, a crucial feature of $R(V_{us})$ is the enhanced sensitivity to new physics due to $(V_{ud}/V_{us})^2 \approx 20$. Experimental data favours the ratio to be smaller than 1 with a significance between 1σ and 2σ, depending on the number of quark flavours assumed for the calculation of the relevant decay constant; see Table 4.6.

4.3.3.3 Discussion

The constraints arising from LFU ratios are illustrated in Fig. 4.5. In Type-I Seesaw, the prospects of an observational shift in the Higgsstrahlung cross section are once again at odds with the data, with $R(V_{us})$ acting as an even stronger restraint on the available parameter space than s_w^2. The next-to-most competitive bounds on electron and muon mixing respectively arise from $g_{\mu/e}^K$ and $g_{\mu/e}^\pi$.

In the case of Type-III Seesaw, the most important constraints stem from $g_{\mu/e}^\pi$ and $R(V_{us})$, which demand $|\theta_e| \lesssim 0.04$ and $|\theta_\mu| \lesssim 0.05$ at 2σ, respectively. In a vein similar to m_W, the bounds from $g_{\mu/e}^K$ and $R(V_{us})$ both constrain muon mixing efficiently enough so that no appreciable cancellations of the contributions to Higgsstrahlung from electron mixing can occur.

As can be seen in Fig. 4.5b, LFU data constrains tau mixing to $|\theta_\tau| \lesssim 0.06$ for either Seesaw model, which arises from $g_{\tau/\mu}^\ell$ in Type-I, and $g_{\tau/\mu}^\pi$ for Type-III. These constraints can in principle be weakened if $|\theta_\mu|$ is more sizeable; still, large changes are only observed for $\mathcal{O}(0.1)$ muon mixing, a scenario which is nonetheless excluded by other observables. While the contributions to $R(V_{us})$ from electron and tau mixing may cancel, this does not open up parameter space in Type-I, as tau mixing itself is too constrained.

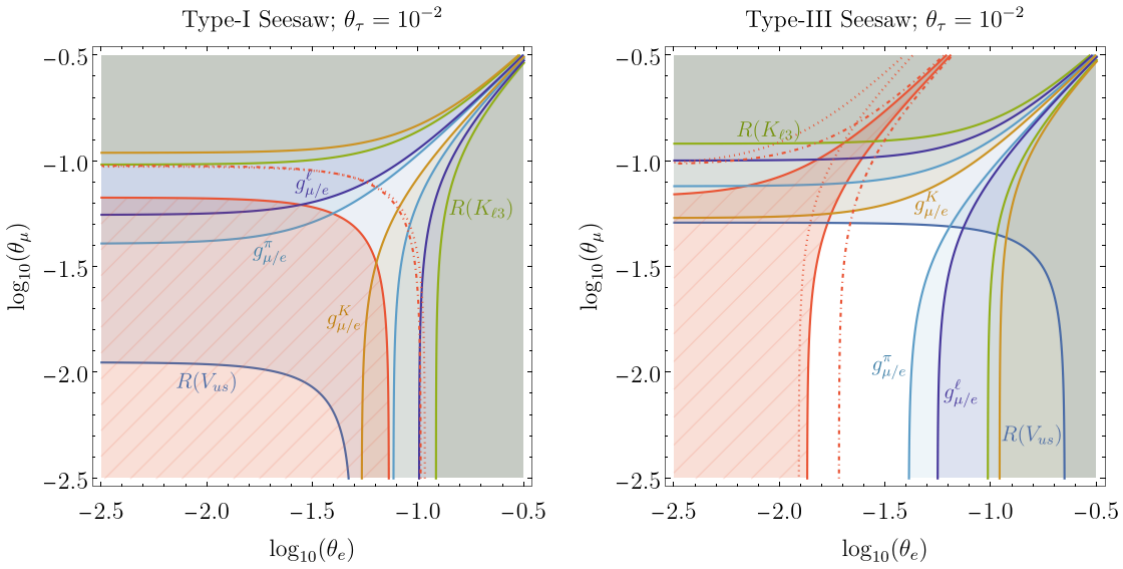

(a) LFU constraints in the θ_e–θ_μ plane.

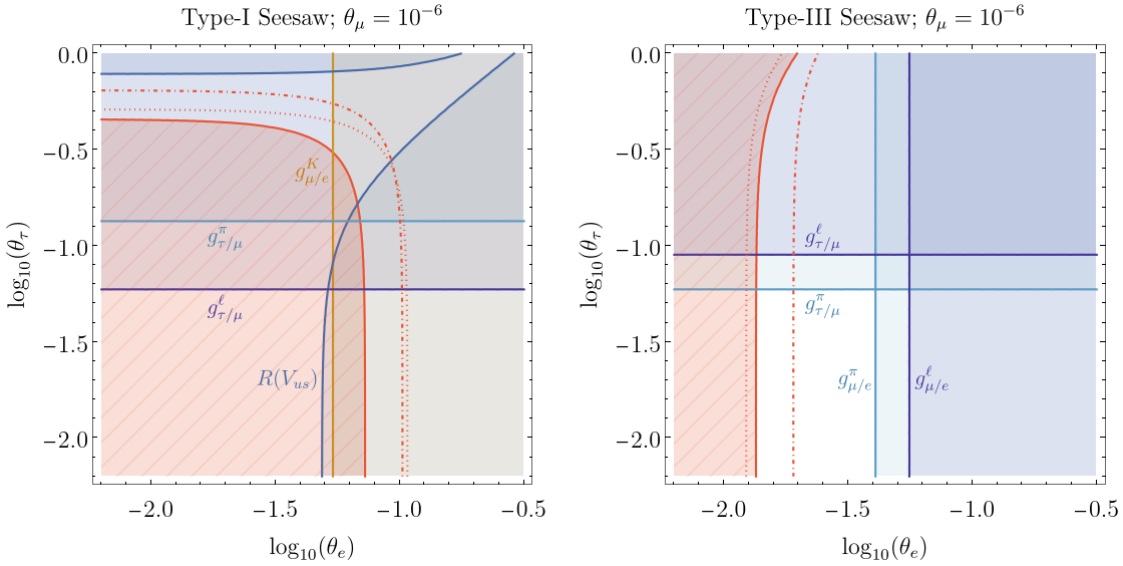

(b) LFU constraints in the θ_e–θ_τ plane. To avoid clutter, subdominant constraints like the one from $R(K_{\ell 3})$ are not drawn, but their locations may be inferred from the above plots.

Figure 4.5: Current constraints arising from LFU ratios at 2σ in comparison with projected sensitivities of precision Higgsstrahlung measurements. The red-ruled regions indicate $|\Delta\sigma/\sigma| < 0.5\%$ at $\sqrt{s} = 240\,\text{GeV}$. The dot-dashed and dotted red lines are the corresponding 1% contours at $\sqrt{s} = 240\,\text{GeV}$ and $365\,\text{GeV}$, respectively.

Further LFU ratios not contained in Table 4.6 deviate from the SM prediction by close to 2σ and thus present moderate anomalies in themselves, see Ref. [278]. Explicitly, $g^K_{\tau/\mu}$ is measured to be smaller than 1, while $g^\ell_{\tau/e}$ and $g^W_{\tau/e}$ exceed the SM expectation. If the models under consideration are to accommodate the data on $g^K_{\tau/\mu}$, one requires $|\theta_\tau| > |\theta_\mu|$ for Type-I Seesaw, and vice-versa for Type-III Seesaw. The restriction $|\theta_\mu| > |\theta_\tau|$ is unlikely to be satisfied in Type-III for scenarios which are testable via Higgsstrahlung measurements, as a large $\Delta\sigma/\sigma_0$ induced by electron mixing demands muon mixing to be very small due to the bounds arising from LFV, as we will see in the next section. Similarly, the other two ratios necessitate that tau mixing substantially exceeds electron mixing in Type-III – a similarly unpromising scenario, particularly in light of the bound on $\mathrm{BR}(\tau \to 3e)$.

4.3.4 Lepton Flavour Violation

For our next set of constraints we turn to a particularly potent probe of BSM physics: that of **lepton flavour violation** (LFV). The premise behind LFV searches is found in the fact that lepton flavour is conserved in the SM on account of the three $\mathrm{U}(1)_{L_i}$ symmetries,[6] which take

$$L_i \to e^{\mathrm{i}\theta_i} L_i \quad \text{and} \quad e_{Ri} \to e^{\mathrm{i}\theta_i} e_{Ri}, \tag{4.53}$$

or equivalently

$$\ell_i \to e^{\mathrm{i}\theta_i} \ell_i \quad \text{and} \quad \nu_{Li} \to e^{\mathrm{i}\theta_i} \nu_{Li}. \tag{4.54}$$

Much akin to LFU violation, the observed neutrino masses and mixings signal that these symmetries are in fact violated, meaning it should in principle be possible to observe flavour-violating decays such as $\mu^\pm \to e^\pm\gamma$ or $\tau^- \to e^-e^-e^+$ (or $\tau \to 3e$ for short), or the conversion of muons to electrons in scatterings with nuclei. As is generically the case for models of

[6] Though these symmetries are anomalous [122; 157; 158], the consequent rate of flavour violation in the SM is unobservably small [280]. The partial baryon-minus-lepton numbers $B/3 - L_i$ are better symmetries, but this strays beyond relevance to the present discussion.

Lepton Flavour Violation						
Observable	Experiment				Model predictions	
	Current bound		Future reach		Type-I	Type-III
BR($\mu \to e\gamma$)	4.2×10^{-13}	[282]	6×10^{-14}	[283]	$0.82 \times 10^{-3}\,\lvert\theta_e\theta_\mu\rvert^2$	$1.27 \times 10^{-3}\,\lvert\theta_e\theta_\mu\rvert^2$
BR($\mu \to 3e$)	1×10^{-12}	[284]	1×10^{-16}	[285]	$0.14 \times 10^{-3}\,\lvert\theta_e\theta_\mu\rvert^2$	$0.72\,\lvert\theta_e\theta_\mu\rvert^2$
CR($\mu - e$; Au)	7×10^{-13}	[286]	—		$0.04 \times 10^{-3}\,\lvert\theta_e\theta_\mu\rvert^2$	$27.1\,\lvert\theta_e\theta_\mu\rvert^2$
CR($\mu - e$; Al)	—		2.6×10^{-17} 8×10^{-17}	[287] [288]	$0.15 \times 10^{-3}\,\lvert\theta_e\theta_\mu\rvert^2$	$6.7\,\lvert\theta_e\theta_\mu\rvert^2$
CR($\mu - e$; Ti)	6.1×10^{-13}	[289]	$\mathcal{O}(10^{-18})$	[290]	$0.18 \times 10^{-3}\,\lvert\theta_e\theta_\mu\rvert^2$	$13.5\,\lvert\theta_e\theta_\mu\rvert^2$
CR($\mu - e$; Pb)	4.6×10^{-11}	[291]	—		$0.02 \times 10^{-3}\,\lvert\theta_e\theta_\mu\rvert^2$	$20.3\,\lvert\theta_e\theta_\mu\rvert^2$
CR($\mu - e$; S)	7×10^{-11}	[292]	—		$0.21 \times 10^{-3}\,\lvert\theta_e\theta_\mu\rvert^2$	$6.4\,\lvert\theta_e\theta_\mu\rvert^2$
BR($\tau \to e\gamma$)	3.3×10^{-8}	[293]	9×10^{-9}	[294]	$0.15 \times 10^{-3}\,\lvert\theta_e\theta_\tau\rvert^2$	$0.23 \times 10^{-3}\,\lvert\theta_e\theta_\tau\rvert^2$
BR($\tau \to 3e$)	2.7×10^{-8}	[295]	4.7×10^{-10}	[294]	$0.02 \times 10^{-3}\,\lvert\theta_e\theta_\tau\rvert^2$	$0.13\,\lvert\theta_e\theta_\tau\rvert^2$

Table 4.7: Current and projected constraints on the LFV observables taken into account in this work, together with the model predictions. The current bounds hold at 90% C.L. The future reach listed for BR($\mu \to 3e$) refers to Phase II of the Mu3e experiment; an initial sensitivity of BR($\mu \to 3e$) $\lesssim 2 \times 10^{-15}$ is expected after Phase I. The upper (lower) value listed for the future reach of CR($\mu - e$; Al) refers to COMET (Mu2e). The model predictions are obtained from matching onto SMEFT at the Seesaw scale $\mu = M = 1\,\text{TeV}$, running to the electroweak scale $\mu = m_Z$, matching onto LEFT and running to the low scale $\mu = 5\,\text{GeV}$.

neutrino mass generation, the Seesaw models predict sizeable rates for these flavour-violating decays and scatterings, and the to-date non-observation of these processes thus imparts stringent bounds on their parameter spaces. These bounds will likely be further refined in the near future due to several ongoing or upcoming experiments – see Table 4.7. Since our focus is on the comparison with the sensitivities to the Higgsstrahlung process at colliders, we restrict ourselves to observables involving electron-flavoured transitions. A comprehensive investigation of LFV effects in the symmetry-protected Type-I Seesaw model can for instance be found in Ref. [281].

In SMEFT, LFV manifests through the off-diagonal entries of Wilson coefficients such as $C_{HL}^{(1)}$ and $C_{HL}^{(3)}$. Since the scales involved in the flavour-violating processes we consider are far removed from the electroweak scale, it is however more appropriate to discuss them in terms of LEFT operators. The explicit matching conditions between SMEFT and LEFT used in this section can be found in Section 4.A in the appendix of this chapter.

4.3.4.1 Radiative Charged Lepton Decays

The branching ratios for radiative flavour-violating charged lepton decays read [296]

$$\mathrm{BR}(\ell_i \to \ell_j \gamma) = \frac{m_{\ell_i}^3}{4\pi\Gamma_{\ell_i}} \left(|C_{e\gamma,ij}|^2 + |C_{e\gamma,ji}|^2 \right), \tag{4.55}$$

with the full decay width Γ_{ℓ_i}. With the matching of SMEFT onto LEFT and the RG running accounted for, this approximately evaluates to

$$\begin{aligned} \mathrm{BR}(\mu \to e\gamma) &\approx 7.117 \times 10^6 \left| \hat{C}_{eB,12} - 0.55\, \hat{C}_{eW,12} + \left(1.77\, \hat{C}^{(3)}_{HL,12} - 0.48\, \hat{C}^{(1)}_{HL,12} \right) 10^{-6} \right|^2 \text{ and} \\ \mathrm{BR}(\tau \to e\gamma) &\approx 0.004 \times 10^6 \left| \hat{C}_{eB,13} - 0.55\, \hat{C}_{eW,13} + \left(29.69\, \hat{C}^{(3)}_{HL,13} - 8.12\, \hat{C}^{(1)}_{HL,13} \right) 10^{-6} \right|^2 \end{aligned} \tag{4.56}$$

in the Seesaw models, where the SMEFT Wilson coefficients are evaluated at the electroweak scale $\mu = m_Z$. In both models the one-loop matching contributions to the electromagnetic dipole operator $\mathcal{O}_{e\gamma}$ from the electroweak dipole operators $\mathcal{O}_{eB}$ and $\mathcal{O}_{eW}$ are of the same order of magnitude as the contributions from $\mathcal{O}^{(1)}_{HL}$ and $\mathcal{O}^{(3)}_{HL}$ which originate from RG running; see also Eq. (4.63) in the appendix.

4.3.4.2 Trilepton Decays

The branching ratio for trilepton decays with identical flavours in the final state is given by [297][7]

$$\begin{aligned} \mathrm{BR}(\ell_i \to \ell_j \ell_j \overline{\ell_j}) = \frac{m_{\ell_i}^5}{3(16\pi)^3 \Gamma_{\ell_i}} \Bigg[& 64 \left| C^{VLL}_{ee,jijj} \right|^2 + 64 \left| C^{VRR}_{ee,jijj} \right|^2 + 8 \left| C^{VLR}_{ee,jijj} \right|^2 + 8 \left| C^{VLR}_{ee,jjji} \right|^2 \\ & + \frac{256 e^2}{m_{\ell_i}^2} \left(\ln \frac{m_{\ell_i}^2}{m_{\ell_j}^2} - \frac{11}{4} \right) \left(\left| C^{ij}_{e\gamma} \right|^2 + \left| C^{ji}_{e\gamma} \right|^2 \right) \\ & - \frac{64 e}{m_{\ell_i}} \mathrm{Re} \left[\left(4\, C^{VLL}_{ee,jijj} + C^{VLR}_{ee,jijj} \right) C^{ji*}_{e\gamma} + \left(4\, C^{VRR}_{ee,jijj} + C^{VLR}_{ee,jjji} \right) C^{ij}_{e\gamma} \right] \Bigg]. \end{aligned} \tag{4.57}$$

[7] See also Refs. [296; 298] for earlier work. In the case of τ decays, we should not expect significantly stronger constraints if some of the final state electrons are swapped for muons.

In Type-III Seesaw, these decays are dominated by the vector operators $\mathcal{O}_{ee}^{VLL}$ and $\mathcal{O}_{ee}^{VLR}$, which receive large contributions in the tree-level matching onto SMEFT, and then onto LEFT (see Section 4.A). By neglecting all Wilson coefficients apart from $C_{ee,jijj}^{VLL}$ and $C_{ee,jijj}^{VLR}$, we thus find

$$\mathrm{BR}(\mu \to 3e) \approx 1.2 \times 10^{-4} \left[64 \left| 0.27 \left(\hat{C}_{HL,12}^{(1)} + \hat{C}_{HL,12}^{(3)} \right) \right|^2 + 8 \left| 0.49 \left(\hat{C}_{HL,12}^{(1)} + \hat{C}_{HL,12}^{(3)} \right) \right|^2 \right] \tag{4.58}$$

and

$$\mathrm{BR}(\tau \to 3e) \approx 0.2 \times 10^{-4} \left[64 \left| 0.27 \left(\hat{C}_{HL,13}^{(1)} + \hat{C}_{HL,13}^{(3)} \right) \right|^2 + 8 \left| 0.49 \left(\hat{C}_{HL,13}^{(1)} + \hat{C}_{HL,13}^{(3)} \right) \right|^2 \right], \tag{4.59}$$

where the SMEFT Wilson coefficients on the right are evaluated at the scale $\mu = m_Z$. In Type-I Seesaw, the above combinations of coefficients are zero at the matching scale, and only depart from zero at $\mu = m_Z$ due to RG running. In this case, the branching ratios are relatively more sensitive to the contributions from the electromagnetic dipole operator $\mathcal{O}_{e\gamma}$, and the above approximations are only accurate to about 20%.

4.3.4.3 $\mu - e$ Conversion in Nuclei

Our third probe of LFV—the conversion between lepton flavours in scatterings with nuclei—enters the murky world of nuclear physics, where many complicated effects become important and the physics is often best expressed in terms of various form factors. Fortunately for us, as the scalar and gluon operators are suppressed in the fermionic Seesaw models, the $\mu - e$ conversion rate in nuclei takes the simple form [299; 300]

$$\omega_{\mathrm{conv}} = \left| -\frac{C_{e\gamma,12}}{2m_\mu} D + \tilde{g}_{LV}^{(p)} V^{(p)} + \tilde{g}_{LV}^{(n)} V^{(n)} \right|^2 + \left| -\frac{C_{e\gamma,21}^*}{2m_\mu} D + \tilde{g}_{RV}^{(p)} V^{(p)} + \tilde{g}_{RV}^{(n)} V^{(n)} \right|^2 , \tag{4.60}$$

where the overlap integrals D, $V^{(p)}$ and $V^{(n)}$ can be found in Refs. [299; 301], and the

effective coupling constants are

$$\tilde{g}_{LV}^{(p)} = 2\left(C_{eu,1211}^{VLL} + C_{eu,1211}^{VLR}\right) + \left(C_{ed,1211}^{VLL} + C_{ed,1211}^{VLR}\right), \tag{4.61a}$$

$$\tilde{g}_{RV}^{(p)} = 2\left(C_{eu,1211}^{VRR} + C_{ue,1112}^{VLR}\right) + \left(C_{ed,1211}^{VRR} + C_{de,1112}^{VLR}\right), \tag{4.61b}$$

$$\tilde{g}_{LV}^{(n)} = \left(C_{eu,1211}^{VLL} + C_{eu,1211}^{VLR}\right) + 2\left(C_{ed,1211}^{VLL} + C_{ed,1211}^{VLR}\right), \quad \text{and} \tag{4.61c}$$

$$\tilde{g}_{RV}^{(n)} = \left(C_{eu,1211}^{VRR} + C_{ue,1112}^{VLR}\right) + 2\left(C_{ed,1211}^{VRR} + C_{de,1112}^{VLR}\right); \tag{4.61d}$$

see Section 4.A for approximate matching expressions.

We are interested in the conversion ratio $\mathrm{CR}(\mu \to e)$, defined as the ratio of the $\mu - e$ conversion rate ω_{conv} over the muon capture rate ω_{capt}. Using the values for ω_{capt} given in Refs. [299; 301], the conversion ratio in the Seesaw models approximates to

$$\begin{aligned}\mathrm{CR}(\mu \to e) \approx \left(\frac{m_\mu}{\mathrm{GeV}}\right)^5 \left\{\begin{array}{c} 5.87 \\ 1.16 \\ 21.54 \end{array}\right\} \times 10^5 \\ \times \left| \left[2\left(\hat{C}_{eu,1211}^{VLL} + \hat{C}_{eu,1211}^{VLR}\right) + \left(\hat{C}_{ed,1211}^{VLL} + \hat{C}_{ed,1211}^{VLR}\right)\right] \left\{\begin{array}{c} 0.0396 \\ 0.0974 \\ 0.0161 \end{array}\right\} \right. \\ \left. + \left[\left(\hat{C}_{eu,1211}^{VLL} + \hat{C}_{eu,1211}^{VLR}\right) + 2\left(\hat{C}_{ed,1211}^{VLL} + \hat{C}_{ed,1211}^{VLR}\right)\right] \left\{\begin{array}{c} 0.0468 \\ 0.146 \\ 0.0173 \end{array}\right\} \right|^2,\end{aligned} \tag{4.62}$$

where the Wilson coefficients on the right are evaluated at the low scale $\mu = 5\,\mathrm{GeV}$, and where the upper, middle and lower entry in the braces refers to a titanium (Ti), gold (Au) and aluminium (Al) target, respectively. Though the predictions for the conversion ratios for lead (Pb) and sulfur (S) are also featured in Table 4.7, we can infer that the current bounds from these elements do not impose relevant constraints. As is reflected by the above approximation, $\mu - e$ conversion is dominated by contributions from left-handed vector operators in both Seesaw models. This is evident in Type-III where these contributions are sourced at tree level, but also holds in Type-I. The electromagnetic dipole operator $\mathcal{O}_{e\gamma}$ plays a subdominant role in both models.

4.3.4.4 Discussion

The current and projected constraints due to the non-observation of LFV are pictured in Fig. 4.6. For both Seesaw models, these constraints impose a pronounced hierarchy between $|\theta_e|$ and $|\theta_\mu|$ if we wish to have an observable shift in the Higgsstrahlung cross section (though of course this is not so relevant for Type-I, where such a scenario has already been ruled out by earlier considerations), as well as a slight hierarchy between $|\theta_e|$ and $|\theta_\tau|$.

In Type-I Seesaw, the most competitive bounds currently arise from $\mu \to e\gamma$ and $\tau \to e\gamma$. Future measurements of $\mathrm{BR}(\mu \to 3e)$ and $\mathrm{CR}(\mu - e)$ are expected to improve the θ_e–θ_μ bound by two orders of magnitude, while more precise measurements of $\mathrm{BR}(\tau \to 3e)$ and $\mathrm{BR}(\tau \to e\gamma)$ will likely improve the θ_e–θ_τ bound by less than an order of magnitude. Interestingly, the LFV bounds for Type-I shuffle around when the Seesaw scale is raised on account of the fine-tuned manner in which the model predictions depend on the RG running of the SMEFT operators – for example, $\mathrm{CR}(\mu - e; \mathrm{Au})$ is tremendously enhanced when $M = 10\,\mathrm{TeV}$. A lucid discussion of this effect can be found for instance in Ref. [302], and we will also have more to say in Section 4.3.5.

In Type-III Seesaw, the bounds from $\mathrm{BR}(\mu \to 3e)$ and $\mathrm{CR}(\mu - e)$ are stricter than that of $\mathrm{BR}(\mu \to e\gamma)$ due to tree-level contributions to the respective pertinent operators, and $\tau \to 3e$ is similarly more competitive than $\tau \to e\gamma$. (In fact, the projected sensitivities of $\mathrm{BR}(\mu \to e\gamma)$ and $\mathrm{BR}(\tau \to e\gamma)$ cannot even be expected to supersede the current bounds.) The strongest current bound on θ_e–θ_μ mixing, from $\mu - e$ conversion in gold, enforces the hierarchy $|\theta_\mu/\theta_e| \lesssim 10^{-3}$ for an observable shift to Higgsstrahlung, and if $\mu \to 3e$ and $\mu - e$ conversion in aluminium are not detected by the Mu3e and COMET experiments, respectively, then the required hierarchy may increase to $|\theta_\mu/\theta_e| \lesssim 10^{-5}$. In a similar vein, the limit on $|\theta_\tau|$ may be strengthened by an order of magnitude if $\tau \to 3e$ is not observed by Belle II, necessitating a hierarchy of $|\theta_\tau/\theta_e| \lesssim 10^{-1}$.

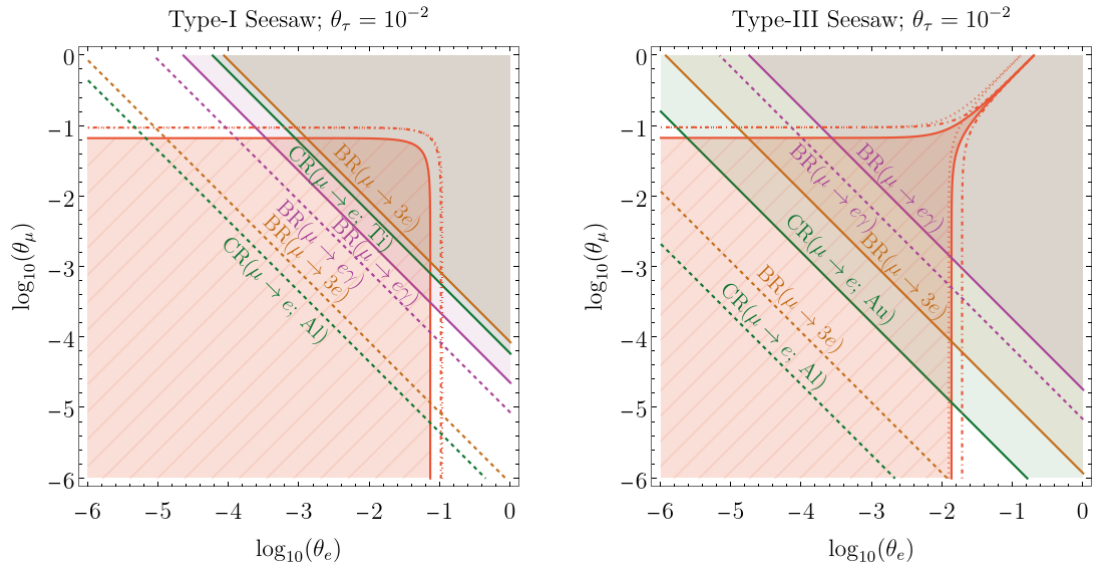

(a) LFV constraints in the θ_e–θ_μ plane. To minimise clutter, only the most competitive bounds are displayed. The PRISM/PRIME proposal [290] may even further extend the new-physics reach of $\mu - e$ conversion.

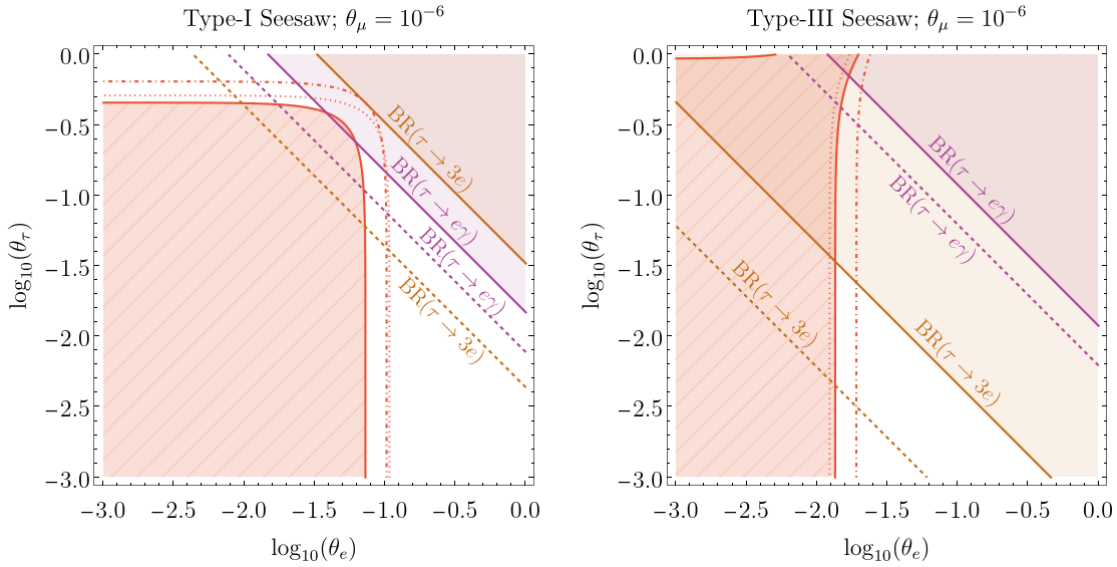

(b) LFV constraints in the θ_e–θ_τ plane.

Figure 4.6: Current constraints from LFV observables depicted at 90% C.L., together with their prospective future reaches, in comparison with projected sensitivities of precision Higgsstrahlung measurements. The red-ruled regions indicate $|\Delta\sigma/\sigma| < 0.5\%$ at $\sqrt{s} = 240\,\text{GeV}$. The dot-dashed and dotted red lines are the corresponding 1% contours at $\sqrt{s} = 240\,\text{GeV}$ and 365 GeV, respectively. The bounds from tau-flavoured processes are not shown in the θ_e–θ_μ plots, and vice versa. If included, they would appear as vertical lines with positioning highly dependent on the choice of the third mixing angle, which limits their relevance.

	Type-I	Type-III
$\Delta\sigma/\sigma_0$ (240 GeV)	$0.74\,\lvert\theta_e\rvert^2 + 1.11\,\lvert\theta_\mu\rvert^2 + 0.06\,\lvert\theta_\tau\rvert^2$	$26.30\,\lvert\theta_e\rvert^2 - 1.07\,\lvert\theta_\mu\rvert^2 - 0.01\,\lvert\theta_\tau\rvert^2$
$\Delta\sigma/\sigma_0$ (365 GeV)	$0.41\,\lvert\theta_e\rvert^2 + 1.18\,\lvert\theta_\mu\rvert^2 + 0.12\,\lvert\theta_\tau\rvert^2$	$63.12\,\lvert\theta_e\rvert^2 - 1.09\,\lvert\theta_\mu\rvert^2 - 0.03\,\lvert\theta_\tau\rvert^2$
$\Delta\sigma/\sigma_0$ (500 GeV)	$-0.05\,\lvert\theta_e\rvert^2 + 1.26\,\lvert\theta_\mu\rvert^2 + 0.19\,\lvert\theta_\tau\rvert^2$	$120.66\,\lvert\theta_e\rvert^2 - 1.11\,\lvert\theta_\mu\rvert^2 - 0.05\,\lvert\theta_\tau\rvert^2$
δs_w^2	$-0.151(\lvert\theta_e\rvert^2 + \lvert\theta_\mu\rvert^2) + 0.005\,\lvert\theta_\tau\rvert^2$	$0.021(\lvert\theta_e\rvert^2 + \lvert\theta_\mu\rvert^2) - 0.135\,\lvert\theta_\tau\rvert^2$
δm_W/GeV	$7.95(\lvert\theta_e\rvert^2 + \lvert\theta_\mu\rvert^2) - 0.24\,\lvert\theta_\tau\rvert^2$	$-8.44(\lvert\theta_e\rvert^2 + \lvert\theta_\mu\rvert^2) - 0.24\,\lvert\theta_\tau\rvert^2$
$g^X_{\mu/e}$	$1 + 0.47(\lvert\theta_e\rvert^2 - \lvert\theta_\mu\rvert^2)$	$1 - 0.47(\lvert\theta_e\rvert^2 - \lvert\theta_\mu\rvert^2)$
$g^X_{\tau/\mu}$	$1 + 0.47(\lvert\theta_\mu\rvert^2 - \lvert\theta_\tau\rvert^2)$	$1 - 0.47(\lvert\theta_\mu\rvert^2 - \lvert\theta_\tau\rvert^2)$
$R(V_{us})$	$1 + 0.44\,\lvert\theta_e\rvert^2 + 8.58\,\lvert\theta_\mu\rvert^2 - 0.07\,\lvert\theta_\tau\rvert^2$	$1 - 0.44\,\lvert\theta_e\rvert^2 - 8.58\,\lvert\theta_\mu\rvert^2 + 0.07\,\lvert\theta_\tau\rvert^2$
$\mathrm{BR}(\mu \to e\gamma)$	$0.80 \times 10^{-3}\,\lvert\theta_e\theta_\mu\rvert^2$	$1.21 \times 10^{-3}\,\lvert\theta_e\theta_\mu\rvert^2$
$\mathrm{BR}(\mu \to 3e)$	$0.34 \times 10^{-3}\,\lvert\theta_e\theta_\mu\rvert^2$	$0.66\,\lvert\theta_e\theta_\mu\rvert^2$
$\mathrm{CR}(\mu \to e; \mathrm{Au})$	$0.94 \times 10^{-3}\,\lvert\theta_e\theta_\mu\rvert^2$	$24.7\,\lvert\theta_e\theta_\mu\rvert^2$
$\mathrm{CR}(\mu \to e; \mathrm{Al})$	$0.03 \times 10^{-3}\,\lvert\theta_e\theta_\mu\rvert^2$	$6.1\,\lvert\theta_e\theta_\mu\rvert^2$
$\mathrm{CR}(\mu \to e; \mathrm{Ti})$	$0.15 \times 10^{-3}\,\lvert\theta_e\theta_\mu\rvert^2$	$12.3\,\lvert\theta_e\theta_\mu\rvert^2$
$\mathrm{CR}(\mu \to e; \mathrm{Pb})$	$0.76 \times 10^{-3}\,\lvert\theta_e\theta_\mu\rvert^2$	$18.5\,\lvert\theta_e\theta_\mu\rvert^2$
$\mathrm{CR}(\mu \to e; \mathrm{S})$	$0.01 \times 10^{-3}\,\lvert\theta_e\theta_\mu\rvert^2$	$5.8\,\lvert\theta_e\theta_\mu\rvert^2$
$\mathrm{BR}(\tau \to e\gamma)$	$0.15 \times 10^{-3}\,\lvert\theta_e\theta_\tau\rvert^2$	$0.23 \times 10^{-3}\,\lvert\theta_e\theta_\tau\rvert^2$
$\mathrm{BR}(\tau \to 3e)$	$0.06 \times 10^{-3}\,\lvert\theta_e\theta_\tau\rvert^2$	$0.12\,\lvert\theta_e\theta_\tau\rvert^2$

Table 4.8: Contributions to the observables considered in the phenomenology study in this work, but obtained from matching onto SMEFT at a Seesaw scale $\mu = M = 10\,\mathrm{TeV}$.

4.3.5 Larger Seesaw Scale

Lastly, it is worth commenting on the scenario with a larger matching scale. The model predictions for all observables considered in this chapter, given the increased Seesaw scale $M = 10\,\mathrm{TeV}$, are collected in Table 4.8.

In the case of the Type-III Seesaw model, our discussed results appear to be fairly robust under the raising of the triplet mass scale, at least to $\mathcal{O}(10\,\mathrm{TeV})$ – that is, the numerical coefficients entering the expressions for the considered observables typically change by less than 20%. The only notable differences lie in the sensitivity of δm_W and $\Delta\sigma/\sigma_0$ at larger centre-of-mass energies to tau-flavour mixing, where the respective coefficients grow by a factor of 2–5. Still, it is a subleading effect, as these observables remain much more sensitive to electron- and muon-flavour mixing. Therefore, the results for the Type-III Seesaw model discussed so far, for which $M = 1\,\mathrm{TeV}$ is assumed, will also approximately hold for (moderately) larger masses.

In contrast, the observable phenomenology of Type-I Seesaw morphs somewhat nontrivially upon raising the Seesaw scale to $M = \mathcal{O}(10\,\text{TeV})$. Most profoundly, the Higgsstrahlung shift $\Delta\sigma/\sigma_0$ now experiences a crossing near $\sqrt{s} = 500\,\text{GeV}$, whereupon the dependence on the squared electron mixing angle $|\theta_e|^2$ reverses from positive to negative. Additionally, the trilepton decay rates receive a relative numerical boost of 200%, and the $\mu - e$ conversion rates are, in general, significantly altered. Specifically, $\mu - e$ conversion in gold and lead increase substantially due to the fact that the effective left-handed vector couplings to neutrons increase by a factor larger than 2, while the proton couplings and the dipole operator remain largely unchanged, and thus the cancellations between the two are much less efficient. Conversely, $\mu - e$ conversion in aluminium and titanium experience a suppression. This implies in particular that the current bound arising from $\mu - e$ conversion in gold is clearly stronger than the one from titanium, unlike the scenario with $M = 1\,\text{TeV}$.

4.4 Summary

In this work we have computed the correction to the tree-level cross section of the Higgsstrahlung process $e^+e^- \to Zh$ in the LN-conserving limit of the Type-I and Type-III Seesaw models, and compared several benchmark sensitivities of next-generation lepton colliders to existing and prospective constraints from electroweak precision measurements, and LFU and LFV probes. Summary plots in the θ_e–θ_μ and θ_e–θ_τ planes are presented in Fig. 4.7.

As a major result, we have found that existing data on the effective leptonic weak mixing angle and LFU observables preclude substantial corrections to the Higgsstrahlung cross section for Type-I Seesaw. The most likely signature of this model at a future lepton collider is therefore the *absence* of a detectable deviation from the SM prediction, at least if no further new physics modifying the electroweak and LFU sectors is introduced. For Type-III Seesaw, the current constraints (at 2σ) leave genuinely viable parameter space that can be probed at an e^+e^- Higgs factory. Fig. 4.8 provides a magnified view of this region. Concretely, for a centre-of-mass energy $\sqrt{s} = 240\,\text{GeV}$ the largest permitted shift

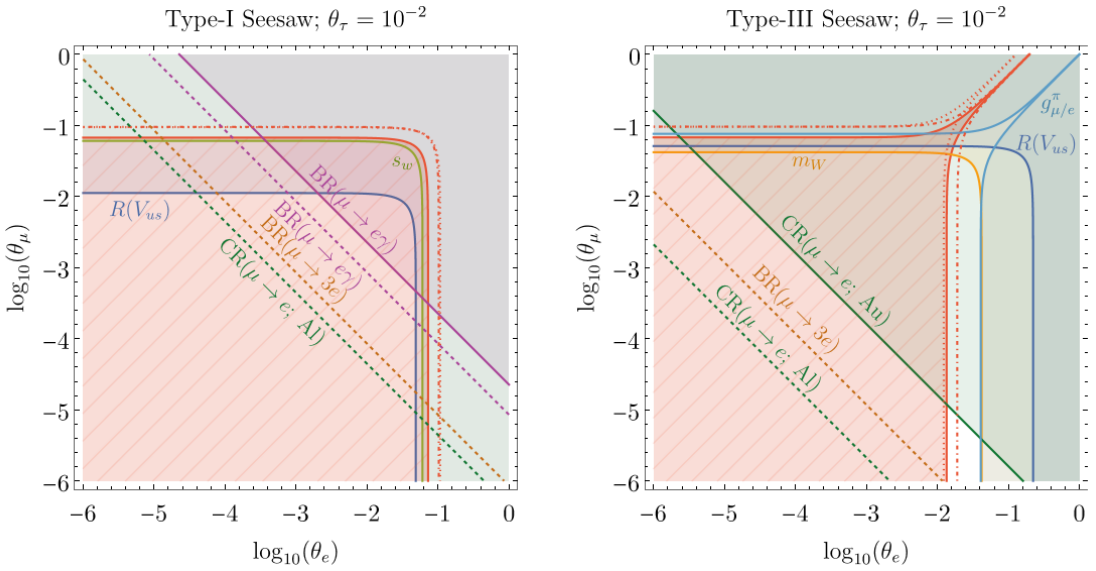

(a) Summary plots in the θ_e–θ_μ plane.

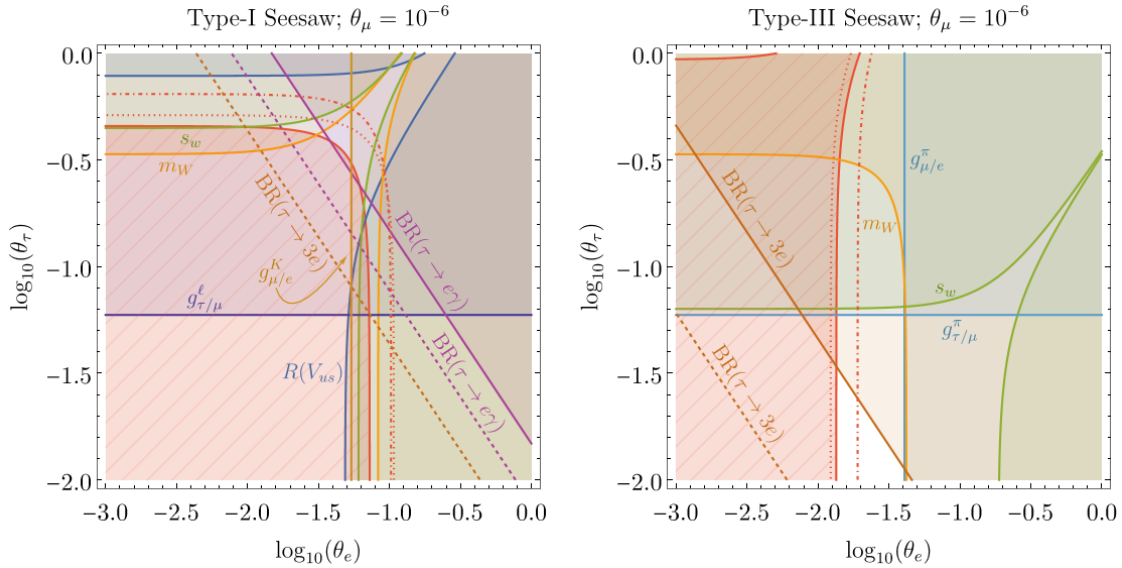

(b) Summary plots in the θ_e–θ_τ plane.

Figure 4.7: Summary plots featuring the most competitive current constraints as well as future reaches considered in this work in comparison with projected sensitivities of precision Higgsstrahlung measurements. The red-ruled regions indicate $|\Delta\sigma/\sigma| < 0.5\%$ at $\sqrt{s} = 240\,\mathrm{GeV}$. The dot-dashed and dotted red lines are the corresponding 1% contours at $\sqrt{s} = 240\,\mathrm{GeV}$ and $365\,\mathrm{GeV}$, respectively.

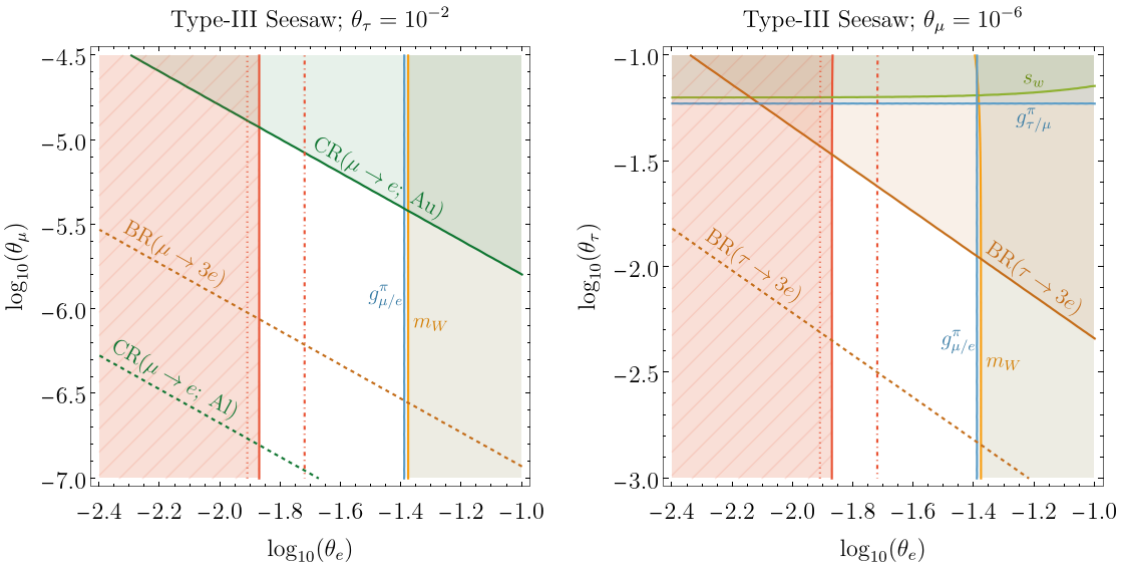

Figure 4.8: Plots zoomed in on the viable parameter regions in the Type-III Seesaw model. Only the most constraining observables are depicted. The red-ruled regions indicate $|\Delta\sigma/\sigma| < 0.5\%$ at $\sqrt{s} = 240\,\text{GeV}$. The dot-dashed and dotted red lines are the corresponding 1% contours at $\sqrt{s} = 240\,\text{GeV}$ and 365 GeV, respectively.

in the Higgsstrahlung cross section is ∼5%; at $\sqrt{s} = 365\,\text{GeV}$ it is ∼12%. It is worth noting, however, that the viability of this region is contingent upon the existence of at least three sterile states, as oscillation data imposes $|\theta_e| \lesssim 10^{-2.3}$ at 2σ in the minimal two-triplet scenario [174].

Assuming at least three sterile states, the viable region in Type-III is isolated by three main considerations. Firstly, the non-observation of LFV tightly constrains any scenario with sizeable mixing of heavy fermion singlets or triplets with two lepton flavours. These constraints are particularly strong for Type-III Seesaw, which induces tree-level contributions to trilepton decays and $\mu - e$ conversion. Indeed, a detectable deviation in $\sigma(e^+e^- \to Zh)$ already necessitates a sizeable hierarchy between θ_e and θ_μ which will become more pronounced if signals of LFV remain elusive in the future. (The situation is similar for Type-I Seesaw, where in the absence of contributions to LFV at tree level, the radiative decays $\mu \to e\gamma$ and $\tau \to e\gamma$ are more important.) Secondly (and thirdly), both the W boson mass m_W and LFU data currently disfavour detectable corrections induced via muon mixing at the level of 2σ, but leave room for visible effects due to electron-flavoured couplings, which

together with the LFV constraints enforces a hierarchy $|\theta_\mu/\theta_e| \lesssim 10^{-3}$.

Focusing on the viable region in Fig. 4.8, the constraints arising from the LFU ratio $g^\pi_{\mu/e}$ and m_W are similarly competitive and provide the most stringent constraint on electron mixing in the Type-III Seesaw model, with $|\theta_e| \lesssim 0.04$ at 2σ. In the region of parameter space where $\Delta\sigma/\sigma_0$ is detectable, tau-flavour mixing is more strictly constrained by the current bound on $\mathrm{BR}(\tau \to 3e)$ than by measurements of the weak mixing angle or pion decays. As is expected from Section 4.3.4, the most competitive upper limit on muon mixing in this context currently arises from the non-observation of $\mu - e$ conversion in gold, and will be further constrained by Mu3e as well as the searches for $\mu - e$ conversion in aluminium at COMET and Mu2e. If an observation of these transitions remains elusive in the future, the currently viable parameter space will retreat to $|\theta_\mu| \lesssim 10^{-7.5}$. Similarly, if $\tau \to 3e$ is not observed at Belle II, tau mixing would need to be smaller than $\theta_\tau = 10^{-2}$.

Since fermion triplets induce a tree-level contribution to $e^+e^- \to Zh$ which is not mediated via the s channel as in the SM, deviations from the cross section induced via electron-flavour mixing grow approximately with s. In that sense, if the drop in statistics can be compensated by higher luminosity, the Type-III Seesaw model motivates precision measurements of the Higgsstrahlung process at higher centre-of-mass energies as well, whereas this is not indicated for Type-I Seesaw.

Overall, we have corroborated the expectation that a rich interplay of neutrino, Higgs, electroweak and flavour physics is to be expected for Seesaw models at low energies, and demonstrated the benefit of measuring the Higgsstrahlung cross section at multiple centre-of-mass energies for the Type-III Seesaw model. One may extend the research conducted in this work along two major avenues. Firstly, although the list of processes which we have considered captures a wide range of phenomenology of the fermionic Seesaw models, it is not exhaustive. In particular, taking into account observables sensitive to angular distributions for Higgs physics [303] as well as a comprehensive global fit in the electroweak sector should help to further differentiate between the low-energy signatures of Seesaw models. Secondly, since we relied on the assumption of an exactly conserved LN symmetry on the Lagrangian level, existing data on lepton mixing and the mass hierarchies in the

neutrino sector was *per definition* not incorporated. While we expect the implications of lepton number breaking for the induced low-energy phenomenology to be small (at least when there are three or more sterile states [174; 264]), any viable model of neutrino mass generation eventually needs to be tested against them. Lastly, similar studies for different models of neutrino mass generation are left for future work.

4.A Approximate Matching Conditions

From `DsixTools` we numerically obtain the matching condition

$$\begin{aligned}\frac{C_{e\gamma,ij}(\mu = 5\,\text{GeV})}{\text{GeV}} \approx\ & 150.732\, C_{eB,ij} - 82.394\, C_{eW,ij} + 3.204\, C^{(3)}_{LeQu,ij33} \\ & + A_{ij}\left(C^{(3)}_{HL,ij} - 0.27353\, C^{(1)}_{HL,ij}\right)\end{aligned} \tag{4.63}$$

for the electromagnetic dipole operator, where the Wilson coefficients on the right-hand side are evaluated at the scale $\mu = m_Z$, repeated indices do not indicate summation, and

$$A_{ij} = 10^{-3}\begin{pmatrix} - & 0.2661 & 4.4758 \\ 0.0013 & - & - \\ 0.0013 & - & - \end{pmatrix}_{ij}, \tag{4.64}$$

with the dashed entries being irrelevant for our purposes.

My coauthors and I are conscious that the scales associated with the decays of taus and muons are smaller than $\mu = 5\,\text{GeV}$. The largest contributions from RG running at lower scales can be expected to originate from QCD. The only SMEFT operator which one may a priori expect to yield a sizeable contribution to LEFT operators which involve quark fields and mix into $\mathcal{O}_{e\gamma}$ is $\mathcal{O}^{(3)}_{LeQu} = (\overline{L}\sigma_{\mu\nu}e_R)\epsilon(\overline{Q}\sigma^{\mu\nu}u_R)$. Still, this operator is not induced at one-loop level in the Seesaw models under consideration [256–258], and it only yields a tiny sub-percent contribution to $\mathcal{O}_{e\gamma}$. Therefore, we do not expect to have missed any sizeable effects from RG running below $\mu = 5\,\text{GeV}$.[8] The same holds for the (semi-)leptonic vector operators mediating trilepton decays and $\mu - e$ conversion; we have explicitly checked that the contribution from quark operators is at most 1% in Eqs. (4.65) and (4.66) below.

For all the matching conditions listed in the following, the respective LEFT Wilson coefficient on the left-hand side is given at $\mu = 5\,\text{GeV}$, while the SMEFT Wilson coefficients

[8] To paraphrase, even if the numerical factor multiplying $C^{(3)}_{LeQu}(m_Z)$ in Eq. (4.63) changes appreciably upon further lowering the scale on the left-hand side to, say, $\mu = m_\mu$, $C^{(3)}_{LeQu}(m_Z)$ itself is so small for the fermionic Seesaw models that we do not expect the resulting (relative) contribution to $C_{e\gamma}(m_\mu)$ to become sizeable in any way.

entering on the right-hand side are evaluated at the scale $\mu = m_Z$. For the operators relevant to trilepton decays we find:

$$C^{VLL}_{ee,jijj} \approx -0.266\, C^{(1)}_{HL,ji} - 0.271\, C^{(3)}_{HL,ji} + 0.973\, C_{LL,jjji}, \tag{4.65a}$$
$$C^{VRR}_{ee,jijj} \approx 0.974\, C_{ee,jjji} + 0.235\, C_{He,ji} - 0.006\, C_{eu,ji33} + 0.003\, C_{Qe,33ji}, \tag{4.65b}$$
$$C^{VLR}_{ee,jijj} \approx 0.4912\, C^{(1)}_{HL,ji} + 0.4909\, C^{(3)}_{HL,ji} + 1.018\, C_{Le,jijj} - 0.012\, C_{Lu,ji33}, \quad \text{and} \tag{4.65c}$$
$$C^{VLR}_{ee,jjji} \approx -0.556\, C_{He,ji} + 1.018\, C_{Le,jjji} - 0.015\, C_{Qe,33ji} + 0.011\, C_{eu,ji33}. \tag{4.65d}$$

For $\mu - e$ conversion the matching conditions for the vector operators are

$$C^{VLL}_{eu,1211} \approx 0.708\, C^{(1)}_{HL,12} + 0.734\, C^{(3)}_{HL,12} - 1.047\, C^{(3)}_{LQ,1211}, \tag{4.66a}$$
$$C^{VLR}_{eu,1211} \approx -0.3172 C^{(1)}_{HL,12} - 0.3170\, C^{(3)}_{HL,12} + 0.984\, C_{Lu,1211}, \tag{4.66b}$$
$$C^{VRR}_{eu,1211} \approx -0.321\, C_{He,12} + 0.008\, C_{eu,1233} - 0.005\, C_{Qe,3312}, \tag{4.66c}$$
$$C^{VLR}_{ue,1112} \approx 0.696\, C_{He,12} + 0.017\, C_{Qe,3312} - 0.014\, C_{eu,1233}, \tag{4.66d}$$
$$C^{VLL}_{ed,1211} \approx -0.856\, C^{(1)}_{HL,12} - 0.864\, C^{(3)}_{HL,12} + 0.987\, C^{(3)}_{LQ,1211}, \tag{4.66e}$$
$$C^{VLR}_{ed,1211} \approx 0.1617\, C^{(1)}_{HL,12} + 0.1615\, C^{(3)}_{HL,12} + 1.006\, C_{Ld,1211}, \tag{4.66f}$$
$$C^{VRR}_{ed,1211} \approx 0.158\, C_{He,12} - 0.004\, C_{eu,1233} + 0.002\, C_{Qe,3312}, \quad \text{and} \tag{4.66g}$$
$$C^{VLR}_{de,1112} \approx -0.867\, C_{He,12} - 0.020\, C_{Qe,3312} + 0.018\, C_{eu,1233}. \tag{4.66h}$$

Bing bing boom bing boom!

Guy Moore,
on finite temperature field theory.

5

Theory: Leptogenesis

Contents

5.1 Ingredients **92**

5.2 *CP* Violation and the Cutting Rules **95**

5.3 A Detour: Results from Unitarity **102**

5.4 Modelling Leptogenesis **109**

5.A Further Details on Real Intermediate State Subtraction **139**

As you may have noticed, the world around us happens to be made up of matter, and not antimatter. In fact, this is almost certainly true for the whole universe, as quantified by cosmic measurements of the baryon-to-photon ratio [90; 304]

$$\frac{n_b - n_{\overline{b}}}{n_\gamma} \simeq \frac{n_b}{n_\gamma} = (6.10 \pm 0.4) \times 10^{-10}. \tag{5.1}$$

Imagining for extreme simplicity that all photons were produced in the pair annihilation of quarks and antiquarks, this ratio suggests an excess of one quark for every 3×10^8 quark-antiquark pairs in the primordial universe – a miniscule, yet clearly important imbalance.

This observed matter dominance presents a rather delicious problem, for it turns out that the Standard Model is incapable of explaining this observed baryon abundance [98; 99; 101], leaving us in need of a BSM mechanism of **baryogenesis**. In this chapter we'll explore one such method for tipping the cosmic scales: **leptogenesis**, in which a lepton asymmetry is first generated before being converted to a baryon asymmetry. Good overviews of baryogenesis and a selection of its myriad approaches can be found for instance in Refs. [89; 100; 101; 304].

As far as theory chapters go, this is a rather long one. After a brief discussion on the generalities of baryogenesis in the next section, I'll review the topic of CP asymmetries and the technique of Cutkosky cuts for evaluating them in Sections 5.2 and 5.3. Then, in Section 5.4 I'll establish the Boltzmann equation as the means of tracking the baryon asymmetry as the universe evolves.

5.1 Ingredients

It is the law that anyone introducing the topic of baryogenesis must first mention **Sakharov's conditions** [91], and I don't intend to make a criminal out of myself. These conditions mandate that to generate a baryon asymmetry in the early universe, one requires

1. baryon number violation,
2. C and CP violation, and

3. a departure from equilibrium.

These requirements can be understood quite intuitively: were the first not true, baryon number would always be conserved and an asymmetry could never be generated from a baryon-symmetric universe; were the second not true, matter and antimatter would be treated on equal footing; and were the third not true, any process generating an asymmetry would have the reverse process just as easily erase it.

In the SM these conditions *are* actually satisfied, as follows:

1. Baryon number, while a classical symmetry of the SM in which all quark fields transform with charge 1/3, is violated at the quantum level by the *ABJ triangle anomaly* [157; 158], also known as the *chiral anomaly*. While the probability of baryon number violation due to this anomaly is unobservably small at zero temperature [280], it is tremendously enhanced between $T \approx 130\,\text{GeV}$ and $T \approx 10^{12}\,\text{GeV}$ when electroweak sphalerons are in thermal equilibrium [305]. An **electroweak sphaleron** is a topological quasiparticle [306–311] consisting of nine quarks and three leptons, and baryon-plus-lepton number $B+L$ is efficiently violated during the period in which they are active.

2. C-symmetry is maximally violated in the SM by the weak interaction, and CP is violated by the complex phase in the CKM matrix, as captured by the Jarlskog invariant $J_{\text{CKM}} \approx 3.12 \times 10^{-5}$ [124]. The CP violation in the PMNS matrix is currently constrained to be at most $J^{\text{max}}_{\text{PMNS}} \approx 3 \times 10^{-2}$ [152], though it is likely much smaller than this bound. In principle CP is also violated by the *strong CP phase* $\overline{\theta}$ appearing in the topological QCD term $\mathcal{L} \sim \overline{\theta} G\widetilde{G}$, but measurements of the neutron dipole moment constrain it to be very small, $\overline{\theta} \lesssim 10^{-10}$ [9; 312].

3. A departure from equilibrium can occur during the electroweak phase transition (EWPT), in which the $\text{SU}(2)_{\text{W}} \times \text{U}(1)_Y$ symmetry is broken by the Higgs' vacuum expectation value in isolated regions, or *bubbles*, which expand until they fill the entire universe. During this time, particles inside the bubbles are unable to equilibrate

with those outside, and CP-asymmetric scatterings against the bubble walls could offer a means of generating the required particle number asymmetries [313–316].

More generically, the decay of any unstable particle can occur out of equilibrium when the temperature drops below its mass and the inverse decay hence becomes inefficient. Since none of the SM particles have baryon number-violating decays, this is however a moot point.

Unfortunately, while these ingredients are present they are nevertheless inadequate when put to the task of explaining the observed baryon abundance. For the EWPT to stand a chance of achieving successful baryogenesis it needs to be strongly *first-order*, meaning there must be a potential barrier between the broken and unbroken phases at the time of transition, such that regions of the broken phase can nucleate with well-defined bubble walls. This turns out to require a Higgs mass below 70 GeV [317; 318], and that this is not the case means that the EWPT in the SM is rather of a crossover type, in which the new phase instead smoothly permeates the universe. One may attempt to introduce new physics to make the phase transition first-order, and this approach forms an essential part of the scheme of *electroweak baryogenesis*; see for example Refs. [100; 101; 316; 319] and [320–329]. Even if this is realised, however, the amount of CP violation in the CKM matrix has been shown to be many orders of magnitude too small to generate the required baryon abundance [98; 99], and so additional sources of CP violation are required.

This brings us to the idea of *leptogenesis* [102–105; 330]. The key premise behind this approach is that the lepton number violation due to Majorana neutrino masses together with the CP violation in the PMNS matrix (or elsewhere in a given mass model) could lead to a significant lepton asymmetry, which can then transmute into a baryon asymmetry through the action of electroweak sphalerons.[1] Many leptogenesis scenarios achieve the lepton number generation through the out-of-equilibrium decay of a heavy particle, most often a sterile neutrino. The canonical example is the decay $N \to LH$ of a sterile neutrino in Type-I Seesaw [102; 335].

[1]Leptogenesis is also possible without Majorana masses, in which case it is often referred to as *Dirac leptogenesis*; see e.g. Refs. [331–334].

In the next chapter we will investigate whether leptogenesis can be accomplished in the Zee model of neutrino masses via the CP-violating decay of a new heavy scalar h^-. As the baryon number violation and out-of-equilibrium conditions are automatically met, we therefore require only that there is sufficient CP violation.

5.2 CP Violation and the Cutting Rules

Let us begin by studying how CP violation comes to be. For a grounded definition, we say that CP is violated when the rate of a process and its CP conjugate are unequal,[2]

$$\Gamma(i \to f) \neq \Gamma(\overline{i} \to \overline{f}). \tag{5.2}$$

For us, it is more convenient to study this at the level of invariant matrix elements, so we'll instead say that we require

$$\Delta|\mathcal{M}|^2 \equiv |\mathcal{M}_{fi}|^2 - |\mathcal{M}_{\overline{f}\overline{i}}|^2 \neq 0, \tag{5.3}$$

where I use the shorthand $\mathcal{M}_{fi} \equiv \mathcal{M}(i \to f)$. In typical scenarios this asymmetry arises from the interference of tree- and loop-level diagrams. To see how, let's write

$$\mathcal{M}_{fi} = c_0\mathcal{A}_0 + c_1\mathcal{A}_1 \quad \text{and} \tag{5.4a}$$
$$\mathcal{M}_{\overline{f}\overline{i}} = c_0^*\overline{\mathcal{A}}_0 + c_1^*\overline{\mathcal{A}}_1, \tag{5.4b}$$

where we decompose the tree- and loop-level amplitudes into their coupling constants $c_{0,1}$ and so-called *dynamical amplitudes* $\mathcal{A}_{0,1}$. Then

$$\begin{aligned}\Delta|\mathcal{M}|^2 &= |c_0\mathcal{A}_0 + c_1\mathcal{A}_1|^2 - |c_0^*\overline{\mathcal{A}}_0 + c_1^*\overline{\mathcal{A}}_1|^2 \\ &= |c_0|^2(|\mathcal{A}_0|^2 - |\overline{\mathcal{A}}_0|^2) + |c_1|^2(|\mathcal{A}_1|^2 - |\overline{\mathcal{A}}_1|^2) \\ &\quad + 2\,\mathrm{Re}(c_0^*c_1)\,\mathrm{Re}(\mathcal{A}_0^*\mathcal{A}_1 - \overline{\mathcal{A}}_0^*\overline{\mathcal{A}}_1) - 2\,\mathrm{Im}(c_0^*c_1)\,\mathrm{Im}(\mathcal{A}_0^*\mathcal{A}_1 + \overline{\mathcal{A}}_0^*\overline{\mathcal{A}}_1).\end{aligned} \tag{5.5}$$

[2]Here I will use notation and terminology for decays, though the discussion in this chapter applies equally well to scatterings.

As it generically transpires that $|\mathcal{A}_0|^2 = |\overline{\mathcal{A}}_0|^2$, $|\mathcal{A}_1|^2 = |\overline{\mathcal{A}}_1|^2$, and $\mathcal{A}_0^*\mathcal{A}_1 = \overline{\mathcal{A}}_0^*\overline{\mathcal{A}}_1$ [104], this reduces to the compact expression

$$\Delta|\mathcal{M}|^2 = -4\,\mathrm{Im}(c_0^* c_1)\,\mathrm{Im}(\mathcal{A}_0^*\mathcal{A}_1). \tag{5.6}$$

That is, CP violation requires the existence of a complex phase in *both* the coupling constants and the dynamical amplitudes. (This immediately explains why, by the way, the phase δ in the CKM matrix is referred to as its CP-violating phase.)

It is conventional to introduce the ***CP* asymmetry parameter** ε by wrapping Eq. (5.6) up into a ratio of decay rates,

$$\begin{aligned}\varepsilon &\equiv \frac{\Gamma(i \to f) - \Gamma(\bar{i} \to \bar{f})}{\Gamma(i \to f) + \Gamma(\bar{i} \to \bar{f})} && (5.7)\\ &\approx \frac{\int \mathrm{d}\Pi_f\, \Delta|\mathcal{M}|^2}{\int \mathrm{d}\Pi_f\, 2|c_0\mathcal{A}_0|^2} \\ &= -\frac{\mathrm{Im}(c_0^* c_1)}{|c_0|^2}\frac{\int \mathrm{d}\Pi_f\, [2\,\mathrm{Im}(\mathcal{A}_0^*\mathcal{A}_1)]}{\int \mathrm{d}\Pi_f\, |\mathcal{A}_0|^2}, && (5.8)\end{aligned}$$

where the sum in the denominator is dominated by the tree-level contribution. In anticipation of what is to come I have left the factor of 2 where it is, rather than pulling it out the front.

Example

To make this all concrete, let's explore a specific example: the decay of the lightest sterile neutrino, $N_1 \to LH$, in Type-I Seesaw. (Note that $N_1 = \nu_{R1}$ in the notation of previous chapters.) Our Feynman rules are

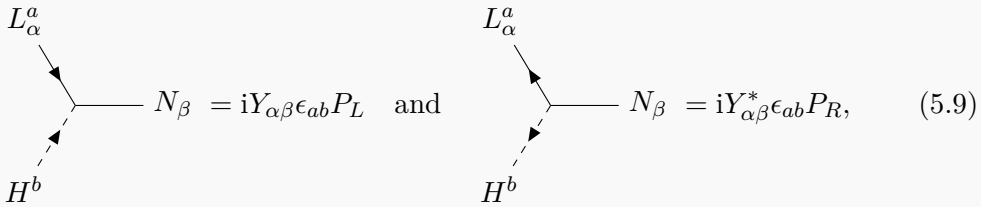

(5.9)

where here α, β index flavours and a, b index $\mathrm{SU}(2)_\mathrm{W}$ components. At one-loop there is a triangular vertex correction and a wavefunction renormalization correction, but

for this example we will just look at the contribution of the triangle diagram:

$$\mathrm{i}\mathcal{M}(N_1 \to L^a_\alpha H^b) =$$

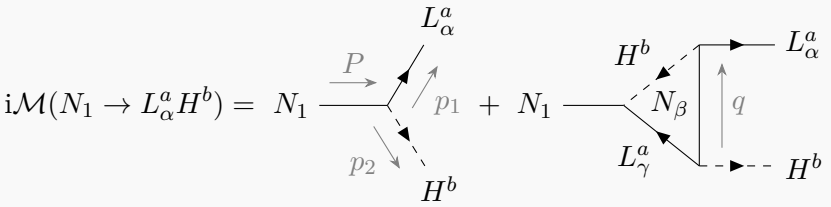

$$= \overline{u}(\mathbf{p}_1)(\mathrm{i}Y^*_{\alpha 1}\epsilon_{ab}P_R)u(\mathbf{P}) \tag{5.10}$$
$$+ (\epsilon_{ab})^3 \int \frac{\mathrm{d}^4q}{(2\pi)^4}\overline{u}(\mathbf{p}_1)\Big(\mathrm{i}Y^*_{\alpha\beta}P_R\Big)\frac{\mathrm{i}}{\not{q} - m_\beta}\Big(\mathrm{i}Y^*_{\gamma\beta}P_R\Big)\frac{\mathrm{i}}{\not{p}_2 + \not{q}}(\mathrm{i}Y_{\gamma 1}P_L)u(\mathbf{P})\frac{\mathrm{i}}{(q-p_1)^2}.$$

We are working in the unbroken phase where L is massless but N still has a Majorana mass, and we moreover neglect the mass of the Higgs doublet. To make sense of the diagrams I have used the fermion flow rules for Majorana fermions developed in Refs. [336; 337]. From the above we can identify

$$c_0 = Y^*_{\alpha 1}\epsilon_{ab}, \tag{5.11a}$$
$$\mathcal{A}_0 = \overline{u}(\mathbf{p}_1)P_R u(\mathbf{P}), \tag{5.11b}$$
$$c_1 = Y^*_{\alpha\beta}Y^*_{\gamma\beta}Y_{\gamma 1}(\epsilon_{ab})^3, \quad \text{and} \tag{5.11c}$$
$$\mathcal{A}_1 = \mathrm{i}\int \frac{\mathrm{d}^4q}{(2\pi)^4}\overline{u}(\mathbf{p}_1)P_R\frac{1}{\not{q} - m_\beta}P_R\frac{1}{\not{p}_2 + \not{q}}P_L u(\mathbf{P})\frac{1}{(q-p_1)^2}. \tag{5.11d}$$

We naturally have some freedom in choosing which factors we lump in with the c's and which with the $\mathcal{A}$'s; here and onwards I will choose to put *only* the coupling constants (including possible minus signs) from the Feynman rules into the c's, and everything else (including all factors of i) into the $\mathcal{A}$'s.

Summing over spins and carrying out the loop integral, we arrive at

$$\mathcal{A}_0^*\mathcal{A}_1 = -\frac{1}{2}\frac{m_1 m_\beta}{96\pi^2}\Big[6 + \pi^2(1+x_\beta) + 6\ln(-x_\beta) + 3(1+x_\beta)\ln(-x_\beta)^2 + 6(1+x_\beta)\mathrm{Li}_2(1+x_\beta)\Big] \tag{5.12}$$
$$\implies \mathrm{Im}(\mathcal{A}_0^*\mathcal{A}_1) = -\frac{m_1 m_\beta}{32\pi}\left[1 - (1+x_\beta)\ln\left(\frac{1+x_\beta}{x_\beta}\right)\right], \tag{5.13}$$

where $x_\beta \equiv m_\beta^2/m_1^2$, Li_2 is the dilogarithm (which satisfies $\mathrm{Im}\,\mathrm{Li}_2(x) = -\pi\ln(x)$),

and the extra factor of $\frac{1}{2}$ comes from averaging over the spin of N_1. By plugging into Eq. (5.8) and summing over all virtual flavours β, γ, and outgoing particles a, b, we find that the asymmetry parameter is

$$\begin{aligned}\varepsilon &= \frac{\Gamma(N_1 \to LH) - \Gamma(N_1 \to \bar{L}\bar{H})}{\Gamma(N_1 \to LH) + \Gamma(N_1 \to \bar{L}\bar{H})} \\ &= \frac{1}{8\pi} \sum_{\beta} \frac{\mathrm{Im}[(Y^\dagger Y)^2_{\beta 1}]}{(Y^\dagger Y)_{11}} \sqrt{x_\beta} \left[1 - (1 + x_\beta) \ln\left(\frac{1 + x_\beta}{x_\beta} \right) \right], \end{aligned} \tag{5.14}$$

which is a well-known result [335].

If that example appeared straightforward it is likely because I skipped over the evaluation of the loop integral. Such integrals are typically the most troublesome part of any asymmetry computation, and they have the potential to become downright nasty if—as in the next chapter—we have to deal with two- or higher-loop diagrams. Fortunately for us, there exists a powerful technique to simplify asymmetry calculations: the **cutting rules**.

These rules, also called the **Cutkosky rules** [338], state that the imaginary part of an amplitude arises from virtual particles going on-shell, via[3]

$$2\,\mathrm{Im}\,\mathcal{A}(i \to f) = \sum_{\text{cuts}} \mathcal{A} \equiv \sum_X \int \mathrm{d}\Pi_X\, \mathcal{A}(i \to X) \mathcal{A}^*(f \to X). \tag{5.15}$$

In words, we can compute $\mathrm{Im}\,\mathcal{A}$ by:

(a) cutting the diagram for $\mathcal{A}$ in all possible ways to put any number of virtual particles on shell,

(b) writing down the separate amplitudes $\mathcal{A}(i \to X)$ and $\mathcal{A}^*(f \to X)$, and

(c) taking their product, summing over the spins and integrating over the phase space of the intermediate particles.

[3]The cutting rules are customarily formulated in a somewhat different manner; see for example Ref. [339] for an excellent treatment. Eq. (5.15) however suffices for our purposes.

If the amplitude $\mathcal{A}(f \to X)$ does not permit cuts of its own (i.e. it doesn't carry an imaginary part), then $\mathcal{A}^*(f \to X) = \mathcal{A}(X \to f)$, and the cutting rules reduce to the slightly neater form

$$2\,\mathrm{Im}\,\mathcal{A}(i \to f) = \sum_X \int \mathrm{d}\Pi_X\, \mathcal{A}(i \to X)\mathcal{A}(X \to f). \tag{5.16}$$

The simple way to gain intuition for the cutting rules is by noting that a propagator becomes imaginary precisely when it is on-shell,

$$\mathrm{Im}\left(\frac{1}{p^2 - m^2 + \mathrm{i}\epsilon}\right) = -\pi\delta(p^2 - m^2). \tag{5.17}$$

In fact, an equivalent way to compute $2\,\mathrm{Im}\,\mathcal{A}$, assuming Eq. (5.16) is valid, is to take $-\mathrm{i}\mathcal{A}$ and make the replacement

$$\frac{\mathrm{i}}{p^2 - m^2 + \mathrm{i}\epsilon} \to 2\pi\delta(p^2 - m^2)\theta(p^0) \tag{5.18}$$

for all cut particles.

EXAMPLE

Let's repeat the above calculation of the asymmetry parameter for Type-I Seesaw, but this time using the cutting rules. There are in principle three possible ways to cut the loop diagram:

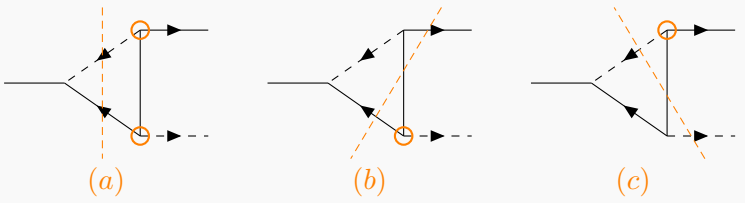

One can systematically list all cuts by enumerating over all possible circlings of vertices, where a line is cut if it connects a circled vertex to an uncircled one [111; 339; 340]. The incoming external lines are treated as implicitly uncircled while the outgoing lines are implicitly circled, and a circling configuration only generates a valid cut if it completely partitions the diagram into a left side, containing only

uncircled vertices, and a right side containing only circled vertices. It is okay for one or both sides to have disconnected parts, but each side must contain at least one vertex, so that it is not completely trivial. The use of circlings is overkill for our triangle diagram, but the technique is increasingly useful for more complicated ones.

Anyhow, cuts (b) and (c) vanish as they are kinematically impossible – cut (b), for example, contains the disconnected subprocess $N_\beta \bar{L} \to H$, which cannot simultaneously conserve energy and momentum. This leaves us with (a) as the only viable cut, and as there are no more valid cuts Eq. (5.16) holds, which reads

$$2\,\mathrm{Im}\,\mathcal{A}_1(N_1 \to LH) = \int \mathrm{d}\Pi_2\,\mathcal{A}(N_1 \to \bar{H}\bar{L})\mathcal{A}(\bar{H}\bar{L} \to LH), \tag{5.19}$$

or, diagrammatically (up to factors of i),

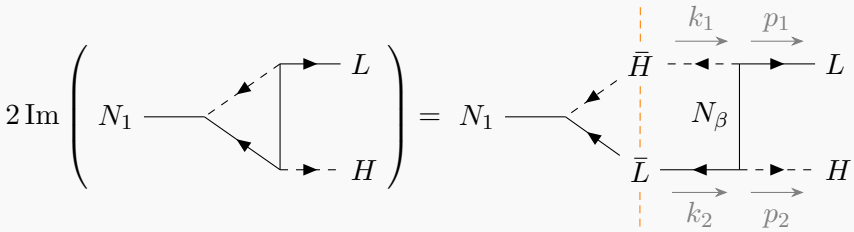

Since we are focusing on the amplitudes and not the coupling constants (which we anyway already know from Eq. (5.11)), here I suppress the flavour and $\mathrm{SU}(2)_\mathrm{W}$ indices for the H's and L's.

From the diagrams above we can read off

$$\mathrm{i}\mathcal{A}(N_1 \to \bar{H}\bar{L}) = \overline{u}(k_2)(\mathrm{i}P_L)u(P) \quad \text{and} \tag{5.21a}$$

$$\mathrm{i}\mathcal{A}(\bar{H}\bar{L} \to LH) = \overline{u}(p_1)(\mathrm{i}P_R)\frac{\mathrm{i}}{\not{p}_1 - \not{k}_1 - m_\beta}(\mathrm{i}P_R)u(k_2); \tag{5.21b}$$

multiplying the two and summing over the spin of the intermediate on-shell $\bar{L}$ gives

$$\mathcal{A}(N_1 \to \bar{H}\bar{L})\mathcal{A}(\bar{H}\bar{L} \to LH) = -\overline{u}(p_1)P_R\frac{1}{\not{p}_1 - \not{k}_1 - m_\beta}P_R\not{k}_2 P_L u(P). \tag{5.22}$$

Eq. (5.19) now instructs us to integrate over the two body phase space of k_1 and k_2, but—while doable—this is somewhat tedious as the four-vectors are not formed into invariant combinations. Instead, remembering that the CP asymmetry is proportional to

$$2\,\mathrm{Im}(\mathcal{A}_0^*\mathcal{A}_1) = \mathcal{A}_0^* \sum_{\text{cuts}} \mathcal{A}_1, \tag{5.23}$$

we multiply out by $\mathcal{A}_0(N_1 \to LH)^* = \overline{u}(\mathbf{P})P_L u(\mathbf{p}_1)$, which gives a closed spinor chain that we can trace over. Upon summing or averaging over the appropriate spins we end up with

$$\begin{aligned}
&\mathcal{A}_0(N_1 \to LH)^*\mathcal{A}(N_1 \to \bar{H}\bar{L})\mathcal{A}(\bar{H}\bar{L} \to LH) \\
&\qquad = -\frac{1}{2}\frac{\mathrm{Tr}\left[(\not{P} + m_1)P_L \not{p}_1 P_R(\not{p}_1 - \not{k}_1 + m_\beta)P_R \not{k}_2 P_L\right]}{(p_1 - k_1)^2 - m_\beta^2} && (5.24)\\
&\qquad = m_1 m_\beta \frac{p_1 \cdot k_2}{2p_1 \cdot k_1 + m_\beta^2}. && (5.25)
\end{aligned}$$

This is a much friendlier expression. To carry out the phase space integral we work in the rest frame of N_1 and choose our z-axis to align with $\mathbf{p}_1$, so that $p_1 \cdot k_1 = \frac{1}{4}m_1^2(1 - \cos\theta)$ and $p_1 \cdot k_2 = \frac{1}{4}m_1^2(1 + \cos\theta)$. Then

$$\begin{aligned}
2\,\mathrm{Im}(\mathcal{A}_0^*\mathcal{A}_1) &= \int \mathrm{d}\Pi_2 \left[m_1 m_\beta \frac{p_1 \cdot k_2}{2p_1 \cdot k_1 + m_\beta^2}\right] && (5.26)\\
&= \frac{m_1 m_\beta}{8\pi}\int_{-1}^{1} \frac{\mathrm{d}\cos\theta}{2} \frac{\frac{1}{4}m_1^2(1 + \cos\theta)}{\frac{1}{2}m_1^2(1 - \cos\theta) + m_\beta^2} && (5.27)\\
&= -\frac{m_1 m_\beta}{16\pi}\left[1 - (1 + x_\beta)\ln\left(\frac{1 + x_\beta}{x_\beta}\right)\right], && (5.28)
\end{aligned}$$

where once again $x_\beta \equiv m_\beta^2/m_1^2$. This agrees with Eq. (5.13), and so we recover the same result for the asymmetry!

With practice, the cutting rules quickly become a very efficient way to compute asymmetries. As in the above example it will almost always be easier to work out $2\,\mathrm{Im}(\mathcal{A}_0^*\mathcal{A}_1)$ than $2\,\mathrm{Im}\,\mathcal{A}_1$ directly. In the rare case that $\mathcal{A}_0$ contains an imaginary part—for instance, one

might have an s-channel scattering where the tree-level mediator can go on-shell—we must generalise to

$$\begin{aligned} 2\,\mathrm{Im}(\mathcal{A}_0^*\mathcal{A}_1) &= 2\,\mathrm{Re}(\mathcal{A}_0)\,\mathrm{Im}(\mathcal{A}_1) - 2\,\mathrm{Im}(\mathcal{A}_0)\,\mathrm{Re}(\mathcal{A}_1) \\ &= \mathrm{Re}(\mathcal{A}_0)\sum_{\text{cuts}}\mathcal{A}_1 - \mathrm{Re}(\mathcal{A}_1)\sum_{\text{cuts}}\mathcal{A}_0. \end{aligned} \tag{5.29}$$

5.3 A Detour: Results from Unitarity

Before proceeding onwards with our discussion of leptogenesis it is a good idea to take a pit stop to review and explore some implications of S-matrix unitarity. We will first derive a consistency condition on CP asymmetries, and then we will explore an alternative unitarity-based approach to their computation. In doing so we will come to appreciate some important nuances that will become relevant to us later.

Our starting point is of course the S-matrix itself, which can roughly be understood as $S = e^{i\hat{H}t}$, with $\hat{H}$ the Hamiltonian of our quantum field theory. Elements of the S-matrix are denoted $S_{fi} = \langle f|S|i\rangle$. There are a number of subtleties associated with the S-matrix, such as the precise definition of asymptotic states $|i\rangle$ and $|f\rangle$ and the treatment of unstable and massless states. I will not go into a great amount of detail here – for this, one should consult their favourite QFT textbook.

As we all know, it is conventional to define the T-matrix (also called the *transition* or *transfer matrix*) to capture the nontrivial part of the S-matrix, via

$$S = 1 + \mathrm{i}T. \tag{5.30}$$

The familiar invariant matrix elements $\mathcal{M}_{fi}$ that we have encountered up to this point are precisely the T-matrix elements up to an overall four-momentum conserving delta function,

$$\mathrm{i}T_{fi} = (2\pi)^4\delta^{(4)}(p_i - p_f)\mathrm{i}\mathcal{M}_{fi}. \tag{5.31}$$

Now, unitarity of S translates to two important conditions for T:

$$S^\dagger S = 1 \quad \Longrightarrow \quad \mathrm{i}T - \mathrm{i}T^\dagger - \mathrm{i}T^\dagger \mathrm{i}T = 0, \tag{5.32a}$$

and

$$S^\dagger S = S S^\dagger \quad \Longrightarrow \quad T^\dagger T = T T^\dagger. \tag{5.32b}$$

The former leads to powerful non-perturbative results such as the *generalised optical theorem*—which is almost equivalent to the form of the cutting rules presented in Eq. (5.15)—and also forms the basis of the so-called *holomorphic cutting rules*, to be introduced below. The latter (which is actually implied by the former) leads to an important constraint on CP asymmetries, which we will explore first.

5.3.1 The Total CP Asymmetry is Zero

Consider a diagonal entry of Eq. (5.32b), $(T^\dagger T)_{ii} = (TT^\dagger)_{ii}$, or in full

$$\sum_f \int [\mathrm{d}P_f] \, \langle i|T^\dagger|f\rangle\langle f|T|i\rangle = \sum_f \int [\mathrm{d}P_f] \, \langle i|T|f\rangle\langle f|T^\dagger|i\rangle \,, \tag{5.33}$$

where the resolution of identity involves a sum over a complete set of states f and an integration over their phase space.[4] At the $\mathcal{M}$ level this reads

$$\sum_f \int \mathrm{d}\Pi_f \, |\mathcal{M}(i \to f)|^2 = \sum_f \int \mathrm{d}\Pi_f \, |\mathcal{M}(f \to i)|^2, \tag{5.34}$$

where a common factor of $V_4 \equiv (2\pi)^4 \delta^{(4)}(0)$ has been removed from both sides. To proceed we call upon the CPT *theorem*, which offers the corollary [341]

$$\mathcal{M}(f \to i) = \mathcal{M}(\bar{i} \to \bar{f}). \tag{5.35}$$

[4] Recall that in my notation $[\mathrm{d}P_f]$ differs from $\mathrm{d}\Pi_f$ by the absence of an explicit four-momentum conserving delta function; see Eq. (1.4).

Applying this to the right hand side of Eq. (5.34) gives

$$\sum_f \int \mathrm{d}\Pi_f \, |\mathcal{M}(i \to f)|^2 = \sum_f \int \mathrm{d}\Pi_f \, |\mathcal{M}(\bar{i} \to \bar{f})|^2, \tag{5.36}$$

or more succinctly,

$$\sum_f \Delta\Gamma(i \to f) = \sum_f \Big[\Gamma(i \to f) - \Gamma(\bar{i} \to \bar{f})\Big] = 0 \tag{5.37}$$

– that is, the total CP asymmetry *must* be zero, and moreover the total decay rate of a particle and its antiparticle must be equal. This offers a very important cross check on asymmetry calculations. If ever it does not appear to hold, something has gone awry.

EXAMPLE

In our Type-I Seesaw example, this condition holds rather trivially since N_1 is Majorana:

$$\begin{aligned}\sum_f \Delta\Gamma(N_1 \to f) &= \Delta\Gamma(N_1 \to LH) + \Delta\Gamma(N_1 \to \bar{L}\bar{H}) \\ &= \Gamma(N_1 \to LH) - \Gamma(N_1 \to \bar{L}\bar{H}) + \Gamma(N_1 \to \bar{L}\bar{H}) - \Gamma(N_1 \to LH) \\ &= 0.\end{aligned} \tag{5.38}$$

A more interesting case study would be $\sum_f \Delta\sigma(LH \to f)$ (see Ref. [104]), but it would present too much of a detour.

5.3.2 Holomorphic Cutting Rules

Let us now study the first unitary condition, Eq. (5.32a), where following Ref. [342] we will derive an alternate formulation of the cutting rules. This will give us a powerful tool for organising perturbative calculations, making results such as Eq. (5.37) evident at the diagram level.

In this study the critical step is the first one, where we observe that we may use Eq. (5.32a) to solve for $T^\dagger$ in terms of T:

$$\mathrm{i}T^\dagger = \mathrm{i}T(1+\mathrm{i}T)^{-1} = \mathrm{i}T - (\mathrm{i}T)^2 + (\mathrm{i}T)^3 - (\mathrm{i}T)^4 + \dots . \tag{5.39}$$

Component-wise this reads

$$\mathrm{i}T^*_{fi} = \mathrm{i}T_{if} - (\mathrm{i}T)^2_{if} + (\mathrm{i}T)^3_{if} - (\mathrm{i}T)^4_{if} + \dots , \tag{5.40}$$

where $(\mathrm{i}T)^n_{if}$ is understood as the sum over diagrams for $f \to i$ with $n-1$ on-shell cuts. This is a very useful relation, and it is worthwhile to work through an example to gain an understanding of what it is telling us.

EXAMPLE

Let us consider a fictional process at a fixed perturbative order,

$\mathrm{i}\mathcal{M}_{fi} =$ 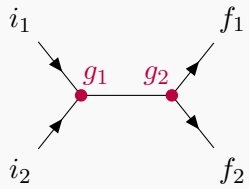

$= (\mathrm{i}g_1)\dfrac{\mathrm{i}}{p^2 - m^2 + \mathrm{i}\epsilon}(\mathrm{i}g_2),$ (5.41)

for which we can immediately read off

$$\mathrm{i}\mathcal{M}^*_{fi} = \frac{-\mathrm{i}g_1^* g_2^*}{p^2 - m^2 - \mathrm{i}\epsilon}. \tag{5.42}$$

The right-hand side of Eq. (5.40), which at $\mathcal{O}(g_1^* g_2^*)$ only receives contributions from the first two terms, reads at the $\mathcal{M}$ level

$\mathrm{i}\mathcal{M}_{if} - (\mathrm{i}\mathcal{M})^2_{if} =$ 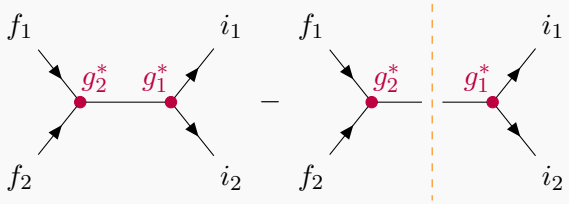

(5.43)

$$= (\mathrm{i}g_2^*)\frac{\mathrm{i}}{p^2 - m^2 + \mathrm{i}\epsilon}(\mathrm{i}g_1^*) - (\mathrm{i}g_2^*)2\pi\delta(p^2 - m^2)(\mathrm{i}g_1^*) \tag{5.44}$$

$$= -\mathrm{i}g_1^* g_2^* \left[\frac{1}{p^2 - m^2 + \mathrm{i}\epsilon} + 2\pi\mathrm{i}\delta(p^2 - m^2)\right], \tag{5.45}$$

where we recall Eq. (5.18) in realising the cut as a delta function. To reconcile this expression with Eq. (5.42) we must call upon the *Sokhotski-Plemelj identity*

$$\frac{1}{p^2 - m^2 + \mathrm{i}\epsilon} = \mathcal{P}\frac{1}{p^2 - m^2} - \mathrm{i}\pi\delta(p^2 - m^2), \tag{5.46}$$

where $\mathcal{P}$ denotes the Cauchy principal value. Then

$$\frac{1}{p^2 - m^2 + \mathrm{i}\epsilon} + 2\pi\mathrm{i}\delta(p^2 - m^2) = \mathcal{P}\frac{1}{p^2 - m^2} + \mathrm{i}\pi\delta(p^2 - m^2) \tag{5.47}$$

$$= \frac{1}{p^2 - m^2 - \mathrm{i}\epsilon}, \tag{5.48}$$

and we have agreement.

Thus, Eq. (5.39) is telling us that to conjugate $\mathcal{M} = c\mathcal{A}$ we first mirror the diagram and reverse the arrows, which conjugates the couplings[5] $c \to c^*$, and then subtract all one-cut diagrams, add all two-cut diagrams, and so on, which amounts to conjugating the dynamical amplitude, $\mathcal{A} \to \mathcal{A}^*$. Through a slight abuse of notation we may roughly express this as

$$\mathrm{i}(c\mathcal{A})^* = \mathrm{i}c^*\mathcal{A} - c^*(\mathrm{i}\mathcal{A})^2 + c^*(\mathrm{i}\mathcal{A})^3 - \ldots, \qquad \text{or} \tag{5.49}$$

$$\mathrm{i}\mathcal{A}^* = \mathrm{i}\mathcal{A} - (\mathrm{i}\mathcal{A})^2 + (\mathrm{i}\mathcal{A})^3 - \ldots, \tag{5.50}$$

where we now understand $(\mathrm{i}\mathcal{A})^n$ to mean $\mathrm{i}\mathcal{A}$ with $n-1$ on-shell cuts. Incidentally this implies

$$2\,\mathrm{Im}\,\mathcal{A} = -(\mathrm{i}\mathcal{A})^2 + (\mathrm{i}\mathcal{A})^3 - (\mathrm{i}\mathcal{A})^4 + \ldots. \tag{5.51}$$

Notice that we recover the simplified cutting rule of Eq. (5.16) when the $(\mathrm{i}\mathcal{A})^3$ and higher terms vanish. When they do not we instead understand this result to be

[5] It also conjugates any spinor chains, $\langle u|\gamma^\mu\gamma^\nu\cdots|u\rangle \to \langle u|\gamma^\mu\gamma^\nu\cdots|u\rangle^\dagger$, which can result in a complex conjugate if, for example, there appears a $\mathrm{Tr}(\gamma^\mu\gamma^\nu\gamma^\rho\gamma^\sigma\gamma^5) = -4\mathrm{i}\epsilon^{\mu\nu\rho\sigma}$. The inclusion of spinor chains complicates our simple argument somewhat, as we treat the them as part of $\mathcal{A}$ instead of c. Fortunately, though I don't do so here, it isn't too difficult to generalise.

equivalent to the more general form of Eq. (5.15).

The above example should kindle a greater appreciation for the role of the $\mathrm{i}\epsilon$ in propagators, which are demonstrably important even at tree-level. Indeed, unitarity depends on their inclusion. This will be of relevance to us in the next two chapters, where in one I will explicitly argue away the imaginary part of some propagators, and in the other I will use the imaginary part to demonstrate infrared finiteness.

Returning to the topic of CP asymmetries, we may use Eq. (5.40) in concert with the CPT theorem to show that the asymmetry at the T-matrix level is

$$\begin{aligned}
\Delta|T_{fi}|^2 &= |T_{fi}|^2 - |T_{\overline{fi}}|^2 \\
&= |T_{fi}|^2 - |T_{if}|^2 \\
&= -\mathrm{i}T^*_{fi}\mathrm{i}T_{fi} - (i \leftrightarrow f) \\
&= \left[-\mathrm{i}T_{if} + (\mathrm{i}T)^2_{if} - (\mathrm{i}T)^3_{if} + \ldots\right]\mathrm{i}T_{fi} - (i \leftrightarrow f) \qquad (5.52) \\
&= \left[(\mathrm{i}T)^2_{if}\mathrm{i}T_{fi} - \mathrm{i}T_{if}(\mathrm{i}T)^2_{fi}\right] - \left[(\mathrm{i}T)^3_{if}\mathrm{i}T_{fi} - \mathrm{i}T_{if}(\mathrm{i}T)^3_{fi}\right] + \ldots . \qquad (5.53)
\end{aligned}$$

This result goes by the name of the **holomorphic cutting rules** [342–345], named so because there are no surviving complex conjugates. These rules make explicit from the outset the need for cutting through amplitudes, and unlike Eq. (5.6) their derivation did not rely on the assertions $|\mathcal{A}_0|^2 = |\overline{\mathcal{A}}_0|^2$, $|\mathcal{A}_1|^2 = |\overline{\mathcal{A}}_1|^2$, and $\mathcal{A}_0^*\mathcal{A}_1 = \overline{\mathcal{A}}_0^*\overline{\mathcal{A}}_1$ that, while easy to check for concrete examples, are difficult to prove generally.

Example

To confirm that the holomorphic cutting rules reproduce the result of the conventional Cutkosky approach, let us return to our trusty Type-I Seesaw example for one last time. In accordance with Eq. (5.53) we have that

$\Delta|T(N_1 \to LH)|^2 =$

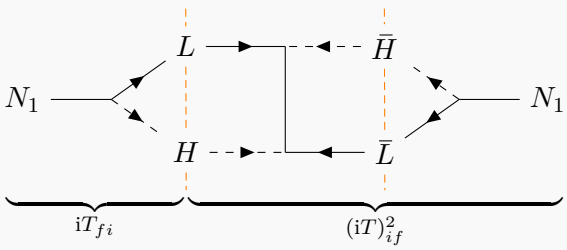

(5.54)

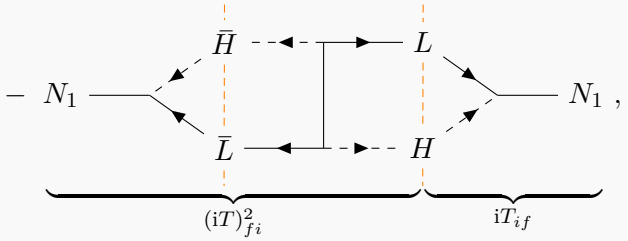

with no integration over the phase space of the final state LH, and where the series terminates at the first term as there are no more valid cuts. By now we are experienced enough to identify that the first line is equal at the $\mathcal{M}$ level to

$$c_0 c_1^* \int \mathrm{d}\Pi_{\bar{H}\bar{L}}\, \mathrm{i}\mathcal{A}_0(N_1 \to LH)\mathrm{i}\mathcal{A}(LH \to \bar{H}\bar{L})\mathrm{i}\mathcal{A}(\bar{H}\bar{L} \to N_1), \tag{5.55}$$

while the second is

$$-c_0^* c_1 \int \mathrm{d}\Pi_{\bar{H}\bar{L}}\, \mathrm{i}\mathcal{A}(N_1 \to \bar{H}\bar{L})\mathrm{i}\mathcal{A}(\bar{H}\bar{L} \to LH)\mathrm{i}\mathcal{A}_0(LH \to N_1). \tag{5.56}$$

Because there are no further valid cuts the amplitudes are all individually real, allowing us to use $\mathcal{A}(i \to f) = \mathcal{A}(f \to i)^* = \mathcal{A}(f \to i)$ to observe that the amplitude factors in each line are in fact identical to each other, and moreover equal to

$$\int \mathrm{d}\Pi_{\bar{H}\bar{L}}\, \mathrm{i}\mathcal{A}_0(N_1 \to LH)^*\mathrm{i}\mathcal{A}(N_1 \to \bar{H}\bar{L})\mathrm{i}\mathcal{A}(\bar{H}\bar{L} \to LH) = -2\mathrm{i}\,\mathrm{Im}(\mathcal{A}_0^*\mathcal{A}_1) \tag{5.57}$$

per the cutting rules in reverse. We therefore see that, up to delta function factors found in transit between the T level and $\mathcal{M}$ level,

$$\begin{aligned} \Delta|T|^2 &= (c_0 c_1^* - c_0^* c_1) \times (-2\mathrm{i})\,\mathrm{Im}(\mathcal{A}_0^*\mathcal{A}_1) && (5.58)\\ &= -4\,\mathrm{Im}(c_0^* c_1)\,\mathrm{Im}(\mathcal{A}_0^*\mathcal{A}_1), && (5.59) \end{aligned}$$

in exact agreement with Eq. (5.6).

A useful application of the holomorphic cutting rules is that they allow us to immediately and easily see that the total CP asymmetry is zero:

$$\begin{aligned}\sum_f \int \mathrm{d}\Pi_f \, \Delta|T_{fi}|^2 &= \sum_f \int \mathrm{d}\Pi_f \left\{ \left[(\mathrm{i}T)^2_{if} \mathrm{i}T_{fi} - \mathrm{i}T_{if} (\mathrm{i}T)^2_{fi} \right] - \left[(\mathrm{i}T)^3_{if} \mathrm{i}T_{fi} - \mathrm{i}T_{if} (\mathrm{i}T)^3_{fi} \right] + \ldots \right\} \\ &= \left[(\mathrm{i}T)^3_{ii} - (\mathrm{i}T)^3_{ii} \right] - \left[(\mathrm{i}T)^4_{ii} - (\mathrm{i}T)^4_{ii} \right] + \ldots \\ &= 0. \end{aligned} \tag{5.60}$$

By examining the terms

$$\sum_f \int \mathrm{d}\Pi_f \left[(\mathrm{i}T)^2_{if} \mathrm{i}T_{fi} - \mathrm{i}T_{if} (\mathrm{i}T)^2_{fi} \right] = \sum_{f,k} \int \mathrm{d}\Pi_f \, \mathrm{d}\Pi_k \left[\mathrm{i}T_{ik} \mathrm{i}T_{kf} \mathrm{i}T_{fi} - \mathrm{i}T_{if} \mathrm{i}T_{fk} \mathrm{i}T_{ki} \right] \tag{5.61}$$

more closely, we can pinpoint that the asymmetry due to $i \to k \to f$ (that is, due to the cut with intermediate state k in the process $i \to f$) cancels against the asymmetry due to $i \to f \to k$. This gives us an even stronger condition than Eq. (5.37), as it allows us to identify the cancellation of asymmetries on a per-diagram basis. We will return to this point in the next chapter, where it will turn out that the asymmetries in the BSM decays $h^- \to e\bar{L}\bar{H} \to LL$ and $h^- \to LL \to e\bar{L}\bar{H}$ cancel within the Boltzmann equation for L, but not in the way we might expect from this discussion.

5.4 Modelling Leptogenesis

It is not enough to say there exists *some* CP asymmetry in our theory – we would like to quantitatively assess whether it is enough to reproduce the observed matter abundance. To determine this we will ultimately need to model the evolution of the early universe and carefully track the number of particles and antiparticles through a network of Boltzmann equations [346]. This is in principle a rather difficult undertaking, but with the right application of statistical methods and approximations it can be made manageable. General references for this section and the remainder of this chapter include Refs. [89; 94; 104; 347; 348], with Refs. [104; 347; 348] offering more of a focus on the leptogenesis aspect. As we have a lot of ground to cover I will defer many of the details to these references and present only the important points. I apologise in advance for the impending overdensity

of new definitions and notation, but it is regrettably unavoidable.

5.4.1 The Expanding Universe

The stage on which this drama plays out is that of an expanding universe, described by the celebrated **Friedmann–Lemaître–Robertson–Walker** (FLRW) **metric**,

$$\mathrm{d}s^2 = \mathrm{d}t^2 - a^2(t)\left(\frac{\mathrm{d}r^2}{1-kr^2} + r^2\mathrm{d}\Omega^2\right). \tag{5.62}$$

The parameter $a(t)$ is called the **scale factor**, and it captures the expansion of the universe, with the normalisation $a_0 \equiv a(\text{today}) = 1$. The other parameter, k, describing the spatial curvature of the universe, is observed to be close to, if not zero [90].

The time evolution of the scale factor is governed by the *Friedmann equations*,

$$\frac{\dot{a}^2}{a^2} = \frac{8\pi G}{3}\rho - \frac{k}{a^2} + \frac{\Lambda}{3} \quad \text{and} \tag{5.63a}$$

$$\frac{\ddot{a}}{a} = -\frac{4\pi G}{3}(\rho + 3P) + \frac{\Lambda}{3}, \tag{5.63b}$$

which are the form taken by the Einstein equations,

$$G_{\mu\nu} + \Lambda g_{\mu\nu} = 8\pi G T_{\mu\nu}, \tag{5.64}$$

when the matter content of an FLRW universe is modelled as a perfect fluid, $T^{\mu}{}_{\nu} = \mathrm{diag}(\rho, -P, -P, -P)$. Here ρ and P are respectively the energy and pressure densities of the fluid. Baryogenesis is expected to have occurred during the *radiation-dominated* era of the universe, where temperatures were large enough that most particles were relativistic, contributing to the energy density and pressure budget with $P = \rho/3$, and dominating over both k and the cosmological constant Λ. In this era the Friedmann equations then imply

$$\rho \propto a^{-4} \quad \text{and} \quad a \propto t^{-1/2}, \tag{5.65}$$

and we may understand the first proportionality as stating that the energy density decreases as a^{-3} due to the volume expansion of the universe, and additionally as a^{-1} due to the redshifting of radiation. Often it will turn out to be more convenient to work in terms of the **Hubble rate**[6]

$$\mathcal{H} \equiv \frac{\dot{a}}{a} = \sqrt{\frac{8\pi G}{3}\rho} \qquad \text{(in radiation domination)}, \tag{5.66}$$

as we will shortly see.

5.4.2 Equilibrium Thermodynamics

With our backdrop in place, we turn to the study of the relativistic particles populating the early universe. At early times these particles constitute a thermal plasma, rapidly scattering and reacting in whichever way possible. To trace their physics—their *thermal history*—one might think to input these interactions into a grand collection of Boltzmann equations (to be introduced in the next section) and let it run, but this is overkill. Instead, we recognise that as long as these interactions are suitably fast (meaning the interaction rate Γ is much larger than the rate of expansion $\mathcal{H}$), they will serve to drive the particles in the plasma to a state of thermal equilibrium. We may therefore capture the effect of these fast interactions simply by presupposing that the participating particles follow equilibrium distributions.

There are two important forms of equilibria: *kinetic* and *chemical*. Kinetic equilibrium is achieved through scatterings which do not change particle number, such as the gauge scattering $e^{\pm}B \to e^{\pm}B$.[7] A particle species i in kinetic equilibrium follows the distribution

[6]Though it is more common to use the notation H for the Hubble rate, I will use $\mathcal{H}$ to avoid confusing it with the Higgs field.

[7]Recall that B is the $\mathrm{U}(1)_Y$ gauge boson. The electroweak phase transition is thought to occur at around $T \approx 159.5\,\mathrm{GeV}$ [349], so at greater temperatures we should speak in terms of B instead of photons.

$$f_i(\mathbf{p}) = \frac{1}{e^{(E_p - \mu_i)/T} - \eta_i}, \quad \text{where} \quad E_p = \sqrt{\mathbf{p}^2 + m_i^2}. \tag{5.67}$$

Bosons have $\eta_i = 1$, in which case this distribution is known as the **Bose-Einstein distribution**, and fermions have $\eta_i = -1$, with f_i the **Fermi-Dirac distribution**. The parameter μ_i is called the **chemical potential** of i, and a non-zero value captures an excess (when $\mu_i > 0$) or scarcity (when $\mu_i < 0$) of particles. Chemical equilibrium is achieved through particle number-changing processes, where a generic fast process $ab\ldots \leftrightarrow ij\ldots$ ensures that

$$\mu_a + \mu_b + \ldots = \mu_i + \mu_j + \ldots. \tag{5.68}$$

In particular, the non-conservation of gauge bosons, for instance due to double Compton scattering $e^{\pm}B \leftrightarrow e^{\pm}BB$, imposes $\mu_B = 0$, and the annihilation process $e^+e^- \leftrightarrow BB$ therefore demands in turn that a particle and its antiparticle have opposite chemical potentials:

$$\mu_i = -\mu_{\bar{i}}. \tag{5.69}$$

Fast gauge interactions with the $\mathrm{SU}(2)_\mathrm{W}$ gauge bosons similarly ensures that the two components of an $\mathrm{SU}(2)_\mathrm{W}$ doublet have the same chemical potential, allowing us to treat the doublet as a single species.

To achieve leptogenesis we will naturally wish to generate a non-zero chemical potential for the baryons. The necessary value of μ will turn out to be small compared to the temperature during leptogenesis, allowing us to expand around the distributions

$$f_i^{\mathrm{eq}} \equiv f_i\Big|_{\mu_i = 0} = \frac{1}{e^{E_p/T} - \eta_i}. \tag{5.70}$$

At zeroth order in μ/T the number density of a relativistic species i with g_i internal degrees of freedom is

$$n_i \approx n_i^{\rm eq} = g_i \int \frac{{\rm d}^3\mathbf{p}}{(2\pi)^3} f_i^{\rm eq}(\mathbf{p}) \approx \frac{\zeta(3)}{\pi^2} g_i T^3 \times \begin{cases} 1 & \text{bosons} \\ \frac{3}{4} & \text{fermions} \end{cases}, \tag{5.71}$$

where $\zeta(x)$ is the Riemann zeta function, with $\zeta(3) = 1.202\ldots$; and its energy density is

$$\rho_i \approx \rho_i^{\rm eq} = g_i \int \frac{{\rm d}^3\mathbf{p}}{(2\pi)^3} f_i^{\rm eq}(\mathbf{p}) E_p \approx \frac{\pi^2}{30} g_i T^4 \times \begin{cases} 1 & \text{bosons} \\ \frac{7}{8} & \text{fermions} \end{cases}. \tag{5.72}$$

Plugging the latter into the Hubble rate, Eq. (5.66), then gives

$$\mathcal{H} = \sqrt{\frac{4\pi^3 G}{45} g_\star} T^2, \tag{5.73}$$

where

$$g_\star \equiv \sum_{\rm bosons} g_i \left(\frac{T_i}{T_\gamma}\right)^4 + \frac{7}{8} \sum_{\rm fermions} g_i \left(\frac{T_i}{T_\gamma}\right)^4 \tag{5.74}$$

is known as the *effective number of relativistic degrees of freedom*. Above the electroweak phase transition all SM particles are relativistic and $g_\star = 106.75$, while today only photons and neutrinos remain so, and $g_{\star 0} \approx 3.36$ [94]. It is common to express the Hubble constant in terms of the *Planck mass* $M_{\rm P} = (\hbar c/G)^{1/2} \approx 1.2 \times 10^{19}\,{\rm GeV}$,

$$\mathcal{H} \approx 1.66 \sqrt{g_\star} \frac{T^2}{M_{\rm P}}, \tag{5.75}$$

and it is usually this form that is used in back-of-the-envelope calculations of $\Gamma/\mathcal{H}$ to assess whether a process is 'fast'.

Now, in the absence of interactions the total particle number $N_i = n_i V \propto n_i a^3$ is constant, implying that the number density must dilute due to the expansion of the universe:

$$\frac{{\rm d}N_i}{{\rm d}t} = 0 \quad \Longrightarrow \quad \frac{{\rm d}n_i}{{\rm d}t} = -3\mathcal{H} n_i. \tag{5.76}$$

It will be more convenient to work with a 'comoving' quantity that scales out this dilution.

For this purpose we first consider the *entropy density*

$$s = \frac{\rho + P}{T} \simeq \frac{2\pi^2}{45} g_{\star S} T^3. \tag{5.77}$$

Here the *effective number of degrees of freedom in entropy*

$$g_{\star S} \equiv \sum_{\text{bosons}} g_i \left(\frac{T_i}{T_\gamma}\right)^3 + \frac{7}{8} \sum_{\text{fermions}} g_i \left(\frac{T_i}{T_\gamma}\right)^3 \tag{5.78}$$

is for most temperatures equal to $g_\star$, differing only in the present day due to the decoupling of neutrinos, with $g_{\star S,0} \approx 3.91$ [94]. The usefulness of s is derived from the fact that the total entropy is conserved in equilibrium (and even to a good approximation in non-equilibrium), $sa^3 = \text{const}$, which one can demonstrate using the Friedmann equations and basic thermodynamical arguments [94; 348]. From this it is straightforward to verify that the **entropy-normalised number density**

$$Y_i \equiv \frac{n_i}{s}, \tag{5.79}$$

is what we are after:

$$s\frac{\mathrm{d}Y_i}{\mathrm{d}t} = \frac{\mathrm{d}n_i}{\mathrm{d}t} - 3\mathcal{H}n_i = 0 \quad \text{(without interactions)}. \tag{5.80}$$

Assuming there are no additional baryon number-changing interactions after baryogenesis ends, the generated asymmetry $Y_B \equiv Y_b - Y_{\bar{b}}$ will therefore match exactly onto the measured asymmetry today, with

$$\begin{aligned} Y_B(\text{end of baryogenesis}) &= Y_B(\text{today}) \\ &= \frac{n_{B,0}}{n_{\gamma,0}} \frac{n_{\gamma,0}}{s_0} \\ &= \frac{n_{B,0}}{n_{\gamma,0}} \frac{45\zeta(3)}{2\pi^4} \frac{g_\gamma}{g_{\star S,0}} \\ &\approx (8.68 \pm 0.57) \times 10^{-11}, \end{aligned} \tag{5.81}$$

where we have used the observed baryon-to-photon ratio $n_{B,0}/n_{\gamma,0} = (6.10 \pm 0.4) \times 10^{-10}$ from the beginning of this chapter. If we are able to formulate the asymmetry generation

in terms of Y_B, Eq. (5.81) is the target we must meet. Such a formulation is fortuitously easy in the μ/T expansion, since for a relativistic species i we have at leading order

$$n_{\Delta i} = n_i - n_{\bar{i}} \approx \frac{T^3}{6} g_i \zeta_i \frac{\mu_i}{T}, \quad \text{where} \quad \zeta_i = \begin{cases} 2 & \text{bosons} \\ 1 & \text{fermions} \end{cases}, \tag{5.82}$$

and so we may use

$$Y_{\Delta i} = \frac{15\zeta_i}{4\pi^2} \frac{g_i}{g_{\star S}} \frac{\mu_i}{T} \tag{5.83}$$

to freely exchange μ_i/T for $Y_{\Delta i}$. Note that because $Y_B \sim 10^{-10}$ and $g_{\star S}$ is at most $\mathcal{O}(100)$, we see that our expansion in small μ_i/T is justified (at least for baryons).

Before moving on we will lastly need to amend parts of the above discussion for non-relativistic particles, which are of relevance to us because the leptogenesis scenario we will consider involves the out-of-equilibrium decay of a heavy species. As these decays generally occur when the temperature falls below the mass of the heavy species, we will take it to follow the **Maxwell-Boltzmann distribution**

$$f_i = e^{-(E_i - \mu_i)/T} \equiv f_i^{\text{eq}} e^{\mu_i/T}, \tag{5.84}$$

which arises from the Bose-Einstein and Fermi-Dirac distributions in the low-temperature limit $T \ll m_i$. A species following this distribution has the number density

$$Y_i = \frac{45}{4\pi^2} \frac{m_i^2}{T^2} \frac{g_i}{g_{\star S}} K_2\left(\frac{m_i}{T}\right) e^{\mu_i/T} \equiv Y_i^{\text{eq}} e^{\mu_i/T}, \tag{5.85}$$

where

$$K_n(z) \equiv \frac{\sqrt{\pi}}{\Gamma(n+\frac{1}{2})} \frac{z^n}{2^n} \int_1^\infty (x^2-1)^{n-\frac{1}{2}} e^{-zx} \, \mathrm{d}x \tag{5.86}$$

is the modified Bessel function of the second kind. Out of equilibrium we cannot assume that $\mu_i = -\mu_{\bar{i}}$, and the μ/T expansion instead takes the form

$$\frac{Y_i}{Y_i^{\text{eq}}} = e^{\mu_i/T} \approx 1 + \frac{\mu_i}{T}, \tag{5.87}$$

and moreover

$$\frac{Y_{\Delta i}}{Y_i^{\rm eq}} \approx \frac{\mu_i}{T} - \frac{\mu_{\bar{i}}}{T}. \tag{5.88}$$

5.4.3 The Boltzmann Equation

Now that we have the infrastructure with which to understand a baryon asymmetry we are ready to discuss our main tool for computing it. The **Boltzmann equation** (BE) governs the non-equilibrium dynamics of our particles, dictating that the (entropy-normalised) number density of a given particle species i evolves in accordance with

$$s\frac{{\rm d}Y_i}{{\rm d}t} = \frac{{\rm d}n_i}{{\rm d}t} + 3\mathcal{H}n_i = \sum_{a,b,j,\ldots} [ab\ldots \leftrightarrow ij\ldots]. \tag{5.89}$$

The rather compact notation of the right-hand side stands for

$$[ab\ldots \leftrightarrow ij\ldots] \equiv [ab\ldots \to ij\ldots] - [ij\ldots \to ab\ldots], \tag{5.90}$$

where

$$\begin{aligned}[ab\ldots \to ij\ldots] \equiv \int [{\rm d}p_a][{\rm d}p_b]\cdots[{\rm d}p_i][{\rm d}p_j]\cdots (2\pi)^4\delta^{(4)}(p_a+p_b+\ldots-p_i-p_j-\ldots) \\ \times |\mathcal{M}(ab\ldots\to ij\ldots)|^2 f_a f_b\cdots(1+\eta_i f_i)(1+\eta_j f_j)\cdots\end{aligned} \tag{5.91}$$

is the thermally-averaged reaction rate for the process $ab\ldots \to ij\ldots$. Here $|\mathcal{M}|^2$ is summed over all initial- and final-state spins, and the form in which the final state distributions appear, $1+\eta_i f_i$, captures the Bose-enhancement of bosons and Pauli-blocking of fermions. When all particles are in kinetic equilibrium we can relate the distributions appearing in $[ab\ldots \to ij\ldots]$ and $[ij\ldots \to ab\ldots]$ by

$$f_a f_b\cdots(1+\eta_i f_i)(1+\eta_j f_j)\cdots = e^{(\mu_a+\mu_b+\ldots-\mu_i-\mu_j-\ldots)/T} f_i f_j\cdots(1+\eta_a f_a)(1+\eta_a f_a)\cdots, \tag{5.92}$$

which follows from the identity

$$1 + \eta_i f_i = e^{(E_i - \mu_i)/T} f_i \tag{5.93}$$

and conservation of energy. From the exponential factor in Eq. (5.92) we can see that the Boltzmann equation acts to push the participating particles towards chemical equilibrium – for example, if there are too many a particles then $[ab\ldots \to ij\ldots] > [ij\ldots \to ab\ldots]$. Note that if there is no CP violation, $|\mathcal{M}(ab\ldots \to ij\ldots)|^2 = |\mathcal{M}(ij\ldots \to ab\ldots)|^2$, and the particles *are* in chemical equilibrium, we instead have $[ab\ldots \leftrightarrow ij\ldots] = 0$, and the number density dilutes solely due to the Hubble expansion as claimed in the previous section.

In practice, it is more convenient to parameterise the evolution as a function of temperature, or better, the dimensionless variable

$$z \equiv \frac{m}{T}, \tag{5.94}$$

where m is a conveniently chosen mass scale. Using the conservation of entropy $\frac{\mathrm{d}}{\mathrm{d}t}(sa^3) \propto \frac{\mathrm{d}}{\mathrm{d}t}(g_{\star S} T^3 a^3) = 0$ and assuming that $g_{\star S}$ remains constant during baryogenesis, it is then not too difficult to show that the Boltzmann equation may be recast as

$$sz\mathcal{H}\frac{\mathrm{d}Y_i}{\mathrm{d}z} = \sum_{a,b,j,\ldots} [ab\ldots \leftrightarrow ij\ldots]. \tag{5.95}$$

To completely bring the BE into the form of a system of equations in the variables $\{Y_i(z)\}$ we must also finesse the right-hand side. As you might guess, this involves an expansion in the chemical potentials μ/T around the equilibrium reaction rate

$$\begin{aligned}\gamma(ab \to ij) \equiv \int [\mathrm{d}p_a][\mathrm{d}p_b][\mathrm{d}p_i][\mathrm{d}p_j](2\pi)^4 \delta^{(4)}(p_a + p_b - p_i - p_j) \\ \times |\mathcal{M}(ab \to ij)|^2 f_a^{\mathrm{eq}} f_b^{\mathrm{eq}} (1 + \eta_i f_i^{\mathrm{eq}})(1 + \eta_j f_j^{\mathrm{eq}}),\end{aligned} \tag{5.96}$$

where here and onwards I will drop the explicit ellipses and trust that the generalisation to an arbitrary number of particles is clear. We then have

$$[ab \to ij] = \gamma(ab \to ij) \frac{f_a f_b (1+\eta_i f_i)(1+\eta_j f_j)}{f_a^{\rm eq} f_b^{\rm eq} (1+\eta_i f_i^{\rm eq})(1+\eta_j f_j^{\rm eq})} \tag{5.97}$$

(for which I stress that the ratio of distributions remains under the integral of $\gamma(ab \to ij)$), and the relevant expansion, assuming all particles are in kinetic equilibrium, is

$$\frac{f_a f_b (1+\eta_i f_i)(1+\eta_j f_j)}{f_a^{\rm eq} f_b^{\rm eq} (1+\eta_i f_i^{\rm eq})(1+\eta_j f_j^{\rm eq})} = 1 + \sum_{I=a,b} \frac{\mu_I}{T} + \sum_{I=a,b,i,j} \eta_I f_I^{\rm eq} \frac{\mu_I}{T} + \mathcal{O}\left(\frac{\mu^2}{T^2}\right) \tag{5.98}$$

$$\equiv 1 + \sum_{I=a,b} \frac{Y_{\Delta I}}{2Y_I^{\rm nor}} + \sum_{I=a,b,i,j} \eta_I f_I^{\rm eq} \frac{Y_{\Delta I}}{2Y_I^{\rm nor}} + \mathcal{O}\left(\frac{\mu^2}{T^2}\right), \tag{5.99}$$

where we have used Eq. (5.83) and defined the convenient quantity

$$Y_I^{\rm nor} \equiv \frac{15\zeta_I}{8\pi^2} \frac{g_I}{g_{\star S}}. \tag{5.100}$$

If any of the particles are out of equilibrium we must instead use

$$\frac{f_i}{f_i^{\rm eq}} = \frac{Y_i}{Y_i^{\rm eq}} \approx 1 + \frac{\mu_i}{T} \quad \text{and} \quad \frac{1+\eta_i f_i}{1+\eta_i f_i^{\rm eq}} \approx 1, \tag{5.101}$$

as per Eq. (5.87).

Example

In the next chapter we will attempt to achieve leptogenesis through the out-of-equilibrium decay of a heavy scalar h^- introduced in the Zee model. Applying the above expansions to its decay into two lepton doublets, $h^- \to L_\alpha L_\beta$ (which, for now, we don't need to know anything about other than the fact that it's allowed), we find

$$\begin{aligned}
[h^- \to L_\alpha L_\beta] &= \gamma(h^- \to L_\alpha L_\beta) \frac{f_{h^-}(1-f_{L_\alpha})(1-f_{L_\beta})}{f_{h^-}^{\rm eq}(1-f_{L_\alpha}^{\rm eq})(1-f_{L_\beta}^{\rm eq})} \\
&\approx \gamma(h^- \to L_\alpha L_\beta) \left(1 + \frac{\mu_{h^-}}{T}\right)\left(1 - f_{L_\alpha}^{\rm eq}\frac{\mu_{L_\alpha}}{T} - f_{L_\beta}^{\rm eq}\frac{\mu_{L_\beta}}{T}\right) \\
&\approx \gamma(h^- \to L_\alpha L_\beta) \left(1 + \frac{\mu_{h^-}}{T} - f_{L_\alpha}^{\rm eq}\frac{\mu_{L_\alpha}}{T} - f_{L_\beta}^{\rm eq}\frac{\mu_{L_\beta}}{T}\right)
\end{aligned}$$

$$\approx \gamma(h^- \to L_\alpha L_\beta)\left(\frac{Y_{h^-}}{Y_{h^-}^{\rm eq}} - f_{L_\alpha}^{\rm eq}\frac{Y_{\Delta L_\alpha}}{2Y_{L_\alpha}^{\rm nor}} - f_{L_\beta}^{\rm eq}\frac{Y_{\Delta L_\beta}}{2Y_{L_\beta}^{\rm nor}}\right)$$
$$= \gamma(h^- \to L_\alpha L_\beta)\left(\frac{Y_{h^-}}{Y_{h}^{\rm eq}} - f_{L_\alpha}^{\rm eq}\frac{Y_{\Delta L_\alpha}}{2Y_{L}^{\rm nor}} - f_{L_\beta}^{\rm eq}\frac{Y_{\Delta L_\beta}}{2Y_{L}^{\rm nor}}\right), \tag{5.102}$$

which I have notationally simplified in the last line by writing $Y_{h^-}^{\rm eq} = Y_{h^+}^{\rm eq} \equiv Y_h^{\rm eq}$ and $Y_{L_\alpha}^{\rm nor} = Y_{L_\beta}^{\rm nor} \equiv Y_L^{\rm nor}$. For the inverse decay we similarly find

$$[L_\alpha L_\beta \to h^-] \approx \gamma(L_\alpha L_\beta \to h^-)\left(1 + (1 - f_{L_\alpha}^{\rm eq})\frac{\mu_{L_\alpha}}{T} + (1 - f_{L_\beta}^{\rm eq})\frac{\mu_{L_\beta}}{T}\right)$$
$$\approx \gamma(L_\alpha L_\beta \to h^-)\left(1 + (1 - f_{L_\alpha}^{\rm eq})\frac{Y_{\Delta L_\alpha}}{2Y_{L}^{\rm nor}} + (1 - f_{L_\beta}^{\rm eq})\frac{Y_{\Delta L_\beta}}{2Y_{L}^{\rm nor}}\right). \tag{5.103}$$

We note that the equilibrium distributions $f_{L_\alpha}^{\rm eq}$ and $f_{L_\beta}^{\rm eq}$ in Eqs. (5.102) and (5.103) inconveniently remain under the phase space integrals of $\gamma(h^- \to L_\alpha L_\beta)$ and $\gamma(L_\alpha L_\beta \to h^-)$, meaning that the parenthesised quantities still do not cleanly factor out from the γ's. Happily, this wrinkle will be (accidentally) resolved by our forthcoming manipulation.

Because we are interested in asymmetry generation it is smarter to track the evolution of the combinations

$$Y_{\Delta i} \equiv Y_i - Y_{\bar{i}} \quad \text{and} \quad Y_{\Sigma i} \equiv Y_i + Y_{\bar{i}} \tag{5.104}$$

instead of Y_i and $Y_{\bar{i}}$ separately. Here the Boltzmann equation for $Y_{\bar{i}}$ is

$$sz\mathcal{H}\frac{{\rm d}Y_{\bar{i}}}{{\rm d}z} = \sum_{a,b,j}[\bar{a}\,\bar{b} \leftrightarrow \bar{i}\,\bar{j}], \tag{5.105}$$

and using the fact that

$$\gamma(\bar{a}\,\bar{b} \to \bar{i}\,\bar{j}) = \gamma(ij \to ab), \tag{5.106}$$

which follows from the CPT theorem and the identity Eq. (5.92), we may write

$$[\overline{a}\,\overline{b} \to \overline{i}\,\overline{j}] = \gamma(ij \to ab)\frac{f_{\overline{a}} f_{\overline{b}}(1+\eta_i f_{\overline{i}})(1+\eta_j f_{\overline{j}})}{f_a^{\mathrm{eq}} f_b^{\mathrm{eq}}(1+\eta_i f_i^{\mathrm{eq}})(1+\eta_j f_j^{\mathrm{eq}})}. \tag{5.107}$$

Defining now the combinations

$$\Sigma\gamma(ab \to ij) \equiv \gamma(ab \to ij) + \gamma(ij \to ab) \quad \text{and} \tag{5.108a}$$
$$\Delta\gamma(ab \to ij) \equiv \gamma(ab \to ij) - \gamma(ij \to ab), \tag{5.108b}$$

as well as—for our own sanity—the abbreviated notation

$$f_{ab,ij} \equiv \frac{f_a f_b(1+\eta_i f_i)(1+\eta_j f_j)}{f_a^{\mathrm{eq}} f_b^{\mathrm{eq}}(1+\eta_i f_i^{\mathrm{eq}})(1+\eta_j f_j^{\mathrm{eq}})} \quad \text{and} \tag{5.109a}$$
$$\overline{f}_{ab,ij} \equiv \frac{f_{\overline{a}} f_{\overline{b}}(1+\eta_i f_{\overline{i}})(1+\eta_j f_{\overline{j}})}{f_a^{\mathrm{eq}} f_b^{\mathrm{eq}}(1+\eta_i f_i^{\mathrm{eq}})(1+\eta_j f_j^{\mathrm{eq}})}, \tag{5.109b}$$

we can now bring it all together, and after some straightforward algebra we find the Boltzmann equations for the difference and sum of number densities to be

$$sz\mathcal{H}\frac{\mathrm{d}Y_{\Delta i}}{\mathrm{d}z} = \sum_{a,b,j}\Big[\frac{1}{2}\Sigma\gamma(ab \to ij)\Big(f_{ab,ij} - f_{ij,ab} - \overline{f}_{ab,ij} + \overline{f}_{ij,ab}\Big) + \frac{1}{2}\Delta\gamma(ab \to ij)\Big(f_{ab,ij} + f_{ij,ab} + \overline{f}_{ab,ij} + \overline{f}_{ij,ab}\Big)\Big] \tag{5.110}$$

and

$$sz\mathcal{H}\frac{\mathrm{d}Y_{\Sigma i}}{\mathrm{d}z} = \sum_{a,b,j}\Big[\frac{1}{2}\Sigma\gamma(ab \to ij)\Big(f_{ab,ij} - f_{ij,ab} + \overline{f}_{ab,ij} - \overline{f}_{ij,ab}\Big) + \frac{1}{2}\Delta\gamma(ab \to ij)\Big(f_{ab,ij} + f_{ij,ab} - \overline{f}_{ab,ij} - \overline{f}_{ij,ab}\Big)\Big]. \tag{5.111}$$

Example

To gain a handle on this form of the BEs, let us construct the equations for a fixed lepton doublet flavour L_α using the decay $h^- \to L_\alpha L_\beta$ from our previous example. From Eqs. (5.102) and (5.103) we can read off

$$f_{h^-,L_\alpha L_\beta} = \frac{Y_{h^-}}{Y_h^{\rm eq}} - f_{L_\alpha}^{\rm eq}\frac{Y_{\Delta L_\alpha}}{2Y_L^{\rm nor}} - f_{L_\beta}^{\rm eq}\frac{Y_{\Delta L_\beta}}{2Y_L^{\rm nor}} \quad \text{and} \tag{5.111a}$$

$$f_{L_\alpha L_\beta,h^-} = 1 + (1-f_{L_\alpha}^{\rm eq})\frac{Y_{\Delta L_\alpha}}{2Y_L^{\rm nor}} + (1-f_{L_\beta}^{\rm eq})\frac{Y_{\Delta L_\beta}}{2Y_L^{\rm nor}}, \tag{5.111b}$$

and using $Y_{\Delta\overline{L}_\alpha} = -Y_{\Delta L_\alpha}$ we may similarly write

$$\overline{f}_{h^-,L_\alpha L_\beta} = \frac{Y_{h^+}}{Y_h^{\rm eq}} + f_{L_\alpha}^{\rm eq}\frac{Y_{\Delta L_\alpha}}{2Y_L^{\rm nor}} + f_{L_\beta}^{\rm eq}\frac{Y_{\Delta L_\beta}}{2Y_L^{\rm nor}} \quad \text{and} \tag{5.111c}$$

$$\overline{f}_{L_\alpha L_\beta,h^-} = 1 - (1-f_{L_\alpha}^{\rm eq})\frac{Y_{\Delta L_\alpha}}{2Y_L^{\rm nor}} - (1-f_{L_\beta}^{\rm eq})\frac{Y_{\Delta L_\beta}}{2Y_L^{\rm nor}}. \tag{5.111d}$$

Plugging into Eqs (5.110) and (5.111), we end up obtaining

$$\begin{aligned} sz\mathcal{H}\frac{{\rm d}Y_{\Delta L_\alpha}}{{\rm d}z} = &\sum_\beta \frac{1}{2}\Sigma\gamma(h^-\to L_\alpha L_\beta)\left(\frac{Y_{\Delta h}}{Y_h^{\rm eq}} - \frac{Y_{\Delta L_\alpha}+Y_{\Delta L_\beta}}{Y_L^{\rm nor}}\right) \\ &+ \sum_\beta \frac{1}{2}\Delta\gamma(h^-\to L_\alpha L_\beta)\left(\frac{Y_{\Sigma h}}{Y_h^{\rm eq}} + 2\right) \end{aligned} \tag{5.112}$$

and

$$\begin{aligned} sz\mathcal{H}\frac{{\rm d}Y_{\Sigma L_\alpha}}{{\rm d}z} = &\sum_\beta \frac{1}{2}\Sigma\gamma(h^-\to L_\alpha L_\beta)\left(\frac{Y_{\Sigma h}}{Y_h^{\rm eq}} - 2\right) \\ &+ \sum_\beta \frac{1}{2}\Delta\gamma(h^-\to L_\alpha L_\beta)\left(\frac{Y_{\Delta h}}{Y_h^{\rm eq}} + \frac{Y_{\Delta L_\alpha}+Y_{\Delta L_\beta}}{Y_L^{\rm nor}} + 2\frac{f_{L_\alpha}^{\rm eq}Y_{\Delta L_\alpha} + f_{L_\beta}^{\rm eq}Y_{\Delta L_\beta}}{Y_L^{\rm nor}}\right). \end{aligned} \tag{5.113}$$

(In principle there should be a factor of $(1+\delta_{\alpha\beta})$ under each of the sums to account for the case where $\beta = \alpha$, but it turns out that the decay rate vanishes when the leptons are the same flavour, and so the factor is unnecessary.) But for the second line of Eq. (5.113), there are no longer any $f_{L_\alpha}^{\rm eq}$ factors, and the parenthesised number densities all factor out from the γ's. If we wanted to, we could however justifiably neglect the second line of Eq. (5.113) as it is proportional to the product of the CP-violating difference $\Delta\gamma(h^-\to L_\alpha L_\beta)$ and the number density differences $Y_{\Delta i}$, both of which are tiny.

In fact, we may go one step further and drop Eq. (5.113) entirely: we are ultimately interested only in modelling the asymmetry $Y_{\Delta L}$, and since $Y_{\Sigma L}$ does not enter into Eq. (5.112) it is not necessary for us to track its evolution. Evidently we will however need to track both $Y_{\Delta h}$ and $Y_{\Sigma h}$.

For the remainder of this section we will hijack the above example to motivate the discussion. The first line of Eq. (5.112),

$$sz\mathcal{H}\frac{\mathrm{d}Y_{\Delta L_\alpha}}{\mathrm{d}z} \supset \sum_\beta \frac{1}{2}\Sigma\gamma(h^- \to L_\alpha L_\beta)\left(\frac{Y_{\Delta h}}{Y_h^{\mathrm{eq}}} - \frac{Y_{\Delta L_\alpha} + Y_{\Delta L_\beta}}{Y_L^{\mathrm{nor}}}\right), \tag{5.114}$$

and more generally of Eq. (5.110), is known as the *washout term*. Its purpose is to work against us, erasing any extant lepton number asymmetry. This is easy enough to see: when we have an excess of lepton doublets or a deficit of h^-'s, the term in parentheses is negative and the inverse decay $L_\alpha L_\beta \to h^-$ will act more quickly to reduce $Y_{\Delta L}$.

The second line of Eq. (5.112),

$$sz\mathcal{H}\frac{\mathrm{d}Y_{\Delta L_\alpha}}{\mathrm{d}z} \supset \sum_\beta \frac{1}{2}\Delta\gamma(h^- \to L_\alpha L_\beta)\left(\frac{Y_{\Sigma h}}{Y_h^{\mathrm{eq}}} + 2\right), \tag{5.115}$$

and of Eq. (5.110), is known as the *source term*, and its purpose is to generate a lepton asymmetry. However, there is a problem – when h^- is in chemical equilibrium, meaning $Y_{\Sigma h} = 2Y_h^{\mathrm{eq}}$, we should expect the source term to be suppressed, but it is clearly not. Where have we gone wrong?

It turns out that we have not so much erred as we have failed to account for all effects. The fix comes from considering the scattering process $L_\gamma L_\delta \to L_\alpha L_\beta$, which occurs through an s-channel h^- mediator. The critical insight is that this scattering process contains the decay $h^- \to L_\alpha L_\beta$ as a subprocess when the h^- is exchanged on-shell, and so the physical effect of the decay is double-counted in the Boltzmann equation. There are two equivalent options available to us: we may remove the decay from the Boltzmann equation, or we may subtract the on-shell piece from the scattering. It is more conventional to take the latter approach, giving this procedure the name of **real intermediate state** (RIS)

subtraction [346; 347; 350].

Let us therefore add to the Boltzmann equation the combination

$$[L_\gamma L_\delta \leftrightarrow L_\alpha L_\beta]_{\text{off-shell}} = [L_\gamma L_\delta \leftrightarrow L_\alpha L_\beta] - [L_\gamma L_\delta \leftrightarrow L_\alpha L_\beta]_{\text{on-shell}}, \tag{5.116}$$

which, as you can check, contributes to $Y_{\Delta L_\alpha}$ as

$$\begin{aligned} sz\mathcal{H}\frac{\mathrm{d}Y_{\Delta L_\alpha}}{\mathrm{d}z} \supset \sum_\beta \frac{1}{2} \sum_{\gamma,\delta\neq\alpha} \frac{1}{2}\Sigma\gamma(L_\gamma L_\delta \to L_\alpha L_\beta)_{\text{off-shell}} \left(\frac{Y_{\Delta L_\gamma} + Y_{\Delta L_\delta} - Y_{\Delta L_\alpha} - Y_{\Delta L_\beta}}{Y_L^{\text{nor}}} \right) \\ + \sum_\beta \frac{1}{2} \sum_{\gamma,\delta\neq\alpha} \frac{1}{2}\Delta\gamma(L_\gamma L_\delta \to L_\alpha L_\beta)_{\text{off-shell}} \times 4, \end{aligned} \tag{5.117}$$

where here the additional factor of $\frac{1}{2}$ is to avoid double-counting the initial states, and we exclude $\gamma, \delta = \alpha$ from the sum over flavours because e.g. $L_\alpha L_\delta \to L_\alpha L_\beta$ does not change the number of L_α particles. The first line, containing the off-shell scattering contribution to the washout, is higher-order in the couplings than the washout from $\Sigma\gamma(h^- \to L_\alpha L_\beta)$ in Eq. (5.114), and so it is usually acceptable to neglect it unless these couplings are $\mathcal{O}(1)$. We may also drop the scattering asymmetry $\Delta\gamma(L_\gamma L_\delta \to L_\alpha L_\beta)$ from the second line, as it will similarly be higher-order than the decay asymmetry $\Delta\gamma(h^- \to L_\alpha L_\beta)$. This leaves us with just the subtracted on-shell piece,

$$sz\mathcal{H}\frac{\mathrm{d}Y_{\Delta L_\alpha}}{\mathrm{d}z} \gtrsim -\sum_\beta \sum_{\gamma,\delta\neq\alpha} \Delta\gamma(L_\gamma L_\delta \to L_\alpha L_\beta)_{\text{on-shell}}. \tag{5.118}$$

To deal with this piece we use that

$$\gamma(L_\gamma L_\delta \to L_\alpha L_\beta)_{\text{on-shell}} = \frac{\gamma(L_\gamma L_\delta \to h^-)\gamma(h^- \to L_\alpha L_\beta)}{\frac{1}{2}\sum_{\rho,\sigma}\gamma(h^- \to L_\rho L_\sigma)} \tag{5.119}$$

—for which I'll defer a proof to Section 5.A—and then in turn

$$\begin{aligned} &\Delta\gamma(L_\gamma L_\delta \to L_\alpha L_\beta)_{\text{on-shell}} \\ &\quad = \frac{\Sigma\gamma(h^- \to L_\gamma L_\delta)\Delta\gamma(h^- \to L_\alpha L_\beta) - \Delta\gamma(h^- \to L_\gamma L_\delta)\Sigma\gamma(h^- \to L_\alpha L_\beta)}{\sum_{\rho,\sigma}\gamma(h^- \to L_\rho L_\sigma)}. \end{aligned} \tag{5.120}$$

When inserted into Eq. (5.118), we notice (perhaps with some effort) that we can now

extend the sums to include $\gamma, \delta = \alpha$ since the additional terms either vanish or cancel against each other. The complete sum then allows us to use

$$\sum_{\gamma,\delta} \frac{\Sigma\gamma(h^- \to L_\gamma L_\delta)}{\sum_{\rho,\sigma} \gamma(h^- \to L_\rho L_\sigma)} = 2 \tag{5.121}$$

for the first term, and—to be demonstrated in the next chapter—

$$\sum_{\gamma,\delta} \Delta\gamma(h^- \to L_\gamma L_\delta) = 0 \tag{5.122}$$

for the second, leaving us at last with

$$sz\mathcal{H}\frac{\mathrm{d}Y_{\Delta L_\alpha}}{\mathrm{d}z} \supset -2\sum_\beta \Delta\gamma(h^- \to L_\alpha L_\beta). \tag{5.123}$$

Adding this to Eq. (5.115), we finally obtain a source term with the correct equilibrium behaviour, and the full corrected form of the Boltzmann equation for $Y_{\Delta L_\alpha}$ is therefore

$$\begin{aligned} sz\mathcal{H}\frac{\mathrm{d}Y_{\Delta L_\alpha}}{\mathrm{d}z} = \sum_\beta \frac{1}{2}\Sigma\gamma(h^- \to L_\alpha L_\beta)\left(\frac{Y_{\Delta h}}{Y_h^{\mathrm{eq}}} - \frac{Y_{\Delta L_\alpha} + Y_{\Delta L_\beta}}{Y_L^{\mathrm{nor}}}\right) \\ + \sum_\beta \frac{1}{2}\Delta\gamma(h^- \to L_\alpha L_\beta)\left(\frac{Y_{\Sigma h}}{Y_h^{\mathrm{eq}}} - 2\right). \end{aligned} \tag{5.124}$$

In the future we will simply write down the Boltzmann equation(s) with the correct source term(s) without explicitly carrying out the RIS subtraction procedure.

5.4.4 Evaluating the Equilibrium Rates

Let us now discuss how to evaluate the equilibrium reaction rates

$$\begin{aligned} \gamma(ab \to ij) = \int [\mathrm{d}p_a][\mathrm{d}p_b][\mathrm{d}p_i][\mathrm{d}p_j](2\pi)^4\delta^{(4)}(p_a + p_b - p_i - p_j) \\ \times |\mathcal{M}(ab \to ij)|^2 f_a^{\mathrm{eq}} f_b^{\mathrm{eq}}(1 + \eta_i f_i^{\mathrm{eq}})(1 + \eta_j f_j^{\mathrm{eq}}). \end{aligned} \tag{5.125}$$

This is rather difficult to do on account of the distributions, which (1) have inconvenient functional forms, and (2) spoil Lorentz invariance through their dependence on $\mathbf{p}$, or rather

$E_p = p^0 = p \cdot u$, with u the plasma velocity vector. Point (2) forces us to express the γ's with a careful set of angular integrals, and together with point (1) this means that we will doubtless need to resort to numerics for their evaluation.

As is the physicist's way, we may however regain some analytical purchase through the art of approximation. The approximation we will use is

$$f_i^{\text{eq}} \approx e^{-E_i/T} \quad \text{and} \quad 1 + \eta_i f_i^{\text{eq}} \approx 1 \tag{5.126}$$

– that is, we will take the Maxwell-Boltzmann limit for all our distributions. Because this limit is suitable only when $T \ll m_i$ (or more correctly $T \ll E_i$), this obviously does great violence to the distributions of particles for which this is not satisfied, which in the context of leptogenesis is typically everything but our heavy decaying particle. However, this is not a problem: the kinematics of the relevant decay (e.g. $h^- \to L_\alpha L_\beta$) forces the energies of the product particles to be of the same order as that of the heavy decaying particle, and for such energies the Maxwell-Boltzmann approximation is acceptable. We may therefore use this approximation with impunity as long as we are considering processes featuring at least one heavy particle.

Now, applying Eq. (5.126) to $\gamma(ab \to ij)$ reduces it to

$$\gamma(ab \to ij) \approx \int [\mathrm{d}p_a][\mathrm{d}p_b][\mathrm{d}p_i][\mathrm{d}p_j](2\pi)^4 \delta^{(4)}(p_a + p_b - p_i - p_j)|\mathcal{M}|^2 e^{-(E_a+E_b)/T}, \tag{5.127}$$

and by cleverly inserting a factor of $1 = \int \frac{\mathrm{d}^4 Q}{(2\pi)^4}(2\pi)^4\delta^{(4)}(Q - p_a - p_b)$ we obtain

$$\gamma(ab \to ij) = \int \frac{\mathrm{d}^4 Q}{(2\pi)^4} e^{-Q^0/T} \hat{\gamma}_{ab\to ij}(Q^2), \tag{5.128}$$

where

$$\hat{\gamma}_{ab\to ij}(Q^2) \equiv \underbrace{\int [\mathrm{d}p_a][\mathrm{d}p_b](2\pi)^4\delta^{(4)}(Q - p_a - p_b)}_{\text{Lorentz-invariant initial state phase space}} \underbrace{\int [\mathrm{d}p_i][\mathrm{d}p_j](2\pi)^4\delta^{(4)}(Q - p_i - p_j)}_{\text{Lorentz-invariant final state phase space}} |\mathcal{M}|^2. \tag{5.129}$$

Having happily recovered Lorentz invariance, we may straightforwardly compute $\hat{\gamma}$ using standard zero-temperature techniques. For a $2 \to n$ scattering process it relates to the usual spin-averaged cross section

$$\sigma(s) = \frac{1}{s_a s_b} \frac{1}{2\lambda^{1/2}(s, m_a^2, m_b^2)} \int \mathrm{d}\Pi_n \, |\mathcal{M}|^2 \tag{5.130}$$

by

$$\hat{\gamma}_{ab \to ij\ldots}(s) = s_a s_b \frac{\lambda(s, m_a^2, m_b^2)}{4\pi s} \sigma(s), \tag{5.131}$$

where

$$\lambda(x, y, z) \equiv x^2 + y^2 + z^2 - 2xy - 2xz - 2yz. \tag{5.132}$$

For a $1 \to n$ decay it relates to the decay rate

$$\Gamma = \frac{1}{s_a} \frac{1}{2m_a} \int \mathrm{d}\Pi_n \, |\mathcal{M}|^2 \tag{5.133}$$

by

$$\hat{\gamma}_{a \to ij\ldots}(s) = 2\pi\delta(s - m_a^2) \times 2m_a s_a \Gamma. \tag{5.134}$$

Independent of the form of $\hat{\gamma}$ we can write

$$\gamma = \int \frac{\mathrm{d}^4 Q}{(2\pi)^4} e^{-Q^0/T} \hat{\gamma}(Q^2) \tag{5.135}$$

$$= \frac{1}{4\pi^3} \int \mathrm{d}|\mathbf{Q}| \, \mathrm{d}Q^0 \, |\mathbf{Q}|^2 e^{-Q^0/T} \hat{\gamma}(Q^2), \tag{5.136}$$

and changing integration variables from $(Q^0, |\mathbf{Q}|)$ to $(Q^0, s = Q^2)$, with[8]

$$\mathrm{d}|\mathbf{Q}| \, \mathrm{d}Q^0 = \frac{1}{2|\mathbf{Q}|} \, \mathrm{d}s \, \mathrm{d}Q^0 = \frac{1}{2\sqrt{(Q^0)^2 - s}} \, \mathrm{d}s \, \mathrm{d}Q^0 \,, \tag{5.137}$$

[8] A naïve reading of $\mathrm{d}|\mathbf{Q}| = -\frac{1}{2|\mathbf{Q}|} \, \mathrm{d}s$ gives the wrong sign if, as we are doing now, we do not concurrently track how the limits of integration are altered under this change of variables.

gives

$$\gamma = \frac{1}{8\pi^3}\int_{s_{\min}}^{\infty} \mathrm{d}s \int_{\sqrt{s}}^{\infty} \mathrm{d}Q^0 \sqrt{(Q^0)^2 - s} e^{-Q^0/T} \hat{\gamma}(s) \tag{5.138}$$

$$= \frac{T}{8\pi^3}\int_{s_{\min}}^{\infty} \mathrm{d}s \sqrt{s} K_1\left(\frac{\sqrt{s}}{T}\right) \hat{\gamma}(s), \tag{5.139}$$

where K_1 is a Bessel function as defined in Eq. (5.86). Here $s_{\min}$ depends on the kinematics of the process; for a 2-to-2 scattering it is $s_{\min} = \max\{(m_a + m_b)^2, (m_i + m_j)^2\}$. In the special case of a decay or inverse decay we can plug in Eq. (5.134) to obtain

$$\gamma = \frac{T}{8\pi^3}\int \mathrm{d}s \sqrt{s} K_1\left(\frac{\sqrt{s}}{T}\right) \times 2\pi\delta(s - m_a^2) \times 2 m_a s_a \Gamma \tag{5.140}$$

$$= \frac{T}{2\pi^2} m_a^2 K_1\left(\frac{m_a}{T}\right) s_a \Gamma. \tag{5.141}$$

At last, we can now see that the reaction asymmetry $\Delta\gamma$ relates to the zero temperature decay asymmetry

$$\varepsilon_{ij} = \frac{\Gamma(a \to ij) - \Gamma(ji \to a)}{\Gamma(a \to ij) + \Gamma(ji \to a)} \tag{5.142}$$

defined at the start of this chapter simply through

$$\Delta\gamma(a \to ij) = \varepsilon_{ij} \Sigma\gamma(a \to ij), \tag{5.143}$$

where now

$$\Sigma\gamma(a \to ij) = \frac{T}{\pi^2} m_a^2 K_1\left(\frac{m_a}{T}\right) s_a \Gamma_0(a \to ij), \tag{5.144}$$

with $\Gamma_0(a \to ij)$ the tree-level decay rate.

5.4.5 Spectator Processes and Conserved Charges

So far, we have made good progress: we are able to write down the Boltzmann equations as a coupled system of relatively simple equations in the variables $Y_{\Delta i}(z)$ and $Y_{\Sigma i}(z)$ using a very reasonable set of approximations. This puts us very close to our goal of computing the predicted baryon abundance Y_B. In a leptogenesis scenario our final step is therefore to determine exactly how a generated lepton asymmetry $Y_{\Delta L}$ transmits to Y_B. Though we know this transmission will be due to electroweak sphalerons, we will obtain the correct result only if we also consider the effect of all other so-called *spectator processes*.

A spectator process is any 'fast' reaction (meaning $\Gamma \gg \mathcal{H}$) which does not directly enter the Boltzmann equations, but instead serves to impose relations between the chemical potentials of participating species. As we recall from Section 5.4.2, a generic spectator process $ab\ldots \leftrightarrow ij\ldots$ demands that

$$\mu_a + \mu_b + \ldots = \mu_i + \mu_j + \ldots . \tag{5.145}$$

In particular, the effect of sphalerons, which can be understood to generate the interaction operator [280; 351]

$$\mathcal{O}_{\text{Sph}} \sim \prod_{\alpha} (QQQL)_\alpha, \tag{5.146}$$

with α a generation index, is to enforce

$$\sum_{\alpha} (3\mu_{Q_\alpha} + \mu_{L_\alpha}) = 0. \tag{5.147}$$

If we can list the constraints from all such processes and solve for μ_B, it seems our job will be done. However, in doing this we will miss an important effect – the sphalerons should also change the number of leptons, thereby altering $Y_{\Delta L}$ and μ_L. It therefore appears that the only way to consistently account for the effect of sphalerons, and potentially other spectator processes as well, is to include them in the Boltzmann equations too.

This conclusion is however too hasty, for there is a better way deal with this complication.

Consider the partial baryon-minus-lepton number

$$\Delta_\alpha \equiv \frac{B}{3} - L_\alpha, \tag{5.148}$$

for which[9]

$$Y_{\Delta_\alpha} = \frac{1}{9}\sum_\beta \left(Y_{\Delta Q_\beta} + Y_{\Delta u_{R\beta}} + Y_{\Delta d_{R\beta}}\right) - Y_{\Delta L_\alpha} - Y_{\Delta e_{R\alpha}}. \tag{5.149}$$

Owing to the fact that sphalerons obey the selection rule

$$\frac{1}{3}\Delta Q_\alpha = \Delta L_\alpha = \pm 1 \tag{5.150}$$

(which we can read off from Eq. (5.146)), and therefore

$$\frac{1}{3}\Delta B = \Delta L_\alpha = \pm 1, \tag{5.151}$$

they do not alter Δ_α. This gives us our way out: if we track Y_{Δ_α} instead of $Y_{\Delta L_\alpha}$ then we are immune to their interruption. In fact, since Δ_α is conserved by every Standard Model process,[10] we can guarantee that the only processes we will need to include in the BE for Y_{Δ_α} are lepton number-violating ones of BSM origin.

This change of strategy now requires us to determine both Y_B and $Y_{\Delta L_\alpha}$ as functions of Y_{Δ_α}, where knowing $Y_{\Delta L_\alpha}$ is necessary to be able to re-express the source and washout terms of the Boltzmann equations in the correct variables Y_{Δ_α}. Doing this, subject to the constraints imposed by spectator processes, has the potential to become quite tedious.

[9] Note that the lepton number L_α includes not just the number of left-handed lepton doublets L_α, but also the right-handed lepton singlets $e_{R\alpha}$. Though this makes for an unfortunate clash of notation, I will do my best to keep the following discussion free of ambiguity.

[10] In principle Δ_α is violated anomalously if there are no right-handed neutrinos [122], but as the rate of violation is small and does not get enhanced by thermal effects we may safely ignore it. The reason for the lack of enhancement is that $B-L$ only has a $\mathrm{U}(1)^3_{B-L}$ anomaly, whereas the $\mathrm{SU}(2)^2_\mathrm{W}\,\mathrm{U}(1)_{B+L}$ anomaly allows $B+L$ to be violated by topological gauge configurations such as sphalerons [309; 311].

Fortunately for us, a rather slick approach due to Ref. [352] (see also Ref. [353]) greatly simplifies this task. The approach, termed the *symmetry formalism*, exploits the key observation that Eq. (5.145) is of exactly the same form as the equations we would write to determine the active U(1) symmetries at a given temperature. (Here and in what follows I use the terminology 'active' to refer to a symmetry respected by all spectator processes. An active symmetry may not necessarily be a symmetry of the full theory.) For example, assuming $\mathrm{U}(1)_Y$ is unbroken (which it is prior to the electroweak phase transition), the hypercharges of all particles in a spectator process $ab\ldots \leftrightarrow ij\ldots$ must satisfy

$$Y_a + Y_b + \ldots = Y_i + Y_j + \ldots, \tag{5.152}$$

and more generally, their charges under an active $\mathrm{U}(1)_X$ symmetry should obey

$$q_a^X + q_b^X + \ldots = q_i^X + q_j^X + \ldots. \tag{5.153}$$

From this we may conjecture that the chemical potentials are given by

$$\mu_i = \sum_X C_X q_i^X, \tag{5.154}$$

where the sum is over all $\mathrm{U}(1)_X$ symmetries, which I will shortly list, and the C_X's are yet-undetermined constants. With this ansatz, Eq. (5.145) is automatically satisfied for all spectator processes as long as $C_X = 0$ for all inactive symmetries (that is, symmetries broken by at least one spectator process).

To determine the constants C_X we first use Eq. (5.83) to write

$$Y_{\Delta i} = \frac{15\zeta_i}{4\pi^2}\frac{g_i}{g_{\star S}}\frac{\mu_i}{T} = \frac{15\zeta_i}{4\pi^2}\frac{g_i}{g_{\star S}}\frac{1}{T}\sum_X C_X q_i^X, \tag{5.155}$$

and then the charge densities Y_X in turn as

$$\begin{aligned} Y_X &= \sum_i q_i^X Y_{\Delta i} \\ &= \frac{15}{4\pi^2 g_{\star S}}\frac{1}{T}\sum_i \zeta_i g_i q_i^X \sum_Y C_Y q_i^Y \end{aligned} \tag{5.156}$$

$$\equiv \frac{15}{4\pi^2 g_{\star S}} \frac{1}{T} \sum_Y J_{XY} C_Y, \tag{5.157}$$

where it is helpful to define the matrix

$$J_{XY} \equiv \sum_i \zeta_i g_i q_i^X q_i^Y. \tag{5.158}$$

Inverting, we then obtain

$$C_X = \frac{4\pi^2 g_{\star S}}{15} T \sum_Y (J^{-1})_{XY} Y_Y. \tag{5.159}$$

Note that when there are n active symmetries, and therefore n non-zero C_X's, Eq. (5.157) tells us that only n of the Y_X's are independent. We therefore can (and should) restrict J to the n-by-n submatrix in the active symmetries before taking the inverse, and understand Eq. (5.159) to be equivalent to

$$C_X = \begin{cases} \dfrac{4\pi^2 g_{\star S}}{15} T \sum_{Y'} (J^{-1})_{XY'} Y_{Y'} & X \text{ active} \\ 0 & X \text{ inactive} \end{cases}, \tag{5.160}$$

where I use a primed notation to indicate that the sum is over the active symmetries only. Plugging this back into Eq. (5.155), we find that the number density of a species i is

$$Y_{\Delta i} = \zeta_i g_i \sum_{X',Y'} q_i^{X'} (J^{-1})_{X'Y'} Y_{Y'}, \tag{5.161}$$

and feeding this into Eq. (5.156) tells us that the baryon number asymmetry is therefore to be computed as

$$Y_B = \sum_{X',Y'} J_{BX'} (J^{-1})_{X'Y'} Y_{Y'}. \tag{5.162}$$

As a sanity check, this equation reduces to $Y_X = Y_X$ if we apply it to an active symmetry instead of baryon number, as we should expect.

	u	c	t	d	s	b	e	μ	τ	ν_e	ν_μ	ν_τ	W^-
Δ_e	$\frac{1}{9}$	$\frac{1}{9}$	$\frac{1}{9}$	$\frac{1}{9}$	$\frac{1}{9}$	$\frac{1}{9}$	-1	0	0	-1	0	0	0
Δ_μ	$\frac{1}{9}$	$\frac{1}{9}$	$\frac{1}{9}$	$\frac{1}{9}$	$\frac{1}{9}$	$\frac{1}{9}$	0	-1	0	0	-1	0	0
Δ_τ	$\frac{1}{9}$	$\frac{1}{9}$	$\frac{1}{9}$	$\frac{1}{9}$	$\frac{1}{9}$	$\frac{1}{9}$	0	0	-1	0	0	-1	0
Q	$\frac{2}{3}$	$\frac{2}{3}$	$\frac{2}{3}$	$-\frac{1}{3}$	$-\frac{1}{3}$	$-\frac{1}{3}$	-1	-1	-1	0	0	0	-1
B	$\frac{1}{3}$	$\frac{1}{3}$	$\frac{1}{3}$	$\frac{1}{3}$	$\frac{1}{3}$	$\frac{1}{3}$	0	0	0	0	0	0	0
g_i	6	6	6	6	6	6	2	2	2	1	1	1	3

Table 5.1: SM particles after the electroweak phase transition and their conserved charges. As the Higgs boson, photon, Z-boson and gluons are real, they cannot carry a charge and are hence excluded from the table. The degrees of freedom g_i of the particles are also shown for convenience.

EXAMPLE

Equations (5.161) and (5.162) are admittedly somewhat impenetrable, so let's explicitly use the latter to work out how Y_B relates to Y_{Δ_α} in the SM. If we want to be able to compare to the baryon abundance today it is imperative that we compute this only when baryon number stops changing – i.e. when the electroweak sphalerons freeze out. Lattice studies indicate that this occurs at $T \approx 130\,\text{GeV}$ [305], *after* the electroweak phase transition, which itself happens at $T_{\text{EWPT}} \approx 160\,\text{GeV}$ [349]. At this point the only surviving symmetries from higher temperatures are Δ_e, Δ_μ, Δ_τ, and Q (electric charge), and so the matrix J will be 4-by-4. Using the charges from Table 5.1 we can then compute

$$J = \frac{1}{27}\begin{pmatrix} 93 & 12 & 12 & 72 \\ 12 & 93 & 12 & 72 \\ 12 & 12 & 93 & 72 \\ 72 & 72 & 72 & 594 \end{pmatrix} \tag{5.163}$$

and

$$J_{BX'} = \begin{pmatrix} \frac{4}{3} & \frac{4}{3} & \frac{4}{3} & 2 \end{pmatrix}_{X'}. \tag{5.164}$$

Inverting J and plugging into Eq. (5.162), we hence find

$$Y_B = \frac{12}{37}(Y_{\Delta_1} + Y_{\Delta_2} + Y_{\Delta_3}) - \frac{1}{37}Y_Q. \tag{5.165}$$

Since we do not violate conservation of charge during leptogenesis (and the universe is moreover observed to be electrically neutral), we can set $Y_Q = 0$ to at last obtain

$$Y_B = \frac{12}{37} Y_{B-L}, \tag{5.166}$$

where $Y_{B-L} \equiv Y_{\Delta_1} + Y_{\Delta_2} + Y_{\Delta_3}$ is the total baryon-minus-lepton number density at the time of sphaleron freeze out (which is in turn equal to Y_{B-L} at the end of leptogenesis).

As an aside, I should comment that the top quark is non-relativistic at $T = 130\,\text{GeV}$, meaning $\zeta_t = 1$ should strictly speaking be replaced by the more general expression [94]

$$\zeta_t = \frac{6}{\pi^2} \int_{z_t}^{\infty} \mathrm{d}x\, x \sqrt{x^2 - z_t^2} \frac{e^x}{(e^x - \eta_t)^2} \approx 0.77, \quad \text{where} \quad z_t = \frac{m_t}{T} \quad \text{and} \quad \eta_t = -1. \tag{5.167}$$

This slightly modifies Y_B from $\frac{12}{37} Y_{B-L} \approx 0.324 Y_{B-L}$ to $0.321 Y_{B-L}$.

If sphalerons instead freeze out before the electroweak phase transition (which could conceivably happen in a given BSM model) then our fourth conserved charge is hypercharge Y instead of electric charge Q, and repeating the calculation with the particle content of Table 5.2 instead gives [354]

$$Y_B = \frac{28}{79} Y_{B-L} \approx 0.354 Y_{B-L}. \tag{5.168}$$

It is worth taking a moment to appreciate the ease with which we obtained the above result. Even though—granted—I skipped over the working in obtaining J, we crucially did not need to identify any spectator processes or solve any chemical constraint equations. Using Eq. (5.161) or (5.162) to determine a number or charge density is as simple as listing the active symmetries and then turning the crank, which is straightforward enough to be easily automated with e.g. Mathematica.

	Q_1	Q_2	Q_3	u_R	c_R	t_R	d_R	s_R	b_R	L_1	L_2	L_3	e_R	μ_R	τ_R	H	$T_{\rm br}$ [GeV]
Δ_e	$\frac{1}{9}$	$\frac{1}{9}$	$\frac{1}{9}$	$\frac{1}{9}$	$\frac{1}{9}$	$\frac{1}{9}$	$\frac{1}{9}$	$\frac{1}{9}$	$\frac{1}{9}$	-1	0	0	-1	0	0	0	—
Δ_μ	$\frac{1}{9}$	$\frac{1}{9}$	$\frac{1}{9}$	$\frac{1}{9}$	$\frac{1}{9}$	$\frac{1}{9}$	$\frac{1}{9}$	$\frac{1}{9}$	$\frac{1}{9}$	0	-1	0	0	-1	0	0	—
Δ_τ	$\frac{1}{9}$	$\frac{1}{9}$	$\frac{1}{9}$	$\frac{1}{9}$	$\frac{1}{9}$	$\frac{1}{9}$	$\frac{1}{9}$	$\frac{1}{9}$	$\frac{1}{9}$	0	0	-1	0	0	-1	0	—
Y	$\frac{1}{6}$	$\frac{1}{6}$	$\frac{1}{6}$	$\frac{2}{3}$	$\frac{2}{3}$	$\frac{2}{3}$	$-\frac{1}{3}$	$-\frac{1}{3}$	$-\frac{1}{3}$	$-\frac{1}{2}$	$-\frac{1}{2}$	$-\frac{1}{2}$	-1	-1	-1	$\frac{1}{2}$	$T_{\rm EWPT}$
e	0	0	0	0	0	0	0	0	0	0	0	0	1	0	0	0	3×10^4
$u - d$	0	0	0	1	0	0	-1	0	0	0	0	0	0	0	0	0	2×10^6
$B_3 + B_2 - 2B_1$	$-\frac{2}{3}$	$\frac{1}{3}$	$\frac{1}{3}$	$-\frac{2}{3}$	$\frac{1}{3}$	$\frac{1}{3}$	$-\frac{2}{3}$	$\frac{1}{3}$	$\frac{1}{3}$	0	0	0	0	0	0	0	10^7
$u - s$	0	0	0	1	0	0	0	-1	0	0	0	0	0	0	0	0	3×10^8
$B_3 - B_2$	0	$-\frac{1}{3}$	$\frac{1}{3}$	0	$-\frac{1}{3}$	$\frac{1}{3}$	0	$-\frac{1}{3}$	$\frac{1}{3}$	0	0	0	0	0	0	0	9×10^8
μ	0	0	0	0	0	0	0	0	0	0	0	0	0	1	0	0	10^9
$u - c$	0	0	0	1	-1	0	0	0	0	0	0	0	0	0	0	0	2×10^{10}
$u - b$	0	0	0	1	0	0	0	0	-1	0	0	0	0	0	0	0	3×10^{11}
τ	0	0	0	0	0	0	0	0	0	0	0	0	0	0	1	0	4×10^{11}
B	$\frac{1}{3}$	$\frac{1}{3}$	$\frac{1}{3}$	$\frac{1}{3}$	$\frac{1}{3}$	$\frac{1}{3}$	$\frac{1}{3}$	$\frac{1}{3}$	$\frac{1}{3}$	0	0	0	0	0	0	0	2×10^{12}
u	0	0	0	1	0	0	0	0	0	0	0	0	0	0	0	0	2×10^{13}
t	0	0	0	0	0	1	0	0	0	0	0	0	0	0	0	0	10^{15}
g_i	6	6	6	3	3	3	3	3	3	2	2	2	1	1	1	2	N/A

Table 5.2: SM particles and their charges at temperatures above the electroweak phase transition. As all gauge bosons are real, they cannot carry a charge and are hence excluded from the table. Estimates for the breaking temperatures $T_{\rm br}$ can be found in Ref. [356]; see also Refs. [104; 355]. The degrees of freedom g_i of the particles are also shown for convenience.

Our final job is therefore to more generally identify the $\mathrm{U}(1)_X$ symmetries that are active at any given temperature. There are up to sixteen such symmetries in the SM: one for each of $\{Q_\alpha, u_{R\alpha}, d_{R\alpha}, L_\alpha, e_{R\alpha}, H\}$, though in practice it is more convenient to use a basis such as the one listed in Table 5.2.[11] As the universe cools down more spectator processes will enter equilibrium, breaking incrementally more symmetries until the only ones remaining are Δ_e, Δ_μ, Δ_τ, and Y (pre-EWPT) or Q (post-EWPT), which remain true symmetries of the SM. If we can determine the temperatures at which the symmetries are broken, then our work is done.

To this end, consider for example the symmetry $\tau = \mathrm{U}(1)_\tau$, under which $\tau_R = e_{R3}$ carries the charge $q^\tau_\tau = 1$ and all other particles are uncharged, $q^\tau_i = 0$. While this $\mathrm{U}(1)_\tau$ is violated by the Yukawa interaction

[11] Other basis choices can also be made; see for example Ref. [355].

$$\mathcal{L} \supset -Y_\tau \overline{L_3} H \tau_R + \text{h.c.}, \tag{5.169}$$

it remains an active symmetry as long as $LH\tau$ interactions are slow, $\Gamma \ll \mathcal{H}$. Estimating the reaction rate to be $\Gamma \sim Y_\tau^2 T$ by dimensional analysis (though actually, a better estimate is $\Gamma \simeq 5 \times 10^{-3} \times Y_\tau^2 T$ [357–359]) and comparing against the Hubble rate, Eq. (5.75), tells us that $\mathrm{U}(1)_\tau$ is broken when

$$1 \simeq \frac{\Gamma}{\mathcal{H}} \simeq \frac{5 \times 10^{-3} \times Y_\tau^2 T}{1.66\sqrt{g_\star}\frac{T^2}{M_\mathrm{P}}} \quad \Longrightarrow \quad T \simeq 4 \times 10^{11}\,\mathrm{GeV}. \tag{5.170}$$

I will not go into detail for the other symmetries in Table 5.2, as the breaking pattern of the quark and baryon number symmetries is somewhat more complicated [356]. In brief, t is first broken by the top Yukawa interaction at $T_\mathrm{br} \approx 10^{15}\,\mathrm{GeV}$, followed by one of the quark symmetries, which we choose to be u, when the $\mathrm{SU}(3)_\mathrm{C}$ sphalerons

$$\mathcal{O}_{\mathrm{Sph},\,\mathrm{SU}(3)_\mathrm{C}} \sim \prod_\alpha (QQu_R^c d_R^c)_\alpha \tag{5.171}$$

enter equilibrium at $T \approx 2 \times 10^{13}\,\mathrm{GeV}$. Baryon number B is then broken when electroweak sphalerons enter equilibrium at $T \approx 2 \times 10^{12}\,\mathrm{GeV}$, and the sequence in which the remaining quark symmetries are broken is due to the quark masses and CKM effects.

Example

Leptogenesis in the Zee model, through the decay of the scalar h^-, will occur when the h^- particles exit equilibrium at $T \sim m_h$, and it will turn out that we will need to take $m_h \gtrsim 10^{12}\,\mathrm{GeV}$. To determine how $Y_{\Delta L_\alpha}$ relates to Y_{Δ_α} during leptogenesis, as is needed for the Boltzmann equation, Table 5.2 tells us that we will need to account for all the symmetries but B, u and t. There is however a catch – the Zee model also introduces a second Higgs doublet (and we will later want to introduce a third), and the Yukawa couplings of this second Higgs to the leptons will turn out to be large enough that e, μ, and τ will be broken above $10^{12}\,\mathrm{GeV}$. This leaves us in actuality with only ten active symmetries. Additionally, we should not forget to include h^- and the new Higgs doublet(s) when summing over all particles in the

computation of J, though for practical purposes we can set $\zeta_{h^-} = 0$ as it drops out of equilibrium.

The eventual result of writing out the 10-by-10 matrix J, inverting, and plugging into Eq. (5.161) is

$$\begin{pmatrix} Y_{\Delta L_1} \\ Y_{\Delta L_2} \\ Y_{\Delta L_3} \end{pmatrix} = \frac{2}{117} \begin{pmatrix} -35 - C & 4 - C & 4 - C \\ 4 - C & -35 - C & 4 - C \\ 4 - C & 4 - C & -35 - C \end{pmatrix} \begin{pmatrix} Y_{\Delta_1} \\ Y_{\Delta_2} \\ Y_{\Delta_3} \end{pmatrix}, \tag{5.172}$$

where

$$C = \frac{756}{111 + 91 n_H}, \tag{5.173}$$

with n_H the number of Higgs doublets. The densities of the other seven charges such as Y_Y can be assumed to be zero as they are, after all, conserved and unbroken during leptogenesis. When $n_H = 2$, as in the minimal Zee model, this becomes

$$\begin{pmatrix} Y_{\Delta L_1} \\ Y_{\Delta L_2} \\ Y_{\Delta L_3} \end{pmatrix} = \frac{2}{2637} \begin{pmatrix} -847 & 32 & 32 \\ 32 & -847 & 32 \\ 32 & 32 & -847 \end{pmatrix} \begin{pmatrix} Y_{\Delta_1} \\ Y_{\Delta_2} \\ Y_{\Delta_3} \end{pmatrix} \approx \begin{pmatrix} -0.64 & 0.02 & 0.02 \\ 0.02 & -0.64 & 0.02 \\ 0.02 & 0.02 & -0.64 \end{pmatrix} \begin{pmatrix} Y_{\Delta_1} \\ Y_{\Delta_2} \\ Y_{\Delta_3} \end{pmatrix}, \tag{5.174}$$

and when $n_H = 3$ we instead get

$$\begin{pmatrix} Y_{\Delta L_1} \\ Y_{\Delta L_2} \\ Y_{\Delta L_3} \end{pmatrix} = \frac{1}{144} \begin{pmatrix} -91 & 5 & 5 \\ 5 & -91 & 5 \\ 5 & 5 & -91 \end{pmatrix} \begin{pmatrix} Y_{\Delta_1} \\ Y_{\Delta_2} \\ Y_{\Delta_3} \end{pmatrix} \approx \begin{pmatrix} -0.63 & 0.03 & 0.03 \\ 0.03 & -0.63 & 0.03 \\ 0.03 & 0.03 & -0.63 \end{pmatrix} \begin{pmatrix} Y_{\Delta_1} \\ Y_{\Delta_2} \\ Y_{\Delta_3} \end{pmatrix}. \tag{5.175}$$

We will also end up needing expressions for the number densities of the Higgs doublets, so while we're here we can also compute

$$Y_{\Delta H_i} = -\frac{112 n_H}{111 + 91 n_H} (Y_{\Delta_1} + Y_{\Delta_2} + Y_{\Delta_3}) \tag{5.176}$$

$$= \begin{cases} -\frac{224}{293} (Y_{\Delta_1} + Y_{\Delta_2} + Y_{\Delta_3}) & n_H = 2 \\ -\frac{7}{8} (Y_{\Delta_1} + Y_{\Delta_2} + Y_{\Delta_3}) & n_H = 3 \end{cases}. \tag{5.177}$$

5.4.6 Summary

With the μ/T expansion, RIS subtraction, Maxwell-Boltzmann approximation, and spectator effects fully accounted for, we have brought our main Boltzmann equation from its original form

$$\frac{\mathrm{d}n_{L_\alpha}}{\mathrm{d}t} + 3\mathcal{H}n_{L_\alpha} = \sum_\beta [h^- \leftrightarrow L_\alpha L_\beta] \tag{5.178}$$

to the final incarnation

$$\begin{aligned} sz\mathcal{H}\frac{\mathrm{d}Y_{\Delta_\alpha}}{\mathrm{d}z} &= -\sum_\beta \frac{1}{2}\Sigma\gamma(h^- \to L_\alpha L_\beta)\left(\frac{Y_{\Delta h}}{Y_h^{\mathrm{eq}}} - \frac{Y_{\Delta L_\alpha} + Y_{\Delta L_\beta}}{Y_L^{\mathrm{nor}}}\right) \\ &\quad -\sum_\beta \frac{1}{2}\Delta\gamma(h^- \to L_\alpha L_\beta)\left(\frac{Y_{\Sigma h}}{Y_h^{\mathrm{eq}}} - 2\right). \end{aligned} \tag{5.179}$$

$$\begin{aligned} &= -\sum_\beta \frac{m_h^3}{2\pi^2 z}K_1(z)\Gamma_0(h^- \to L_\alpha L_\beta)\left(\frac{Y_{\Delta h}}{Y_h^{\mathrm{eq}}} - \frac{Y_{\Delta L_\alpha} + Y_{\Delta L_\beta}}{Y_L^{\mathrm{nor}}}\right) \\ &\quad -\sum_\beta \frac{m_h^3}{2\pi^2 z}K_1(z)\varepsilon_{\alpha\beta}\Gamma_0(h^- \to L_\alpha L_\beta)\left(\frac{Y_{\Sigma h}}{Y_h^{\mathrm{eq}}} - 2\right), \end{aligned} \tag{5.180}$$

where

$$z = \frac{m_h}{T}, \qquad \varepsilon_{\alpha\beta} = \frac{\Gamma(h^- \to L_\alpha L_\beta) - \Gamma(L_\alpha L_\beta \to h^-)}{\Gamma(h^- \to L_\alpha L_\beta) + \Gamma(L_\alpha L_\beta \to h^-)}, \tag{5.181}$$

and

$$\begin{pmatrix} Y_{\Delta L_1} \\ Y_{\Delta L_2} \\ Y_{\Delta L_3} \end{pmatrix} \approx \begin{pmatrix} -0.64 & 0.02 & 0.02 \\ 0.02 & -0.64 & 0.02 \\ 0.02 & 0.02 & -0.64 \end{pmatrix} \begin{pmatrix} Y_{\Delta_1} \\ Y_{\Delta_2} \\ Y_{\Delta_3} \end{pmatrix}. \tag{5.182}$$

Assuming the additional Higgs doublets are non-relativistic when the electroweak sphalerons freeze out, Eq. (5.166) still holds and the generated baryon asymmetry is equal to

$$Y_B = \frac{12}{37}(Y_{\Delta_1} + Y_{\Delta_2} + Y_{\Delta_3}) = \frac{12}{37}Y_{B-L}. \tag{5.183}$$

To successfully explain the observed baryon abundance of the universe we therefore require

that

$$Y_{B-L} \approx \frac{37}{12} \times 8.68 \times 10^{-11} \approx 2.68 \times 10^{-10} \tag{5.184}$$

at the end of leptogenesis. In the next chapter we will write down the Boltzmann equations for $Y_{\Sigma h}$ and $Y_{\Delta h}$, and extend Eq. (5.179) to include additional processes.

5.A Further Details on Real Intermediate State Subtraction

Let's try to convince ourselves of the relation

$$\gamma(L_\gamma L_\delta \to L_\alpha L_\beta)_{\text{on-shell}} = \frac{\gamma(L_\gamma L_\delta \to h^-)\gamma(h^- \to L_\alpha L_\beta)}{\frac{1}{2}\sum_{\rho,\sigma}\gamma(h^- \to L_\rho L_\sigma)}, \tag{5.185}$$

which was critical to the success of the RIS subtraction scheme in Section 5.4.3. This is most easily achieved using the results derived in Section 5.4.4 by approximating the distributions as Maxwell-Boltzmann, though it can be shown without doing so [347].

To begin, we have from Eq. (5.139) that

$$\gamma(L_\gamma L_\delta \to L_\alpha L_\beta) = \frac{T}{8\pi^3}\int \mathrm{d}s\,\sqrt{s}K_1\left(\frac{\sqrt{s}}{T}\right)\int \mathrm{d}\Pi_{\gamma\delta}\,\mathrm{d}\Pi_{\alpha\beta}\,|\mathcal{M}(L_\gamma L_\delta \to L_\alpha L_\beta)|^2. \tag{5.186}$$

The matrix element for this scattering is

$$\mathrm{i}\mathcal{M}(L_\gamma L_\delta \to L_\alpha L_\beta) = \tag{5.187}$$

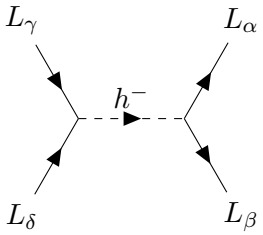

$$= \mathrm{i}\mathcal{M}_{\mathrm{ID}}\frac{\mathrm{i}}{s - m^2 + \mathrm{i}m_h\Gamma_h}\mathrm{i}\mathcal{M}_{\mathrm{D}}, \tag{5.188}$$

where $\mathcal{M}_{\mathrm{ID}}$ and $\mathcal{M}_{\mathrm{D}}$ are the (inverse) decay matrix elements, and we use the resummed form of the propagator for the intermediate h^-. To identify the on-shell part of this scattering the conventional approach is to appropriate the *narrow width approximation*

$$\left|\frac{1}{s - m_h^2 + \mathrm{i}m_h\Gamma_h}\right|^2 \approx \frac{\pi}{m_h\Gamma_h}\delta(s - m_h^2), \tag{5.189}$$

which holds in the limit $\Gamma_h \ll m_h$, to write

$$|\mathcal{M}(L_\gamma L_\delta \to L_\alpha L_\beta)|^2_{\text{on-shell}} = |\mathcal{M}_{\mathrm{ID}}|^2|\mathcal{M}_{\mathrm{D}}|^2\frac{\pi}{m_h\Gamma_h}\delta(s - m^2); \tag{5.190}$$

the off-shell piece then contains the difference between this approximation and the unapproximated amplitude. Using this, Eq. (5.186) becomes

$$\begin{aligned}\gamma(L_\gamma L_\delta \to L_\alpha L_\beta)_{\text{on-shell}} &= \frac{T}{8\pi^3} m_h K_1\left(\frac{m_h}{T}\right) \frac{\pi}{m_h \Gamma_h} \underbrace{\left(\int \mathrm{d}\Pi_{\gamma\delta}\, |\mathcal{M}_{\text{ID}}|^2\right)}_{2m_h\Gamma(L_\gamma L_\delta \to h^-)} \underbrace{\left(\int \mathrm{d}\Pi_{\alpha\beta}\, |\mathcal{M}_{\text{D}}|^2\right)}_{2m_h\Gamma(h^- \to L_\alpha L_\beta)} \\ &= \frac{T}{2\pi^2} m_h^2 K_1\left(\frac{m_h}{T}\right) \frac{\Gamma(L_\gamma L_\delta \to h^-)\Gamma(h^- \to L_\alpha L_\beta)}{\Gamma_h}. \end{aligned} \tag{5.191}$$

To convert from the uppercase Γ's to lowercase ones we recall from Eq. (5.141) that

$$\gamma(h^- \to L_\alpha L_\beta) = \frac{T}{2\pi^2} m_h^2 K_1\left(\frac{m_h}{T}\right) \Gamma(h^- \to L_\alpha L_\beta), \tag{5.192}$$

and assuming that h^- has no other decay modes, so that

$$\Gamma_h = \frac{1}{2} \sum_{\rho,\sigma} \Gamma(h^- \to L_\rho L_\sigma) \tag{5.193}$$

(the factor of $\frac{1}{2}$ is to avoid double-counting final states), we at last obtain

$$\gamma(L_\gamma L_\delta \to L_\alpha L_\beta)_{\text{on-shell}} = \frac{\gamma(L_\gamma L_\delta \to h^-)\gamma(h^- \to L_\alpha L_\beta)}{\frac{1}{2}\sum_{\rho,\sigma} \gamma(h^- \to L_\rho L_\sigma)}, \tag{5.194}$$

as claimed.

Some comments are in order. First, it is not correct to assume that h^- has no other decay modes – for instance, it can also decay into two Higgs doublets, $h^- \to \bar{H}\bar{H}$. While this means Eq. (5.194) must be altered, it does *not* change the result of the RIS subtraction procedure. The reason for this is that the additional RIS-subtracted scattering $\bar{H}\bar{H} \to LL$, which when added alongside $LL \to LL$ in the Boltzmann equation, results in an overall factor that correctly cancels against the full decay rate in the denominator. Other additional decay channels are handled similarly.

Next, it is worth acknowledging that RIS subtraction admittedly appears to be a somewhat ad hoc prescription. The use of the narrow width approximation is moreover arbitrary, and the eventual cancellation of the total decay rate Γ_h in the denominator suggests that

there may be another way to execute the subtraction. Indeed, RIS subtraction can be made to work using the principal value decomposition of a propagator,

$$\frac{1}{p^2 - m^2 + \mathrm{i}\epsilon} = \mathcal{P}\frac{1}{p^2 - m^2} - \mathrm{i}\pi\delta(p^2 - m^2), \tag{5.195}$$

though care must be taken when squaring it to obtain sensible results [350; 360; 361]. All that said, RIS subtraction can in fact be justified through use of the **closed time path** (CTP) **formalism** for finite temperature quantum field theory; see for example Refs. [105; 120; 362–372]. The CTP formalism provides one with the means of deriving the evolution equations for quantum correlators in a thermal background from first principles, and these *Kadanoff-Baym equations* [373] can be shown to reduce to the Boltzmann equations under the right set of approximations. Importantly, the Kadanoff-Baym equations automatically imply RIS subtraction [365], and without going into detail, this is because propagators in the CTP formalism include additional on-shell parts bearing distributional factors representing the exchange of a particle with the thermal bath. For more details I refer you to the above references, though I recommend Ref. [120] for a relatively gentle first introduction to the formalism.

I am altering the model.
Pray I don't alter it any further.

Darth Vader,
in *The Empire Strikes Back*,
reimagined

6

Leptogenesis in the Zee Model

Contents

6.1 Introduction **144**

6.2 The Zee Model **146**

6.3 A Benchmark Scenario **157**

6.4 Minimal Extensions **160**

6.5 Summary **163**

6.A Feynman Rules **165**

6.B The Cutkosky Cuts in Detail **165**

6.C The Explicit Boltzmann Equations **174**

The time has come for us to apply what we have learnt in the previous chapter to the

study of a concrete leptogenesis scenario – that in which a lepton asymmetry is generated through the CP-violating decay of the singly-charged scalar singlet h^- introduced in the Zee model of neutrino masses. It will turn out that this scenario is unable to adequately explain the observed baryon asymmetry of the universe, and so the Zee model will need to be extended if it is to do so.

This chapter is representative of an ongoing work [2] and therefore does not form a complete package. In particular, a thorough examination of the available parameter space from present-day experimental constraints is absent, the flavour-covariant Boltzmann equations are not presented, and the study of the minimally-extended variants of the Zee model is yet to be performed. My largest sole contribution to this work is the calculation of the CP asymmetries, though I have also had a hand in most other parts. All plots and figures in this chapter were created by me.

6.1 Introduction

As we discussed somewhat exhaustively (and exhaustingly) in the previous chapter, the SM falls short of explaining the observed baryon abundance of the universe [90; 304],

$$Y_B \approx (8.68 \pm 0.57) \times 10^{-11}, \tag{6.1}$$

leaving us in need of a BSM mechanism of baryogenesis. A particularly appealing one is that of leptogenesis, where the lepton number violation inherent to Majorana neutrino mass models is leveraged to generate a lepton asymmetry which is transformed to a baryon asymmetry by equilibrium sphaleron processes. Countlessly many leptogenesis scenarios have been studied (see for example Refs. [102; 104–107; 331–335; 374–393]), and in this wide berth of literature it is often observed that successful leptogenesis is generically more difficult to attain in radiative mass models, where the lepton number-violating interactions giving rise to neutrino masses have a tendency to erase any existing lepton (and therefore baryon) asymmetry [38; 106; 107; 394; 395]. This is particularly true for $\mathcal{O}$(TeV)-scale

scenarios—which attract the most attention due to their testability at colliders and in other terrestrial experiments—as the couplings required to explain neutrino masses are typically orders of magnitude greater than what is required to satisfy the out-of-equilibrium Sakharov condition [106; 107; 396].

One of the most well-known radiative mass models is the Zee model [23], where the introduction of a second Higgs doublet H_2 and a singly-charged scalar singlet h^- is used to generate neutrino masses at one-loop. For the reasons cited above, the model has been ruled out as a viable progenitor of leptogenesis, at least at the 1–100 TeV scale [106; 107; 385] where it is most likely to reside [179]. If we untether ourselves from naturality requirements, however, it is possible to entertain a high-scale realisation of the model, where H_2 and h^- almost entirely decouple from the low-scale phenomenology and their respective couplings become nearly unconstrained.

The purpose of this chapter is to study this high-scale scenario, and in doing so determine whether it is at all possible for the Zee model to successfully explain the observed baryon abundance of the universe via leptogenesis. In this scenario a lepton asymmetry is generated through the out-of-equilibrium CP-violating decays $h^- \to LL$ and $h^- \to e\bar{L}\bar{H}$, with the heavy charged scalar h^- requiring a mass of $\mathcal{O}(10^{12}\,\text{GeV})$. Standing in the way of successful leptogenesis are two main obstacles: first, the CP-violating interferences are *two-loop* suppressed, and second, the total CP asymmetry of these decays is zero, necessitating the intervention of flavour effects to preserve a net non-zero asymmetry.

The rest of this chapter is organised as follows. In Section 6.2 I will review the Zee model and its CP-violating decays, giving a reasonably in-depth discussion of their important features. This includes a brief qualitative overview in Section 6.2.4 of the ingredients needed to maximise the asymmetry generated. Then, in Section 6.3 we will quantitatively examine a promising benchmark scenario, before canvassing some minimal extensions to the model in Section 6.4. Finally, I will summarise our findings in Section 6.5. A more detailed examination of the CP-violating Cutkosky cuts is provided in the appendix section 6.B, which is sandwiched between two other appendices on the Feynman rules and Boltzmann equations for the model.

6.2 The Zee Model

Let us begin by reintroducing the Zee model and reviewing its properties. The model [23] extends the SM with a new charged scalar $h^- \sim (1, 1, -1)$ and one new Higgs doublet $H_2 \sim (1, 2, 1/2)$, with the relevant Lagrangian terms

$$\mathcal{L} \supset -m_h^2 h^+ h^- + \left(\mu \widetilde{H}_1^\dagger H_2 h^- - \overline{\widetilde{L}} f L h^+ - \overline{L}(Y_1^\dagger H_1 + Y_2^\dagger H_2) e_R + \text{h.c.}\right). \tag{6.2}$$

We will operate in the so-called 'Higgs basis', where H_1 acquires a vacuum expectation value $v \simeq 246\,\text{GeV}$, and we have the freedom to rotate our leptons so that either Y_1 or Y_2 can be made real, diagonal, and positive (the conventional choice is of course Y_1). The coupling matrix f is antisymmetric, $f = -f^T$, and we may take it to be real by simultaneously rephasing L and e_R, so that the diagonal Yukawa matrix remains unaffected. By rephasing h^- we may also take μ to be real.

Notationally I will use a, b in superscripts to label $\text{SU}(2)_\text{W}$ indices, Greek letters in subscripts for flavour indices, and i, j to index the Higgses – for example, I might write H_i^a, L_β^b, or e_γ (in this chapter I will drop the R subscript from e_R). I will use both subscript and superscript placement for the Higgs indices based on a subjective sense of neatness, so you may see e.g. $Y_{\alpha\beta}^i$ and $Y_j^\dagger$.

Now, the Zee model is foremost a model for neutrino masses, which arise at the one-loop level, and are equal in the decoupling limit to [179]

$$m_{\alpha\beta}^\nu = -\frac{s_{2\varphi}}{16\pi^2}\frac{v}{\sqrt{2}} \ln \frac{m_{h_2^+}^2}{m_{h_1^+}^2} \left(f Y_1 Y_2 + Y_2^T Y_1^T f^T\right)_{\alpha\beta}, \tag{6.3}$$

where the charged mass eigenstates are defined by

$$\begin{pmatrix} h_1^+ \\ h_2^+ \end{pmatrix} = \begin{pmatrix} s_\varphi & c_\varphi \\ c_\varphi & -s_\varphi \end{pmatrix} \begin{pmatrix} h^+ \\ H_2^+ \end{pmatrix}, \quad \text{with} \quad s_{2\varphi} = \frac{\sqrt{2} v \mu}{m_{h_2^+}^2 - m_{h_1^+}^2}. \tag{6.4}$$

For small mixing angles, $\varphi \ll 1$, we have $h_1^+ \approx H_2^+$ and $h_2^+ \approx h^+$, and for $m_h \gg m_{H_2}$ the mass matrix simplifies further to

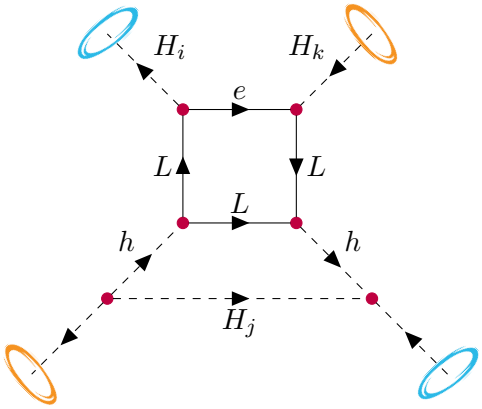

Figure 6.1: The two-loop vacuum diagram from which we derive our CP-violating interferences. It is non-planar, so some portals have been used to make it look nice.[1] At the same order in the couplings we can construct another vacuum diagram by instead joining the Higgs lines at the top and bottom, but this does not generate any CP asymmetries.

$$m^{\nu}_{\alpha\beta} = \frac{\mu v^2}{16\pi^2 m_h^2} \ln \frac{m^2_{H_2^+}}{m^2_{h^+}} \left(f Y_1 Y_2 + Y_2^T Y_1^T f^T \right)_{\alpha\beta}. \tag{6.5}$$

6.2.1 *CP*-Violating Decays

With the model established, our first task is to take stock of the CP-asymmetric decays relevant to leptogenesis. Where possible, it is conventional to express these asymmetries in the form of an asymmetry parameter

$$\varepsilon = \frac{\Gamma(h^- \to f) - \Gamma(h^+ \to \bar{f})}{\Gamma(h^- \to f) + \Gamma(h^+ \to \bar{f})} = -\frac{\mathrm{Im}(c_0^* c_1)}{|c_0|^2} \frac{\int \mathrm{d}\Pi_f \, [2\,\mathrm{Im}(\mathcal{A}_0^* \mathcal{A}_1)]}{\int \mathrm{d}\Pi_f \, |\mathcal{A}_0|^2}, \tag{6.6}$$

where we recall from the previous chapter the decomposition $\mathcal{M}(h^- \to f) = c_0 \mathcal{A}_0 + c_1 \mathcal{A}_1$.

All asymmetries we will consider originate from the vacuum diagram in Fig. 6.1, which we must cut three times: once for the initial state, once for the final state, and once

[1] Though the use of colours is not faithful to the `Portal` franchise, I hope that this choice of colouring is more intuitive to the average reader than the canonical one. The portal graphic was sourced from Ref. [397].

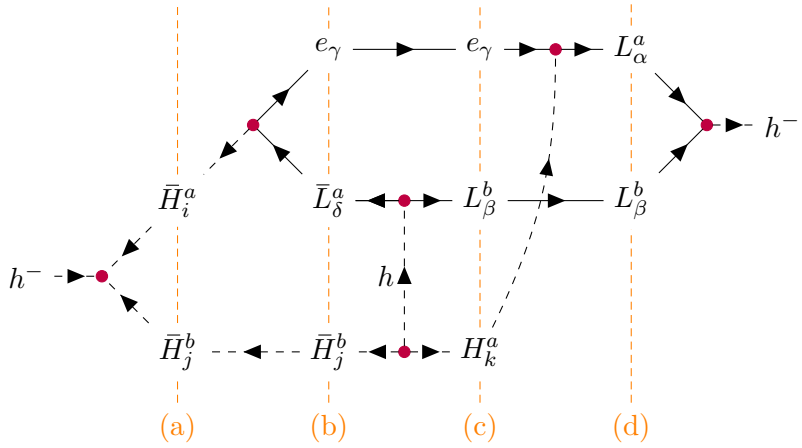

Figure 6.2: A two-loop self energy diagram for h^- obtained by cutting through an h line in the vacuum diagram of Fig. 6.1. Shown in orange are all cuts relevant to the main text. There are also two four-body cuts, shown in Fig. 6.7.

for the Cutkosky cut. For example, by cutting through an h line we arrive at the self energy diagram in Fig. 6.2; cutting then through (d) gives us the final state $L_\alpha L_\beta$, where everything to the left of cut (d) is the loop-level amplitude for $h^- \to L_\alpha L_\beta$, and to the right is (the conjugate of) the tree-level amplitude. Lastly, the Cutkosky cut will then be one of (a), (b), (c), (e), or (f), of which the latter two can be found in Fig. 6.7. Notice that the vacuum diagram is four-loop, and that the loop-level amplitude for $h^- \to L_\alpha L_\beta$ is *two-loop*. There are no CP-violating interferences for this decay at one-loop in the Zee model, so this is the leading order at which we should expect to find an asymmetry.

An important feature of the vacuum diagram is that it can *only* generate asymmetries in L number. To understand this, note that when we construct the Boltzmann equation (BE) for a particle, say e_α, we must sum over the flavours of all other particles in the diagram since they will either be virtual or spectators as far as the BE is concerned. From the Feynman rules listed in Section 6.A, doing so leads to the combination of couplings $\sum_i \mu^2 (Y_i f^\dagger f Y_i^\dagger)_{\alpha\alpha}$, which, as the diagonal element of a self-adjoint matrix, has no imaginary part and thus no asymmetry:

$$\varepsilon_{e_\alpha} \propto \sum_i \mu^2 \,\mathrm{Im}(Y_i f^\dagger f Y_i^\dagger)_{\alpha\alpha} = 0. \tag{6.7}$$

It is only when leaving the flavour of the vertical L lines in Fig. 6.1 unsummed, with

$$\varepsilon_{L_\alpha} \propto \sum_i \mu^2 \,\mathrm{Im}(Y_i^\dagger Y_i f^\dagger f)_{\alpha\alpha}, \tag{6.8}$$

that an asymmetry can arise. Note however that the *total* asymmetry, when summed over all L_α flavours, is zero:

$$\sum_\alpha \varepsilon_{L_\alpha} \propto \sum_i \mu^2 \,\mathrm{Im}\mathrm{Tr}(Y_i^\dagger Y_i f^\dagger f) = 0. \tag{6.9}$$

This forces us into a *purely flavoured leptogenesis* scenario [398; 399], meaning we are dependent on flavour effects to obtain a net non-zero lepton asymmetry. In practice this implies that we will need to protect the negative asymmetry in one flavour while washing out the positive asymmetries in the remaining flavours.[2]

In the following subsections I will present and briefly discuss the results for the relevant asymmetries. More details are provided in Appendix 6.B.

6.2.1.1 $h^- \to LL$

The most important decay channel for h^- is $h^- \to LL$, for which the tree-level decay rate is

$$\Gamma_0(h^- \to L_\alpha L_\beta) = \frac{m_h |f_{\alpha\beta}|^2}{2\pi}. \tag{6.10}$$

Of the available Cutkosky cuts, there are only two that contribute a non-zero asymmetry to this decay: cuts (a) and (b) in Fig. 6.2. Cut (a) produces the decay asymmetry

$$\Delta\Gamma(h^- \to L_\alpha L_\beta)_{(\mathrm{a})} = \frac{\pi^2 - (\ln 4)^2}{512\pi^4} \frac{\mu^2}{m_h} \sum_i \mathrm{Im}\left[(Y_i^\dagger Y_i f^\dagger)_{\alpha\beta} f_{\beta\alpha} + (Y_i^\dagger Y_i f^\dagger)_{\beta\alpha} f_{\alpha\beta}\right]. \tag{6.11}$$

[2] Since sphalerons conserve $\Delta_\alpha = B/3 - L_\alpha$, a negative lepton asymmetry leads to a positive baryon asymmetry.

The asymmetry due to cut (b) cannot be expressed analytically—at least not easily—as it features the IR-divergent three-body decay $h^- \to e\bar{L}\bar{H}$. However, it turns out that the asymmetry from this cut cancels exactly against the asymmetry due to the complementary cut $h^- \to LL \to e\bar{L}\bar{H}$ of the three-body decay in the Boltzmann equation Eq. (6.27) (see Section 6.B for details), so we can ignore it without consequence.

Owing to the flavoured nature of leptogenesis in the model, the most useful CP parameter we can define is

$$\varepsilon_\alpha^{(a)} \equiv \frac{\sum_\beta \Delta\Gamma(h^- \to L_\alpha L_\beta)_{(\mathrm{a})}}{\sum_\beta 2\Gamma_0(h^- \to L_\alpha L_\beta)} = \frac{\pi^2 - (\ln 4)^2}{512\pi^3}\frac{\mu^2}{m_h^2}\sum_i \frac{\mathrm{Im}(Y_i^\dagger Y_i f^\dagger f)_{\alpha\alpha}}{(f^\dagger f)_{\alpha\alpha}}, \tag{6.12}$$

instead of a more conventional one in which all flavours are summed over. This isolates the asymmetry contribution to a fixed flavour α.

6.2.1.2 $h^- \to e\bar{L}\bar{H}$

The second-most important decay channel is $h^- \to e\bar{L}\bar{H}$, whose tree-level diagram can be found to the left of cut (b) in Fig. 6.2. This decay is IR divergent in the limit that h^- is much heavier than the product particles, whose masses we have—up to this point—been neglecting. In Chapter 7 we will investigate how to cancel the divergence, but for now it is more practical to regulate it by introducing thermal masses and decay widths to these particles. Thermal masses arise from resumming interactions with the early universe plasma, and are given by $m_i^2(T) = c_i T^2$, where (see e.g. Refs. [104; 347; 369; 372; 400–402])

$$c_{H_1} = \frac{1}{16}(g_1^2 + 3g_2^2) + \frac{1}{6}(6\lambda_1 + 2\lambda_3 + \lambda_4) + \frac{1}{4}Y_t^2, \tag{6.13a}$$

$$c_{H_2} = \frac{1}{16}(g_1^2 + 3g_2^2) + \frac{1}{6}(6\lambda_2 + 2\lambda_3 + \lambda_4) + \frac{1}{12}\mathrm{Tr}(Y_2^\dagger Y_2), \tag{6.13b}$$

$$c_{L,\alpha\beta} = \frac{1}{32}(g_1^2 + 3g_2^2)\delta_{\alpha\beta} + \frac{1}{48}\sum_i (Y_i^\dagger Y_i)_{\alpha\beta}, \quad \text{and} \tag{6.13c}$$

$$c_{e,\alpha\beta} = \frac{1}{8}g_1^2\delta_{\alpha\beta} + \frac{1}{24}\sum_i (Y_i Y_i^\dagger)_{\alpha\beta}. \tag{6.13d}$$

When $T < m_h$ the h^- particles no longer contribute hard thermal loops to the self-energies of these light particles, and so there are no terms proportional to the couplings μ or f. In c_{H_1} we can neglect the contribution from Y_1 as it is far smaller than the top quark Yukawa entry Y_t. In principle c_{H_2} should receive contributions from its own quark Yukawas, but for simplicity we will assume they are zero. The couplings λ_i appearing in c_{H_i} originate from the scalar potential

$$\begin{aligned} V(H_1, H_2) = &-\mu_1^2 H_1^\dagger H_1 - \mu_2^2 H_2^\dagger H_2 + \Big[\mu_3^2 H_2^\dagger H_1 + \text{h.c.}\Big] + \lambda_1 (H_1^\dagger H_1)^2 + \lambda_2 (H_2^\dagger H_2)^2 \\ &+ \lambda_3 (H_1^\dagger H_1)(H_2^\dagger H_2) + \lambda_4 (H_1^\dagger H_2)(H_2^\dagger H_1) + \lambda_5 \Big[(H_1^\dagger H_2)^2 + (H_2^\dagger H_1)^2\Big]. \end{aligned} \tag{6.14}$$

Since the virtual Higgs doublet in the three-body decay can still go on-shell even after the institution of thermal masses, we also require the widths

$$m_{H_i}\Gamma_{H_i} = T^2 \sum_{\alpha,\beta} |Y^i_{\alpha\beta}|^2 \frac{\lambda^{1/2}(c_{H_i}, c_{e_\alpha}, c_{L_\beta})}{16\pi c_{H_i}} (c_{H_i} - c_{e_\alpha} - c_{L_\beta}), \tag{6.15}$$

arising from the decay $H \to \bar{e}L$ and computed using the zero-temperature rates with the thermal masses. With this the Higgs propagators are replaced by

$$\frac{\mathrm{i}}{p^2 + \mathrm{i}\epsilon} \to \frac{\mathrm{i}}{p^2 - m_{H_i}^2 + \mathrm{i} m_{H_i}\Gamma_{H_i}}, \tag{6.16}$$

and the three-body decay rate must be evaluated numerically. Correctly accounting for all thermal effects is a far more involved undertaking [347; 371; 372], but Eqs. (6.13) and (6.15) are sufficient to capture the dominant ones. When this is done we obtain a tree-level decay rate satisfying

$$\frac{\Gamma_0(h^- \to e_\gamma \bar{L}_\delta \bar{H}_i)}{\Gamma_0(h^- \to L_\alpha L_\beta)} = \frac{\mu^2}{m_h^2} \frac{|Y^j_{\gamma\delta}|^2}{|f_{\alpha\beta}|^2} g(m_h/T), \tag{6.17}$$

where $j \neq i$ (meaning if $i = 1$ then $j = 2$, and vice-versa), and the function $g(z)$ is plotted in Fig. 6.3. For the parameter values we will want to consider, this leads to a washout rate that is reasonably suppressed compared to that of the two-body decay, so it will be acceptable for us to neglect it. Even though the decays with an $\bar{H}_2$ in the final state are

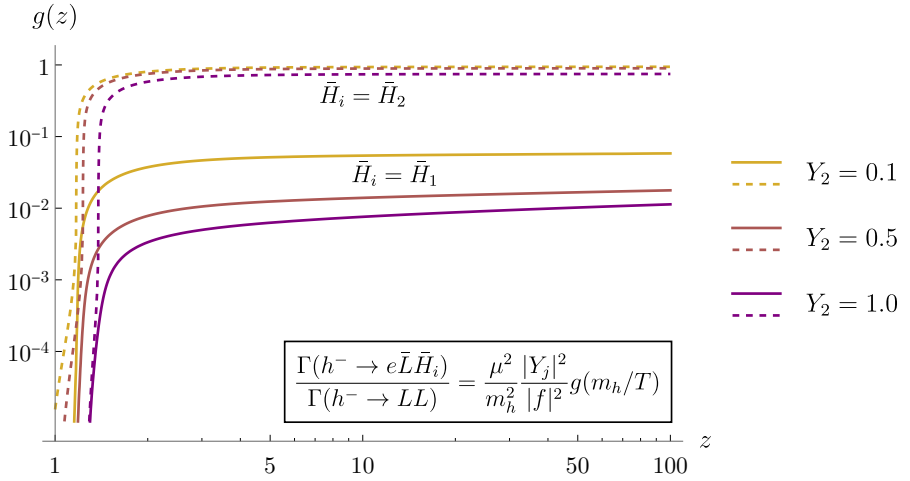

Figure 6.3: A plot illustrating the magnitude of the three-body decay rate relative to the two-body rate, given the benchmark values $\lambda_1 = \lambda_2 = 0.1$ and $\lambda_3 = \lambda_4 = 0$, and assuming for simplicity that Y_2 is proportional to the identity matrix with entries $Y_2 = \{0.1, 0.5, 1.0\}$. For consistency, the thermal mass corrections to the two-body rate are accounted for in the ratio. The precipitous drop as $z \to 1$, due to the final state masses growing comparable to m_h, is an unphysical feature which would not appear if we also accounted for the thermal contributions to the mass of h^-.

resonantly enhanced by the narrow width of the virtual H_1, the overall proportionality of the rate to $|Y_1|^2 \lesssim 0.01$ keeps it small.

Now, there are two non-zero Cutkosky cuts for this decay: cuts (c) and (d). Neither cut permits an analytical expression, though as discussed above, cut (d) cancels in the Boltzmann equation Eq. (6.27), leaving only the contribution from cut (c). Numerically the asymmetry due to cut (c) is about 17% as large as the asymmetry due to cut (a) in the 2-body decay, and of opposite sign (see Section 6.B for details):

$$\Delta\Gamma(h^- \to e\bar{L}_\alpha \bar{H})_{(\mathrm{c})} \approx -0.17 \times \Delta\Gamma(h^- \to L_\alpha L)_{(\mathrm{a})} \tag{6.18}$$

$$= -0.17 \times \frac{\pi^2 - (\ln 4)^2}{512\pi^4} \frac{\mu^2}{m_h} \sum_i \mathrm{Im}(Y_i^\dagger Y_i f^\dagger f)_{\alpha\alpha}. \tag{6.19}$$

(Here, to declutter the notation, the absence of an index means it has been summed over.) Unlike the cut (a) asymmetry, this is not so easy to express as a ratio parameter since we don't have an analytic expression for the tree-level rate. Because the dominant contribution

to the washout comes from the two-body inverse decay, however, we can instead define

$$\varepsilon_\alpha^{(\mathrm{c})} \equiv \frac{\Delta\Gamma(h^- \to e\bar{L}_\alpha \bar{H})_{(\mathrm{c})}}{2\Gamma_0(h^- \to L_\alpha L)} \approx -0.17 \frac{\pi^2 - (\ln 4)^2}{512\pi^3} \frac{\mu^2}{m_h^2} \sum_i \frac{\mathrm{Im}(Y_i^\dagger Y_i f^\dagger f)_{\alpha\alpha}}{(f^\dagger f)_{\alpha\alpha}}. \tag{6.20}$$

As the two- and three-body decays enter the Boltzmann equation Eq. (6.27) with opposite signs, the total relevant asymmetry parameter is therefore

$$\varepsilon_\alpha \equiv \varepsilon_\alpha^{(\mathrm{a})} - \varepsilon_\alpha^{(\mathrm{c})} = 1.17 \frac{\pi^2 - (\ln 4)^2}{512\pi^3} \frac{\mu^2}{m_h^2} \sum_i \frac{\mathrm{Im}(Y_i^\dagger Y_i f^\dagger f)_{\alpha\alpha}}{(f^\dagger f)_{\alpha\alpha}}. \tag{6.21}$$

6.2.2 Flavour Covariance

As was mentioned when introducing the Zee model, it is conventional to work in the charged lepton mass basis, where Y_1 is diagonal and real, and f is also made real. In this basis the CP asymmetries become proportional to

$$\varepsilon_\alpha \propto \sum_i \mathrm{Im}(Y_i^\dagger Y_i f^\dagger f)_{\alpha\alpha} = \mathrm{Im}(Y_2^\dagger Y_2 f^\dagger f)_{\alpha\alpha}, \tag{6.22}$$

and Y_1 does not contribute to the asymmetry at all. However, we could equally well rotate to the diagonal basis of Y_2, in which case

$$\varepsilon_\alpha \propto \mathrm{Im}(Y_1^\dagger Y_1 f^\dagger f)_{\alpha\alpha}. \tag{6.23}$$

It appears we have an inconsistency, and a potentially important one at that, for this distinction may mean the difference between an asymmetry large enough to explain the observed baryon abundance and one that is not. The way to resolve this is to establish flavour-covariant forms of the Boltzmann equations [104; 358; 359; 403–409], which are constructed in such a way that the total asymmetry generated, $Y_{\Delta_1} + Y_{\Delta_2} + Y_{\Delta_3}$, is manifestly invariant under flavour rotations. At the time of this writing this remains an ongoing work, so in the meantime we will need to make do with the Boltzmann equations written in the next section.

This being the case, the next best thing we can do is work in the basis that we expect should most accurately represent the true physics. With the flavours distinguished predominantly by their Yukawa interactions and thermal masses, the most suitable basis is the one that diagonalises these [104]. Since the mass basis will be most closely aligned with whichever Yukawa matrix is larger, this dashes our hopes of enlarging the asymmetry by choosing Y_2 to be large. Nevertheless, it turns out that we will still want Y_2 to be significantly larger than Y_1, and so we will use the diagonal basis of Y_2.

To be concrete, it is helpful to note that under the unitary basis rotations

$$L \to UL \quad \text{and} \quad e \to Ve, \tag{6.24}$$

the coupling matrices transform to

$$f \to U^* f U^\dagger \quad \text{and} \quad Y_i \to V Y_i U^\dagger. \tag{6.25}$$

Upon these rotations, which will be used to diagonalise Y_2, the flavoured part of the CP asymmetry parameter transforms in turn to

$$\sum_i \frac{\mathrm{Im}(Y_i^\dagger Y_i f^\dagger f)_{\alpha\alpha}}{(f^\dagger f)_{\alpha\alpha}} \to \sum_i \frac{\mathrm{Im}(U Y_i^\dagger Y_i f^\dagger f U^\dagger)_{\alpha\alpha}}{(U f^\dagger f U^\dagger)_{\alpha\alpha}}. \tag{6.26}$$

6.2.3 Boltzmann Equations

Let us now drape our asymmetries in the appropriate Boltzmann equations. We will need equations for the partial baryon-minus-lepton number densities Y_{Δ_α}, as well as for $Y_{\Sigma h}$ and $Y_{\Delta h}$. The remaining particle number densities—namely those of the leptons L_α, e_α and the Higgs doublets H_i—are fixed by spectator processes, as discussed in Section 5.4.5 of the previous chapter. At leading order the equation for Y_{Δ_α} is

$$sz\mathcal{H}\frac{\mathrm{d}Y_{\Delta_\alpha}}{\mathrm{d}z} = \frac{1}{2}\left[-\sum_\beta \Delta\gamma(h^- \to L_\alpha L_\beta) + \sum_{\beta,i} \Delta\gamma(h^- \to e_\beta \bar{L}_\alpha \bar{H}_i)\right]\left(\frac{Y_{\Sigma h}}{Y_h^{\mathrm{eq}}} - 2\right) \\ -\sum_\beta \frac{1}{2}\Sigma\gamma(h^- \to L_\alpha L_\beta)\left(\frac{Y_{\Delta h}}{Y_h^{\mathrm{eq}}} - \frac{Y_{\Delta L_\alpha} + Y_{\Delta L_\beta}}{Y_L^{\mathrm{nor}}}\right), \tag{6.27}$$

where $z = m_h/T$, and all other symbols are defined in Chapter 5. In principle there should be a washout term from the three-body decay of the form[3]

$$\sum_{\beta,\gamma,i}(\delta_{\alpha\beta} - \delta_{\alpha\gamma})\frac{1}{2}\Sigma\gamma(h^- \to e_\gamma \bar{L}_\beta \bar{H}_i)\left(\frac{Y_{\Delta h}}{Y_h^{\mathrm{eq}}} - \frac{Y_{\Delta e_\gamma}}{Y_e^{\mathrm{nor}}} + \frac{Y_{\Delta L_\beta}}{Y_L^{\mathrm{nor}}} + \frac{Y_{\Delta H_i}}{Y_H^{\mathrm{nor}}}\right), \tag{6.28}$$

as well as from other decay channels such as $h^- \to e_\beta L_\alpha H_i$, but as discussed above, they are acceptable to neglect. Generically we should also prepend a factor of $(1 + \delta_{\alpha\beta})$ to the two-body decay, but since the rate vanishes when $\alpha = \beta$ due to the antisymmetry of f, such a factor is unnecessary.

The equations for the heavy scalar $h^\pm$ are

$$sz\mathcal{H}\frac{\mathrm{d}Y_{\Sigma h}}{\mathrm{d}z} = -\frac{1}{4}\left[\sum_{\alpha,\beta}\Sigma\gamma(h^- \to L_\alpha L_\beta) + \sum_{i,j}\Sigma\gamma(h^- \to \bar{H}_i\bar{H}_j)\right]\left(\frac{Y_{\Sigma h}}{Y_h^{\mathrm{eq}}} - 2\right) \tag{6.29a}$$
$$-\left[\Sigma\gamma(h^+h^- \to BB) + \sum_i \Sigma\gamma(h^+h^- \to H_i\bar{H}_i) \right.$$
$$\left. + \sum_f \Sigma\gamma(h^+h^- \to f\bar{f})\right]\left(\frac{Y_{\Sigma h}^2}{4(Y_h^{\mathrm{eq}})^2} - 1\right) \quad \text{and}$$
$$sz\mathcal{H}\frac{\mathrm{d}Y_{\Delta h}}{\mathrm{d}z} = -\frac{1}{4}\sum_{\alpha,\beta}\Sigma\gamma(h^- \to L_\alpha L_\beta)\left(\frac{Y_{\Delta h}}{Y_h^{\mathrm{eq}}} - \frac{Y_{\Delta L_\alpha} + Y_{\Delta L_\beta}}{Y_L^{\mathrm{nor}}}\right) \tag{6.29b}$$
$$-\frac{1}{4}\sum_{i,j}\Sigma\gamma(h^- \to \bar{H}_i\bar{H}_j)\left(\frac{Y_{\Delta h}}{Y_h^{\mathrm{eq}}} - \frac{Y_{\Delta H_i} + Y_{\Delta H_j}}{Y_H^{\mathrm{nor}}}\right).$$

The decays $h^- \to L_\alpha L_\beta$ and $h^- \to \bar{H}_i\bar{H}_j$ both include additional factors of 1/2 to avoid

[3]The Kronecker deltas here would be necessary because both L and e carry lepton number. The reason for the absence of similar deltas in the source term of Eq. (6.27) is that there is no asymmetry generated in e, as we have discussed.

double-counting the final states. The annihilation processes appearing in the second and third lines of Eq. (6.29a) are all mediated by the $\mathrm{U}(1)_Y$ gauge boson B, and the sum f runs over all SM fermions. Expressions for these processes are given in Section 6.C.

6.2.4 Qualitative Discussion

It is a good idea to now orient ourselves by discussing what we will need to maximise our chances of achieving successful leptogenesis. As a reminder, the asymmetry parameter is

$$\varepsilon_\alpha = 1.17 \frac{\pi^2 - (\ln 4)^2}{512\pi^3} \frac{\mu^2}{m_h^2} \sum_i \frac{\mathrm{Im}(Y_i^\dagger Y_i f^\dagger f)_{\alpha\alpha}}{(f^\dagger f)_{\alpha\alpha}}, \tag{6.30}$$

meaning that the asymmetry generation for a flavour α is proportional to $\mu^2 \,\mathrm{Im}(Y_i^\dagger Y_i f^\dagger f)_{\alpha\alpha}$, while the washout in that flavour is proportional to $(f^\dagger f)_{\alpha\alpha}$. Since this is a flavoured leptogenesis scenario, we require f to be hierarchical in order to preserve the asymmetry in one flavour – for example, $|f_{12}|, |f_{13}| \ll |f_{23}|$ in the diagonal mass basis will preserve $Y_{\Delta L_1}$ while washing out $Y_{\Delta L_2}$ and $Y_{\Delta L_3}$.

To obtain a large asymmetry the most direct thing we can do is increase μ, since—as discussed in Section 6.2.2—increasing Y_2 does not necessarily increase the asymmetry. The limit on the size of μ is set by perturbativity, which requires $\mu \lesssim \sqrt{4\pi} m_h$. Ref. [179] argues that $\mu \lesssim 15\,\mathrm{TeV}$ is needed to avoid a fine-tuned Higgs boson mass, but since this is not a strict requirement we will ignore it (and likewise for the similar naturality bounds on m_h and m_{H_2}). An important point to consider is that the decay rate of $h^- \to \bar{H}\bar{H}$ is proportional to μ, so to avoid depleting the population of h^- particles before they can decay to leptons we will need $\Gamma(h^- \to \bar{H}\bar{H}) \sim \Gamma(h^- \to LL)$, which translates to $\mu/m_h \sim |f|$.

Regarding m_h, we generically expect a larger mass scale to fare better than a smaller one. The reason for this is that the efficiency of the inverse decay,[4]

[4]Here we use that $\Gamma(LL \to h^-) \simeq \Gamma(h^- \to LL) z^{3/2} e^{-z}$ for $z > 1$ [89, Ch. 6]. See also Ref. [410] for an earlier work on the out-of-equilibrium condition for $h^- \leftrightarrow LL$.

$$\frac{\Gamma}{\mathcal{H}} \approx 10^5 z^{7/2} e^{-z} \left(\frac{110.75}{g_\star}\right)^{1/2} \left(\frac{|f|}{1}\right)^2 \left(\frac{10^{12}\,\text{GeV}}{m_h}\right), \tag{6.31}$$

scales inversely with m_h, and so a larger value is preferred to ensure the out-of-equilibrium condition $\Gamma/\mathcal{H} < 1$ is more quickly satisfied. (The numerical factor of 10^5 here may appear distressing, but it will largely cancel against the hierarchically small entries of f.) To see how we might obtain a large m_h we may consult the neutrino mass formula,

$$m^\nu_{\alpha\beta} = \frac{\mu v^2}{16\pi^2 m_h^2} \ln \frac{m^2_{H_2^+}}{m^2_{h^+}} \left(f Y_1 Y_2 + Y_2^T Y_1^T f^T\right)_{\alpha\beta}. \tag{6.32}$$

With m_ν and Y_1 fixed, we see that increasing μ, f or Y_2, or decreasing $m_{H_2^+}$, will allow us to raise m_h. Increasing Y_2 and μ/m_h up to the perturbative limit of $\sqrt{4\pi}$ is easily done, though raising f is counterproductive since $\Gamma/\mathcal{H} \propto |f|^2$ – that said, increasing f and μ/m_h proportionally in accordance with the demand $\mu/m_h \sim |f|$ leaves $\Gamma/\mathcal{H}$ unaltered. The most stringent limits on $m_{H_2^+}$ are set by flavour physics searches, which, assuming $Y_2 \sim \mathcal{O}(1)$, impose $m_{H_2^+} \gtrsim 100\,\text{TeV}$ [411][5]; direct collider searches for charged Higgs decays additionally imply the weaker bound $m_{H_2^+} > 3\,\text{TeV}$ [124; 412; 413].

6.3 A Benchmark Scenario

In order to assess the general feasibility of successful leptogenesis within the Zee model it is productive to study a benchmark scenario. To accomplish this we performed a numerical scan over the parameter space of the model and collected a set of benchmark parameter points that successfully fit the observed neutrino oscillation data [152] for both normal ordering and inverted ordering. The result of this scan is shown in Fig. 6.4, where for each point we have rotated to the diagonal basis of Y_2, computed the asymmetry parameters

[5]The bounds shown in Fig. 5.1 of Ref. [411] must be appropriately rescaled since the contributions to the pertinent Wilson coefficients are typically loop-suppressed. Though the trilepton decays occur at tree-level in the Zee model, they are suppressed in proportion to the charged lepton masses [179].

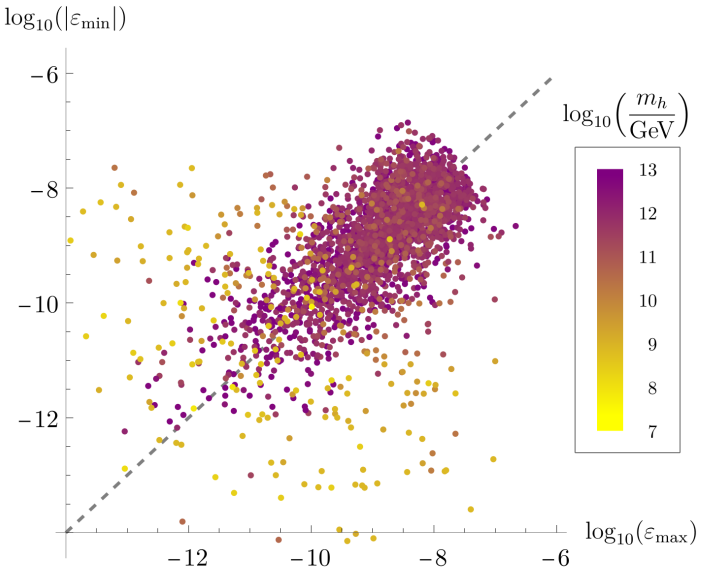

(a) Normal ordering

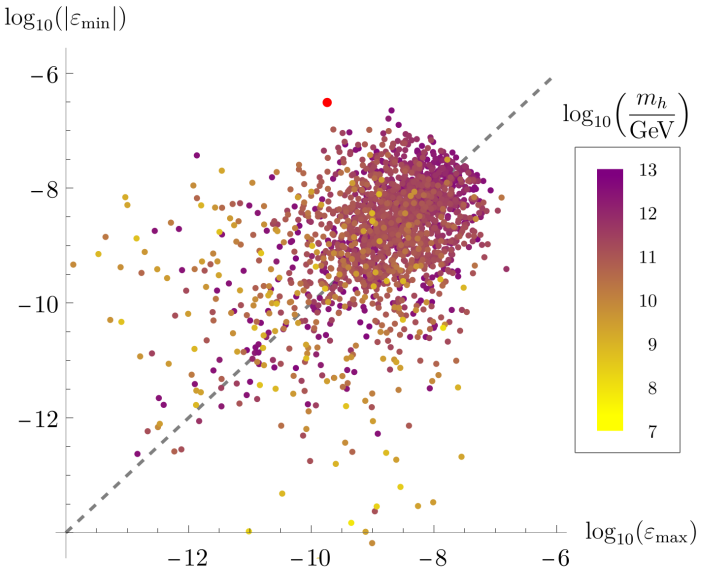

(b) Inverted ordering

Figure 6.4: Benchmark parameter points fitting neutrino oscillation data, showing $\varepsilon_{\min} = \min\{\varepsilon_1, \varepsilon_2, \varepsilon_2\}$ (i.e. the largest negative asymmetry parameter) against $\varepsilon_{\max} = \max\{\varepsilon_1, \varepsilon_2, \varepsilon_2\}$ (i.e. the largest positive asymmetry parameter). The colour of a point denotes the value of m_h computed in the manner described in the main text, with the exception of the most promising benchmark point between the two orderings, which is indicated with an enlarged red dot.

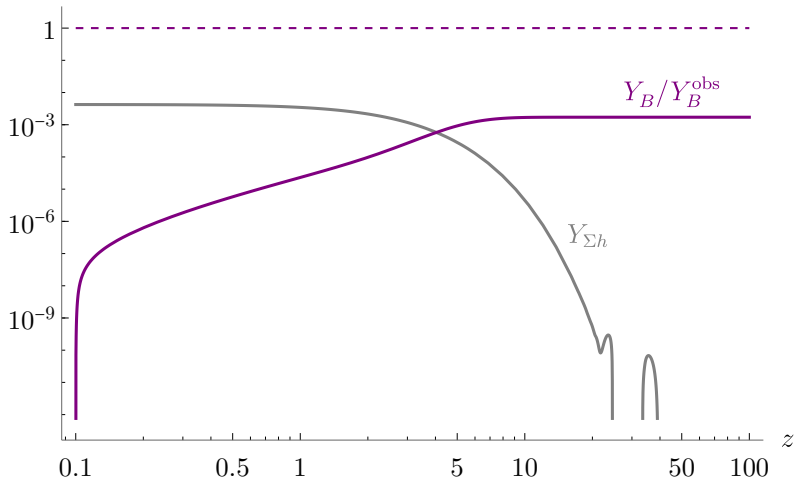

Figure 6.5: The result of running the Boltzmann equations in our benchmark scenario. The oscillations in $Y_{\Sigma h}$ at large z are due to numerical instability, and are unphysical.

$\varepsilon_1, \varepsilon_2, \varepsilon_3$, and positioned it based on its largest negative ε and largest positive ε. For concreteness, m_h is computed for each point by fixing $m_{H_2^+} = 100\,\text{TeV}$, $\mu/m_h = 1$, and rescaling both Y_2 and f so that their largest absolute entries are 1 in the original basis; this leads to a spread of m_h values from around $10^7\,\text{GeV}$ to $10^{13}\,\text{GeV}$. For each of these values the mixing angle φ in Eq. (6.4) is indeed small, justifying the use of the simplified mass formula, Eq. (6.5).

The most promising points for leptogenesis are those near the top of the plots in Fig. 6.4, as these have a relatively large negative asymmetry (as is needed to generate a positive baryon asymmetry), and a small positive asymmetry. To be as generous as possible to the model, let's take the highest benchmark point from Fig. 6.4b, for which the three asymmetry parameters read

$$\varepsilon_1 \approx -3.10 \times 10^{-7}, \qquad \varepsilon_2 \approx 1.82 \times 10^{-10}, \quad \text{and} \quad \varepsilon_3 \approx -6.10 \times 10^{-13}, \tag{6.33}$$

with $m_h \approx 2.73 \times 10^{12}\,\text{GeV}$. The result of running the Boltzmann equations for this benchmark scenario is shown in Fig. 6.5, where we can plainly see that the generated baryon asymmetry $Y_B = \frac{12}{37}(Y_{\Delta_1} + Y_{\Delta_2} + Y_{\Delta_3})$ falls short of reproducing the observed asymmetry $Y_B^{\rm obs} \approx 8.68 \times 10^{-11}$ by three orders of magnitude. Reducing the size of f or increasing Y_2 and μ/m_h up to $\sqrt{4\pi}$, and correspondingly rescaling m_h, does little to

improve the result. We similarly do not expect a 10^3 enhancement to arise from running the more correct flavour-covariant Boltzmann equations. Since all other benchmark points have a worse outlook than this one, we may conclude that *the Zee model is incapable of explaining the observed baryon asymmetry of the universe*, even in a high-scale leptogenesis scenario.

6.4 Minimal Extensions

The failure of the Zee model to successfully achieve leptogenesis is somewhat disappointing, so to avoid ending on a null result we are endeavouring to study the viability of minimal extensions of the model with additional sources of CP violation. This part of the work is presently ongoing, so for now I will simply present the extensions without discussing their phenomenology or prospects for leptogenesis.

6.4.1 A Third Higgs Doublet

One possible way to extend the model is to introduce a third Higgs doublet $H_3 \sim (1, 2, 1/2)$, wherein the interactions relevant to this work generalise to

$$\mathcal{L} \supset -m_h^2 h^+ h^- + \left(\frac{1}{2}\mu_{ij}\widetilde{H}_i^\dagger H_j h^- - \overline{\widetilde{L}} f L h^+ - \overline{L} Y_i^\dagger H_i e_R + \text{h.c.}\right), \tag{6.34}$$

where μ_{ij} is antisymmetric and equal to $\mu\epsilon_{ij}$ in the original model. Much like the original Zee model, we can rotate to a lepton basis where one Yukawa matrix Y_i is real and diagonal and f is also real. Moreover, μ_{ij} may also be made real by rephasing h^- and the two Higgs doublets with non-diagonal Yukawa matrices.

In this extended model the neutrino mass formula generalises to[6]

[6]To evaluate the loop diagrams we have used the results of Ref. [414]. If we drop the contribution of the third Higgs doublet and parameterise U by $U_{11} = -U_{22} = \sin\varphi$ and $U_{12} = U_{21} = \cos\varphi$, then $U_{21}U_{11}^* = -U_{22}U_{12}^* = \frac{1}{2}\sin(2\varphi)$, and we recover Eq. (6.3).

$$m^{\nu}_{\alpha\beta} = \frac{1}{8\pi^2}\frac{v}{\sqrt{2}}\sum_{k\neq 1}(G_{12,k}+G_{23,k}+G_{31,k})(fY_1Y_k + Y_k^T Y_1^T f^T)_{\alpha\beta} \tag{6.35}$$

with

$$G_{ij,k} = \frac{U_{ki}U^*_{1i}m^2_{h_j^+} + U_{kj}U^*_{1j}m^2_{h_i^+}}{m^2_{h_j^+} - m^2_{h_i^+}} \ln\frac{m^2_{h_i^+}}{m^2_{h_j^+}}, \tag{6.36}$$

where U is the unitary matrix relating the charged scalar mass eigenstates h^- to the interaction eigenstates $\hat{h}^-$: $\hat{h}^-_i = U_{ij}h^-_j$. Here $\hat{h}^-_1$ is the singly-charged scalar and h^+_i for $i = 2, 3$ are the charged components of H_i.

The CP asymmetry factor similarly generalises to

$$\begin{aligned}\varepsilon_\alpha &\simeq 1.17\frac{\pi^2 - (\ln 4)^2}{512\pi^3}\sum_{i,j}\mathrm{Im}\left[\frac{(\mu\mu^\dagger)_{ij}}{m^2_h}\frac{(Y_j^\dagger Y_i f^\dagger f)_{\alpha\alpha}}{(f^\dagger f)_{\alpha\alpha}}\right] \\ &= 1.17\frac{\pi^2 - (\ln 4)^2}{512\pi^3}\sum_{i,j}\frac{(\mu\mu^\dagger)_{ij}}{m^2_h}\frac{1}{2\mathrm{i}}\frac{(Y_j^\dagger Y_i f^\dagger f - f^\dagger f Y_j^\dagger Y_i)_{\alpha\alpha}}{(f^\dagger f)_{\alpha\alpha}},\end{aligned} \tag{6.37}$$

and the total asymmetry $\sum_{\alpha,\beta}\Delta\Gamma(h^- \to L_\alpha L_\beta)$ is zero. Leptogenesis therefore remains flavoured in this extension, and a hierarchical f is still required.

The main advantage to introducing a third Higgs doublet lies in the observation that only one Yukawa matrix can in general be diagonalised at a time. If we then have, say, $|Y_3| > |Y_2| > |Y_1|$, the thermal lepton masses will be most closely aligned with Y_3, and so even when Y_3 is diagonalised we may entertain the possibility of enhancing the CP asymmetry through its proportionality to Y_2, which may be much larger than Y_1. That said, it is unclear how well this advantage carries over in a more correct flavour-covariant treatment of the asymmetry generation.

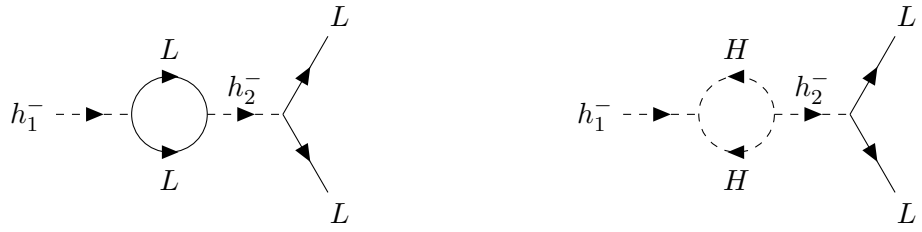

(a) LL loop (b) HH loop

Figure 6.6: The one-loop corrections to $h_1^- \to LL$ in the two singlet extension that generate CP-violating interferences with the tree-level decay.

6.4.2 A Second Singly-Charged Scalar

Another way to extend the Zee model is to introduce a second singly-charged scalar[7] $h_2^- \sim (1, 1, -1)$, with the relevant interactions

$$\mathcal{L} \supset -m_{h_1}^2 h_1^+ h_1^- - m_{h_2}^2 h_2^+ h_2^- + \left(\mu_i \widetilde{H}_1^\dagger H_2 h_i^- - \overline{\widetilde{L}} f_i L h_i^+ - \overline{L} Y_i^\dagger H_i e_R + \text{h.c.}\right). \tag{6.38}$$

In this extension, CP violation in the decay $h_1^- \to LL$ can arise at one-loop through the diagrams in Fig. 6.6, generating an asymmetry of the form

$$\Delta\Gamma(h_1^- \to L_\alpha L_\beta) = \text{Im}\left[\text{Tr}(f_1^\dagger f_2) f_{\alpha\beta}^1 f_{\alpha\beta}^{2*}\right] g_1\left(\frac{m_{h_2}^2}{m_{h_1}^2}\right) + \text{Im}\left[\mu_1 \mu_2^* f_{\alpha\beta}^1 f_{\alpha\beta}^{2*}\right] g_2\left(\frac{m_{h_2}^2}{m_{h_1}^2}\right), \tag{6.39}$$

where $g_1(x)$ and $g_2(x)$ are presently-undetermined functions. The contribution of the first term is zero when summed over flavours, leaving

$$\sum_{\alpha,\beta} \Delta\Gamma(h_1^- \to L_\alpha L_\beta) = \text{Im}\left[\mu_1 \mu_2^* \,\text{Tr}(f_2^\dagger f_1)\right] g_2\left(\frac{m_{h_2}^2}{m_{h_1}^2}\right). \tag{6.40}$$

This version of the model has the advantage that the asymmetry is only one-loop (instead of two-loop) suppressed, and moreover it can be resonantly enhanced when $m_{h_2} \approx m_{h_1}$. The fact that the asymmetry is no longer purely flavoured additionally lowers the difficulty

[7] This extension was suggested by Eung Jin Chun. It is also mentioned in a footnote in Ref. [107].

barrier to generating a large net asymmetry. These considerations greatly improve the prospects of this extension compared to the original Zee model.

A similar extension to this one has been studied in Ref. [107], featuring in addition three right-handed sterile neutrinos $N_R \sim (1,1,0)$ of mass 1 TeV. There the three-body decays $N_R \to \bar{e}LL$ and $N_R \to \bar{e}HH$ mediated by h^- generated the requisite lepton asymmetry. Another related extension was studied in Ref. [385], where the authors additionally introduced a third singly-charged scalar $\chi^- \sim (1,1,-1)$ and three left-handed sterile neutrinos $N_L \sim (1,1,0)$, as well as a softly-broken $\mathrm{U}(1)_{B-L}$ symmetry. The asymmetry generation in their model then came from the decay $h_1^- \to eN_L$, with the spectator process $e\bar{e} \leftrightarrow L\bar{L}$ transmitting the symmetry to the left-handed leptons, and therefore the baryons.

6.5 Summary

In this chapter we have investigated the leptogenesis prospects of a high-scale realisation of the Zee model of neutrino masses, in which a lepton asymmetry is generated through the decays of the new scalar h^- with a mass of $\mathcal{O}(10^{12}\,\mathrm{GeV})$. Unfortunately, this scenario is heavily marred by the fact that it is purely flavoured, and this compounded with the two-loop suppression of the CP asymmetries and the difficulty in enhancing them due to effects related to flavour covariance means that it fails to reproduce the observed baryon asymmetry by at least three orders of magnitude even under the most optimistic circumstances. This finding is complementary to previous works demonstrating the inability of the model to successfully achieve leptogenesis at the TeV scale, and thereby corroborates the claim that it is unachievable at *any* scale.

The Zee model must therefore be extended if it is to generate enough of a baryon asymmetry. To this end, we have identified two minimal extensions of the model—one adding another Higgs doublet and the other adding another charged singlet—that have improved prospects, and the study of these extensions remains an ongoing part of this work. If successful leptogenesis is indeed possible in either of these models, it will be interesting to see how far

the new mass scales can be lowered, as well as if there are any low-scale observables (such as the Dirac CP phase of the PMNS matrix in the upcoming JUNO [168], DUNE [169], and Hyper-K [170] experiments[8]) that we can use to probe these scenarios. To ensure we do not miss any important effects and that any conclusions drawn about these extensions are therefore as robust as possible, we will want to carry out this study using a flavour-covariant formulation of the Boltzmann equations.

[8]See for example Refs. [415–419] for discussions of the connection between the Dirac phase and (Seesaw) leptogenesis, and Ref. [420] for a more general discussion of probes of leptogenesis.

6.A Feynman Rules

As a reminder, the relevant part of the Zee model interaction Lagrangian consists of

$$\mathcal{L} \supset \frac{1}{2}\mu_{ij}\widetilde{H}_i^\dagger H_j h^- - \overline{\widetilde{L}} f L h^+ - \overline{L} Y_i^\dagger H_i e_R + \text{h.c.} \tag{6.41}$$

when generalised to an arbitrary number of Higgs doublets. This gives rise to the following Feynman rules, which are each independent of prescribed fermion flow (see Refs. [336; 337]):

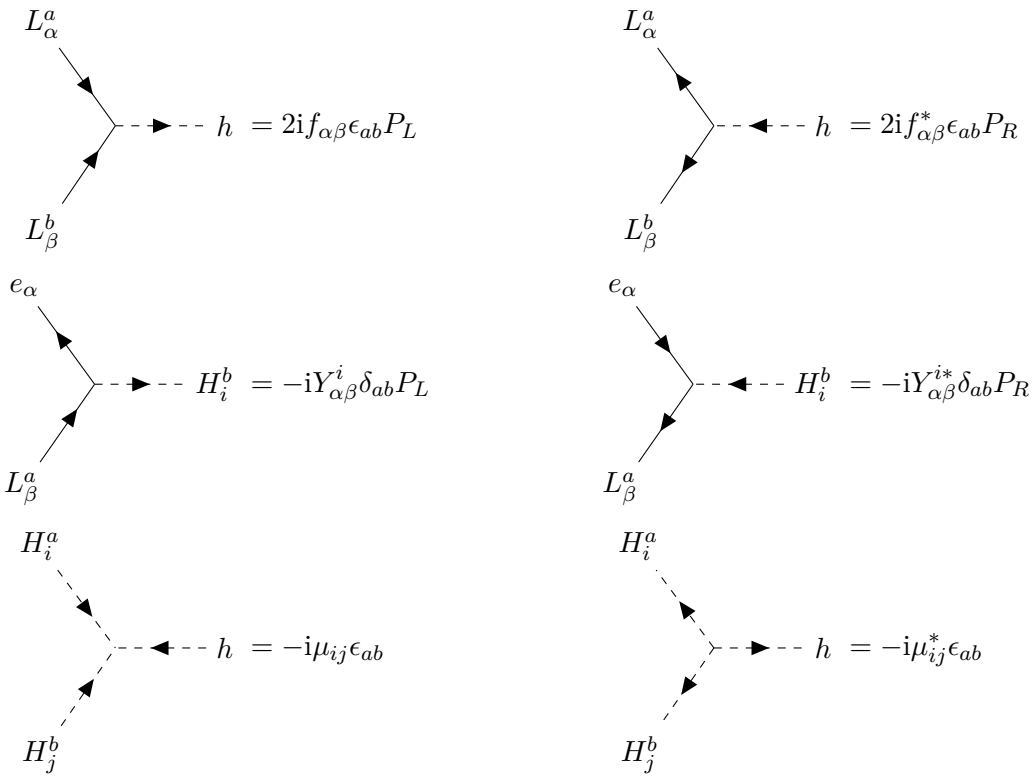

The rules for the original Zee model are recovered by replacing $\mu_{ij} \to \mu\epsilon_{ij}$.

6.B The Cutkosky Cuts in Detail

There are six possible cuttings of our two-loop self-energy diagram for h^-, shown in Figs. 6.2 and 6.7, and labelled (a) to (f). We must consider all possible pairings of cuts, with one

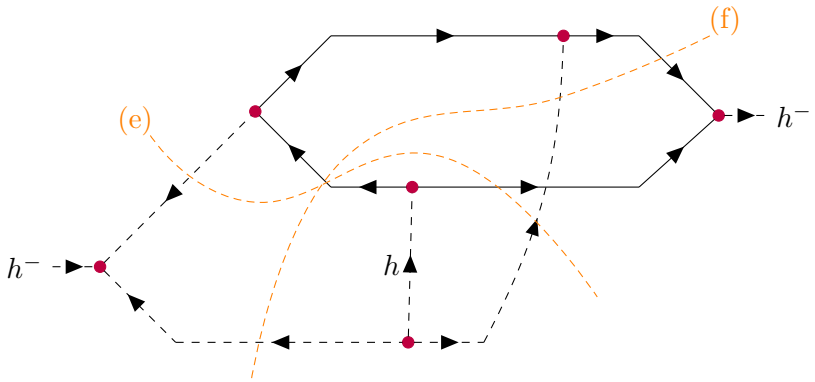

Figure 6.7: The two additional four-body cuts, (e) and (f), not shown in Fig. 6.2. They do not contribute to any CP asymmetries.

Decay	Cut	Cutkosky cuts (a)	(b)	(c)	(d)	(e)	(f)	Imaginary couplings?	Asymmetry?
$h^- \to HH$	(a)		PS	✓	✓	PS	PS	None	✗
$h^- \to e\bar{L}\bar{H}$	(b)	PS		✓	✓	—	PS	$\bar{L}$	✓
$h^- \to eLH$	(c)	✓	✓		PS	PS	—	None	✗
$h^- \to LL$	(d)	✓	✓	PS		PS	PS	L	✓
$h^- \to \bar{H}LLH$	(e)	PS	—	PS	PS		—	L	✗
$h^- \to L\bar{H}\bar{L}\bar{H}$	(f)	PS	PS	—	PS	—		$L, \bar{L}$	✗

Table 6.1: Summary of cuts. A dash (—) means a cut is incompatible with that row's decay. "PS" means that a cut contains a phase space of vanishing measure, and so is zero. The remaining non-zero pairings are ticked (✓). A decay can generate an asymmetry if it allows at least one non-zero Cutkosky cut and has imaginary couplings for at least one final state particle.

functioning as the final state cut and one as the Cutkosky cut. Some pairings, such as (e) and (f), are incompatible as they cross over each other and so cannot occur simultaneously. Of the compatible pairings, most are trivially zero as they contain a phase space integral with zero measure. For example, the combination of cuts (a) and (b) includes the process $H \to e\bar{L}$ as a disconnected subprocess, which has measure zero phase space when all particles are treated as massless.

The non-zero cuts are marked with a tick in Table 6.1, contributing imaginary parts to the loop-level amplitudes of the decays $h^- \to HH$, $h^- \to e\bar{L}\bar{H}$, $h^- \to eLH$, and $h^- \to LL$. However, as discussed in Section 6.2.1, only the decays $h^- \to LL$ and $h^- \to e\bar{L}\bar{H}$ feature imaginary couplings, and even then only when considering a final state lepton doublet of

fixed flavour, L_α. We therefore only need to work out the asymmetries in these two decays.

Note that the phase space and imaginary couplings arguments no longer apply when we institute thermal masses to H_i, L, and e, meaning we in principle should consider additional cuts and decays. These new contributions will however be suppressed in powers of m/m_h, and can be safely neglected.

6.B.1 $h^- \to LL$

Common to all cuts for the decay $h^- \to L^a_\alpha L^b_\beta$ are the coupling constants

$$\mathrm{Im}(c_0^* c_1) = 4\mu_{ij}\mu^*_{kj}\epsilon^4_{ab}\,\mathrm{Im}(f_{\alpha\beta}f^*_{\delta\beta}Y^i_{\gamma\delta}Y^{k*}_{\gamma\alpha}) + (\alpha \leftrightarrow \beta, a \leftrightarrow b), \tag{6.42}$$

obtained by using the particle indices of Figs. 6.2 and 6.8. The second term, labelled $(\alpha \leftrightarrow \beta, a \leftrightarrow b)$, comes from the diagram where the final state lepton doublets are swapped. To avoid exaggerating the differences between the original Zee model (where μ appears simply as $|\mu|^2$) and the three-Higgs-doublet extension, I have assumed that we have rephased our fields to make μ real so that it factors out of the imaginary part (though to maintain some semblance of generality I have left the now-meaningless conjugate on μ^*_{kj} in place).[9] Summing over the $\mathrm{SU(2)_W}$ indices a, b, virtual lepton flavours γ, δ, and virtual Higgses i, j, k brings this to the form

$$\mathrm{Im}(c_0^* c_1) \to \sum_{i,k} 8(\mu\mu^\dagger)_{ik}\,\mathrm{Im}\left[(Y_k^\dagger Y_i f^\dagger)_{\alpha\beta}f_{\beta\alpha} + (Y_k^\dagger Y_i f^\dagger)_{\beta\alpha}f_{\alpha\beta}\right]. \tag{6.43}$$

In the Boltzmann equation for Y_{Δ_α} we additionally sum over the flavour β, so the couplings appear there as

$$\mathrm{Im}(c_0^* c_1) \to \sum_{i,j} 8(\mu\mu^\dagger)_{ij}\,\mathrm{Im}(Y_j^\dagger Y_i f^\dagger f)_{\alpha\alpha}, \tag{6.44}$$

where I have relabelled $k \to j$.

[9] The fully general form of $\mathrm{Im}(c_0^* c_1)$, without assuming the reality of μ, can be found in Eq. (6.37).

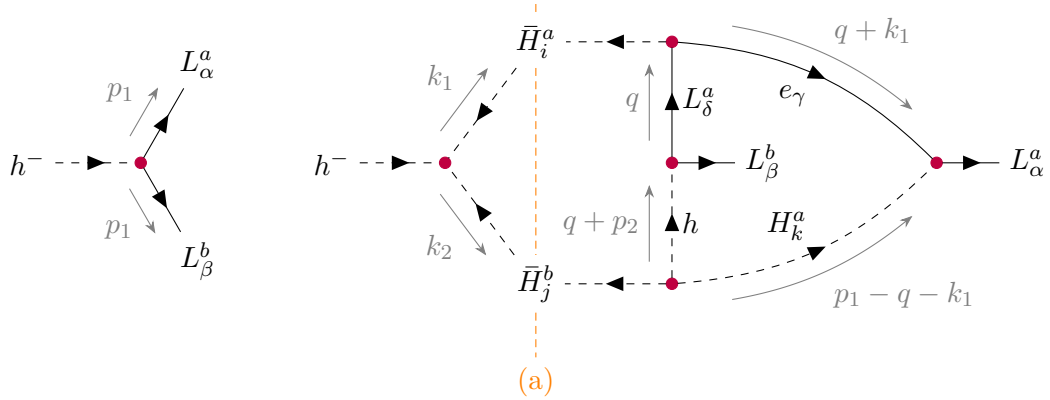

(a) Tree-level.

(b) Loop-level, with the two-body cut (a). This diagram is non-planar, so for visual clarity the final state L^b_β line terminates in the centre instead of exiting to the right.

Figure 6.8: Diagrams for the two-body decay $h^- \to LL$.

6.B.1.1 Cut (a)

For this cut,

$$h^- \to \bar{H}^a_i(\mathbf{k}_1)\bar{H}^b_j(\mathbf{k}_2) \to L^a_\alpha(\mathbf{p}_1)L^b_\beta(\mathbf{p}_2), \tag{6.45}$$

which is shown in Fig. 6.8b, we have

$$2\,\mathrm{Im}(\mathcal{A}_0^*\mathcal{A}_1)_{(\mathrm{a})} = \int \mathrm{d}\Pi(k_1,k_2)\,\frac{1}{\mathrm{i}}\int \frac{\mathrm{d}^4q}{(2\pi)^4}\frac{1}{(q+k_1)^2}\frac{1}{q^2}\frac{\mathrm{Tr}[\not{p}_1(\not{q}+\not{k}_1)\not{q}\not{p}_2 P_L]}{(q+p_2)^2-m_h^2}\frac{1}{(p_1-q-k_1)^2}. \tag{6.46}$$

The loop integral can be carried out using e.g. `Package-X` [421], resulting in a somewhat complicated—but finite—expression. Integrating then over the two-body phase spaces of (k_1,k_2) and (p_1,p_2), the latter of which is trivial, leads to the remarkably simple result

$$\int \mathrm{d}\Pi_f\, 2\,\mathrm{Im}(\mathcal{A}_0^*\mathcal{A}_1)_{(\mathrm{a})} = -\frac{\pi^2-(\ln 4)^2}{(8\pi)^4} \approx -2\times 10^{-5}. \tag{6.47}$$

In accordance with $\Delta|\mathcal{M}|^2 = -4\,\mathrm{Im}(c_0^*c_1)\,\mathrm{Im}(\mathcal{A}_0^*\mathcal{A}_1)$ (see Eq. (5.6)), the asymmetry in the two-body decay $h^- \to L_\alpha L_\beta$ due to cut (a) is therefore

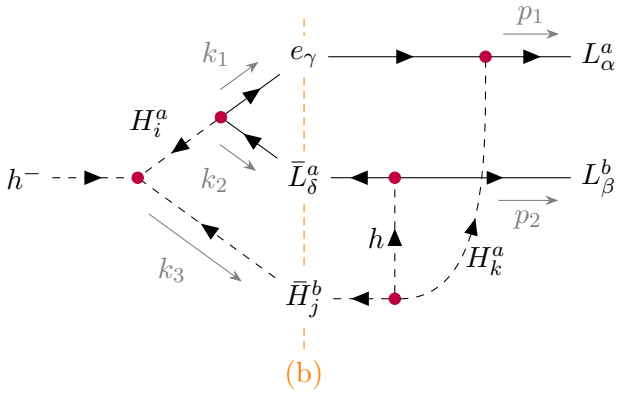

Figure 6.9: The loop-level diagram for $h^- \to LL$ with the three-body cut (b).

$$\begin{aligned}\Delta\Gamma(h^- \to L_\alpha L_\beta)_{(\mathrm{a})} &= \frac{1}{2m_h}\int \mathrm{d}\Pi_f\,(-4)\,\mathrm{Im}(c_0^* c_1)\,\mathrm{Im}(\mathcal{A}_0^*\mathcal{A}_1)_{(\mathrm{a})} \\ &= \frac{\pi^2-(\ln 4)^2}{512\pi^4}\sum_{i,j}\frac{(\mu\mu^\dagger)_{ij}}{m_h}\,\mathrm{Im}\left[(Y_j^\dagger Y_i f^\dagger)_{\alpha\beta}f_{\beta\alpha}+(Y_j^\dagger Y_i f^\dagger)_{\beta\alpha}f_{\alpha\beta}\right]. \quad (6.48)\end{aligned}$$

In the original Zee model, in which $\mu_{ij} = \mu\epsilon_{ij}$, this becomes the asymmetry given in Eq. (6.11).

6.B.1.2 Cut (b)

This cut, which is shown in Fig. 6.9, reads

$$h^- \to e_\gamma(\mathbf{k}_1)\bar{L}^a_\delta(\mathbf{k}_2)\bar{H}^b_j(\mathbf{k}_3) \to L^a_\alpha(\mathbf{p}_1)L^b_\beta(\mathbf{p}_1), \quad (6.49)$$

and it is IR divergent when all particles but h^- are treated as massless. When regulated with the thermal masses in Section 6.2.1.2, we have

$$\begin{aligned}2\,\mathrm{Im}(\mathcal{A}_0^*\mathcal{A}_1)_{(\mathrm{b})} = -\int \mathrm{d}\Pi(k_1,k_2,k_3)\,&\frac{\mathrm{Tr}\left[\not{p}_1\not{k}_1\not{k}_2\not{p}_2 P_L\right]}{(p_2-k_2)^2-m_h^2} \\ &\times\frac{1}{(k_1+k_2)^2-m_{H_i}^2+\mathrm{i}m_{H_i}\Gamma_{H_i}}\,\frac{1}{(p_1-k_1)^2-m_{H_k}^2+\mathrm{i}m_{H_k}\Gamma_{H_k}}. \quad (6.50)\end{aligned}$$

Due to the imaginary widths this expression is no longer purely real, so we must modify

it by taking the real parts of these propagators:

$$2\,\mathrm{Im}(\mathcal{A}_0^*\mathcal{A}_1)_{(\mathrm{b})} = -\int \mathrm{d}\Pi(k_1,k_2,k_3)\,\frac{\mathrm{Tr}\left[\not{p}_1\not{k}_1\not{k}_2\not{p}_2 P_L\right]}{(p_2-k_2)^2-m_h^2} \times \frac{(k_1+k_2)^2-m_{H_i}^2}{[(k_1+k_2)^2-m_{H_i}^2]^2+[m_{H_i}\Gamma_{H_i}]^2}\,\frac{(p_1-k_1)^2-m_{H_k}^2}{[(p_1-k_1)^2-m_{H_k}^2]^2+[m_{H_k}\Gamma_{H_k}]^2}. \tag{6.51}$$

While necessary, this alteration is somewhat ad hoc, and we should attempt to justify it. One way to do this is to note that in the absence of the widths, the propagators are equal to

$$\frac{1}{p^2-m^2+\mathrm{i}\epsilon} = \mathrm{Re}\left(\frac{1}{p^2-m^2+\mathrm{i}\epsilon}\right) - \mathrm{i}\pi\delta(p^2-m^2). \tag{6.52}$$

The imaginary part corresponds to an on-shell cut, and since all further cuts in combination with (b) and (d) are zero (see Table 6.1), it vanishes, allowing us to replace each propagator with its real part. Unfortunately, this argument does not straightforwardly carry over to the resummed propagators since their imaginary parts have support at more than just $p^2 = m^2$. This being the case, the correct approach is to resolve the cuts *before* resumming the Dyson series, treating each self-energy insertion as a higher-order loop correction to be cut through in accordance with the Cutkosky or holomorphic cutting rules; see Refs. [342; 360].

In any case, we will soon see that Eq. (6.51) is of the exact same form as cut (d) in the three-body decay, meaning they will cancel against each other in the Boltzmann equation Eq. (6.27). This spares us from needing to evaluate it.

6.B.2 $h^- \to e\bar{L}\bar{H}$

Common to all cuts for the decay $h^- \to e_\gamma \bar{L}^a_\delta \bar{H}^b_j$ are the coupling constants

$$\mathrm{Im}(c_0^* c_1) = 4\mu_{ij}^*\mu_{kj}\epsilon_{ab}^4\,\mathrm{Im}(f^*_{\alpha\beta}f_{\delta\beta}Y^{i*}_{\gamma\delta}Y^k_{\gamma\alpha}). \tag{6.53}$$

Summing over all indices and flavours but δ gives

$$\mathrm{Im}(c_0^* c_1) \to \sum_{i,k} 8(\mu\mu^\dagger)_{ki}\,\mathrm{Im}(Y_i^\dagger Y_k f^\dagger f)_{\delta\delta}, \tag{6.54}$$

which is of the exact same form as the couplings entering the $h^- \to LL$ asymmetries, Eq. (6.44), upon relabelling $\delta \to \alpha$, $i \to j$, and $k \to i$. Note that $\mathrm{Im}(c_0^* c_1) \to 0$ when all indices but γ are summed over, meaning that this decay does not generate any asymmetries in the number of e_γ particles.

6.B.2.1 Cut (d)

Though our alphabetical sensibilities compel us to first study cut (c), let us discuss cut (d) in order to relieve the suspense of the promised cancellation against cut (b) of the two-body decay. This cut reads

$$h^- \to L^a_\alpha(\mathbf{p}_1) L^b_\beta(\mathbf{p}_1) \to e_\gamma(\mathbf{k}_1)\bar{L}^a_\delta(\mathbf{k}_2)\bar{H}^b_j(\mathbf{k}_3), \tag{6.55}$$

and for it we find

$$\begin{aligned} 2\,\mathrm{Im}(\mathcal{A}_0^*\mathcal{A}_1)_{(\mathrm{d})} = &-\int \mathrm{d}\Pi(p_1,p_2)\,\frac{\mathrm{Tr}\left[\not{p}_1\not{k}_1\not{k}_2\not{p}_2 P_L\right]}{(p_2-k_2)^2-m_h^2} \\ &\times \frac{(k_1+k_2)^2-m_{H_i}^2}{[(k_1+k_2)^2-m_{H_i}^2]^2+[m_{H_i}\Gamma_{H_i}]^2}\,\frac{(p_1-k_1)^2-m_{H_k}^2}{[(p_1-k_1)^2-m_{H_k}^2]^2+[m_{H_k}\Gamma_{H_k}]^2}, \end{aligned} \tag{6.56}$$

where the relevant diagram is very similar to the one in Fig. 6.9, and as before we take the real parts of the resummed propagators. The integrand is exactly the same as that of Eq. (6.51); the only difference here is that we are integrating over the phase space of (p_1, p_2) instead of (k_1, k_2, k_3). When computing the decay rate asymmetry this difference disappears, as we must integrate over both phase spaces. Altogether, we then have

$$\Delta\Gamma(h^- \to e\bar{L}_\alpha\bar{H})_{(\mathrm{d})} = \frac{1}{2m_h}\int \mathrm{d}\Pi_f\,(-4)\,\mathrm{Im}(c_0^* c_1)\,\mathrm{Im}(\mathcal{A}_0^*\mathcal{A}_1)_{(\mathrm{d})} \tag{6.57}$$

$$= \sum_{i,k} 8 \frac{(\mu\mu^\dagger)_{ki}}{m_h} \operatorname{Im}(Y_i^\dagger Y_k f^\dagger f)_{\alpha\alpha} \int \mathrm{d}\Pi(p_1,p_2)\,\mathrm{d}\Pi(k_1,k_2,k_3)\, \frac{\operatorname{Tr}\left[\not{p}_1 \not{k}_1 \not{k}_2 \not{p}_2 P_L\right]}{(p_2-k_2)^2 - m_h^2} \tag{6.58}$$

$$\times \frac{(k_1+k_2)^2 - m_{H_i}^2}{[(k_1+k_2)^2 - m_{H_i}^2]^2 + [m_{H_i}\Gamma_{H_i}]^2} \frac{(p_1-k_1)^2 - m_{H_k}^2}{[(p_1-k_1)^2 - m_{H_k}^2]^2 + [m_{H_k}\Gamma_{H_k}]^2}$$

$$= \Delta\Gamma(h^- \to L_\alpha L)_{(\mathrm{b})}, \tag{6.59}$$

where I use the absence of an index to indicate that it has been summed over. Since these two cuts enter the Boltzmann equation Eq. (6.27) with opposite signs, they therefore cancel against each other.

It is worth commenting on the consistency of this finding with the requirement that the asymmetry from $h^- \to e\bar{L}\bar{H} \to LL$ and $h^- \to LL \to e\bar{L}\bar{H}$ should cancel when *summed*, per the discussion following Eq. (5.61) in Chapter 5. The resolution to this apparent inconsistency is found in noting that we have summed over different flavour indices in the two decays, and that the asymmetries do in fact cancel when summed if we consider a fixed selection of flavours. Using the notation $\Delta\Gamma(i \to k \to f)$ to denote the asymmetry in $\Gamma(i \to f)$ due to the cut $i \to k \to f$, we can see from Eqs. (6.42) and (6.53) that[10]

$$\Delta\Gamma(h^- \to e_\gamma \bar{L}^a_\delta \bar{H}^b_j \to L^a_\alpha L^b_\beta) \propto 4\epsilon^4_{ab} \operatorname{Im}(\mu_{ij}\mu^*_{kj} f_{\alpha\beta} f^*_{\delta\beta} Y^i_{\gamma\delta} Y^{k*}_{\gamma\alpha}) \quad \text{and} \tag{6.60a}$$

$$\Delta\Gamma(h^- \to L^a_\alpha L^b_\beta \to e_\gamma \bar{L}^a_\delta \bar{H}^b_j) \propto 4\epsilon^4_{ab} \operatorname{Im}(\mu^*_{ij}\mu_{kj} f^*_{\alpha\beta} f_{\delta\beta} Y^{i*}_{\gamma\delta} Y^k_{\gamma\alpha}) \tag{6.60b}$$

(where I have elided the identical $\operatorname{Im}(\mathcal{A}_0^*\mathcal{A}_1)$ factors, and for maximum transparency dropped the assumption that μ is real), from which we can immediately read off

$$\Delta\Gamma(h^- \to e_\gamma \bar{L}^a_\delta \bar{H}^b_j \to L^a_\alpha L^b_\beta) + \Delta\Gamma(h^- \to L^a_\alpha L^b_\beta \to e_\gamma \bar{L}^a_\delta \bar{H}^b_j) = 0. \tag{6.61}$$

6.B.2.2 Cut (c)

For this cut,

[10] The $+(\alpha \leftrightarrow \beta, a \leftrightarrow b)$ term in Eq. (6.42) does not contribute here since the three-body cut fixes the indices of all the couplings – see Fig. 6.2 to convince yourself of this.

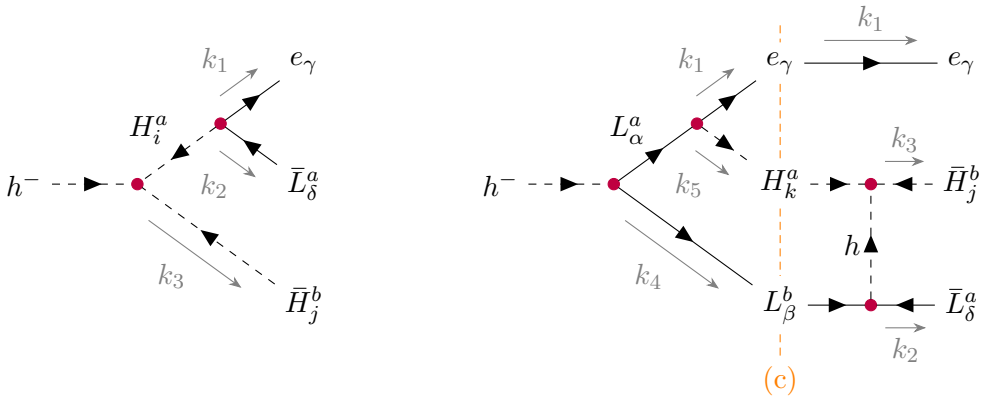

(a) Tree-level. (b) Loop-level, with the three-body cut (c).

Figure 6.10: Diagrams for the three-body decay $h^- \to e\bar{L}\bar{H}$.

$$h^- \to e_\gamma(\mathbf{k}_1) L_\beta^b(\mathbf{k}_4) H_k^a(\mathbf{k}_5) \to e_\gamma(\mathbf{k}_1) \bar{L}_\delta^a(\mathbf{k}_2) \bar{H}_j^b(\mathbf{k}_3), \tag{6.62}$$

which is illustrated in Fig. 6.10b, one finds

$$\begin{aligned} 2\,\mathrm{Im}(\mathcal{A}_0^* \mathcal{A}_1)_{(\mathrm{c})} = -\int \mathrm{d}\Pi(k_4, k_5)\, \frac{\mathrm{Tr}[(\not{k}_1 + \not{k}_5)\not{k}_4 \not{k}_2 \not{k}_1 P_L]}{(k_3 - k_5)^2 - m_h^2} \\ \times \frac{(k_1 + k_2)^2 - m_{H_i}^2}{[(k_1 + k_2)^2 - m_{H_i}^2]^2 + [m_{H_i}\Gamma_{H_i}]^2} \frac{1}{(k_1 + k_5)^2 - m_{L_\alpha}^2}. \end{aligned} \tag{6.63}$$

This must be evaluated numerically, and doing so leads to Fig. 6.11, where the result of this cut is plotted alongside the result of cut (a) in the two-body decay. We are interested in the asymptotic value at large z, which is about 0.17 times as large as cut (a), and of opposite sign (though the plot doesn't show the sign). As the drop at low z is unphysical, we can for our purposes treat this cut as constant and equal to

$$\begin{aligned} \Delta\Gamma(h^- \to e\bar{L}_\alpha \bar{H})_{(\mathrm{c})} &\approx -0.17 \times \Delta\Gamma(h^- \to L_\alpha L)_{(\mathrm{a})} \\ &= -0.17 \frac{\pi^2 - (\ln 4)^2}{512\pi^4} \frac{\mu^2}{m_h} \sum_i \mathrm{Im}(Y_i^\dagger Y_i f^\dagger f)_{\alpha\alpha}. \end{aligned} \tag{6.64}$$

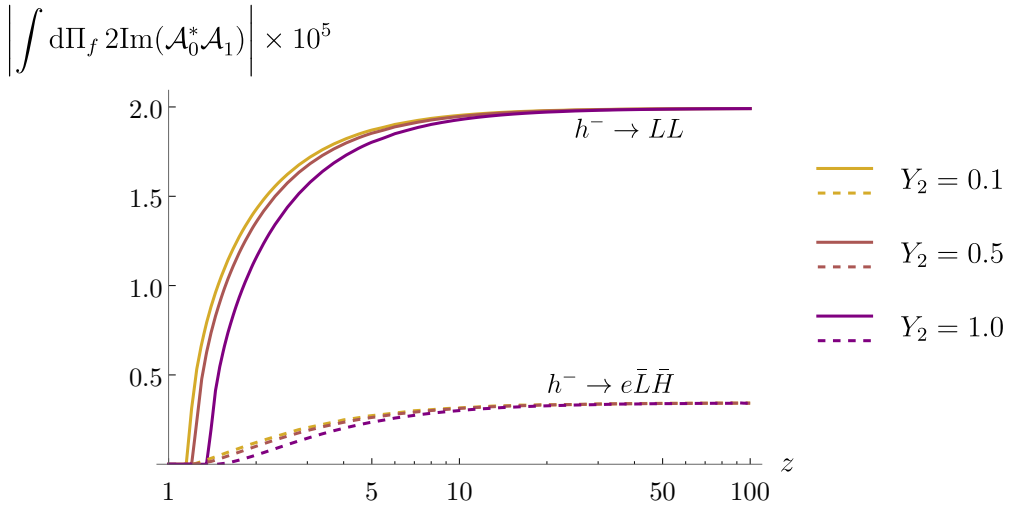

Figure 6.11: A plot illustrating the size of cut (a) in $h^- \to LL$ (solid lines) and cut (c) in $h^- \to e\bar{L}\bar{H}$ (dashed lines) as a function of $z = m_h/T$, given the benchmark values $\lambda_1 = \lambda_2 = 0.1$ and $\lambda_3 = \lambda_4 = 0$, and assuming for simplicity that Y_2 is proportional to the identity matrix with entries $Y_2 = \{0.1, 0.5, 1.0\}$. For consistency, cut (a) has also been evaluated with the appropriate thermal masses; note that at large z it approaches the zero-temperature value $\frac{\pi^2-(\ln 4)^2}{(8\pi)^4} \approx 2 \times 10^{-5}$. The drop as $z \to 1$, due to the final state masses growing comparable to m_h, is an unphysical feature which would not appear if we also accounted for the thermal contributions to the mass of h^-.

6.C The Explicit Boltzmann Equations

To translate the Boltzmann equations in Section 6.2.3 to their explicit functional forms one would need to trawl both through this chapter and the previous one in search of all the relevant formulas. This is not anyone's idea of fun, and while I imagine most readers are not too interested in these forms anyway, I will nevertheless present them here in service of the subset that is (which includes me).

Our Boltzmann equations are

$$sz\mathcal{H}\frac{\mathrm{d}Y_{\Delta_\alpha}}{\mathrm{d}z} = -\frac{1}{2}\sum_\beta \gamma_{D,\alpha\beta}\left[\varepsilon_\alpha\left(\frac{Y_{\Sigma h}}{Y_h^{\mathrm{eq}}} - 2\right) + \frac{Y_{\Delta h}}{Y_h^{\mathrm{eq}}} - \frac{Y_{\Delta L_\alpha} + Y_{\Delta L_\beta}}{Y_L^{\mathrm{nor}}}\right], \tag{6.65a}$$

$$sz\mathcal{H}\frac{\mathrm{d}Y_{\Sigma h}}{\mathrm{d}z} = -\frac{1}{4}\left(\sum_{\alpha,\beta}\gamma_{D,\alpha\beta} + \sum_{i,j}\gamma_{D,ij}\right)\left(\frac{Y_{\Sigma h}}{Y_h^{\mathrm{eq}}} - 2\right) - \gamma_S\left(\frac{Y_{\Sigma h}^2}{4(Y_h^{\mathrm{eq}})^2} - 1\right), \text{ and} \tag{6.65b}$$

$$sz\mathcal{H}\frac{\mathrm{d}Y_{\Delta h}}{\mathrm{d}z} = -\frac{1}{4}\sum_{\alpha,\beta}\gamma_{D,\alpha\beta}\left(\frac{Y_{\Delta h}}{Y_h^{\mathrm{eq}}} - \frac{Y_{\Delta L_\alpha} + Y_{\Delta L_\beta}}{Y_L^{\mathrm{nor}}}\right) - \frac{1}{4}\sum_{i,j}\gamma_{D,ij}\left(\frac{Y_{\Delta h}}{Y_h^{\mathrm{eq}}} - \frac{2Y_{\Delta H}}{Y_H^{\mathrm{nor}}}\right), \tag{6.65c}$$

where

$$sz\mathcal{H} = \frac{4\pi^{7/2}}{135\sqrt{5}z^4}g_\star^{3/2}\frac{m_h^5}{M_{\mathrm{P}}}, \tag{6.66a}$$

$$Y_h^{\mathrm{eq}} = \frac{45}{4\pi^4 g_\star}z^2K_2(z), \qquad Y_L^{\mathrm{nor}} = \frac{15}{4\pi^2 g_\star}, \qquad Y_H^{\mathrm{nor}} = \frac{15}{2\pi^2 g_\star}, \tag{6.66b}$$

$$\gamma_{D,\alpha\beta} \equiv \Sigma\gamma(h^- \to L_\alpha L_\beta) = \frac{m_h^4}{8\pi^3 z}K_1(z)4|f_{\alpha\beta}|^2, \tag{6.66c}$$

$$\gamma_{D,ij} \equiv \Sigma\gamma(h^- \to \bar{H}_i\bar{H}_j) = \frac{m_h^4}{8\pi^3 z}K_1(z)\frac{|\mu_{ij}|^2}{m_h^2}, \tag{6.66d}$$

$$\gamma_S = \frac{m_h^4}{8\pi^3 z}\int_4^\infty \mathrm{d}x\,\sqrt{x}K_1(z\sqrt{x})\Big[\hat{\gamma}_{hh\to BB}(x) + \hat{\gamma}_{hh\to f\bar{f}}(x) + \hat{\gamma}_{hh\to H\bar{H}}(x)\Big], \tag{6.66e}$$

$$\varepsilon_\alpha = 1.17\frac{\pi^2 - (\ln 4)^2}{512\pi^3}\sum_{i,j}\frac{(\mu\mu^T)_{ij}}{m_h^2}\frac{\mathrm{Im}(Y_j^\dagger Y_i f^\dagger f)_{\alpha\alpha}}{(f^\dagger f)_{\alpha\alpha}}, \tag{6.66f}$$

with $g_\star = 106.75 + 4(n_H - 1)$, n_H being the number of Higgs doublets, and

$$\hat{\gamma}_{hh\to BB}(x) = \frac{g_1^4}{16\pi^2}\frac{(x+4)\sqrt{x-4}}{x^{3/2}} + \frac{g_1^4}{4\pi^2}\frac{x-2}{x^2}\ln\left(\frac{1-\sqrt{1-4/x}}{1+\sqrt{1-4/x}}\right), \tag{6.67a}$$

$$\hat{\gamma}_{hh\to f\bar{f}}(x) = \frac{10g_1^4}{96\pi^2}\left(\frac{x-4}{x}\right)^{3/2}, \quad \text{and} \tag{6.67b}$$

$$\hat{\gamma}_{hh\to H\bar{H}}(x) = \frac{g_1^4}{768\pi^2}\left(\frac{x-4}{x}\right)^{3/2}n_H. \tag{6.67c}$$

Included in $\hat{\gamma}_{hh\to f\bar{f}}$ is a factor of $\sum_f g_f Y_f^2 = 10$ from summing over the contribution of all SM fermions. Accounting for spectator processes, we have

$$\begin{pmatrix} Y_{\Delta L_1} \\ Y_{\Delta L_2} \\ Y_{\Delta L_3} \end{pmatrix} = \frac{2}{2637}\begin{pmatrix} -847 & 32 & 32 \\ 32 & -847 & 32 \\ 32 & 32 & -847 \end{pmatrix}\begin{pmatrix} Y_{\Delta_1} \\ Y_{\Delta_2} \\ Y_{\Delta_3} \end{pmatrix} \quad \text{and} \tag{6.68a}$$

$$Y_{\Delta H} = -\frac{224}{293}(Y_{\Delta_1} + Y_{\Delta_2} + Y_{\Delta_3}), \tag{6.68b}$$

when $n_H = 2$, while for $n_H = 3$ it is instead the case that

$$\begin{pmatrix} Y_{\Delta L_1} \\ Y_{\Delta L_2} \\ Y_{\Delta L_3} \end{pmatrix} = \frac{1}{144} \begin{pmatrix} -91 & 5 & 5 \\ 5 & -91 & 5 \\ 5 & 5 & -91 \end{pmatrix} \begin{pmatrix} Y_{\Delta_1} \\ Y_{\Delta_2} \\ Y_{\Delta_3} \end{pmatrix} \quad \text{and} \tag{6.69a}$$

$$Y_{\Delta H} = -\frac{7}{8}(Y_{\Delta_1} + Y_{\Delta_2} + Y_{\Delta_3}). \tag{6.69b}$$

These relations hold assuming $T \sim 10^{12}\,\text{GeV}$, and should strictly speaking vary continuously as we sweep through the relevant temperature region given by $z \in [10^{-1}, 10^{2}]$ due to more spectator processes entering equilibrium; see Ref. [409, Sec. III.A]. This will be accounted for in the final version of this work.

We should take the divergence and push it somewhere else!

Patrick Star,
in *Spongebob Squarepants*,
reimagined

7

IR Divergences in the Zee Model

Contents

7.1 What is an IR Divergence? **178**

7.2 Zero Temperature Cancellation **185**

7.3 Finite Temperature Cancellation – a Discussion **194**

7.A Regulator Independence of the Final State Sum **199**

In the previous chapter we encountered the infrared (IR) divergent decay $h^- \to e\bar{L}\bar{H}$, pictured in Fig. 7.1, which appeared both as an isolated process and as a subprocess in our Cutkosky cuts. There we regulated the divergence, due to the virtual H going on shell, by introducing thermal masses to e, L, and the H's. In the case that $m_H < m_e + m_L$, it became kinematically impossible for H to go on shell, whereas when $m_H > m_e + m_L$ the

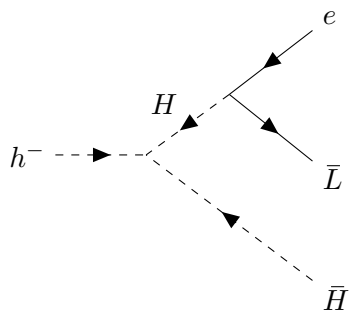

Figure 7.1: The IR-divergent decay $h^- \to e\bar{L}\bar{H}$ in the Zee model.

H acquired a decay width, which when added to its propagator,

$$\frac{\mathrm{i}}{p^2 - m^2} \to \frac{\mathrm{i}}{p^2 - m^2 + \mathrm{i}m\Gamma}, \tag{7.1}$$

prevented it from diverging when $p^2 = m^2$.

However, this is an unsatisfying solution. Though the divergence has formally been removed, its spectre remains in the form of large logarithms such as $\ln(m_e/m_h)$, which threaten perturbativity. To banish this threat we should study how to cancel the divergence properly. As guaranteed by the KLN theorem [109; 110], other processes which add to the decay will generate a logarithm with the opposite sign, resulting in a well-behaved sum. Our task, therefore, is to find these processes and evaluate them.

In this chapter I will chronicle my efforts in this direction in the hope that they may be put to use in future works. We will find that we are able to eliminate the divergence at zero temperature, but encounter difficulties at finite temperature preventing us from carrying the analysis over. The entirety of this chapter is my own work, and I will provide detailed computations here, as they are often skipped over in the literature.

7.1 What is an IR Divergence?

In case you are unfamiliar with IR divergences, allow me to briefly review them. As the name suggests, these divergences are associated with low energies, and they tend to appear

in theories with massless particles, or in high energy limits where the masses of particles can be neglected.

To be concrete, let's assign the momentum labels q and p to the outgoing e and $\bar{L}$ of the three-body decay, so that the H propagator appears as

$$\frac{1}{(q+p)^2} = \frac{1}{2q\cdot p} = \frac{1}{2E_qE_p(1-\cos\theta)}. \tag{7.2}$$

This blows up when either $E_q = 0$, $E_p = 0$, or $\cos\theta = 1$. When the energy of a particle is zero it is called 'soft', and the divergence a **soft divergence**. When $\cos\theta = 1$ the two particles are travelling in the same direction and the divergence is termed a **collinear divergence**.

There are a few ways to regulate an IR divergence, and I will demonstrate two: using a mass regulator, and dimensional regularisation. It is also possible to regulate by considering a finite energy window $E_q, E_p > E_0$ and finite angular window $\theta > \theta_0$, though this is of less interest to us.

Example

Let's first try using a mass regulator. This functions intuitively – by reintroducing a small mass to one or both of e and $\bar{L}$, it becomes kinematically impossible for the virtual H to go on shell, and the divergence is avoided. Because it is simpler to compute, I'll elect to assign a mass m_e to e only.

Here the matrix element for the decay is

$$\mathrm{i}\mathcal{M} = \quad = (-\mathrm{i}\mu)\frac{\mathrm{i}}{(q+p)^2+\mathrm{i}\epsilon}\overline{v}(\mathbf{p})(-\mathrm{i}Y^*P_R)u(\mathbf{q}), \tag{7.3}$$

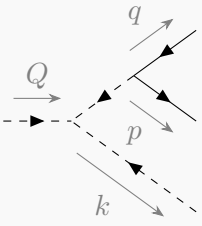

and its spin-summed square is in turn

$$|\mathcal{M}|^2 = \mu^2|Y|^2 \frac{\mathrm{Tr}[\not{p} P_R(\not{q} + m_e) P_L]}{|(q+p)^2 + \mathrm{i}\epsilon|^2} \tag{7.4}$$

$$= \mu^2|Y|^2 \frac{2p\cdot q}{(q+p)^4}, \tag{7.5}$$

where we can drop the $+\mathrm{i}\epsilon$ as the pole of the propagator is never touched in the presence of our regulator. In this chapter I'll suppress all flavour indices, $\mathrm{SU}(2)_\mathrm{W}$ indices, and Higgs indices, as here they are little more than distractions. To be maximally transparent I will not even implicitly sum over these indices, so all processes and diagrams can be understood as involving only a fixed selection of particles. Spins, on the other hand, will be summed over at every available opportunity.

The three-body phase space integral with one massive particle is [122; 422]

$$\int \mathrm{d}\Pi_3 = \frac{m_h^2}{128\pi^3} \int_0^{1-\beta} \mathrm{d}x_k \int_{1-x_k-\beta}^{1-\frac{\beta}{1-x_k}} \mathrm{d}x_p \,, \tag{7.6}$$

where we define the energy fractions $x_i \equiv 2E_i/m_h$ and the squared mass fraction $\beta \equiv m_e^2/m_h^2$. Then, using that

$$m_h^2(1-x_k) = (Q-k)^2 = (q+p)^2 = m_e^2 + 2p\cdot q, \tag{7.7}$$

we may write

$$|\mathcal{M}|^2 = \mu^2|Y|^2 \frac{m_h^2(1-x_k) - m_e^2}{m_h^4(1-x_k)^2} = \frac{\mu^2|Y|^2}{m_h^2} \frac{1-x_k-\beta}{(1-x_k)^2}, \tag{7.8}$$

giving

$$\hat{\Gamma}(h^- \to e\bar{L}\bar{H}) = \int \mathrm{d}\Pi_3 \, |\mathcal{M}|^2 \tag{7.9}$$

$$= \frac{\mu^2|Y|^2}{128\pi^3} \int_0^{1-\beta} \mathrm{d}x_k \int_{1-x_k-\beta}^{1-\frac{\beta}{1-x_k}} \mathrm{d}x_p \, \frac{1-x_k-\beta}{(1-x_k)^2} \tag{7.10}$$

$$= \frac{\mu^2|Y|^2}{128\pi^3} \frac{1}{2} \Big[-5 + 4\beta + \beta^2 - 2(1+2\beta)\ln\beta \Big], \tag{7.11}$$

where to avoid needing to carry around factors of $1/2m_h$ I define the un-normalised

decay rate

$$\hat{\Gamma} \equiv 2m_h\Gamma = \int \mathrm{d}\Pi_f \, |\mathcal{M}|^2. \tag{7.12}$$

Expanding in small β, we find at the lowest order

$$\hat{\Gamma}(h^- \to e\bar{L}\bar{H}) = \frac{\mu^2|Y|^2}{128\pi^3}\left(-\frac{5}{2} - \ln\frac{m_e^2}{m_h^2}\right). \tag{7.13}$$

The divergence manifests in the logarithm, which blows up as we take $m_e \to 0$.

We may alternatively regulate the divergence using the technique of dimensional regularisation, whereby IR divergences are tamed by moving to a *higher*-dimensional space, $d = 4 + \epsilon$.

Example

In d dimensions the massless three-body phase space takes the form [423]

$$\begin{aligned}\int \mathrm{d}\Pi_3 &= \int [\mathrm{d}q][\mathrm{d}p][\mathrm{d}k](2\pi)^d\delta^{(d)}(Q-q-p-k) \\ &= \frac{(m_h^2)^{d-3}}{2(4\pi)^{d-1}\Gamma(d-2)}\int_0^1 x^{d-3}(1-x)^{(d-4)/2}\,\mathrm{d}x\int_0^1 y^{(d-4)/2}(1-y)^{(d-4)/2}\,\mathrm{d}y\,,\end{aligned} \tag{7.14}$$

where the variables x and y are defined such that

$$(p+k)^2 = m_h^2 xy, \tag{7.15a}$$
$$(q+k)^2 = m_h^2(1-x), \quad \text{and} \tag{7.15b}$$
$$(q+p)^2 = m_h^2 x(1-y). \tag{7.15c}$$

As μ and Y have the mass dimensions

$$[\mu] = 1 + \frac{4-d}{2} \quad \text{and} \quad [Y] = \frac{4-d}{2}, \tag{7.16}$$

away from $d = 4$ we must also make the replacements

$$\mu^2 \to \mu^2\left(\tilde{\mu}^2\frac{e^{\gamma_E}}{4\pi}\right)^{(4-d)/2} \quad \text{and} \quad |Y|^2 \to |Y|^2\left(\tilde{\mu}^2\frac{e^{\gamma_E}}{4\pi}\right)^{(4-d)/2}, \tag{7.17}$$

where $\widetilde{\mu}$ is a new dimensionful scale and the other factors, including the Euler-Mascheroni constant $\gamma_E \approx 0.577$, are an $\overline{\text{MS}}$-styled convenience. Ignoring for now the iϵ in the propagator (which is not justified – see Section 7.A), we then have

$$|\mathcal{M}|^2 = \mu^2|Y|^2\frac{2p\cdot q}{(q+p)^4} \to \mu^2|Y|^2\left(\widetilde{\mu}^2\frac{e^{\gamma_E}}{4\pi}\right)^{4-d}\frac{1}{m_h^2 x(1-y)}, \tag{7.18}$$

and

$$\hat{\Gamma} = \mu^2|Y|^2\left(\widetilde{\mu}^2\frac{e^{\gamma_E}}{4\pi}\right)^{4-d}\int \mathrm{d}\Pi_3\,\frac{1}{m_h^2 x(1-y)} \tag{7.19}$$

$$= \mu^2|Y|^2\left(\widetilde{\mu}^2\frac{e^{\gamma_E}}{4\pi}\right)^{4-d}\frac{(m_h^2)^{d-4}}{2(4\pi)^{d-1}\Gamma(d-2)}\frac{\Gamma(\frac{d-4}{2})\Gamma(\frac{d-2}{2})^2}{\Gamma(\frac{3d-8}{2})} \tag{7.20}$$

$$= \frac{\mu^2|Y|^2}{128\pi^3}\left(\frac{2}{\epsilon} - 5 - 2\ln\frac{\widetilde{\mu}^2}{m_h^2}\right), \tag{7.21}$$

where the divergence manifests in the form of the $\frac{1}{\epsilon}$ term. For reasons discussed in Section 7.A, this form of the divergence is not very useful to us, and so I will use the mass regulator for the remainder of this chapter.

One might be tempted to compare IR divergences with ultraviolet (UV) divergences, but they could not be any more different. The latter emerge from the momenta of virtual particles in loops being allowed to run to infinity, and are an unphysical artefact of working with bare fields and couplings instead of renormalized ones.[1] IR divergences, on the other hand, are a result of the fact that it is difficult to define asymptotic states for theories with massless particles, in the sense that a naïvely-defined single particle state may not be physical [111; 426–428]. In view of this, these divergences are cured not with renormalization, but by considering multiple processes together, whereby physically sensible states are found in their sum. To borrow a textbook example, the scatterings $e^+e^- \to \mu^+\mu^-$ and $e^+e^- \to \mu^+\mu^-\gamma$ are both IR divergent at $\mathcal{O}(e^6)$, but finite when summed together [122]:

[1] More rigorously, UV divergences arise because the product of distributions such as $\frac{1}{p^2-m^2+\mathrm{i}\epsilon}\frac{1}{q^2-m^2+\mathrm{i}\epsilon}$ is ill-defined. In this view, the procedure of renormalization and the choice of counterterms in fact amount to a choice of definition of this product [424; 425].

$$\sigma(e^+e^- \to \mu^+\mu^-) + \sigma(e^+e^- \to \mu^+\mu^-\gamma) = \text{finite}. \tag{7.22}$$

The implication of this is that the final states $\mu^+\mu^-$ and $\mu^+\mu^-\gamma$ only make sense when considered together. Sometimes this is phrased in terms of distinguishability, where we might say that a free muon is indistinguishable from one accompanied by one or more soft photons. This isn't too difficult to believe, as muons, being charged particles, carry at all times a photon cloud.

To cancel a given IR divergence it is therefore necessary to consider a sufficiently inclusive set of processes. Our ability to do so is guaranteed by the **Kinoshita–Lee–Nauenberg** (KLN) **theorem** [109; 110] (or rather, the stronger version formulated in Ref. [111]), which states that for a fixed initial state i we will obtain an IR-finite result when summing over all possible final states, and vice-versa:

$$\sum_f \sigma(i \to f) = \text{finite} \quad \text{and} \quad \sum_i \sigma(i \to f) = \text{finite}. \tag{7.23}$$

The proof is rather straightforward to sketch, and follows entirely from unitarity of the S-matrix:

$$\begin{aligned} \sum_f \sigma(i \to f) &\propto \sum_f |\, \langle f|S|i\rangle \,|^2 \\ &= \sum_f \langle i|S|f\rangle\langle f|S^\dagger|i\rangle \\ &= \langle i|SS^\dagger|i\rangle \\ &= \langle i|i\rangle\,, \end{aligned} \tag{7.24}$$

which is finite up to a normalisation of the states. The proof for the initial state sum is identical. The authors of Ref. [111] emphasise that the final state sum *must* include the initial state i for the resolution of the identity to succeed, which means there may be some situations where it is necessary to include the forward scattering $i \to i$ to achieve infrared finiteness. I will return to this point when it becomes relevant to us.

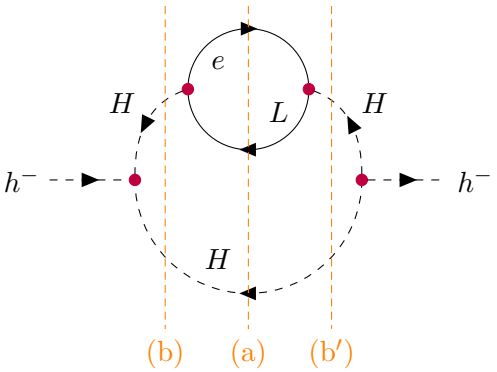

Figure 7.2: The $h^- \to h^-$ forward diagram and its final state cuts.

Practically speaking, it is of course infeasible to sum over *all* possible initial or final states. At a fixed perturbative order, however, there are only finitely many processes available, and it turns out that we may easily enumerate them by cutting through an $i \to i$ (or $f \to f$) diagram. This is best illustrated with an example, so let's apply this discussion to our three-body decay.

Consider the diagram in Fig. 7.2, constructed by taking the three-body decay, mirroring it across (a), and joining it with its reflection. This construction ensures two things. The first is that by cutting through (a) we recover the three-body decay, with the two sides of the cut corresponding to $\mathcal{M}(h^- \to e\bar{L}\bar{H})$ and its conjugate, so that (up to factors of i)

$$\mathcal{M}(h^- \to h^-)_{\text{cut (a)}} = \mathcal{M}\mathcal{M}^* = |\mathcal{M}|^2. \tag{7.25}$$

The second is that any other cut will necessarily be of the same order in the coupling constants. Here there are only two other cuts, (b) and (b′), both of which share the final state $\bar{H}\bar{H}$. This suggests that at $\mathcal{O}(\mu^2|Y|^2)$ we should expect to find

$$\Gamma(h^- \to e\bar{L}\bar{H}) + \Gamma(h^- \to \bar{H}\bar{H}) = \text{finite}. \tag{7.26}$$

This is indeed the case, which I will now demonstrate.

7.2 Zero Temperature Cancellation

7.2.1 Final State Sum

Let us evaluate the contribution to $h^- \to \bar{H}\bar{H}$ as given by the cuts (b) and (b′) in Fig. 7.2. Together these cuts proffer the interference between the tree-level amplitude and a loop correction, viz.

$$|\mathcal{M}_0 + \mathcal{M}_1|^2 = |\mathcal{M}_0|^2 + \underbrace{\mathcal{M}_0^*\mathcal{M}_1 + \mathcal{M}_0\mathcal{M}_1^*}_{|\mathcal{M}|^2_{\text{loop}}} + |\mathcal{M}_1|^2, \tag{7.27}$$

with

$|\mathcal{M}|^2_{\text{loop}} =$ 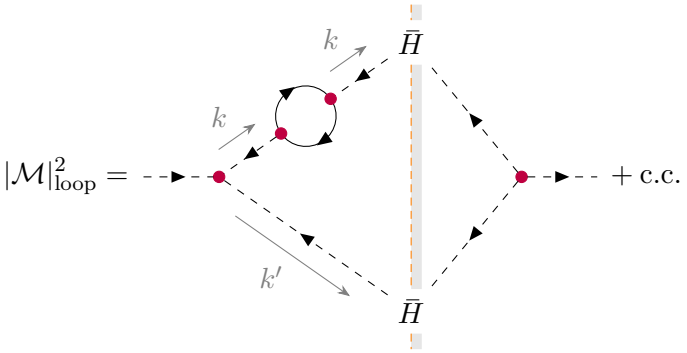

$+ \text{c.c.}$ (7.28)

$$= \mu^2 \frac{\mathrm{i}}{k^2 + \mathrm{i}\epsilon} \mathrm{i}\Sigma(k^2) + \text{c.c.} \tag{7.29}$$

$$= -\mu^2 \Sigma(k^2) \left(\frac{1}{k^2 + \mathrm{i}\epsilon} + \text{c.c.} \right), \tag{7.30}$$

where I have added a shadow to one side of the cut to indicate that it is conjugated. Explicitly, the self energy is

$$\mathrm{i}\Sigma(k^2) = (-1)|Y|^2 \int \frac{\mathrm{d}^4 q}{(2\pi)^4} \frac{\mathrm{Tr}[\not{q}(\not{q} - \not{k})P_R]}{[q^2 - m_e^2 + \mathrm{i}\epsilon][(q-k)^2 + \mathrm{i}\epsilon]}, \tag{7.31}$$

and it is UV divergent, requiring a renormalization of both the Higgs field and its mass. We retain the electron mass m_e as an IR regulator, and with it the self energy is purely real.

This loop diagram is unusual, as we are taught that self energy corrections to external particles are always amputated. As if to remind us why this is so, the virtual $\bar{H}$ is automatically on shell, making the $\frac{1}{k^2}$ propagator a menacing presence. Nevertheless, the diagram's inclusion is vital in obtaining an IR-finite result; we must simply treat the propagator with the respect it deserves – that is, as a distribution. This is a delicate procedure, and so I'll carefully walk us through all the steps in evaluating it.

Step 1: The first of these steps is to write out the quantity of interest—the (hatted) decay rate—in full:

$$\begin{aligned}\hat{\Gamma}(h^- \to \bar{H}\bar{H})_{\text{loop}} &= \int \mathrm{d}\Pi_2 \, |\mathcal{M}|^2_{\text{loop}} \\ &= \int \frac{\mathrm{d}^4k}{(2\pi)^4}\frac{\mathrm{d}^4k'}{(2\pi)^4} 2\pi\delta(k^2)\theta(k_0)2\pi\delta(k'^2)\theta(k'_0)(2\pi)^4\delta^{(4)}(Q-k-k')|\mathcal{M}|^2_{\text{loop}}.\end{aligned} \tag{7.32}$$

With this we can immediately identify the on-shell delta function $\delta(k^2)$ as the source of our angst. Fortunately, we are saved by the distributional identity[2] [111; 360]

$$\delta(k^2)\left(\frac{1}{k^2+\mathrm{i}\epsilon}+\text{c.c.}\right) = -\frac{\partial}{\partial k^2}\delta(k^2) = -\delta'(k^2), \tag{7.33}$$

and so

$$\hat{\Gamma}_{\text{loop}} = -\mu^2 \int \frac{\mathrm{d}^4k}{(2\pi)^4}\frac{\mathrm{d}^4k'}{(2\pi)^4} 2\pi\Big[-\delta'(k^2)\Big]\theta(k_0)2\pi\delta(k'^2)\theta(k'^0)(2\pi)^4\delta^{(4)}(Q-k-k')\Sigma(k^2), \tag{7.34}$$

where I highlight this new distribution with magenta colouring. To handle the derivative we must integrate by parts – however, doing so now is unhelpful since the derivative will hit the other delta functions. We should resolve them first.

[2] An easy way to convince oneself of this identity is to recall

$$2\pi\delta(x) = -2\,\mathrm{Im}\left(\frac{1}{x+\mathrm{i}\epsilon}\right) = \frac{\mathrm{i}}{x+\mathrm{i}\epsilon} - \frac{\mathrm{i}}{x-\mathrm{i}\epsilon},$$

from which it is straightforward to see that

$$2\pi\delta(x)\left(\frac{1}{x+\mathrm{i}\epsilon}+\text{c.c.}\right) = \frac{\mathrm{i}}{(x+\mathrm{i}\epsilon)^2} - \frac{\mathrm{i}}{(x-\mathrm{i}\epsilon)^2} = -2\pi\delta'(x).$$

Step 2: Resolving the four-momentum-conserving delta function eliminates the integral over k', giving

$$\hat{\Gamma}_{\text{loop}} = -\mu^2 \int \frac{\mathrm{d}^4 k}{(2\pi)^4} 2\pi \Big[-\delta'(k^2)\Big] \theta(k_0) 2\pi\delta((Q-k)^2)\theta(Q_0 - k_0)\mu^2\Sigma(k^2) \tag{7.35}$$

$$= -\frac{\mu^2}{\pi} \int \mathrm{d}k_0\, \mathrm{d}|\mathbf{k}|\, |\mathbf{k}|^2 \Big[-\delta'(k^2)\Big] \theta(k_0)\delta((m_h - k_0)^2 - |\mathbf{k}|^2)\theta(m_h - k_0)\Sigma(k^2), \tag{7.36}$$

where it is convenient to proceed in the rest frame of h^-, with $Q = (m_h, 0, 0, 0)$. The remaining delta function may be used to eliminate either k_0 or $|\mathbf{k}|$. Arbitrarily choosing $|\mathbf{k}|$, we write

$$\delta((m_h - k_0)^2 - |\mathbf{k}|^2) = \frac{\delta(|\mathbf{k}| - (m_h - k_0))}{2(m_h - k_0)} \tag{7.37}$$

(the negative root is outside the integration region as enforced by the step functions), and

$$\hat{\Gamma}_{\text{loop}} = -\frac{\mu^2}{2\pi} \int_0^{m_h} \mathrm{d}k_0\, (m_h - k_0) \Big[-\delta'(k^2)\Big] \Sigma(k^2)\Big|_{|\mathbf{k}| = m_h - k_0}. \tag{7.38}$$

Step 3: We are now in a position to handle the $-\delta'(k^2)$. Having set $|\mathbf{k}| = m_h - k_0$ in the previous step, we have $k^2 = 2m_h k_0 - m_h^2$, and so for some test function $f(k_0)$,

$$\int \mathrm{d}k_0\, f(k_0) \Big[-\frac{\partial}{\partial k^2}\delta(k^2)\Big] = \int \mathrm{d}k_0\, f(k_0) \Big[-\frac{1}{2m_h}\frac{\partial}{\partial k_0}\delta(2m_h k_0 - m_h^2)\Big] \tag{7.39}$$

$$= \int \mathrm{d}k_0\, \frac{1}{2m_h}\frac{\partial f}{\partial k_0}\delta(2m_h k_0 - m_h^2) \tag{7.40}$$

$$= \int \mathrm{d}k_0\, \frac{1}{2m_h}\frac{\partial f}{\partial k_0}\frac{\delta(k_0 - \frac{1}{2}m_h)}{2m_h} \tag{7.41}$$

$$= \frac{1}{4m_h^2}\frac{\partial f}{\partial k_0}\Big|_{k_0 = \frac{1}{2}m_h}, \tag{7.42}$$

where in the second line we have integrated by parts. Thus,

$$\hat{\Gamma}_{\text{loop}} = -\frac{\mu^2}{8\pi m_h^2}\frac{\partial}{\partial k_0}\Big[(m_h - k_0)\Sigma(2m_h k_0 - m_h^2)\Big]\Big|_{k_0 = \frac{1}{2}m_h} \tag{7.43}$$

$$= \frac{\mu^2}{8\pi m_h^2}\Big[\Sigma(0) - m_h^2\Sigma'(0)\Big]. \tag{7.44}$$

This is an interesting expression, and we can identify these two terms as representing the

mass correction and LSZ reduction factor encountered in renormalization theory [360]. In the $\overline{\text{MS}}$ scheme the self energy and its derivative are

$$\Sigma(0) = -\frac{|Y|^2}{16\pi^2} 2m_e^2 \left(1 + \ln \frac{\widetilde{\mu}^2}{m_e^2}\right) \to 0 \quad \text{and} \tag{7.45a}$$

$$\Sigma'(0) = \frac{|Y|^2}{16\pi^2} \left(\frac{1}{2} + \ln \frac{\widetilde{\mu}^2}{m_e^2}\right), \tag{7.45b}$$

where $\widetilde{\mu}$ is the same new scale as introduced in Eq. (7.17), and so

$$\hat{\Gamma}(h^- \to \bar{H}\bar{H})_{\text{loop}} = \frac{\mu^2 |Y|^2}{128\pi^3} \left(-\frac{1}{2} - \ln \frac{\widetilde{\mu}^2}{m_e^2}\right). \tag{7.46}$$

Here we see that this loop correction is itself IR divergent, and it is perfectly primed to cancel the divergence in the three-body decay. Indeed, adding this to Eq. (7.13) produces the IR-finite sum

$$\hat{\Gamma}(h^- \to e\bar{L}\bar{H}) + \hat{\Gamma}(h^- \to \bar{H}\bar{H})_{\text{loop}} = \frac{\mu^2 |Y|^2}{128\pi^3} \left(-3 - \ln \frac{\widetilde{\mu}^2}{m_h^2}\right). \tag{7.47}$$

Success! The apparently negative decay rate may be startling, but it should be interpreted as a correction to the leading order two-body rate:

$$\Gamma_{\text{NLO}} = \Gamma_{\text{LO}} \left[1 - \frac{|Y|^2}{16\pi^2} \left(3 + \ln \frac{\widetilde{\mu}^2}{m_h^2}\right)\right], \qquad \Gamma_{\text{LO}} = \frac{1}{2m_h} \frac{\mu^2}{8\pi}. \tag{7.48}$$

7.2.2 Initial State Sum

Our excitement at having successfully cancelled the divergence is swiftly tempered upon realising that while the two-body decay $h^- \to \bar{H}\bar{H}$ enters the Boltzmann equation (BE) for h^-, it does not appear in the BE for e or L, as it features no leptons. Therefore, while it stands a chance of cancelling the divergence within the former, we are forced to consider the initial state sum for the latter ones.

To discover which initial states to use we proceed as before: by constructing a forward

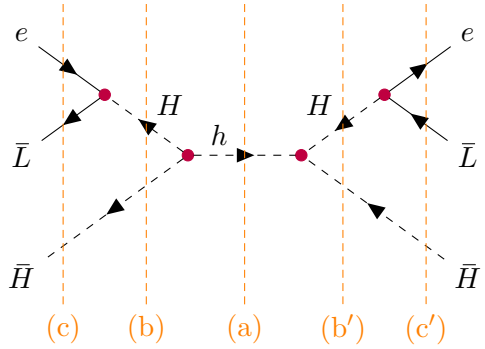

Figure 7.3: The $e\bar{L}\bar{H} \to e\bar{L}\bar{H}$ forward diagram and its initial state cuts, including the forward scattering cuts (c) and (c′).

diagram out of the three-body decay, but this time for $e\bar{L}\bar{H} \to e\bar{L}\bar{H}$. This produces Fig. 7.3, which proposes the initial states h^- and $\bar{H}\bar{H}$. Unfortunately these two alone do not lead to an IR-finite sum,[3] which means that we must also include the forward scattering $e\bar{L}\bar{H} \to e\bar{L}\bar{H}$, suggestively indicated by cuts (c) and (c′). One might object that because the forward scattering doesn't alter any particle numbers, it should not enter the BE. However, as generally argued by Ref. [429], we may treat it as both a production and destruction process, including it twice with opposite signs so that its net contribution is zero. In this light it should be possible to observe the cancellation without it, though we will not pursue this.

For the following discussion it is convenient to work with the 'inverted hat' rates (or cross sections),

$$\check{\Gamma} \text{ or } \check{\sigma} \equiv \int \mathrm{d}\Pi_i \, |\mathcal{M}|^2, \tag{7.49}$$

defined much like the hatted rates $\hat{\Gamma}$ but with an integral over the initial state phase space instead of the final one. In the Boltzmann equation we must of course integrate over both of these phase spaces, but here we only require the initial one to demonstrate IR finiteness.

Now, to accommodate forward scatterings the usual decomposition of the S-matrix into

[3] It would be too much of an unproductive detour to demonstrate this explicitly, so I will decline to do so. Instead, I'll offer a simpler argument for why this is so at the end of this section.

$1 + \mathrm{i}T$ must be superseded with [111]

$$S_{fi} = (2\pi)^4 \delta^{(4)}(p_i - p_f)\mathrm{i}\mathcal{M}_{fi}. \tag{7.50}$$

This allows us to draw the trivial diagram

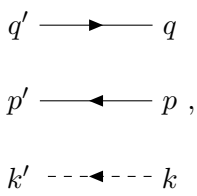

equal at the S-matrix level to

$$\begin{aligned} S_{fi} &= \langle e(\mathbf{q})\bar{L}(\mathbf{p})\bar{H}(\mathbf{k})|e(\mathbf{q}')\bar{L}(\mathbf{p}')\bar{H}(\mathbf{k}')\rangle & (7.51)\\ &= (2\pi)^3 2E_q \delta^{(3)}(\mathbf{q}-\mathbf{q}')(2\pi)^3 2E_p \delta^{(3)}(\mathbf{p}-\mathbf{p}')(2\pi)^3 2E_k \delta^{(3)}(\mathbf{k}-\mathbf{k}'). & (7.52)\end{aligned}$$

Evidently there is no overall four-momentum conserving delta function in Eq. (7.52), so we cannot so easily ascribe a value to this diagram at the $\mathcal{M}$ level. In view of this it is slightly more transparent to write

$$\check{\sigma} = \int [\mathrm{d}P_i] \frac{|S_{fi}|^2}{V_4} = \int [\mathrm{d}q'][\mathrm{d}p'][\mathrm{d}k'] \frac{|S_{fi}|^2}{V_4}, \tag{7.53}$$

where $V_4 = (2\pi)^4 \delta^{(4)}(0)$, instead of Eq. (7.49).

The interference of the trivial diagram with the connected one in Fig. 7.3 is of $\mathcal{O}(\mu^2|Y|^2)$, and is what promises to cancel the IR divergence. The connected diagram gives

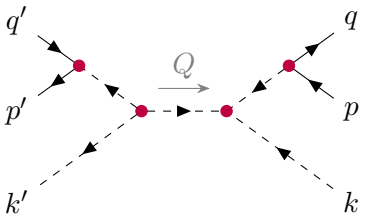

$$\begin{aligned} &= \mu^2 |Y|^2 \frac{\mathrm{i}}{(q'+p')^2 + \mathrm{i}\epsilon} \frac{\mathrm{i}}{Q^2 - m_h^2 + \mathrm{i}\epsilon} \frac{\mathrm{i}}{(q+p)^2 + \mathrm{i}\epsilon}, \quad (7.54)\\ &\quad \times \overline{v}(\mathbf{p}')P_R u(\mathbf{q}')\overline{u}(\mathbf{q})P_L v(\mathbf{p}) \end{aligned}$$

and so the interference between the two, at the S-matrix level, is

$$
\begin{aligned}
|S|^2_{\text{int}} = \Bigg[& \mu^2 |Y|^2 \frac{\mathrm{i}}{(q'+p')^2 + \mathrm{i}\epsilon} \frac{\mathrm{i}}{Q^2 - m_h^2 + \mathrm{i}\epsilon} \frac{\mathrm{i}}{(q+p)^2 + \mathrm{i}\epsilon} + \text{c.c.} \Bigg] \\
& \times \overline{v}(\mathbf{p}') P_R u(\mathbf{q}') \overline{u}(\mathbf{q}) P_L v(\mathbf{p}) \\
& \times (2\pi)^3 2E_q \delta^{(3)}(\mathbf{q} - \mathbf{q}') (2\pi)^3 2E_p \delta^{(3)}(\mathbf{p} - \mathbf{p}') (2\pi)^3 2E_k \delta^{(3)}(\mathbf{k} - \mathbf{k}') \\
& \times (2\pi)^4 \delta^{(4)}(q' + p' + k' - q - p - k).
\end{aligned} \tag{7.55}
$$

In $\check{\sigma}$ the full initial state phase space is wiped out by the delta functions from the trivial diagram, and the four-momentum conserving delta function, which comes from the connected diagram, is reduced to $(2\pi)^4 \delta^{(4)}(0)$ and cancels against the $\frac{1}{V_4}$ in Eq. (7.53). The result is

$$
\check{\sigma}(e\bar{L}\bar{H} \to e\bar{L}\bar{H})_{\text{int}} = \mu^2 |Y|^2 \left(\frac{\mathrm{i}}{(q+p)^2 + \mathrm{i}\epsilon} \right)^2 \frac{\mathrm{i}}{Q^2 - m_h^2 + \mathrm{i}\epsilon} (2q \cdot p) + \text{c.c.}, \tag{7.56}
$$

where I have additionally summed over the spins and taken the resulting trace.[4]

Having understood how the forward scattering contributes, we are now in a position to observe the cancellation of the IR divergences. Unlike the cancellation between the two- and three-body decays in the final state sum, we will do this schematically – that is, without any explicit computations or references to divergent $\ln m_e$ terms. If this makes you suspicious then you have good instincts, and in fact you may have already guessed the result we are building towards. Nonetheless, we press on.

To uncover the cancellation we recall the identity

$$
\frac{1}{p^2 - m^2 + \mathrm{i}\epsilon} = \mathcal{P} \frac{1}{p^2 - m^2} - \mathrm{i}\pi \delta(p^2 - m^2), \tag{7.57}
$$

which I will abbreviate as

$$
\Delta_p = \mathcal{P}_p - \mathrm{i}\pi \delta_p. \tag{7.58}
$$

With this notation we may restate Eq. (7.56) as

[4] The initial state sum includes a sum over spins, so there are no averaging factors.

$$\check{\sigma}(e\bar{L}\bar{H} \to e\bar{L}\bar{H})_{\text{int}} =$$

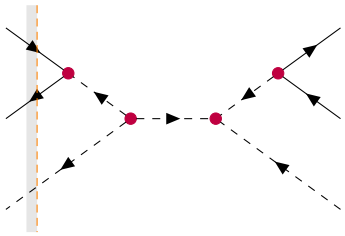

$$+ \text{c.c.}$$

$$\begin{aligned} &\propto \mathrm{i}^7 \Delta_{q+p}^2 \Delta_Q + \text{c.c.} \\ &= -2\pi \mathcal{P}_{q+p}^2 \delta_Q + 2\pi^3 \delta_{q+p}^2 \delta_Q - 4\pi \mathcal{P}_{q+p} \delta_{q+p} \mathcal{P}_Q, \end{aligned} \tag{7.59}$$

where in the proportionality I have dropped the couplings and the factor of $2q \cdot p$ from the spinor structure. The factor of i^7, which I have made explicit, is due to the four vertices and three propagators.

To obtain an analogous expression for the three-body decay we recall from Eq. (5.18) that cutting through a line to put it on shell is equivalent to making the replacement

$$\frac{\mathrm{i}}{p^2 - m^2 + \mathrm{i}\epsilon} \to 2\pi\delta(p^2 - m^2). \tag{7.60}$$

Thus,

$$\check{\Gamma}(h^- \to e\bar{L}\bar{H}) =$$

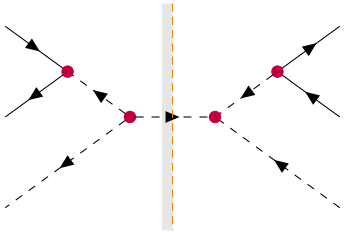

$$\begin{aligned} &\propto (\mathrm{i}^3 \Delta_{q+p})^* \times 2\pi\delta_Q \times \mathrm{i}^3 \Delta_{q+p} \\ &= 2\pi |\Delta_{q+p}|^2 \delta_Q \\ &= 2\pi \mathcal{P}_{q+p}^2 \delta_Q + 2\pi^3 \delta_{q+p}^2 \delta_Q. \end{aligned} \tag{7.61}$$

Both sides of the cut have two vertices and one propagator, and so three factors of i, and as indicated by the shadow we conjugate the left side. I comment that the second term, which contains the extremely dangerous square of a delta function, did not appear in our earlier treatment of the three-body decay because the m_e regulator prevented the virtual H from going on shell. If we were to apply a similar analysis to the two-body decay $h^- \to \bar{H}\bar{H}$,

we would however find a similar term which tames the threat in the final state sum [360] – see Section 7.A in the appendix of this chapter for details.

Lastly, with this recipe the two-to-three scattering is equally easy to express, giving

$\check{\sigma}(\bar{H}\bar{H} \to e\bar{L}\bar{H}) =$ 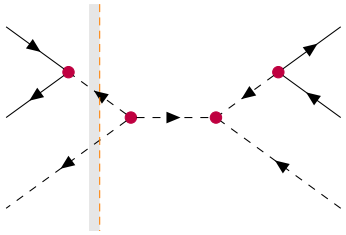 $+ \text{c.c.}$

$$\begin{aligned} &\propto (\mathrm{i})^* \times 2\pi\delta_{q+p} \times \mathrm{i}^5 \Delta_{q+p}\Delta_Q + \text{c.c.} \\ &= 2\pi\Delta_{q+p}\delta_{q+p}\Delta_Q + \text{c.c.} \\ &= 4\pi\mathcal{P}_{q+p}\delta_{q+p}\mathcal{P}_Q - 4\pi^3\delta^2_{q+p}\delta_Q. \end{aligned} \tag{7.62}$$

Summing Eqs. (7.59), (7.61), and (7.62), we observe the complete cancellation

$$\check{\Gamma}(h^- \to e\bar{L}\bar{H}) + \check{\sigma}(\bar{H}\bar{H} \to e\bar{L}\bar{H})_{\text{int}} + \check{\sigma}(e\bar{L}\bar{H} \to e\bar{L}\bar{H})_{\text{int}} = 0. \tag{7.63}$$

This sum is certainly IR-finite, so we have succeeded in cancelling the divergence. That there is no leftover finite part is something we should have expected, as it is a demand of unitarity. To understand why, we can repeat the proof of the KLN theorem to obtain

$$\sum_i \int [\mathrm{d}P_i]\, |S_{fi}|^2 = \langle f|f\rangle\,. \tag{7.64}$$

As the right-hand side has no dependence on the coupling constants, the sum must necessarily be zero at every order but $\mathcal{O}(1)$. A more explicit way to observe this is through Eq. (5.32a),

$$\mathrm{i}T - \mathrm{i}T^\dagger - \mathrm{i}T\mathrm{i}T^\dagger = 0, \tag{7.65}$$

which we recall expressed S-matrix unitarity in terms of the T-matrix. Sandwiching with $\langle f|$ and $|f\rangle$ tells us that

$$(\mathrm{i}T_{ff} + \text{c.c.}) + \sum_i \int [\mathrm{d}P_i]\, |T_{fi}|^2 = 0, \tag{7.66}$$

which we can now understand as

$$(\text{forward scattering}) + (\text{everything else}) = 0. \tag{7.67}$$

In retrospect we could therefore have written Eq. (7.63) without needing to perform any of the busywork beforehand. That said, it is nonetheless satisfying to have observed the cancellation play out in practice.

As a final comment I remark that the (everything else) in Eq. (7.67) is IR divergent only if the forward scattering contribution is. One way to assess whether the forward scattering is required, then, is to directly examine it: if it is divergent, it is needed. In our case it is straightforward to see that $e\bar{L}\bar{H} \to e\bar{L}\bar{H}$ suffers from the same kind of soft and collinear divergences as the three-body decay, and this is enough to conclude that

$$\check{\Gamma}(h^- \to e\bar{L}\bar{H}) + \check{\sigma}(\bar{H}\bar{H} \to e\bar{L}\bar{H})_{\text{int}} = \text{divergent}. \tag{7.68}$$

7.3 Finite Temperature Cancellation – a Discussion

With the cancellation of divergences at zero temperature fully understood, the next step is to examine the finite temperature scenario. In the Boltzmann equation for, say, e, the three-body decay appears as

$$s\frac{\mathrm{d}Y_e}{\mathrm{d}t} \supset [h^- \to e\bar{L}\bar{H}] - [e\bar{L}\bar{H} \to h^-], \tag{7.69}$$

where the thermally-averaged decay rate is

$$[h^- \to e\bar{L}\bar{H}] = \int \mathrm{d}\Pi\, |\mathcal{M}|^2 f_h(1-f_e)(1-f_{\bar{L}})(1+f_{\bar{H}}), \tag{7.70}$$

with

$$\int \mathrm{d}\Pi = \int [\mathrm{d}p_h][\mathrm{d}p_e][\mathrm{d}p_{\bar{L}}][\mathrm{d}p_{\bar{H}}](2\pi)^4\delta^{(4)}(p_h - p_e - p_{\bar{L}} - p_{\bar{H}}). \tag{7.71}$$

Based on our arguments at zero temperature, we might expect to be able to add to this

$$[\bar{H}\bar{H} \to e\bar{L}\bar{H}] = \int \mathrm{d}\Pi\, |\mathcal{M}|^2 f_{\bar{H}} f_{\bar{H}} (1 - f_e)(1 - f_{\bar{L}})(1 + f_{\bar{H}}) \quad \text{and} \tag{7.72a}$$

$$[e\bar{L}\bar{H} \to e\bar{L}\bar{H}] = \int \mathrm{d}\Pi\, |\mathcal{M}|^2 f_e f_{\bar{L}} f_{\bar{H}} (1 - f_e)(1 - f_{\bar{L}})(1 + f_{\bar{H}}) \tag{7.72b}$$

(which have different $\mathcal{M}$'s and $\mathrm{d}\Pi$'s) to obtain a finite result. Unfortunately, since each process carries a different set of distributional factors, they no longer sum together directly at the $\check{\Gamma}$ level and our previous analysis therefore fails to carry over. We can fix this when the chemical potentials for all particles are zero and the Maxwell-Boltzmann approximation holds for each distribution, in which case the interaction rates can be written as

$$[i \to f] \approx \int \frac{\mathrm{d}^4 Q}{(2\pi)^4} e^{-Q^0/T} \int \mathrm{d}\Pi_i\, \mathrm{d}\Pi_f\, |\mathcal{M}|^2 \qquad \text{(see Eq. (5.128))} \tag{7.73}$$

$$= \int \frac{\mathrm{d}^4 Q}{(2\pi)^4} e^{-Q^0/T} \int \mathrm{d}\Pi_f\, \check{\Gamma}, \tag{7.74}$$

giving

$$\begin{aligned} &[h^- \to e\bar{L}\bar{H}] + [\bar{H}\bar{H} \to e\bar{L}\bar{H}] + [e\bar{L}\bar{H} \to e\bar{L}\bar{H}] \\ &\quad \approx \int \frac{\mathrm{d}^4 Q}{(2\pi)^4} e^{-Q^0/T} \int \mathrm{d}\Pi_f \left[\check{\Gamma}(h^- \to e\bar{L}\bar{H}) + \check{\sigma}(\bar{H}\bar{H} \to e\bar{L}\bar{H}) + \check{\sigma}(e\bar{L}\bar{H} \to e\bar{L}\bar{H})\right] \\ &\quad = 0. \end{aligned} \tag{7.75}$$

This special case is however too narrow to be useful, as the Maxwell-Boltzmann limit—which holds when $E \gg T$—is completely unsuitable for soft particles and divergences.

To approach the cancellation more generally we might hope that there is a finite-temperature equivalent of the KLN theorem, but we have no such luck. In spite of this, there are nevertheless a number of works that have successfully demonstrated IR finiteness at finite temperature in certain situations, such as Refs. [112–121]. Today, the most commonly-used approach is to call upon the **closed time path** (CTP) **formalism** [105; 120; 363–372], which I briefly touched on in Section 5.A of Chapter 5. To construct the Boltzmann equation for a particle in the CTP formalism, one draws self-energy diagrams for that particle and enumerates circling configurations of the internal vertices, as in Figs. 7.4 and

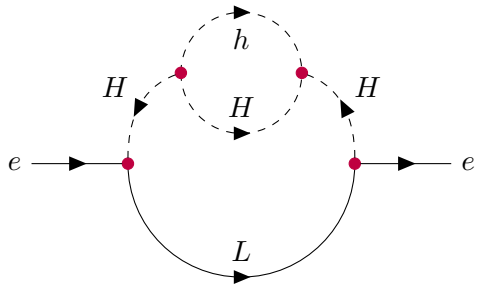

Figure 7.4: The self energy diagram used to construct the Boltzmann equation for e at $\mathcal{O}(\mu^2|Y|^2)$ in the CTP formalism.

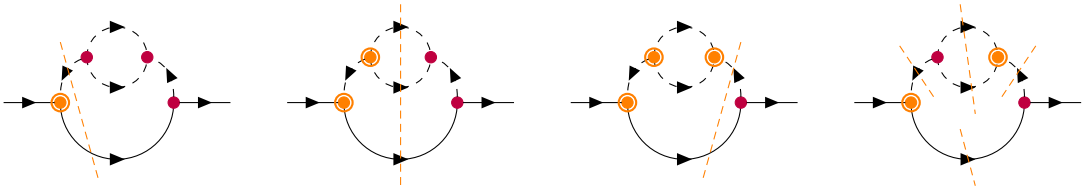

Figure 7.5: The four circling configurations of Fig. 7.4 that give rise to processes with an e in the final state, and the on-shell cuts they roughly correspond to. To obtain processes with an e in the initial state the formalism requires that we uncircle the leftmost vertex and circle the rightmost one.

7.5. Uncircled and circled vertices are labelled type '1' and '2' respectively, and a scalar propagator $\mathrm{i}\Delta$ pointing to a type a vertex from a type b vertex is replaced by $\mathrm{i}\Delta^{ab}$, where[5]

$$\mathrm{i}\Delta^{11}(p) = \frac{\mathrm{i}}{p^2 - m^2 + \mathrm{i}\epsilon} + 2\pi\delta(p^2 - m^2)\Big[\theta(p^0)f(\mathbf{p}) + \theta(-p^0)\bar{f}(-\mathbf{p})\Big], \tag{7.76a}$$

$$\mathrm{i}\Delta^{22}(p) = \frac{-\mathrm{i}}{p^2 - m^2 - \mathrm{i}\epsilon} + 2\pi\delta(p^2 - m^2)\Big[\theta(p^0)f(\mathbf{p}) + \theta(-p^0)\bar{f}(-\mathbf{p})\Big], \tag{7.76b}$$

$$\mathrm{i}\Delta^{12}(p) = 2\pi\delta(p^2 - m^2)\Big[\theta(p^0)f(\mathbf{p}) + \theta(-p^0)(1 + \bar{f}(-\mathbf{p}))\Big], \quad \text{and} \tag{7.76c}$$

$$\mathrm{i}\Delta^{21}(p) = 2\pi\delta(p^2 - m^2)\Big[\theta(p^0)(1 + f(\mathbf{p})) + \theta(-p^0)\bar{f}(-\mathbf{p})\Big]. \tag{7.76d}$$

From these expressions we can see that lines between circled and uncircled vertices are 'cut', and can represent either an initial- or final-state particle or antiparticle as long as it is kinematically allowed. The circling configuration in Fig. 7.5b, for example, therefore contains not only the three body decay $h^- \to e\bar{L}\bar{H}$, but also the three 2-to-2 scattering processes pictured in Fig. 7.6. The peculiar configuration of Fig. 7.5d, which is proportional

[5]The CTP propagators for fermions are similar; see for example Ref. [120, App. A].

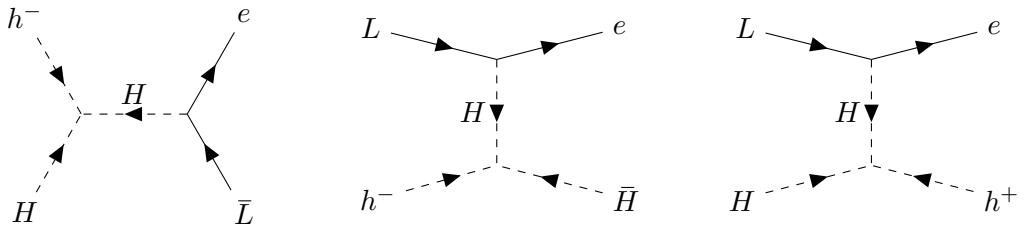

(a) $h^- H \to e\bar{L}$ (b) $Lh^- \to e\bar{H}$ (c) $LH \to eh^+$

Figure 7.6: The three 2-to-2 scatterings originating from the circling configuration in Fig. 7.5b. Scatterings (b) and (c) are both IR divergent.

to the square of a delta function, cancels against similar squares found within the other configurations [117]. Note that none of these CTP diagrams contain the scatterings $\bar{H}\bar{H} \to e\bar{L}\bar{H}$ and $e\bar{L}\bar{H} \to e\bar{L}\bar{H}$, as uncovering them would require being able to cut through some lines twice – once to put a particle in the initial state, and again to put it in the final state. It is rather curious that the processes we are lead to consider at finite temperature are so different to the ones we needed to obtain IR finiteness at zero temperature.

At the time of this writing, a full CTP analysis of the Zee model remains to be carried out, and verifying that the IR divergences cancel at finite temperature is left to future work. In aid of one who embarks on this work (who may well be me), I highlight Ref. [117] for its particularly readable demonstration of a cancellation in a similar scenario, and Ref. [120] for its pedagogical guide to making practical use of the CTP formalism. If needed, Ref. [119] provides a similar presentation to Ref. [117], but it is a far more difficult read. I comment that each of these works assumes zero chemical potential for all particles, and to the best of my knowledge it is not clear that the cancellation can be extended to more general equilibrium and nonequilibrium scenarios.

The cancellation of divergences within CP asymmetries presents another direction for future work. Finiteness at zero temperature is guaranteed by the condition that the total CP asymmetry is zero,

$$\sum_f \Delta\Gamma(i \to f) = 0, \tag{7.77}$$

as well as its initial-state-sum counterpart

$$\sum_i \Delta\check{\Gamma}(i \to f) = 0, \tag{7.78}$$

which can be thought of as equivalents of the KLN theorem for asymmetries. At finite temperature we once again have no such theorem, and CP asymmetries are moreover generically more difficult to study than plain processes within the CTP formalism. The recent theoretical developments of Refs. [121; 342; 430] however offer convenient means of organising finite-temperature computations using zero-temperature techniques, and may provide a promising avenue for future investigations in this direction.

7.A Regulator Independence of the Final State Sum

It is worthwhile to verify that the sum

$$\hat{\Gamma}_{\rm NLO} \equiv \hat{\Gamma}(h^- \to e\bar{L}\bar{H}) + \hat{\Gamma}(h^- \to \bar{H}\bar{H})_{\rm loop} = \frac{\mu^2|Y|^2}{128\pi^3}\left(-3 - \ln\frac{\widetilde{\mu}^2}{m_h^2}\right), \tag{7.79}$$

obtained with an electron mass regulator, is in fact regulator-independent. Our first thought is to turn to dimensional regularisation, as we have already computed the three-body decay in $d = 4 + \epsilon$ dimensions. Unfortunately, the expression we obtained is misleadingly wrong, and moreover any attempt to calculate the loop correction to the two-body decay is ill-fated if we are not careful. In what follows I will describe an approach due to Ref. [360] that successfully navigates this problem. The basic idea is to combine the expressions for the two decays into a common integral over k^2, where they can then be treated together with a judicious application of distributional identities.

Let's begin by re-examining the two-body decay. Similar to the main text, it has the squared matrix element

$|\mathcal{M}|^2_{\rm loop} =$ 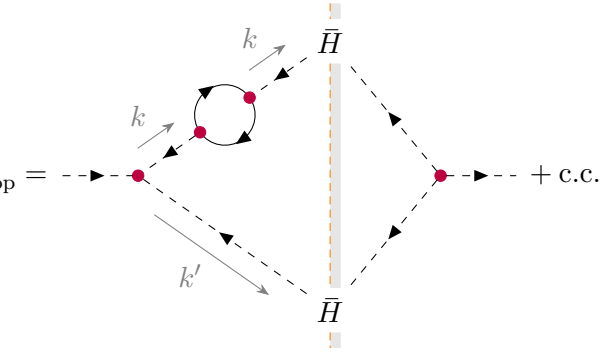

$+ \text{c.c.}$ (7.80)

$$= -\mu^2 \cdot 2\,\mathrm{Re}\left(\frac{\Sigma(k^2)}{k^2 + \mathrm{i}\epsilon}\right) \tag{7.81}$$

$$= -2\mu^2\left[\mathrm{Re}\,\Sigma(k^2)\mathcal{P}\frac{1}{k^2} + \mathrm{Im}\,\Sigma(k^2)\pi\delta(k^2)\right], \tag{7.82}$$

where here we apply the principal value decomposition of the propagator, and in the absence of a mass regulator we do not assume the self energy is real. In fact, without any masses the self energy takes the simple explicit form

$$\mathrm{i}\Sigma(k^2) = -|Y|^2\left(\widetilde{\mu}^2\frac{e^{\gamma_E}}{4\pi}\right)^{(4-d)/2}\int\frac{\mathrm{d}^d q}{(2\pi)^d}\frac{\mathrm{Tr}[\not{q}(\not{q}-\not{k})P_R]}{[q^2+\mathrm{i}\epsilon][(q-k)^2+\mathrm{i}\epsilon]} \tag{7.83}$$

$$= \mathrm{i}\frac{|Y|^2}{16\pi^2}k^2\left[\frac{2}{4-d}+2+\ln\left(-\frac{\widetilde{\mu}^2}{k^2}\right)\right] \tag{7.84}$$

$$\to \mathrm{i}\frac{|Y|^2}{16\pi^2}k^2\left[2+\ln\left(-\frac{\widetilde{\mu}^2}{k^2}\right)\right] \qquad \text{in the } \overline{\text{MS}} \text{ scheme,} \tag{7.85}$$

for which we can read off

$$\mathrm{Re}\,\Sigma(k^2) = \frac{|Y|^2}{16\pi^2}k^2\left(2+\ln\frac{\widetilde{\mu}^2}{|k^2|}\right) \quad \text{and} \quad \mathrm{Im}\,\Sigma(k^2) = \frac{|Y|^2}{16\pi}k^2\theta(k^2). \tag{7.86}$$

When the Higgs is on shell, i.e. $k^2 = 0$, the self energy vanishes, and it is tempting to claim that this correction is zero.[6] This would be premature. Instead, we may follow the same sequence of steps as we did in Section 7.2.1 up to Eq. (7.38), resulting in

$$\hat{\Gamma}(h^- \to \bar{H}\bar{H})_{\text{loop}} = \int \mathrm{d}\Pi_2\,|\mathcal{M}|^2_{\text{loop}} \tag{7.87}$$

$$= -\frac{\mu^2}{2\pi}\int_0^{m_h}\mathrm{d}k_0\,(m_h-k_0)\delta(k^2)2\,\mathrm{Re}\left(\frac{\Sigma(k^2)}{k^2+\mathrm{i}\epsilon}\right)\Big|_{k^2=2m_h k_0-m_h^2}; \tag{7.88}$$

changing the integration variable from k_0 to k^2 gives

$$\hat{\Gamma}(h^- \to \bar{H}\bar{H})_{\text{loop}} = -\frac{\mu^2}{8\pi m_h^2}\int_{-m_h^2}^{m_h^2}\mathrm{d}k^2\,(m_h^2-k^2)\delta(k^2)2\,\mathrm{Re}\left(\frac{\Sigma(k^2)}{k^2+\mathrm{i}\epsilon}\right) \tag{7.89}$$

$$= -\frac{\mu^2}{8\pi m_h^2}\int_{-m_h^2}^{m_h^2}\mathrm{d}k^2\,(m_h^2-k^2)\left[2\,\mathrm{Re}\,\Sigma(k^2)\delta(k^2)\mathcal{P}\frac{1}{k^2}+2\pi\,\mathrm{Im}\,\Sigma(k^2)\delta(k^2)^2\right]. \tag{7.90}$$

To bring the three-body decay into a similar form we can use a two-body decomposition of the three-body phase space, where for

[6] Such a claim is made in Ref. [117], where the authors considered the similar sum $\Gamma(N \to LQU) + \Gamma(N \to LH)$. With the loop correction to the two-body decay vanishing, the authors instead—to the best of my understanding—cancelled the divergence in the three-body decay against the vertex counterterm in the leading order two-body decay. In a footnote, the authors repeated the calculation with a mass regulator, cancelling the UV divergence from the loop against the same counterterm. I am not convinced that such an approach is entirely legitimate.

$$|\mathcal{M}|^2 = \left| \right|^2 = \mu^2 |Y|^2 (2q\cdot p)\left|\frac{1}{k^2+\mathrm{i}\epsilon}\right|^2 = \mu^2|Y|^2k^2\left|\frac{1}{k^2+\mathrm{i}\epsilon}\right|^2 \tag{7.91}$$

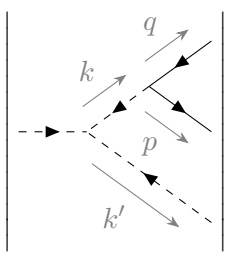

we have [431]

$$\int \mathrm{d}\Pi_3(q,p,k') = \int_0^{m_h^2} \frac{\mathrm{d}k^2}{2\pi} \int \mathrm{d}\Pi_2(k,k')\,\mathrm{d}\Pi_2(q,p) \tag{7.92}$$

$$= \int_{-m_h^2}^{m_h^2} \frac{\mathrm{d}k^2}{2\pi} \int \mathrm{d}\Pi_2(k,k')\,\mathrm{d}\Pi_2(q,p)\,\theta(k^2) \tag{7.93}$$

$$= \int_{-m_h^2}^{m_h^2} \frac{\mathrm{d}k^2}{2\pi} \cdot \frac{m_h^2-k^2}{8\pi m_h^2} \cdot \frac{1}{8\pi}\theta(k^2). \tag{7.94}$$

Observe that the two-body phase space integral over q and p, when considered with the $|Y|^2k^2$ terms from $|\mathcal{M}|^2$, is equal to

$$\int \mathrm{d}\Pi_2(q,p)\,\theta(k^2)|Y|^2k^2 = \frac{|Y|^2}{8\pi}k^2\theta(k^2) = 2\,\mathrm{Im}\,\Sigma(k^2) \tag{7.95}$$

– an identification which should not be surprising given our knowledge of the cutting rules. Thus,

$$\hat{\Gamma}(h^- \to e\bar{L}\bar{H}) = \int \mathrm{d}\Pi_3\,|\mathcal{M}|^2 \tag{7.96}$$

$$= \frac{\mu^2}{8\pi^2 m_h^2}\int_{-m_h^2}^{m_h^2} \mathrm{d}k^2\,(m_h^2-k^2)\,\mathrm{Im}\,\Sigma(k^2)\left|\frac{1}{k^2+\mathrm{i}\epsilon}\right|^2. \tag{7.97}$$

With both the two- and three-body rates now expressed as integrals over k^2, we may combine them to obtain

$$\hat{\Gamma}_{\mathrm{NLO}} = \frac{\mu^2}{8\pi^2 m_h^2}\int_{-m_h^2}^{m_h^2} \mathrm{d}k^2\,(m_h^2-k^2) \tag{7.98}$$

$$\times\left\{\mathrm{Im}\,\Sigma(k^2)\left[\left|\frac{1}{k^2+\mathrm{i}\epsilon}\right|^2 - 2\pi^2\delta(k^2)^2\right] - \mathrm{Re}\,\Sigma(k^2)\left[2\pi\delta(k^2)\mathcal{P}\frac{1}{k^2}\right]\right\}.$$

The bracketed terms multiplying $\operatorname{Re}\Sigma$ and $\operatorname{Im}\Sigma$ must be treated distributionally, so we call upon the identities [111; 360]

$$\left|\frac{1}{k^2+\mathrm{i}\epsilon}\right|^2 - 2\pi^2\delta(k^2)^2 = -\frac{\partial}{\partial k^2}\mathcal{P}\frac{1}{k^2} \quad \text{and} \tag{7.99}$$

$$2\delta(k^2)\mathcal{P}\frac{1}{k^2} = -\frac{\partial}{\partial k^2}\delta(k^2), \tag{7.100}$$

which are easily verified after making the identifications

$$\frac{1}{k^2+\mathrm{i}\epsilon} = \underbrace{\frac{k^2}{k^4+\epsilon^2}}_{\mathcal{P}\frac{1}{k^2}} - \mathrm{i}\,\underbrace{\frac{\epsilon}{k^4+\epsilon^2}}_{\pi\delta(k^2)}. \tag{7.101}$$

As both identities result in distributional derivatives we must integrate by parts, giving

$$\begin{aligned}\hat{\Gamma}_{\mathrm{NLO}} &= \frac{\mu^2}{8\pi^2 m_h^2}\int_{-m_h^2}^{m_h^2}\mathrm{d}k^2\,(m_h^2-k^2)\left\{\operatorname{Im}\Sigma(k^2)\left[-\frac{\partial}{\partial k^2}\mathcal{P}\frac{1}{k^2}\right] - \operatorname{Re}\Sigma(k^2)\left[-\frac{\partial}{\partial k^2}\pi\delta(k^2)\right]\right\} \\ &= \frac{\mu^2}{8\pi^2 m_h^2}\int_{-m_h^2}^{m_h^2}\mathrm{d}k^2\left\{\frac{\partial}{\partial k^2}\Big[(m_h^2-k^2)\operatorname{Im}\Sigma(k^2)\Big]\mathcal{P}\frac{1}{k^2}\right. \\ &\qquad \left. - \frac{\partial}{\partial k^2}\Big[(m_h^2-k^2)\operatorname{Re}\Sigma(k^2)\Big]\pi\delta(k^2)\right\}.\end{aligned} \tag{7.102}$$

Plugging in Eq. (7.86) and carrying out the remaining integrals, we at last arrive at

$$\hat{\Gamma}_{\mathrm{NLO}} = \frac{\mu^2}{8\pi^2 m_h^2}\left\{\left[\int_0^{m_h^2}\mathrm{d}k^2\,\frac{|Y|^2}{16\pi}\frac{m_h^2-2k^2}{k^2}\right] + \pi\Big[\operatorname{Re}\Sigma(0) - m_h^2\operatorname{Re}\Sigma'(0)\Big]\right\} \tag{7.103}$$

$$= \frac{\mu^2}{8\pi^2 m_h^2}\frac{|Y|^2}{16\pi}\left\{m_h^2\left(-2+\ln\frac{m_h^2}{k^2}\right) - m_h^2\left(1+\ln\frac{\widetilde{\mu}^2}{k^2}\right)\right\}\Big|_{k^2\to 0} \tag{7.104}$$

$$= \frac{\mu^2|Y|^2}{128\pi^3}\left(-3-\ln\frac{\widetilde{\mu}^2}{m_h^2}\right), \tag{7.105}$$

which agrees with the sum obtained with the electron mass regulator. Observe that $\operatorname{Re}\Sigma'(0)$ and the $\operatorname{Im}\Sigma(k^2)$ integral are separately ill-defined, and finite only when summed together as in the above. This is precisely why an attempt to compute the two-body decay in dimensional regularisation is destined to have failed.

Aw, a particle? I wanted new physics!
New particles are new physics.
Explain how!
Particles can be exchanged for forces and interactions.

Homer and *his brain*,
in *The Simpsons*,
reimagined

8

Conclusion

Some closing words are due, so allow me to summarise the work of this thesis, offer some personal thoughts, and muse on directions for future work. In all, this thesis was a tour of some rather disparate topics tied together primarily by the common thread of neutrinos and the need to consider quantum effects (i.e. loops) in the study of their mass models. These effects took the form of effective operators in the first half, while in the latter half they were considered explicitly and tamed using cutting techniques.

After beginning with a review of the necessary theory in Chapters 2 and 3, I investigated in Chapter 4 the potential for measurements of the Higgsstrahlung cross section at a next-generation collider to function as a precision probe of the Type-I and -III Seesaw models. It was found that a measurement of $\sigma(e^+e^- \to Zh)$ deviating from the Standard Model

prediction would place the Type-I model in severe tension with preexisting constraints from (in particular) measurements of the weak mixing angle s_w^2 and the CKM ratio $R(V_{us})$, while the Type-III model could accommodate a shift of up to $\sim 10\%$ assuming a pronounced hierarchy between the mixings of ν_e and ν_μ with the sterile states. Conversely, a measurement of $\sigma(e^+e^- \to Zh)$ found to be in agreement with the SM prediction would be compatible with both models, though it would place new constraints on the parameter space of Type-III Seesaw. As such, precision measurements of the Higgsstrahlung cross section can demonstrably complement existing experimental probes of neutrino mass models, and if any of the proposals for next-generation colliders are approved, we will certainly gain more insight into the nature of neutrino masses.

Having been conducted through the lens of effective field theories, the work of Chapter 4 is in principle extendable to the study of any new physics model admitting an EFT description. Naturally, the parameterisation of the fermionic Seesaw models will not carry over to a generic model, nor will the approximate expressions presented therein; nevertheless, the general expressions remain applicable. In a different direction, the study of the Seesaw models has room for further refinement, for instance by considering additional observables (such as angular distributions of the Higgsstrahlung decay products), utilising a comprehensive global fit of electroweak data, or relaxing the assumption of an exactly conserved lepton number symmetry.

The second half of this thesis was by and large devoted to the topic of leptogenesis, which began in Chapter 5 with a rather lengthy introduction to the relevant theory. In Chapter 6 I studied the prospects of achieving successful leptogenesis in the Zee model through the out-of-equilibrium decays $h^- \to LL$ and $h^- \to e\bar{L}\bar{H}$ of the new scalar h^-. This scenario required the mass of h^- to be $\mathcal{O}(10^{12}\,\text{GeV})$, at which scale it decouples from all low-scale observables but neutrino masses and mixings. The CP asymmetries in the decays of this scalar arose from two-loop interferences (at least in the case of the two-body decay), and they had the property that the total asymmetry, when summed over lepton flavours, was zero. This leptogenesis scenario was consequently purely flavoured, relying on hierarchical couplings to protect the asymmetry in one flavour while washing out the asymmetry in the

others in order to obtain a net non-zero asymmetry. Unfortunately, this made the scenario too restrictive to reproduce the observed baryon abundance of the universe, even when the relevant parameters were raised close to their perturbative limits. When considered alongside prior assertions that leptogenesis is unachievable in TeV-scale realisations of the model [106; 107], this therefore indicated that successful leptogenesis is not possible in the Zee model, period.

In a continuation of this work we identified two minimal extensions of the Zee model with improved leptogenesis prospects, the studies of which remain ongoing at the time of this writing. To consistently account for flavour effects and ensure the analysis of these extensions is free of ambiguities, it will be necessary to employ flavour-covariant forms of the Boltzmann equations. This need is not unprecedented [358; 432], and an explicit example of a model where it is important to treat flavour effects covariantly is Type-II Seesaw [19–21], as shown by Ref. [408]. It will be good to additionally apply this treatment to the original Zee model to confirm the conclusions reached in Chapter 5.

As an outgrowth of the study of the Zee model I was lastly lead to investigate the cancellation of infrared divergences in processes such as $h^- \to e\bar{L}\bar{H}$, and this formed the contents of Chapter 7. The successful cancellation of these divergences at zero temperature was underpinned by the strengthened KLN theorem of Ref. [111], and it required the consideration of some rather unconventional diagrams such as a self-energy correction to $h^- \to \bar{H}\bar{H}$, and the forward scattering $e\bar{L}\bar{H} \to e\bar{L}\bar{H}$. A careful distributional treatment was needed to evaluate these diagrams, and in view of this I showed the full details of all computations (which have a tendency to be skipped over in works encountering similar processes, such as Refs. [111; 117; 360]). Extending the cancellation to finite temperature, as would be needed to apply it to the leptogenesis study of Chapter 6, was deemed too impractical to perform in an acceptable timeframe, so I have left it to future work. One of the more well-worn approaches to achieving such a cancellation is found in the machinery of the CTP formalism, as is demonstrated for example by Refs. [117; 119; 120]. That said, I also find the techniques of Refs. [121; 342; 430] to be intriguing, and I would be curious to see if they are also suitable for this task.

All in all, the study of a new physics model can often be distilled down to two main questions: *what can we do for the model?* (i.e. what observations can we use to constrain it?) and *what can the model do for us?* (i.e. which of the SM's deficiencies is it able to resolve?). In this thesis I explored both sides of this symbiosis, first by examining the potential of a next-generation collider to probe the fermionic Seesaw models, and then by studying the capacity of the Zee model to explain the observed baryon asymmetry of the universe (and along the way I elucidated some technicalities of IR divergences). The systematic investigation of new physics models along these two general lines is among our surest ways to gain insight into the fundamental workings of the universe, and it is a tradition that I am proud to now (in some small way) be a part of.

References

[1] T. Felkl, A. Lackner, and M. A. Schmidt, *Riding the Seesaw: What Higgsstrahlung May Reveal about Massive Neutrinos*, Eur. Phys. J. C **83**, 342 (2023), arXiv:2211.15954 [hep-ph].

[2] C. S. Fong, A. Lackner, and M. A. Schmidt, *Leptogenesis in the Zee Model* (2025), in preparation.

[3] G. Aad *et al.* (ATLAS), *Observation of a new particle in the search for the Standard Model Higgs boson with the ATLAS detector at the LHC*, Phys. Lett. B **716**, 1 (2012), arXiv:1207.7214 [hep-ex].

[4] S. Chatrchyan *et al.* (CMS), *Observation of a New Boson at a Mass of 125 GeV with the CMS Experiment at the LHC*, Phys. Lett. B **716**, 30 (2012), arXiv:1207.7235 [hep-ex].

[5] S. Troitsky, *Unsolved problems in particle physics*, Phys. Usp. **55**, 72 (2012), arXiv:1112.4515 [hep-ph].

[6] A. de Gouvea, D. Hernandez, and T. M. P. Tait, *Criteria for Natural Hierarchies*, Phys. Rev. D **89**, 115005 (2014), arXiv:1402.2658 [hep-ph].

[7] C. Csáki and P. Tanedo, *Beyond the Standard Model*, (2015), pp. 169–268, arXiv:1602.04228 [hep-ph].

[8] R. D. Peccei, *The Strong CP problem and axions*, Lect. Notes Phys. **741**, 3 (2008), arXiv:hep-ph/0607268.

[9] A. Hook, *TASI Lectures on the Strong CP Problem and Axions*, PoS **TASI2018**, 004 (2019), arXiv:1812.02669 [hep-ph].

[10] Y. Fukuda *et al.* (Super-Kamiokande), *Evidence for oscillation of atmospheric neutrinos*, Phys. Rev. Lett. **81**, 1562 (1998), arXiv:hep-ex/9807003.

[11] Q. R. Ahmad *et al.* (SNO), *Measurement of the rate of* $\nu_e + d \to p + p + e^-$ *interactions produced by* ^8B *solar neutrinos at the Sudbury Neutrino Observatory*, Phys. Rev. Lett. **87**, 071301 (2001), arXiv:nucl-ex/0106015.

[12] Q. R. Ahmad *et al.* (SNO), *Direct evidence for neutrino flavor transformation from neutral current interactions in the Sudbury Neutrino Observatory*, Phys. Rev. Lett. **89**, 011301 (2002), arXiv:nucl-ex/0204008.

[13] Nobel Media AB, *The Nobel Prize in Physics 2015* (2015), accessed 2024/10/03.

[14] P. Minkowski, $\mu \to e\gamma$ *at a Rate of One Out of* 10^9 *Muon Decays?*, Phys. Lett. **67B**, 421 (1977).

[15] T. Yanagida, *Horizontal gauge symmetry and masses of neutrinos*, *Proceedings: Workshop on the Unified Theories and the Baryon Number in the Universe: Tsukuba, Japan, February 13-14, 1979*, Conf. Proc. **C7902131**, 95 (1979).

[16] M. Gell-Mann, P. Ramond, and R. Slansky, *Complex Spinors and Unified Theories*, *Supergravity Workshop Stony Brook, New York, September 27-28, 1979*, Conf. Proc. **C790927**, 315 (1979), arXiv:1306.4669 [hep-th].

[17] S. L. Glashow, *Quarks and Leptons, Cargèse 1979*, edited by M. Lévy (Plenum Press, New York, 1980), ISBN: 9780306405600, p. 720.

[18] R. N. Mohapatra and G. Senjanovic, *Neutrino Mass and Spontaneous Parity Nonconservation*, Phys. Rev. Lett. **44**, 912 (1980).

[19] M. Magg and C. Wetterich, *Neutrino Mass Problem and Gauge Hierarchy*, Phys. Lett. **94B**, 61 (1980).

[20] G. Lazarides, Q. Shafi, and C. Wetterich, *Proton Lifetime and Fermion Masses in an SO(10) Model*, Nucl. Phys. B **181**, 287 (1981).

[21] R. N. Mohapatra and G. Senjanovic, *Neutrino Masses and Mixings in Gauge Models with Spontaneous Parity Violation*, Phys. Rev. D **23**, 165 (1981).

[22] J. Schechter and J. W. F. Valle, *Neutrino Masses in* $SU(2) \otimes U(1)$ *Theories*, Phys. Rev. **D22**, 2227 (1980).

[23] A. Zee, *A Theory of Lepton Number Violation, Neutrino Majorana Mass, and Oscillation*, Phys. Lett. B **93**, 389 (1980), [Erratum: Phys.Lett.B 95, 461 (1980)].

[24] C. Wetterich, *Neutrino Masses and the Scale of B-L Violation*, Nucl. Phys. **B187**, 343 (1981).

[25] A. Zee, *Quantum Numbers of Majorana Neutrino Masses*, Nucl. Phys. B **264**, 99 (1986).

[26] A. Zee, *Charged Scalar Field and Quantum Number Violations*, Phys. Lett. B **161**, 141 (1985).

[27] K. S. Babu, *Model of "Calculable" Majorana Neutrino Masses*, Phys. Lett. B **203**, 132 (1988).

[28] R. Foot, H. Lew, X. G. He, and G. C. Joshi, *Seesaw Neutrino Masses Induced by a Triplet of Leptons*, Z. Phys. **C44**, 441 (1989).

[29] E. Ma, *Pathways to naturally small neutrino masses*, Phys. Rev. Lett. **81**, 1171 (1998), arXiv:hep-ph/9805219.

[30] L. M. Krauss, S. Nasri, and M. Trodden, *A Model for neutrino masses and dark matter*, Phys. Rev. D **67**, 085002 (2003), arXiv:hep-ph/0210389.

[31] E. Ma, *Neutrino Mass Seesaw Version 3: Recent Developments*, AIP Conf. Proc. **1116**, 239 (2009), arXiv:0810.5574 [hep-ph].

[32] R. N. Mohapatra *et al.*, *Theory of neutrinos: A White paper*, Rept. Prog. Phys. **70**, 1757 (2007), arXiv:hep-ph/0510213.

[33] E. Ma, *Verifiable radiative seesaw mechanism of neutrino mass and dark matter*, Phys. Rev. D **73**, 077301 (2006), arXiv:hep-ph/0601225.

[34] R. N. Mohapatra and A. Y. Smirnov, *Neutrino Mass and New Physics*, Ann. Rev. Nucl. Part. Sci. **56**, 569 (2006), arXiv:hep-ph/0603118.

[35] E. Ma, *Neutrino Mass: Mechanisms and Models* (2009), arXiv:0905.0221 [hep-ph].

[36] C. Giunti and C. W. Kim, *Fundamentals of Neutrino Physics and Astrophysics* (Oxford University Press, 2007), ISBN: 978-0-19-850871-7.

[37] E. Ma, I. Picek, and B. Radovčić, *New Scotogenic Model of Neutrino Mass with $U(1)_D$ Gauge Interaction*, Phys. Lett. B **726**, 744 (2013), arXiv:1308.5313 [hep-ph].

[38] Y. Cai, J. Herrero-García, M. A. Schmidt, A. Vicente, and R. R. Volkas, *From the trees to the forest: a review of radiative neutrino mass models*, Front. in Phys. **5**, 63 (2017), arXiv:1706.08524 [hep-ph].

[39] C. Hagedorn, J. Herrero-García, E. Molinaro, and M. A. Schmidt, *Phenomenology of the Generalised Scotogenic Model with Fermionic Dark Matter*, JHEP **11** (2018), 103, arXiv:1804.04117 [hep-ph].

[40] J. Herrero-García and M. A. Schmidt, *Neutrino mass models: New classification and model-independent upper limits on their scale*, Eur. Phys. J. C **79**, 938 (2019), arXiv:1903.10552 [hep-ph].

[41] V. De Romeri, J. Nava, M. Puerta, and A. Vicente, *Dark matter in the scotogenic model with spontaneous lepton number violation*, Phys. Rev. D **107**, 095019 (2023), arXiv:2210.07706 [hep-ph].

[42] M. Hirsch, M. A. Diaz, W. Porod, J. C. Romao, and J. W. F. Valle, *Neutrino masses and mixings from supersymmetry with bilinear R parity violation: A Theory for solar and atmospheric neutrino oscillations*, Phys. Rev. D **62**, 113008 (2000), [Erratum: Phys.Rev.D 65, 119901 (2002)], arXiv:hep-ph/0004115.

[43] N. Arkani-Hamed, L. J. Hall, H. Murayama, D. Tucker-Smith, and N. Weiner, *Small neutrino masses from supersymmetry breaking*, Phys. Rev. D **64**, 115011 (2001), arXiv:hep-ph/0006312.

[44] D. S. Akerib *et al.* (LZ), *The LUX-ZEPLIN (LZ) Experiment*, Nucl. Instrum. Meth. A **953**, 163047 (2020), arXiv:1910.09124 [physics.ins-det].

[45] E. Aprile *et al.* (XENON), *The XENONnT dark matter experiment*, Eur. Phys. J. C **84**, 784 (2024), arXiv:2402.10446 [physics.ins-det].

[46] X. Cao *et al.* (PandaX), *PandaX: A Liquid Xenon Dark Matter Experiment at CJPL*, Sci. China Phys. Mech. Astron. **57**, 1476 (2014), arXiv:1405.2882 [physics.ins-det].

[47] S. J. Asztalos *et al.* (ADMX), *A SQUID-based microwave cavity search for dark-matter axions*, Phys. Rev. Lett. **104**, 041301 (2010), arXiv:0910.5914 [astro-ph.CO].

[48] V. Anastassopoulos *et al.* (CAST), *New CAST Limit on the Axion-Photon Interaction*, Nature Phys. **13**, 584 (2017), arXiv:1705.02290 [hep-ex].

[49] X. Cui *et al.* (PandaX-II), *Dark Matter Results From 54-Ton-Day Exposure of PandaX-II Experiment*, Phys. Rev. Lett. **119**, 181302 (2017), arXiv:1708.06917 [astro-ph.CO].

[50] Q. Wang *et al.* (PandaX-II), *Results of dark matter search using the full PandaX-II exposure*, Chin. Phys. C **44**, 125001 (2020), arXiv:2007.15469 [astro-ph.CO].

[51] E. Aprile *et al.* (XENON), *Dark Matter Search Results from a One Ton-Year Exposure of XENON1T*, Phys. Rev. Lett. **121**, 111302 (2018), arXiv:1805.12562 [astro-ph.CO].

[52] E. Aprile *et al.* (XENON), *First Search for Light Dark Matter in the Neutrino Fog with XENONnT* (2024), arXiv:2409.17868 [hep-ex].

[53] T. Braine *et al.* (ADMX), *Extended Search for the Invisible Axion with the Axion Dark Matter Experiment*, Phys. Rev. Lett. **124**, 101303 (2020), arXiv:1910.08638 [hep-ex].

[54] J. Aalbers *et al.* (LZ), *First Dark Matter Search Results from the LUX-ZEPLIN (LZ) Experiment*, Phys. Rev. Lett. **131**, 041002 (2023), arXiv:2207.03764 [hep-ex].

[55] M. Aaboud *et al.* (ATLAS), *Combination of the searches for pair-produced vector-like partners of the third-generation quarks at $\sqrt{s} = 13$ TeV with the ATLAS detector*, Phys. Rev. Lett. **121**, 211801 (2018), arXiv:1808.02343 [hep-ex].

[56] G. Aad *et al.* (ATLAS), *Search for type-III seesaw heavy leptons in leptonic final states in pp collisions at $\sqrt{s} = 13$ TeV with the ATLAS detector*, Eur. Phys. J. C **82**, 988 (2022), arXiv:2202.02039 [hep-ex].

[57] G. Aad *et al.* (ATLAS), *Combination of searches for invisible decays of the Higgs boson using 139 fb^{-1} of proton-proton collision data at $\sqrt{s} = 13$ TeV collected with the ATLAS experiment*, Phys. Lett. B **842**, 137963 (2023), arXiv:2301.10731 [hep-ex].

[58] G. Aad *et al.* (ATLAS), *Combination of searches for pair-produced leptoquarks at $\sqrt{s} = 13$ TeV with the ATLAS detector*, Phys. Lett. B **854**, 138736 (2024), arXiv:2401.11928 [hep-ex].

[59] G. Aad *et al.* (ATLAS), *Combination of searches for heavy spin-1 resonances using 139 fb^{-1} of proton-proton collision data at $\sqrt{s} = 13$ TeV with the ATLAS detector*, JHEP **04** (2024), 118, arXiv:2402.10607 [hep-ex].

[60] G. Aad *et al.* (ATLAS), *Combination of searches for singly produced vector-like top quarks in pp collisions at* $\sqrt{s} = 13$ *TeV with the ATLAS detector* (2024), arXiv:2408.08789 [hep-ex].

[61] V. Khachatryan *et al.* (CMS), *Search for dark matter, extra dimensions, and unparticles in monojet events in proton–proton collisions at* $\sqrt{s} = 8$ *TeV*, Eur. Phys. J. C **75**, 235 (2015), arXiv:1408.3583 [hep-ex].

[62] A. M. Sirunyan *et al.* (CMS), *Search for invisible decays of a Higgs boson produced through vector boson fusion in proton-proton collisions at* $\sqrt{s} = 13$ *TeV*, Phys. Lett. B **793**, 520 (2019), arXiv:1809.05937 [hep-ex].

[63] A. M. Sirunyan *et al.* (CMS), *Search for resonant and nonresonant new phenomena in high-mass dilepton final states at* $\sqrt{s} = 13$ *TeV*, JHEP **07** (2021), 208, arXiv:2103.02708 [hep-ex].

[64] A. Tumasyan *et al.* (CMS), *Search for new particles in events with energetic jets and large missing transverse momentum in proton-proton collisions at* $\sqrt{s} = 13$ *TeV*, JHEP **11** (2021), 153, arXiv:2107.13021 [hep-ex].

[65] A. Tumasyan *et al.* (CMS), *Search for long-lived heavy neutral leptons with displaced vertices in proton-proton collisions at* $\sqrt{\text{s}} = 13$ *TeV*, JHEP **07** (2022), 081, arXiv:2201.05578 [hep-ex].

[66] M. Agostini *et al.* (GERDA), *Final Results of GERDA on the Search for Neutrinoless Double-*β *Decay*, Phys. Rev. Lett. **125**, 252502 (2020), arXiv:2009.06079 [nucl-ex].

[67] A. Gando *et al.* (KamLAND-Zen), *Search for Majorana Neutrinos near the Inverted Mass Hierarchy Region with KamLAND-Zen*, Phys. Rev. Lett. **117**, 082503 (2016), [Addendum: Phys.Rev.Lett. 117, 109903 (2016)], arXiv:1605.02889 [hep-ex].

[68] M. Ahmad *et al.*, *CEPC-SPPC Preliminary Conceptual Design Report. 1. Physics and Detector* (2015).

[69] J. B. Guimarães da Costa *et al.* (CEPC Study Group), *CEPC Conceptual Design Report: Volume 2 - Physics & Detector* (2018), arXiv:1811.10545 [hep-ex].

[70] H. Cheng *et al.* (CEPC Physics Study Group), *The Physics potential of the CEPC. Prepared for the US Snowmass Community Planning Exercise (Snowmass 2021)* (2022), arXiv:2205.08553 [hep-ph].

[71] H. Baer *et al.*, *The International Linear Collider Technical Design Report - Volume 2: Physics* (2013), arXiv:1306.6352 [hep-ph].

[72] D. M. Asner *et al.*, *ILC Higgs White Paper*, (2013), arXiv:1310.0763 [hep-ph].

[73] P. Bambade *et al.*, *The International Linear Collider: A Global Project* (2019), arXiv:1903.01629 [hep-ex].

[74] A. Aryshev *et al.* (ILC International Development Team), *The International Linear Collider: Report to Snowmass 2021* (2022), arXiv:2203.07622 [physics.acc-ph].

[75] M. Bicer *et al.* (TLEP Design Study Working Group), *First Look at the Physics Case of TLEP*, JHEP **01** (2014), 164, arXiv:1308.6176 [hep-ex].

[76] A. Pyarelal, H. Song, and S. Su, *FCC-ee: The Lepton Collider: Future Circular Collider Conceptual Design Report Volume 2*, EUROPEAN PHYSICAL JOURNAL-SPECIAL TOPICS 10.1140/epjst/e2019-900045-4 (2019).

[77] I. Agapov *et al.*, *Future Circular Lepton Collider FCC-ee: Overview and Status*, (2022), arXiv:2203.08310 [physics.acc-ph].

[78] G. Bernardi *et al.*, *The Future Circular Collider: a Summary for the US 2021 Snowmass Process* (2022), arXiv:2203.06520 [hep-ex].

[79] P. Lebrun, L. Linssen, A. Lucaci-Timoce, D. Schulte, F. Simon, S. Stapnes, N. Toge, H. Weerts, and J. Wells, *The CLIC Programme: Towards a Staged e^+e^- Linear Collider Exploring the Terascale : CLIC Conceptual Design Report* (2012), arXiv:1209.2543 [physics.ins-det].

[80] J. de Blas *et al.* (CLIC), *The CLIC Potential for New Physics* (2018), arXiv:1812.02093 [hep-ph].

[81] T. K. Charles *et al.* (CLICdp, CLIC), *The Compact Linear Collider (CLIC) - 2018 Summary Report* (2018), arXiv:1812.06018 [physics.acc-ph].

[82] M. Bai *et al.*, *C^3: A "Cool" Route to the Higgs Boson and Beyond*, (2021), arXiv:2110.15800 [hep-ex].

[83] E. A. Nanni *et al.*, *C^3 Demonstration Research and Development Plan*, (2022), arXiv:2203.09076 [physics.acc-ph].

[84] S. Dasu *et al.*, *Strategy for Understanding the Higgs Physics: The Cool Copper Collider*, (2022), arXiv:2203.07646 [hep-ex].

[85] S. Dawson *et al.*, *Report of the Topical Group on Higgs Physics for Snowmass 2021: The Case for Precision Higgs Physics*, (2022), arXiv:2209.07510 [hep-ph].

[86] N. Craig, M. Farina, M. McCullough, and M. Perelstein, *Precision Higgsstrahlung as a Probe of New Physics*, JHEP **03** (2015), 146, arXiv:1411.0676 [hep-ph].

[87] M. Drewes *et al.*, *A White Paper on keV Sterile Neutrino Dark Matter*, JCAP **01** (2017), 025, arXiv:1602.04816 [hep-ph].

[88] A. Boyarsky, M. Drewes, T. Lasserre, S. Mertens, and O. Ruchayskiy, *Sterile neutrino Dark Matter*, Prog. Part. Nucl. Phys. **104**, 1 (2019), arXiv:1807.07938 [hep-ph].

[89] E. W. Kolb and M. S. Turner, *The Early Universe*, Vol. 69 (Taylor and Francis, 2019), ISBN: 978-0-429-49286-0, 978-0-201-62674-2.

[90] N. Aghanim *et al.* (Planck), *Planck 2018 results. VI. Cosmological parameters*, Astron. Astrophys. **641**, A6 (2020), [Erratum: Astron.Astrophys. 652, C4 (2021)], arXiv:1807.06209 [astro-ph.CO].

[91] A. D. Sakharov, *Violation of CP Invariance, C asymmetry, and baryon asymmetry of the universe*, Pisma Zh. Eksp. Teor. Fiz. **5**, 32 (1967).

[92] V. Mukhanov, *Physical Foundations of Cosmology* (Cambridge University Press, Oxford, 2005), ISBN: 978-0-521-56398-7.

[93] S. Dodelson and F. Schmidt, *Modern Cosmology* (Academic Press, 2020),.

[94] D. Baumann, *Cosmology* (Cambridge University Press, 2022), ISBN: 978-1-108-93709-2, 978-1-108-83807-8.

[95] O. Bertolami, D. Colladay, V. A. Kostelecky, and R. Potting, *CPT violation and baryogenesis*, Phys. Lett. B **395**, 178 (1997), arXiv:hep-ph/9612437.

[96] J. M. Carmona, J. L. Cortes, A. K. Das, J. Gamboa, and F. Mendez, *Matter-antimatter asymmetry without departure from thermal equilibrium*, Mod. Phys. Lett. A **21**, 883 (2006), arXiv:hep-th/0410143.

[97] E. Di Grezia, S. Esposito, and G. Salesi, *Baryon asymmetry in the universe resulting from Lorentz violation*, EPL **74**, 747 (2006), arXiv:hep-ph/0508298.

[98] M. B. Gavela, P. Hernandez, J. Orloff, O. Pene, and C. Quimbay, *Standard model CP violation and baryon asymmetry. Part 2: Finite temperature*, Nucl. Phys. B **430**, 382 (1994), arXiv:hep-ph/9406289.

[99] P. Huet and E. Sather, *Electroweak baryogenesis and standard model CP violation*, Phys. Rev. D **51**, 379 (1995), arXiv:hep-ph/9404302.

[100] J. M. Cline, *Baryogenesis*, (2006), arXiv:hep-ph/0609145.

[101] D. Bodeker and W. Buchmuller, *Baryogenesis from the weak scale to the grand unification scale*, Rev. Mod. Phys. **93**, 035004 (2021), arXiv:2009.07294 [hep-ph].

[102] M. Fukugita and T. Yanagida, *Baryogenesis Without Grand Unification*, Phys. Lett. B **174**, 45 (1986).

[103] M. A. Luty, *Baryogenesis via leptogenesis*, Phys. Rev. D **45**, 455 (1992).

[104] S. Davidson, E. Nardi, and Y. Nir, *Leptogenesis*, Phys. Rept. **466**, 105 (2008), arXiv:0802.2962 [hep-ph].

[105] C. S. Fong, E. Nardi, and A. Riotto, *Leptogenesis in the Universe*, Adv. High Energy Phys. **2012**, 158303 (2012), arXiv:1301.3062 [hep-ph].

[106] E. Ma, M. Raidal, and U. Sarkar, *Neutrino masses in supersymmetry: R-parity and leptogenesis*, Phys. Lett. B **460**, 359 (1999), arXiv:hep-ph/9901406.

[107] T. Hambye, *Leptogenesis at the TeV scale*, Nucl. Phys. B **633**, 171 (2002), arXiv:hep-ph/0111089.

[108] F. Bloch and A. Nordsieck, *Note on the Radiation Field of the electron*, Phys. Rev. **52**, 54 (1937).

[109] T. Kinoshita, *Mass singularities of Feynman amplitudes*, J. Math. Phys. **3**, 650 (1962).

[110] T. D. Lee and M. Nauenberg, *Degenerate Systems and Mass Singularities*, Phys. Rev. **133**, B1549 (1964).

[111] C. Frye, H. Hannesdottir, N. Paul, M. D. Schwartz, and K. Yan, *Infrared Finiteness and Forward Scattering*, Phys. Rev. D **99**, 056015 (2019), arXiv:1810.10022 [hep-ph].

[112] R. Baier, B. Pire, and D. Schiff, *Dilepton production at finite temperature: Perturbative treatment at order α_s*, Phys. Rev. D **38**, 2814 (1988).

[113] T. Altherr, P. Aurenche, and T. Becherrawy, *On Infrared and Mass Singularities of Perturbative QCD in a Quark - Gluon Plasma*, Nucl. Phys. B **315**, 436 (1989).

[114] T. Grandou, M. Le Bellac, and D. Poizat, *Remarks on infrared singularities of relativistic thermal field theories*, Phys. Lett. B **249**, 478 (1990).

[115] T. Grandou, M. Le Bellac, and D. Poizat, *Cancellation of infrared and collinear singularities in relativistic thermal field theories*, Nucl. Phys. B **358**, 408 (1991).

[116] P. Aurenche, F. Gelis, and H. Zaraket, *KLN theorem, magnetic mass, and thermal photon production*, Phys. Rev. D **61**, 116001 (2000), arXiv:hep-ph/9911367.

[117] A. Salvio, P. Lodone, and A. Strumia, *Towards leptogenesis at NLO: the right-handed neutrino interaction rate*, JHEP **08** (2011), 116, arXiv:1106.2814 [hep-ph].

[118] M. Laine and Y. Schroder, *Thermal right-handed neutrino production rate in the non-relativistic regime*, JHEP **02** (2012), 068, arXiv:1112.1205 [hep-ph].

[119] B. Garbrecht, F. Glowna, and M. Herranen, *Right-Handed Neutrino Production at Finite Temperature: Radiative Corrections, Soft and Collinear Divergences*, JHEP **04** (2013), 099, arXiv:1302.0743 [hep-ph].

[120] M. Beneke, F. Dighera, and A. Hryczuk, *Relic density computations at NLO: infrared finiteness and thermal correction*, JHEP **10** (2014), 045, [Erratum: JHEP 07, 106 (2016)], arXiv:1409.3049 [hep-ph].

[121] T. Blažek and P. Maták, *Mass-derivative relations for leptogenesis*, Eur. Phys. J. C **82**, 214 (2022), arXiv:2111.03419 [hep-ph].

[122] M. D. Schwartz, *Quantum Field Theory and the Standard Model* (Cambridge University Press, 2014), ISBN: 978-1-107-03473-0.

[123] M. E. Peskin and D. V. Schroeder, *An Introduction to quantum field theory* (Addison-Wesley, Reading, USA, 1995), ISBN: 978-0-201-50397-5, 978-0-429-50355-9, 978-0-429-49417-8.

[124] S. Navas *et al.* (Particle Data Group), *Review of Particle Physics*, Phys. Rev. D **110**, 030001 (2024).

[125] J. C. Romao and J. P. Silva, *A resource for signs and Feynman diagrams of the Standard Model*, Int. J. Mod. Phys. A **27**, 1230025 (2012), arXiv:1209.6213 [hep-ph].

[126] J. Schwichtenberg, *Physics from Symmetry*, Undergraduate Lecture Notes in Physics (Springer, 2018), ISBN: 978-3-319-19201-7, 978-3-319-66630-3, 978-3-319-88288-8, 978-3-319-66631-0.

[127] S. Willenbrock, *Symmetries of the Standard Model* (2004), arXiv:hep-ph/0410370 [hep-ph].

[128] N. Cabibbo, *Unitary Symmetry and Leptonic Decays*, Phys. Rev. Lett. **10**, 531 (1963).

[129] M. Kobayashi and T. Maskawa, *CP Violation in the Renormalizable Theory of Weak Interaction*, Prog. Theor. Phys. **49**, 652 (1973).

[130] L.-L. Chau and W.-Y. Keung, *Comments on the Parametrization of the Kobayashi-Maskawa Matrix*, Phys. Rev. Lett. **53**, 1802 (1984).

[131] C. Jarlskog, *Commutator of the Quark Mass Matrices in the Standard Electroweak Model and a Measure of Maximal CP Nonconservation*, Phys. Rev. Lett. **55**, 1039 (1985).

[132] K. N. Abazajian *et al.*, *Light Sterile Neutrinos: A White Paper* (2012), arXiv:1204.5379 [hep-ph].

[133] T. Wester *et al.* (Super-Kamiokande), *Atmospheric neutrino oscillation analysis with neutron tagging and an expanded fiducial volume in Super-Kamiokande I–V*, Phys. Rev. D **109**, 072014 (2024), arXiv:2311.05105 [hep-ex].

[134] R. Abbasi *et al.* (IceCube), *Measurement of atmospheric neutrino oscillation parameters using convolutional neural networks with 9.3 years of data in IceCube DeepCore* (2024), arXiv:2405.02163 [hep-ex].

[135] C. Arpesella *et al.* (Borexino), *Direct Measurement of the Be-7 Solar Neutrino Flux with 192 Days of Borexino Data*, Phys. Rev. Lett. **101**, 091302 (2008), arXiv:0805.3843 [astro-ph].

[136] K. Abe *et al.* (Super-Kamiokande), *Solar neutrino measurements using the full data period of Super-Kamiokande-IV*, Phys. Rev. D **109**, 092001 (2024), arXiv:2312.12907 [hep-ex].

[137] J. N. Abdurashitov *et al.* (SAGE), *Measurement of the solar neutrino capture rate with gallium metal. III: Results for the 2002–2007 data-taking period*, Phys. Rev. C **80**, 015807 (2009), arXiv:0901.2200 [nucl-ex].

[138] F. Kaether, W. Hampel, G. Heusser, J. Kiko, and T. Kirsten, *Reanalysis of the GALLEX solar neutrino flux and source experiments*, Phys. Lett. B **685**, 47 (2010), arXiv:1001.2731 [hep-ex].

[139] A. Aguilar *et al.* (LSND), *Evidence for neutrino oscillations from the observation of $\bar{\nu}_e$ appearance in a $\bar{\nu}_\mu$ beam*, Phys. Rev. D **64**, 112007 (2001), arXiv:hep-ex/0104049.

[140] K. Abe *et al.* (T2K), *Indication of Electron Neutrino Appearance from an Accelerator-produced Off-axis Muon Neutrino Beam*, Phys. Rev. Lett. **107**, 041801 (2011), arXiv:1106.2822 [hep-ex].

[141] K. Abe *et al.* (T2K), *Measurements of neutrino oscillation parameters from the T2K experiment using* 3.6×10^{21} *protons on target*, Eur. Phys. J. C **83**, 782 (2023), arXiv:2303.03222 [hep-ex].

[142] M. A. Acero *et al.* (NOvA), *First Measurement of Neutrino Oscillation Parameters using Neutrinos and Antineutrinos by NOvA*, Phys. Rev. Lett. **123**, 151803 (2019), arXiv:1906.04907 [hep-ex].

[143] M. A. Acero *et al.* (NOvA), *Expanding neutrino oscillation parameter measurements in NOvA using a Bayesian approach*, Phys. Rev. D **110**, 012005 (2024), arXiv:2311.07835 [hep-ex].

[144] K. Eguchi *et al.* (KamLAND), *First results from KamLAND: Evidence for reactor anti-neutrino disappearance*, Phys. Rev. Lett. **90**, 021802 (2003), arXiv:hep-ex/0212021.

[145] A. Gando *et al.* (KamLAND), *Constraints on* θ_{13} *from A Three-Flavor Oscillation Analysis of Reactor Antineutrinos at KamLAND*, Phys. Rev. D **83**, 052002 (2011), arXiv:1009.4771 [hep-ex].

[146] F. P. An *et al.* (Daya Bay), *Observation of electron-antineutrino disappearance at Daya Bay*, Phys. Rev. Lett. **108**, 171803 (2012), arXiv:1203.1669 [hep-ex].

[147] D. Adey *et al.* (Daya Bay), *Measurement of the Electron Antineutrino Oscillation with 1958 Days of Operation at Daya Bay*, Phys. Rev. Lett. **121**, 241805 (2018), arXiv:1809.02261 [hep-ex].

[148] J. K. Ahn *et al.* (RENO), *Observation of Reactor Electron Antineutrino Disappearance in the RENO Experiment*, Phys. Rev. Lett. **108**, 191802 (2012), arXiv:1204.0626 [hep-ex].

[149] G. Bak *et al.* (RENO), *Measurement of Reactor Antineutrino Oscillation Amplitude and Frequency at RENO*, Phys. Rev. Lett. **121**, 201801 (2018), arXiv:1806.00248 [hep-ex].

[150] Y. Abe *et al.* (Double Chooz), *Indication of Reactor* $\bar{\nu}_e$ *Disappearance in the Double Chooz Experiment*, Phys. Rev. Lett. **108**, 131801 (2012), arXiv:1112.6353 [hep-ex].

[151] H. de Kerret *et al.* (Double Chooz), *Double Chooz* θ_{13} *measurement via total neutron capture detection*, Nature Phys. **16**, 558 (2020), arXiv:1901.09445 [hep-ex].

[152] I. Esteban, M. C. Gonzalez-Garcia, M. Maltoni, I. Martinez-Soler, J. a. P. Pinheiro, and T. Schwetz, *NuFit-6.0: Updated global analysis of three-flavor neutrino oscillations* (2024), arXiv:2410.05380 [hep-ph].

[153] M. Aker *et al.* (KATRIN), *Direct neutrino-mass measurement with sub-electronvolt sensitivity*, Nature Phys. **18**, 160 (2022), arXiv:2105.08533 [hep-ex].

[154] S. Saad, *Simplest Radiative Dirac Neutrino Mass Models*, Nucl. Phys. B **943**, 114636 (2019), arXiv:1902.07259 [hep-ph].

[155] P. B. Pal, *Dirac, Majorana and Weyl fermions*, Am. J. Phys. **79**, 485 (2011), arXiv:1006.1718 [hep-ph].

[156] S. Weinberg, *Baryon and Lepton Nonconserving Processes*, Phys. Rev. Lett. **43**, 1566 (1979).

[157] S. L. Adler, *Axial vector vertex in spinor electrodynamics*, Phys. Rev. **177**, 2426 (1969).

[158] J. S. Bell and R. Jackiw, *A PCAC puzzle:* $\pi^0 \to \gamma\gamma$ *in the* σ *model*, Nuovo Cim. A **60**, 47 (1969).

[159] J. Schechter and J. W. F. Valle, *Neutrinoless Double beta Decay in SU(2)* $\times$ *U(1) Theories*, Phys. Rev. D **25**, 2951 (1982).

[160] I. J. Arnquist *et al.* (Majorana), *Final Result of the Majorana Demonstrator's Search for Neutrinoless Double-*β *Decay in Ge76*, Phys. Rev. Lett. **130**, 062501 (2023), arXiv:2207.07638 [nucl-ex].

[161] S. Abe *et al.* (KamLAND-Zen), *Search for Majorana Neutrinos with the Complete KamLAND-Zen Dataset* (2024), arXiv:2406.11438 [hep-ex].

[162] T. Hahn, *Routines for the diagonalization of complex matrices* (2006), arXiv:physics/0607103.

[163] K. D. Ikramov, *Takagi's decomposition of a symmetric unitary matrix as a finite algorithm*, Computational Mathematics and Mathematical Physics **52**, 1–3 (2012).

[164] B. Pontecorvo, *Inverse beta processes and nonconservation of lepton charge*, Zh. Eksp. Teor. Fiz. **34**, 247 (1957).

[165] Z. Maki, M. Nakagawa, and S. Sakata, *Remarks on the unified model of elementary particles*, Prog. Theor. Phys. **28**, 870 (1962).

[166] S. P. Mikheev and A. Y. Smirnov, *Resonant amplification of neutrino oscillations in matter and solar neutrino spectroscopy*, Nuovo Cim. C **9**, 17 (1986).

[167] L. Wolfenstein, *Neutrino Oscillations in Matter*, Phys. Rev. D **17**, 2369 (1978).

[168] F. An *et al.* (JUNO), *Neutrino Physics with JUNO*, J. Phys. G **43**, 030401 (2016), arXiv:1507.05613 [physics.ins-det].

[169] B. Abi *et al.* (DUNE), *Deep Underground Neutrino Experiment (DUNE), Far Detector Technical Design Report, Volume I Introduction to DUNE*, JINST **15** (08), T08008, arXiv:2002.02967 [physics.ins-det].

[170] K. Abe *et al.* (Hyper-Kamiokande), *Hyper-Kamiokande Design Report* (2018), arXiv:1805.04163 [physics.ins-det].

[171] S. Antusch, C. Biggio, E. Fernandez-Martinez, M. B. Gavela, and J. Lopez-Pavon, *Unitarity of the Leptonic Mixing Matrix*, JHEP **10** (2006), 084, arXiv:hep-ph/0607020.

[172] S. Antusch and O. Fischer, *Non-unitarity of the leptonic mixing matrix: Present bounds and future sensitivities*, JHEP **10** (2014), 094, arXiv:1407.6607 [hep-ph].

[173] A. Abada, C. Biggio, F. Bonnet, M. B. Gavela, and T. Hambye, *Low energy effects of neutrino masses*, JHEP **12** (2007), 061, arXiv:0707.4058 [hep-ph].

[174] C. Biggio, E. Fernandez-Martinez, M. Filaci, J. Hernandez-Garcia, and J. Lopez-Pavon, *Global Bounds on the Type-III Seesaw*, JHEP **05** (2020), 022, arXiv:1911.11790 [hep-ph].

[175] T. D. Lee, *A Theory of Spontaneous T Violation*, Phys. Rev. D **8**, 1226 (1973).

[176] E. Gildener and S. Weinberg, *Symmetry Breaking and Scalar Bosons*, Phys. Rev. D **13**, 3333 (1976).

[177] G. C. Branco, P. M. Ferreira, L. Lavoura, M. N. Rebelo, M. Sher, and J. P. Silva, *Theory and phenomenology of two-Higgs-doublet models*, Phys. Rept. **516**, 1 (2012), arXiv:1106.0034 [hep-ph].

[178] J. F. Gunion and H. E. Haber, *The CP conserving two Higgs doublet model: The Approach to the decoupling limit*, Phys. Rev. D **67**, 075019 (2003), arXiv:hep-ph/0207010.

[179] J. Herrero-García, T. Ohlsson, S. Riad, and J. Wirén, *Full parameter scan of the Zee model: exploring Higgs lepton flavor violation*, JHEP **04** (2017), 130, arXiv:1701.05345 [hep-ph].

[180] I. Cordero-Carrión, M. Hirsch, and A. Vicente, *General parametrization of Majorana neutrino mass models*, Phys. Rev. D **101**, 075032 (2020), arXiv:1912.08858 [hep-ph].

[181] L. Wolfenstein, *A Theoretical Pattern for Neutrino Oscillations*, Nucl. Phys. B **175**, 93 (1980).

[182] Y. Koide, *Can the Zee model explain the observed neutrino data?*, Phys. Rev. D **64**, 077301 (2001), arXiv:hep-ph/0104226.

[183] X.-G. He, *Is the Zee model neutrino mass matrix ruled out?*, Eur. Phys. J. C **34**, 371 (2004), arXiv:hep-ph/0307172.

[184] X.-G. He and S. K. Majee, *Implications of Recent Data on Neutrino Mixing and Lepton Flavour Violating Decays for the Zee Model*, JHEP **03** (2012), 023, arXiv:1111.2293 [hep-ph].

[185] I. Brivio, *SMEFTsim 3.0 — a practical guide*, JHEP **04** (2021), 073, arXiv:2012.11343 [hep-ph].

[186] T. Cohen, *As Scales Become Separated: Lectures on Effective Field Theory*, PoS **TASI2018**, 011 (2019), arXiv:1903.03622 [hep-ph].

[187] A. V. Manohar, in *Effective Field Theory in Particle Physics and Cosmology: Lecture Notes of the Les Houches Summer School: Volume 108, July 2017* (Oxford University Press, 2020), ISBN: 9780198855743, arXiv:1804.05863 [hep-ph].

[188] R. Penco, *An Introduction to Effective Field Theories* (2020), arXiv:2006.16285 [hep-th].

[189] G. Isidori, F. Wilsch, and D. Wyler, *The standard model effective field theory at work*, Rev. Mod. Phys. **96**, 015006 (2024), arXiv:2303.16922 [hep-ph].

[190] R. Alonso, E. E. Jenkins, A. V. Manohar, and M. Trott, *Renormalization Group Evolution of the Standard Model Dimension Six Operators III: Gauge Coupling Dependence and Phenomenology*, JHEP **04** (2014), 159, arXiv:1312.2014 [hep-ph].

[191] L. Berthier and M. Trott, *Towards consistent Electroweak Precision Data constraints in the SMEFT*, JHEP **05** (2015), 024, arXiv:1502.02570 [hep-ph].

[192] I. Brivio and M. Trott, *The Standard Model as an Effective Field Theory*, Phys. Rept. **793**, 1 (2019), arXiv:1706.08945 [hep-ph].

[193] J. Fuentes-Martin, J. Portoles, and P. Ruiz-Femenia, *Integrating out heavy particles with functional methods: a simplified framework*, JHEP **09** (2016), 156, arXiv:1607.02142 [hep-ph].

[194] Z. Zhang, *Covariant diagrams for one-loop matching*, JHEP **05** (2017), 152, arXiv:1610.00710 [hep-ph].

[195] T. Cohen, X. Lu, and Z. Zhang, *Functional Prescription for EFT Matching*, JHEP **02** (2021), 228, arXiv:2011.02484 [hep-ph].

[196] J. Fuentes-Martin, M. König, J. Pagès, A. E. Thomsen, and F. Wilsch, *SuperTracer: A Calculator of Functional Supertraces for One-Loop EFT Matching*, JHEP **04** (2021), 281, arXiv:2012.08506 [hep-ph].

[197] J. Fuentes-Martín, M. König, J. Pagès, A. E. Thomsen, and F. Wilsch, *A proof of concept for matchete: an automated tool for matching effective theories*, Eur. Phys. J. C **83**, 662 (2023), arXiv:2212.04510 [hep-ph].

[198] B. Grzadkowski, M. Iskrzynski, M. Misiak, and J. Rosiek, *Dimension-Six Terms in the Standard Model Lagrangian*, JHEP **10** (2010), 085, arXiv:1008.4884 [hep-ph].

[199] E. E. Jenkins, A. V. Manohar, and P. Stoffer, *Low-Energy Effective Field Theory below the Electroweak Scale: Operators and Matching*, JHEP **03** (2018), 016, arXiv:1709.04486 [hep-ph].

[200] A. Celis, J. Fuentes-Martin, A. Vicente, and J. Virto, *DsixTools: The Standard Model Effective Field Theory Toolkit*, Eur. Phys. J. C **77**, 405 (2017), arXiv:1704.04504 [hep-ph].

[201] J. Fuentes-Martin, P. Ruiz-Femenia, A. Vicente, and J. Virto, *DsixTools 2.0: The Effective Field Theory Toolkit*, Eur. Phys. J. C **81**, 167 (2021), arXiv:2010.16341 [hep-ph].

[202] J. Aebischer, J. Kumar, and D. M. Straub, *Wilson: a Python package for the running and matching of Wilson coefficients above and below the electroweak scale*, Eur. Phys. J. C **78**, 1026 (2018), arXiv:1804.05033 [hep-ph].

[203] I. Brivio, Y. Jiang, and M. Trott, *The SMEFTsim package, theory and tools*, JHEP **12** (2017), 070, arXiv:1709.06492 [hep-ph].

[204] A. Dedes, W. Materkowska, M. Paraskevas, J. Rosiek, and K. Suxho, *Feynman rules for the Standard Model Effective Field Theory in R_ξ-gauges*, JHEP **06** (2017), 143, arXiv:1704.03888 [hep-ph].

[205] A. Dedes, M. Paraskevas, J. Rosiek, K. Suxho, and L. Trifyllis, *SmeftFR – Feynman rules generator for the Standard Model Effective Field Theory*, Comput. Phys. Commun. **247**, 106931 (2020), arXiv:1904.03204 [hep-ph].

[206] A. Dedes, J. Rosiek, M. Ryczkowski, K. Suxho, and L. Trifyllis, *SmeftFR v3 – Feynman rules generator for the Standard Model Effective Field Theory*, Comput. Phys. Commun. **294**, 108943 (2024), arXiv:2302.01353 [hep-ph].

[207] A. Carmona, A. Lazopoulos, P. Olgoso, and J. Santiago, *Matchmakereft: automated tree-level and one-loop matching*, SciPost Phys. **12**, 198 (2022), arXiv:2112.10787 [hep-ph].

[208] F. del Aguila, S. Bar-Shalom, A. Soni, and J. Wudka, *Heavy Majorana Neutrinos in the Effective Lagrangian Description: Application to Hadron Colliders*, Phys. Lett. B **670**, 399 (2009), arXiv:0806.0876 [hep-ph].

[209] Y. Liao and X.-D. Ma, *Operators up to Dimension Seven in Standard Model Effective Field Theory Extended with Sterile Neutrinos*, Phys. Rev. D **96**, 015012 (2017), arXiv:1612.04527 [hep-ph].

[210] J. Aebischer, W. Altmannshofer, E. E. Jenkins, and A. V. Manohar, *Dark matter effective field theory and an application to vector dark matter*, JHEP **06** (2022), 086, arXiv:2202.06968 [hep-ph].

[211] I. Brivio and M. Trott, *Scheming in the SMEFT... and a reparameterization invariance!*, JHEP **07** (2017), 148, [Addendum: JHEP 05, 136 (2018)], arXiv:1701.06424 [hep-ph].

[212] I. Brivio, S. Dawson, J. de Blas, G. Durieux, P. Savard, A. Denner, A. Freitas, C. Hays, B. Pecjak, and A. Vicini, *Electroweak input parameters* (2021), arXiv:2111.12515 [hep-ph].

[213] E. E. Jenkins, A. V. Manohar, and P. Stoffer, *Low-Energy Effective Field Theory below the Electroweak Scale: Anomalous Dimensions*, JHEP **01** (2018), 084, [Erratum: JHEP 12, 042 (2023)], arXiv:1711.05270 [hep-ph].

[214] E. Aslanides *et al.*, *Charting the European Course to the High-Energy Frontier* (2019), arXiv:1912.13466 [hep-ex].

[215] F. del Aguila, J. A. Aguilar-Saavedra, A. Martinez de la Ossa, and D. Meloni, *Flavor and polarisation in heavy neutrino production at e^+e^- colliders*, Phys. Lett. B **613**, 170 (2005), arXiv:hep-ph/0502189.

[216] F. del Aguila and J. A. Aguilar-Saavedra, *$\ell W\nu$ production at CLIC: A Window to TeV scale non-decoupled neutrinos*, JHEP **05** (2005), 026, arXiv:hep-ph/0503026.

[217] S. Antusch and O. Fischer, *Testing sterile neutrino extensions of the Standard Model at future lepton colliders*, JHEP **05** (2015), 053, arXiv:1502.05915 [hep-ph].

[218] S. Antusch, E. Cazzato, and O. Fischer, *Higgs production from sterile neutrinos at future lepton colliders*, JHEP **04** (2016), 189, arXiv:1512.06035 [hep-ph].

[219] S. Antusch, E. Cazzato, and O. Fischer, *Displaced vertex searches for sterile neutrinos at future lepton colliders*, JHEP **12** (2016), 007, arXiv:1604.02420 [hep-ph].

[220] Y. Zhang and B. Zhang, *A potential scenario for Majorana neutrino detection at future lepton colliders*, JHEP **02** (2019), 175, arXiv:1805.09520 [hep-ph].

[221] A. Das, S. Jana, S. Mandal, and S. Nandi, *Probing right handed neutrinos at the LHeC and lepton colliders using fat jet signatures*, Phys. Rev. D **99**, 055030 (2019), arXiv:1811.04291 [hep-ph].

[222] D. Barducci, E. Bertuzzo, A. Caputo, P. Hernandez, and B. Mele, *The see-saw portal at future Higgs Factories*, JHEP **03** (2021), 117, arXiv:2011.04725 [hep-ph].

[223] Y. Gao and K. Wang, *Heavy neutrino searches via same-sign lepton pairs at a Higgs boson factory*, Phys. Rev. D **105**, 076005 (2022), arXiv:2102.12826 [hep-ph].

[224] F. F. Deppisch, P. S. Bhupal Dev, and A. Pilaftsis, *Neutrinos and Collider Physics*, New J. Phys. **17**, 075019 (2015), arXiv:1502.06541 [hep-ph].

[225] Y. Cai, T. Han, T. Li, and R. Ruiz, *Lepton Number Violation: Seesaw Models and Their Collider Tests*, Front. in Phys. **6**, 40 (2018), arXiv:1711.02180 [hep-ph].

[226] A. Das, *Searching for the minimal Seesaw models at the LHC and beyond*, Adv. High Energy Phys. **2018**, 9785318 (2018), arXiv:1803.10940 [hep-ph].

[227] A. M. Abdullahi *et al.*, *The present and future status of heavy neutral leptons*, J. Phys. G **50**, 020501 (2023), arXiv:2203.08039 [hep-ph].

[228] A. Das and S. Mandal, *Bounds on the triplet fermions in type-III seesaw and implications for collider searches*, Nucl. Phys. B **966**, 115374 (2021), arXiv:2006.04123 [hep-ph].

[229] C. A. Argüelles *et al.*, *Snowmass White Paper: Beyond the Standard Model effects on Neutrino Flavor*, Eur. Phys. J. C **83**, 15 (2023), arXiv:2203.10811 [hep-ph].

[230] S.-F. Ge, H.-J. He, and R.-Q. Xiao, *Probing new physics scales from Higgs and electroweak observables at e^+e^- Higgs factory*, JHEP **10** (2016), 007, arXiv:1603.03385 [hep-ph].

[231] J. Baglio and C. Weiland, *The triple Higgs coupling: A new probe of low-scale seesaw models*, JHEP **04** (2017), 038, arXiv:1612.06403 [hep-ph].

[232] J. Baglio and C. Weiland, *Heavy neutrino impact on the triple Higgs coupling*, Phys. Rev. D **94**, 013002 (2016), arXiv:1603.00879 [hep-ph].

[233] A. Freitas and Q. Song, *Two-Loop Electroweak Corrections with Fermion Loops to $e^+e^- \to ZH$*, Phys. Rev. Lett. **130**, 031801 (2023), arXiv:2209.07612 [hep-ph].

[234] X. Chen, X. Guan, C.-Q. He, Z. Li, X. Liu, and Y.-Q. Ma, *Complete two-loop electroweak corrections to $e^+e^- \to HZ$* (2022), arXiv:2209.14953 [hep-ph].

[235] J. Fleischer and F. Jegerlehner, *Radiative corrections to Higgs production by $e^+e^- \to Zh$ in the Weinberg-Salam model*, Nuclear Physics B **216**, 469 (1983).

[236] B. A. Kniehl, *Radiative corrections for associated ZH production at future e^+e^- colliders*, Zeitschrift für Physik C Particles and Fields **55**, 605 (1991).

[237] A. Denner, J. Kublbeck, R. Mertig, and M. Bohm, *Electroweak radiative corrections to $e^+e^- \to Zh$*, Z. Phys. C **56**, 261 (1992).

[238] S. Bondarenko, Y. Dydyshka, L. Kalinovskaya, L. Rumyantsev, R. Sadykov, and V. Yermolchyk, *One-loop electroweak radiative corrections to polarized $e^+e^- \to ZH$*, Phys. Rev. D **100**, 073002 (2019), arXiv:1812.10965 [hep-ph].

[239] Y. Gong, Z. Li, X. Xu, L. L. Yang, and X. Zhao, *Mixed QCD-EW corrections for Higgs boson production at e^+e^- colliders*, Phys. Rev. D **95**, 093003 (2017), arXiv:1609.03955 [hep-ph].

[240] Q.-F. Sun, F. Feng, Y. Jia, and W.-L. Sang, *Mixed electroweak-QCD corrections to $e^+e^- \to ZH$ at Higgs factories*, Phys. Rev. D **96**, 051301 (2017), arXiv:1609.03995 [hep-ph].

[241] W. Chen, F. Feng, Y. Jia, and W.-L. Sang, *Mixed electroweak-QCD corrections to $e^+e^- \to \mu^+\mu^- H$ at CEPC with finite-width effect*, Chin. Phys. C **43**, 013108 (2019), arXiv:1811.05453 [hep-ph].

[242] H. Abramowicz *et al.*, *Higgs physics at the CLIC electron–positron linear collider*, Eur. Phys. J. C **77**, 475 (2017), arXiv:1608.07538 [hep-ex].

[243] J. Kersten and A. Y. Smirnov, *Right-Handed Neutrinos at CERN LHC and the Mechanism of Neutrino Mass Generation*, Phys. Rev. D **76**, 073005 (2007), arXiv:0705.3221 [hep-ph].

[244] M. Drewes, J. Klarić, and P. Klose, *On lepton number violation in heavy neutrino decays at colliders*, JHEP **11** (2019), 032, arXiv:1907.13034 [hep-ph].

[245] A. Abada, P. Escribano, X. Marcano, and G. Piazza, *Collider searches for heavy neutral leptons: beyond simplified scenarios* (2022), arXiv:2208.13882 [hep-ph].

[246] D. Wyler and L. Wolfenstein, *Massless Neutrinos in Left-Right Symmetric Models*, Nucl. Phys. B **218**, 205 (1983).

[247] J. Bernabeu, A. Santamaria, J. Vidal, A. Mendez, and J. W. F. Valle, *Lepton Flavor Nonconservation at High-Energies in a Superstring Inspired Standard Model*, Phys. Lett. B **187**, 303 (1987).

[248] G. C. Branco, W. Grimus, and L. Lavoura, *The Seesaw Mechanism in the Presence of a Conserved Lepton Number*, Nucl. Phys. B **312**, 492 (1989).

[249] D. Tommasini, G. Barenboim, J. Bernabeu, and C. Jarlskog, *Nondecoupling of heavy neutrinos and lepton flavor violation*, Nucl. Phys. B **444**, 451 (1995), arXiv:hep-ph/9503228.

[250] A. Pilaftsis, *Resonant tau-leptogenesis with observable lepton number violation*, Phys. Rev. Lett. **95**, 081602 (2005), arXiv:hep-ph/0408103.

[251] A. Pilaftsis and T. E. J. Underwood, *Electroweak-scale resonant leptogenesis*, Phys. Rev. D **72**, 113001 (2005), arXiv:hep-ph/0506107.

[252] M. Shaposhnikov, *A Possible symmetry of the νMSM*, Nucl. Phys. B **763**, 49 (2007), arXiv:hep-ph/0605047.

[253] M. B. Gavela, T. Hambye, D. Hernandez, and P. Hernandez, *Minimal Flavour Seesaw Models*, JHEP **09** (2009), 038, arXiv:0906.1461 [hep-ph].

[254] O. J. P. Eboli, J. Gonzalez-Fraile, and M. C. Gonzalez-Garcia, *Neutrino Masses at LHC: Minimal Lepton Flavour Violation in Type-III See-saw*, JHEP **12** (2011), 009, arXiv:1108.0661 [hep-ph].

[255] E. Fernandez-Martinez, J. Hernandez-Garcia, J. Lopez-Pavon, and M. Lucente, *Loop level constraints on Seesaw neutrino mixing*, JHEP **10** (2015), 130, arXiv:1508.03051 [hep-ph].

[256] Y. Du, X.-X. Li, and J.-H. Yu, *Neutrino seesaw models at one-loop matching: discrimination by effective operators*, JHEP **09** (2022), 207, arXiv:2201.04646 [hep-ph].

[257] D. Zhang and S. Zhou, *Complete one-loop matching of the type-I seesaw model onto the Standard Model effective field theory*, JHEP **09** (2021), 163, arXiv:2107.12133 [hep-ph].

[258] R. Coy and M. Frigerio, *Effective comparison of neutrino-mass models*, Phys. Rev. D **105**, 115041 (2022), arXiv:2110.09126 [hep-ph].

[259] R. N. Mohapatra, *Mechanism for Understanding Small Neutrino Mass in Superstring Theories*, Phys. Rev. Lett. **56**, 561 (1986).

[260] R. N. Mohapatra and J. W. F. Valle, *Neutrino Mass and Baryon Number Nonconservation in Superstring Models*, Phys. Rev. D **34**, 1642 (1986).

[261] E. K. Akhmedov, M. Lindner, E. Schnapka, and J. W. F. Valle, *Left-right symmetry breaking in NJL approach*, Phys. Lett. B **368**, 270 (1996), arXiv:hep-ph/9507275.

[262] E. K. Akhmedov, M. Lindner, E. Schnapka, and J. W. F. Valle, *Dynamical left-right symmetry breaking*, Phys. Rev. D **53**, 2752 (1996), arXiv:hep-ph/9509255.

[263] A. Donini, P. Hernandez, J. Lopez-Pavon, M. Maltoni, and T. Schwetz, *The minimal 3+2 neutrino model versus oscillation anomalies*, JHEP **07** (2012), 161, arXiv:1205.5230 [hep-ph].

[264] M. Blennow, E. Fernández-Martínez, J. Hernández-García, J. López-Pavón, X. Marcano, and D. Naredo-Tuero, *Bounds on lepton non-unitarity and heavy neutrino mixing*, JHEP **08** (2023), 030, arXiv:2306.01040 [hep-ph].

[265] A. Hayrapetyan *et al.* (CMS), *Review of searches for vector-like quarks, vector-like leptons, and heavy neutral leptons in proton-proton collisions at* $\sqrt{s} = 13$ *TeV at the CMS experiment* (2024), arXiv:2405.17605 [hep-ex].

[266] A. M. Sirunyan *et al.* (CMS), *Search for heavy neutral leptons in events with three charged leptons in proton-proton collisions at* $\sqrt{s} = 13$ *TeV*, Phys. Rev. Lett. **120**, 221801 (2018), arXiv:1802.02965 [hep-ex].

[267] A. Tumasyan *et al.* (CMS), *Probing Heavy Majorana Neutrinos and the Weinberg Operator through Vector Boson Fusion Processes in Proton-Proton Collisions at s=13 TeV*, Phys. Rev. Lett. **131**, 011803 (2023), arXiv:2206.08956 [hep-ex].

[268] B. Kniehl and A. Pilaftsis, *Quantum effects on Higgs-boson production and decay due to Majorana neutrinos*, Nucl. Phys. B **424**, 18 (1994), arXiv:hep-ph/9402314 [hep-ph].

[269] J. Yan, S. Watanuki, K. Fujii, A. Ishikawa, D. Jeans, J. Strube, J. Tian, and H. Yamamoto, *Measurement of the Higgs boson mass and* $e^+e^- \to ZH$ *cross section using* $Z \to \mu^+\mu^-$ *and* $Z \to e^+e^-$ *at the ILC*, Phys. Rev. D **94**, 113002 (2016), [Erratum: Phys.Rev.D 103, 099903 (2021)], arXiv:1604.07524 [hep-ex].

[270] M. Thomson, *Model-independent measurement of the* $e^+e^- \to HZ$ *cross section at a future* e^+e^- *linear collider using hadronic Z decays*, Eur. Phys. J. C **76**, 72 (2016), arXiv:1509.02853 [hep-ex].

[271] A. Miyamoto, *A measurement of the total cross section of* σ_{Zh} *at a future* e^+e^- *collider using the hadronic decay mode of Z* (2013), arXiv:1311.2248 [hep-ex].

[272] S. Schael *et al.* (ALEPH, DELPHI, L3, OPAL, SLD, LEP Electroweak Working Group, SLD Electroweak Group, SLD Heavy Flavour Group), *Precision electroweak measurements on the Z resonance*, Phys. Rept. **427**, 257 (2006), arXiv:hep-ex/0509008 [hep-ex].

[273] J. de Blas, M. Ciuchini, E. Franco, A. Goncalves, S. Mishima, M. Pierini, L. Reina, and L. Silvestrini, *Global analysis of electroweak data in the Standard Model*, Phys. Rev. D **106**, 033003 (2022), arXiv:2112.07274 [hep-ph].

[274] R. L. Workman (Particle Data Group), *Review of Particle Physics*, PTEP **2022**, 083C01 (2022).

[275] T. Aaltonen *et al.* (CDF), *High-precision measurement of the W boson mass with the CDF II detector*, Science **376**, 170 (2022).

[276] A. Crivellin and M. Hoferichter, *β Decays as Sensitive Probes of Lepton Flavor Universality*, Phys. Rev. Lett. **125**, 111801 (2020), arXiv:2002.07184 [hep-ph].

[277] D. Bryman, V. Cirigliano, A. Crivellin, and G. Inguglia, *Testing Lepton Flavor Universality with Pion, Kaon, Tau, and Beta Decays*, Ann. Rev. Nucl. Part. Sci. **72**, 69 (2022), arXiv:2111.05338 [hep-ph].

[278] A. Pich, *Challenges for tau physics at the TeraZ*, Eur. Phys. J. Plus **136**, 1117 (2021), arXiv:2012.07099 [hep-ph].

[279] C.-Y. Seng, D. Galviz, M. Gorchtein, and U.-G. Meißner, *Complete theory of radiative corrections to $K_{\ell 3}$ decays and the V_{us} update*, JHEP **07** (2022), 071, arXiv:2203.05217 [hep-ph].

[280] G. 't Hooft, *Symmetry Breaking Through Bell-Jackiw Anomalies*, Phys. Rev. Lett. **37**, 8 (1976).

[281] A. Crivellin, F. Kirk, and C. A. Manzari, *Comprehensive analysis of charged lepton flavour violation in the symmetry protected type-I seesaw*, JHEP **12** (2022), 031, arXiv:2208.00020 [hep-ph].

[282] A. M. Baldini *et al.* (MEG), *Search for the lepton flavour violating decay $\mu^+ \to e^+\gamma$ with the full dataset of the MEG experiment*, Eur. Phys. J. C **76**, 434 (2016), arXiv:1605.05081 [hep-ex].

[283] A. M. Baldini *et al.* (MEG II), *The Search for $\mu^+ \to e^+\gamma$ with 10^{-14} Sensitivity: the Upgrade of the MEG Experiment*, Symmetry **13**, 1591 (2021), arXiv:2107.10767 [hep-ex].

[284] U. Bellgardt *et al.* (SINDRUM), *Search for the Decay $\mu^+ \to e^+e^+e^-$*, Nucl. Phys. B **299**, 1 (1988).

[285] A. Blondel *et al.*, *Research Proposal for an Experiment to Search for the Decay $\mu \to eee$* (2013), arXiv:1301.6113 [physics.ins-det].

[286] W. H. Bertl *et al.* (SINDRUM II), *A Search for muon to electron conversion in muonic gold*, Eur. Phys. J. C **47**, 337 (2006).

[287] R. Abramishvili *et al.* (COMET), *COMET Phase-I Technical Design Report*, PTEP **2020**, 033C01 (2020), arXiv:1812.09018 [physics.ins-det].

[288] M. T. Hedges (Mu2e), *The Mu2e experiment — Searching for charged lepton flavor violation*, Nucl. Instrum. Meth. A **1045**, 167589 (2023), arXiv:2210.14317 [hep-ex].

[289] P. Wintz, *Results of the SINDRUM-II experiment*, Conf. Proc. C **980420**, 534 (1998).

[290] Y. Kuno, *PRISM/PRIME*, Nucl. Phys. B Proc. Suppl. **149**, 376 (2005).

[291] W. Honecker *et al.* (SINDRUM II), *Improved limit on the branching ratio of $\mu \to e$ conversion on lead*, Phys. Rev. Lett. **76**, 200 (1996).

[292] A. Badertscher *et al.*, *New Upper Limits for Muon - Electron Conversion in Sulfur*, Lett. Nuovo Cim. **28**, 401 (1980).

[293] B. Aubert *et al.* (BaBar), *Searches for Lepton Flavor Violation in the Decays $\tau^\pm \to e^\pm\gamma$ and $\tau^\pm \to \mu^\pm\gamma$*, Phys. Rev. Lett. **104**, 021802 (2010), arXiv:0908.2381 [hep-ex].

[294] S. Banerjee *et al.*, *Snowmass 2021 White Paper: Charged lepton flavor violation in the tau sector*, (2022), arXiv:2203.14919 [hep-ph].

[295] K. Hayasaka *et al.*, *Search for Lepton Flavor Violating Tau Decays into Three Leptons with 719 Million Produced $\tau^+\tau^-$ Pairs*, Phys. Lett. B **687**, 139 (2010), arXiv:1001.3221 [hep-ex].

[296] Y. Kuno and Y. Okada, *Muon decay and physics beyond the standard model*, Rev. Mod. Phys. **73**, 151 (2001), arXiv:hep-ph/9909265.

[297] L. Calibbi, X. Marcano, and J. Roy, *Z lepton flavour violation as a probe for new physics at future e^+e^- colliders*, Eur. Phys. J. C **81**, 1054 (2021), arXiv:2107.10273 [hep-ph].

[298] A. Brignole and A. Rossi, *Anatomy and phenomenology of mu-tau lepton flavor violation in the MSSM*, Nucl. Phys. B **701**, 3 (2004), arXiv:hep-ph/0404211.

[299] R. Kitano, M. Koike, and Y. Okada, *Detailed calculation of lepton flavor violating muon electron conversion rate for various nuclei*, Phys. Rev. D **66**, 096002 (2002), [Erratum: Phys.Rev.D 76, 059902 (2007)], arXiv:hep-ph/0203110.

[300] V. Cirigliano, R. Kitano, Y. Okada, and P. Tuzon, *On the model discriminating power of $\mu \to e$ conversion in nuclei*, Phys. Rev. D **80**, 013002 (2009), arXiv:0904.0957 [hep-ph].

[301] T. Suzuki, D. F. Measday, and J. P. Roalsvig, *Total nuclear capture rates for negative muons*, Phys. Rev. C **35**, 2212 (1987).

[302] R. Alonso, M. Dhen, M. B. Gavela, and T. Hambye, *Muon conversion to electron in nuclei in type-I seesaw models*, JHEP **01** (2013), 118, arXiv:1209.2679 [hep-ph].

[303] N. Craig, J. Gu, Z. Liu, and K. Wang, *Beyond Higgs Couplings: Probing the Higgs with Angular Observables at Future e^+e^- Colliders*, JHEP **03** (2016), 050, arXiv:1512.06877 [hep-ph].

[304] G. Elor *et al.*, *New Ideas in Baryogenesis: A Snowmass White Paper*, (2022), arXiv:2203.05010 [hep-ph].

[305] M. D'Onofrio, K. Rummukainen, and A. Tranberg, *Sphaleron Rate in the Minimal Standard Model*, Phys. Rev. Lett. **113**, 141602 (2014), arXiv:1404.3565 [hep-ph].

[306] F. R. Klinkhamer and N. S. Manton, *A Saddle Point Solution in the Weinberg-Salam Theory*, Phys. Rev. D **30**, 2212 (1984).

[307] P. B. Arnold and L. D. McLerran, *Sphalerons, Small Fluctuations and Baryon Number Violation in Electroweak Theory*, Phys. Rev. D **36**, 581 (1987).

[308] P. B. Arnold and L. D. McLerran, *The Sphaleron Strikes Back*, Phys. Rev. D **37**, 1020 (1988).

[309] V. A. Rubakov, *Classical theory of gauge fields* (Princeton University Press, Princeton, New Jersey, 2002), ISBN: 978-0-691-05927-3, 978-0-691-05927-3.

[310] N. S. Manton and P. Sutcliffe, *Topological solitons*, Cambridge Monographs on Mathematical Physics (Cambridge University Press, 2004), ISBN: 978-0-521-04096-9, 978-0-521-83836-8, 978-0-511-20783-9.

[311] E. J. Weinberg, *Classical solutions in quantum field theory: Solitons and Instantons in High Energy Physics*, Cambridge Monographs on Mathematical Physics (Cambridge University Press, 2012), ISBN: 978-0-521-11463-9, 978-1-139-57461-7, 978-0-521-11463-9, 978-1-107-43805-7.

[312] C. Abel *et al.*, *Measurement of the Permanent Electric Dipole Moment of the Neutron*, Phys. Rev. Lett. **124**, 081803 (2020), arXiv:2001.11966 [hep-ex].

[313] V. A. Kuzmin, V. A. Rubakov, and M. E. Shaposhnikov, *On the Anomalous Electroweak Baryon Number Nonconservation in the Early Universe*, Phys. Lett. B **155**, 36 (1985).

[314] M. E. Shaposhnikov, *Possible Appearance of the Baryon Asymmetry of the Universe in an Electroweak Theory*, JETP Lett. **44**, 465 (1986).

[315] M. E. Shaposhnikov, *Baryon Asymmetry of the Universe in Standard Electroweak Theory*, Nucl. Phys. B **287**, 757 (1987).

[316] D. E. Morrissey and M. J. Ramsey-Musolf, *Electroweak baryogenesis*, New J. Phys. **14**, 125003 (2012), arXiv:1206.2942 [hep-ph].

[317] K. Kajantie, M. Laine, K. Rummukainen, and M. E. Shaposhnikov, *A Nonperturbative analysis of the finite T phase transition in SU(2) x U(1) electroweak theory*, Nucl. Phys. B **493**, 413 (1997), arXiv:hep-lat/9612006.

[318] M. Laine and K. Rummukainen, *What's new with the electroweak phase transition?*, Nucl. Phys. B Proc. Suppl. **73**, 180 (1999), arXiv:hep-lat/9809045.

[319] A. G. Cohen, D. B. Kaplan, and A. E. Nelson, *Progress in electroweak baryogenesis*, Ann. Rev. Nucl. Part. Sci. **43**, 27 (1993), arXiv:hep-ph/9302210.

[320] S. J. Huber and M. G. Schmidt, *Electroweak baryogenesis: Concrete in a SUSY model with a gauge singlet*, Nucl. Phys. B **606**, 183 (2001), arXiv:hep-ph/0003122.

[321] C. Balazs, M. Carena, and C. E. M. Wagner, *Dark matter, light stops and electroweak baryogenesis*, Phys. Rev. D **70**, 015007 (2004), arXiv:hep-ph/0403224.

[322] T. Konstandin, T. Prokopec, M. G. Schmidt, and M. Seco, *MSSM electroweak baryogenesis and flavor mixing in transport equations*, Nucl. Phys. B **738**, 1 (2006), arXiv:hep-ph/0505103.

[323] L. Fromme, S. J. Huber, and M. Seniuch, *Baryogenesis in the two-Higgs doublet model*, JHEP **11** (2006), 038, arXiv:hep-ph/0605242.

[324] S. J. Huber, T. Konstandin, T. Prokopec, and M. G. Schmidt, *Electroweak Phase Transition and Baryogenesis in the nMSSM*, Nucl. Phys. B **757**, 172 (2006), arXiv:hep-ph/0606298.

[325] J. R. Espinosa, B. Gripaios, T. Konstandin, and F. Riva, *Electroweak Baryogenesis in Non-minimal Composite Higgs Models*, JCAP **01** (2012), 012, arXiv:1110.2876 [hep-ph].

[326] G. C. Dorsch, S. J. Huber, T. Konstandin, and J. M. No, *A Second Higgs Doublet in the Early Universe: Baryogenesis and Gravitational Waves*, JCAP **05** (2017), 052, arXiv:1611.05874 [hep-ph].

[327] C. Balazs, G. White, and J. Yue, *Effective field theory, electric dipole moments and electroweak baryogenesis*, JHEP **03** (2017), 030, arXiv:1612.01270 [hep-ph].

[328] I. Baldes and G. Servant, *High scale electroweak phase transition: baryogenesis \& symmetry non-restoration*, JHEP **10** (2018), 053, arXiv:1807.08770 [hep-ph].

[329] I. Baldes, S. Blasi, A. Mariotti, A. Sevrin, and K. Turbang, *Baryogenesis via relativistic bubble expansion*, Phys. Rev. D **104**, 115029 (2021), arXiv:2106.15602 [hep-ph].

[330] W. Buchmuller, R. D. Peccei, and T. Yanagida, *Leptogenesis as the origin of matter*, Ann. Rev. Nucl. Part. Sci. **55**, 311 (2005), arXiv:hep-ph/0502169.

[331] E. K. Akhmedov, V. A. Rubakov, and A. Y. Smirnov, *Baryogenesis via neutrino oscillations*, Phys. Rev. Lett. **81**, 1359 (1998), arXiv:hep-ph/9803255.

[332] K. Dick, M. Lindner, M. Ratz, and D. Wright, *Leptogenesis with Dirac neutrinos*, Phys. Rev. Lett. **84**, 4039 (2000), arXiv:hep-ph/9907562.

[333] H. Murayama and A. Pierce, *Realistic Dirac leptogenesis*, Phys. Rev. Lett. **89**, 271601 (2002), arXiv:hep-ph/0206177.

[334] N. D. Barrie and C. Han, *Affleck-Dine Dirac Leptogenesis* (2024), arXiv:2402.15245 [hep-ph].

[335] L. Covi, E. Roulet, and F. Vissani, *CP violating decays in leptogenesis scenarios*, Phys. Lett. B **384**, 169 (1996), arXiv:hep-ph/9605319.

[336] A. Denner, H. Eck, O. Hahn, and J. Kublbeck, *Compact Feynman rules for Majorana fermions*, Phys. Lett. B **291**, 278 (1992).

[337] A. Denner, H. Eck, O. Hahn, and J. Kublbeck, *Feynman rules for fermion number violating interactions*, Nucl. Phys. B **387**, 467 (1992).

[338] R. E. Cutkosky, *Singularities and Discontinuities of Feynman Amplitudes*, Journal of Mathematical Physics **1**, 429 (1960).

[339] M. L. Bellac and G. Barton, *Quantum and statistical Field Theory* (Oxford University Press, 1992), ISBN: 978-0-19-853964-3.

[340] M. J. G. Veltman, *Diagrammatica: The Path to Feynman rules*, Vol. 4 (Cambridge University Press, 2012), ISBN: 978-1-139-24339-1, 978-0-521-45692-0.

[341] E. W. Kolb and S. Wolfram, *Baryon number generation in the early universe*, Nuclear Physics B **172**, 224 (1980).

[342] T. Blažek and P. Maták, *CP asymmetries and higher-order unitarity relations*, Phys. Rev. D **103**, L091302 (2021), arXiv:2102.05914 [hep-ph].

[343] J. Coster and H. P. Stapp, *Physical-Region Discontinuity Equation*, Journal of Mathematical Physics **11**, 2743 (1970).

[344] J. L. Bourjaily, H. Hannesdottir, A. J. McLeod, M. D. Schwartz, and C. Vergu, *Sequential Discontinuities of Feynman Integrals and the Monodromy Group*, JHEP **01** (2021), 205, arXiv:2007.13747 [hep-th].

[345] H. S. Hannesdottir and S. Mizera, Unitarity implies anomalous thresholds, in *What is the $i\epsilon$ for the S-matrix?* (Springer International Publishing, Cham, 2022), pp. 17–29, ISBN: 978-3-031-18258-7.

[346] E. W. Kolb and S. Wolfram, *The Development of Baryon Asymmetry in the Early Universe*, Phys. Lett. B **91**, 217 (1980).

[347] G. F. Giudice, A. Notari, M. Raidal, A. Riotto, and A. Strumia, *Towards a complete theory of thermal leptogenesis in the SM and MSSM*, Nucl. Phys. B **685**, 89 (2004), arXiv:hep-ph/0310123.

[348] C. S. Fong, *Baryogenesis toolbox in the early universe* (2022), for publicly-accessible resources with overlaps in content see for example Refs. [89; 409; 433].

[349] M. D'Onofrio and K. Rummukainen, *Standard model cross-over on the lattice*, Phys. Rev. D **93**, 025003 (2016), arXiv:1508.07161 [hep-ph].

[350] K. Ala-Mattinen, M. Heikinheimo, K. Tuominen, and K. Kainulainen, *Anatomy of real intermediate state-subtraction scheme*, Phys. Rev. D **108**, 096034 (2023), arXiv:2309.16615 [hep-ph].

[351] V. A. Rubakov and M. E. Shaposhnikov, *Electroweak baryon number nonconservation in the early universe and in high-energy collisions*, Usp. Fiz. Nauk **166**, 493 (1996), arXiv:hep-ph/9603208.

[352] A. Antaramian, L. J. Hall, and A. Rasin, *Hypercharge and the cosmological baryon asymmetry*, Phys. Rev. D **49**, 3881 (1994), arXiv:hep-ph/9311279.

[353] C. S. Fong, *Baryogenesis from Symmetry Principle*, Phys. Lett. B **752**, 247 (2016), arXiv:1508.03648 [hep-ph].

[354] J. A. Harvey and M. S. Turner, *Cosmological baryon and lepton number in the presence of electroweak fermion number violation*, Phys. Rev. D **42**, 3344 (1990).

[355] V. Domcke, Y. Ema, K. Mukaida, and M. Yamada, *Spontaneous Baryogenesis from Axions with Generic Couplings*, JHEP **08** (2020), 096, arXiv:2006.03148 [hep-ph].

[356] C. S. Fong, *Baryogenesis in the Standard Model and its Supersymmetric Extension*, Phys. Rev. D **103**, L051705 (2021), arXiv:2012.03973 [hep-ph].

[357] J. M. Cline, K. Kainulainen, and K. A. Olive, *Protecting the primordial baryon asymmetry from erasure by sphalerons*, Phys. Rev. D **49**, 6394 (1994), arXiv:hep-ph/9401208.

[358] A. Abada, S. Davidson, A. Ibarra, F. X. Josse-Michaux, M. Losada, and A. Riotto, *Flavour Matters in Leptogenesis*, JHEP **09** (2006), 010, arXiv:hep-ph/0605281.

[359] B. Garbrecht and P. Schwaller, *Spectator Effects during Leptogenesis in the Strong Washout Regime*, JCAP **10** (2014), 012, arXiv:1404.2915 [hep-ph].

[360] P. Maták, *Modifying the Dyson series for unstable particles and resonances*, Phys. Rev. D **105**, 076019 (2022), arXiv:2203.01253 [hep-ph].

[361] P. Maták, *Unitarity, real-intermediate states, and fixed-order approach to resonant dark matter annihilation*, Phys. Rev. D **109**, 043008 (2024), arXiv:2305.19238 [hep-ph].

[362] W. Buchmuller and S. Fredenhagen, *Quantum mechanics of baryogenesis*, Phys. Lett. B **483**, 217 (2000), arXiv:hep-ph/0004145.

[363] T. Prokopec, M. G. Schmidt, and S. Weinstock, *Transport equations for chiral fermions to order ħ and electroweak baryogenesis. Part 1*, Annals Phys. **314**, 208 (2004), arXiv:hep-ph/0312110.

[364] T. Prokopec, M. G. Schmidt, and S. Weinstock, *Transport equations for chiral fermions to order ħ and electroweak baryogenesis. Part II*, Annals Phys. **314**, 267 (2004), arXiv:hep-ph/0406140.

[365] M. Beneke, B. Garbrecht, M. Herranen, and P. Schwaller, *Finite Number Density Corrections to Leptogenesis*, Nucl. Phys. B **838**, 1 (2010), arXiv:1002.1326 [hep-ph].

[366] A. Anisimov, W. Buchmüller, M. Drewes, and S. Mendizabal, *Quantum Leptogenesis I*, Annals Phys. **326**, 1998 (2011), [Erratum: Annals Phys. 338, 376–377 (2011)], arXiv:1012.5821 [hep-ph].

[367] M. L. Bellac, *Thermal Field Theory*, Cambridge Monographs on Mathematical Physics (Cambridge University Press, 2011), ISBN: 978-0-511-88506-8, 978-0-521-65477-7.

[368] T. Konstandin, *Quantum Transport and Electroweak Baryogenesis*, Phys. Usp. **56**, 747 (2013), arXiv:1302.6713 [hep-ph].

[369] M. Laine and A. Vuorinen, *Basics of Thermal Field Theory: A Tutorial on Perturbative Computations*, Lecture Notes in Physics (Springer International Publishing, 2016), ISBN: 978-3-319-31932-2.

[370] B. Garbrecht, *Why is there more matter than antimatter? Calculational methods for leptogenesis and electroweak baryogenesis*, Prog. Part. Nucl. Phys. **110**, 103727 (2020), arXiv:1812.02651 [hep-ph].

[371] T. Lundberg and R. Pasechnik, *Thermal Field Theory in real-time formalism: concepts and applications for particle decays*, Eur. Phys. J. A **57**, 71 (2021), arXiv:2007.01224 [hep-th].

[372] M. Becker, E. Copello, J. Harz, and C. Tamarit, *Dark matter freeze-in from non-equilibrium QFT: towards a consistent treatment of thermal effects* (2023), arXiv:2312.17246 [hep-ph].

[373] G. Baym and L. P. Kadanoff, *Conservation Laws and Correlation Functions*, Phys. Rev. **124**, 287 (1961).

[374] B. A. Campbell, S. Davidson, and K. A. Olive, *Inflation, neutrino baryogenesis, and (S)neutrino induced baryogenesis*, Nucl. Phys. B **399**, 111 (1993), arXiv:hep-ph/9302223.

[375] M. Flanz, E. A. Paschos, and U. Sarkar, *Baryogenesis from a lepton asymmetric universe*, Phys. Lett. B **345**, 248 (1995), [Erratum: Phys.Lett.B 384, 487–487 (1996), Erratum: Phys.Lett.B 382, 447–447 (1996)], arXiv:hep-ph/9411366.

[376] M. Plumacher, *Baryon asymmetry, neutrino mixing and supersymmetric SO(10) unification*, Nucl. Phys. B **530**, 207 (1998), arXiv:hep-ph/9704231.

[377] E. Ma and U. Sarkar, *Neutrino masses and leptogenesis with heavy Higgs triplets*, Phys. Rev. Lett. **80**, 5716 (1998), arXiv:hep-ph/9802445.

[378] E. J. Chun and S. K. Kang, *Baryogenesis and degenerate neutrinos*, Phys. Rev. D **63**, 097902 (2001), arXiv:hep-ph/0001296.

[379] T. Hambye, E. Ma, and U. Sarkar, *Supersymmetric triplet Higgs model of neutrino masses and leptogenesis*, Nucl. Phys. B **602**, 23 (2001), arXiv:hep-ph/0011192.

[380] S. Davidson and A. Ibarra, *A Lower bound on the right-handed neutrino mass from leptogenesis*, Phys. Lett. B **535**, 25 (2002), arXiv:hep-ph/0202239.

[381] Y. Grossman, T. Kashti, Y. Nir, and E. Roulet, *Leptogenesis from supersymmetry breaking*, Phys. Rev. Lett. **91**, 251801 (2003), arXiv:hep-ph/0307081.

[382] T. Hambye, Y. Lin, A. Notari, M. Papucci, and A. Strumia, *Constraints on neutrino masses from leptogenesis models*, Nucl. Phys. B **695**, 169 (2004), arXiv:hep-ph/0312203.

[383] W. Buchmuller, P. Di Bari, and M. Plumacher, *Leptogenesis for pedestrians*, Annals Phys. **315**, 305 (2005), arXiv:hep-ph/0401240.

[384] V. Cirigliano, G. Isidori, and V. Porretti, *CP violation and Leptogenesis in models with Minimal Lepton Flavour Violation*, Nucl. Phys. B **763**, 228 (2007), arXiv:hep-ph/0607068.

[385] N. Sahu and U. Sarkar, *Extended Zee model for Neutrino Mass, Leptogenesis and Sterile Neutrino like Dark Matter*, Phys. Rev. D **78**, 115013 (2008), arXiv:0804.2072 [hep-ph].

[386] A. Pilaftsis, *The Little Review on Leptogenesis*, J. Phys. Conf. Ser. **171**, 012017 (2009), arXiv:0904.1182 [hep-ph].

[387] M. Blennow, B. Dasgupta, E. Fernandez-Martinez, and N. Rius, *Aidnogenesis via Leptogenesis and Dark Sphalerons*, JHEP **03** (2011), 014, arXiv:1009.3159 [hep-ph].

[388] C. S. Fong, M. C. Gonzalez-Garcia, E. Nardi, and J. Racker, *Supersymmetric Leptogenesis*, JCAP **12** (2010), 013, arXiv:1009.0003 [hep-ph].

[389] C. S. Fong, M. C. Gonzalez-Garcia, and E. Nardi, *Leptogenesis from Soft Supersymmetry Breaking (Soft Leptogenesis)*, Int. J. Mod. Phys. A **26**, 3491 (2011), arXiv:1107.5312 [hep-ph].

[390] P. Hernández, M. Kekic, J. López-Pavón, J. Racker, and N. Rius, *Leptogenesis in GeV scale seesaw models*, JHEP **10** (2015), 067, arXiv:1508.03676 [hep-ph].

[391] P. Hernández, M. Kekic, J. López-Pavón, J. Racker, and J. Salvado, *Testable Baryogenesis in Seesaw Models*, JHEP **08** (2016), 157, arXiv:1606.06719 [hep-ph].

[392] M. Drewes, B. Garbrecht, P. Hernandez, M. Kekic, J. Lopez-Pavon, J. Racker, N. Rius, J. Salvado, and D. Teresi, *ARS Leptogenesis*, Int. J. Mod. Phys. A **33**, 1842002 (2018), arXiv:1711.02862 [hep-ph].

[393] N. D. Barrie, C. Han, and H. Murayama, *Affleck-Dine Leptogenesis from Higgs Inflation*, Phys. Rev. Lett. **128**, 141801 (2022), arXiv:2106.03381 [hep-ph].

[394] A. E. Nelson and S. M. Barr, *Upper bound on baryogenesis scale from neutrino masses*, Phys. Lett. B **246**, 141 (1990).

[395] B. A. Campbell, S. Davidson, J. R. Ellis, and K. A. Olive, *Cosmological baryon asymmetry constraints on extensions of the standard model*, Phys. Lett. B **256**, 484 (1991).

[396] W. Fischler, G. F. Giudice, R. G. Leigh, and S. Paban, *Constraints on the baryogenesis scale from neutrino masses*, Phys. Lett. B **258**, 45 (1991).

[397] NicePNG, *Royalty free portal*, https://www.nicepng.com/ourpic/u2q8a9q8y3e6e6i1_svg-royalty-free-portal-portal-2-portal-vector/, accessed 2024/08/25.

[398] E. Nardi, Y. Nir, E. Roulet, and J. Racker, *The Importance of flavor in leptogenesis*, JHEP **01** (2006), 164, arXiv:hep-ph/0601084.

[399] D. Aristizabal Sierra, L. A. Munoz, and E. Nardi, *Purely Flavored Leptogenesis*, Phys. Rev. D **80**, 016007 (2009), arXiv:0904.3043 [hep-ph].

[400] H. A. Weldon, *Effective Fermion Masses of Order gT in High Temperature Gauge Theories with Exact Chiral Invariance*, Phys. Rev. D **26**, 2789 (1982).

[401] I. F. Ginzburg, K. A. Kanishev, M. Krawczyk, and D. Sokolowska, *Evolution of Universe to the present inert phase*, Phys. Rev. D **82**, 123533 (2010), arXiv:1009.4593 [hep-ph].

[402] A. Kobakhidze, M. A. Schmidt, and M. Talia, *Mechanism for dark matter depopulation*, Phys. Rev. D **98**, 095026 (2018), arXiv:1712.05170 [hep-ph].

[403] G. Raffelt, G. Sigl, and L. Stodolsky, *NonAbelian Boltzmann equation for mixing and decoherence*, Phys. Rev. Lett. **70**, 2363 (1993), [Erratum: Phys.Rev.Lett. 98, 069902 (2007)], arXiv:hep-ph/9209276.

[404] G. Sigl and G. Raffelt, *General kinetic description of relativistic mixed neutrinos*, Nucl. Phys. B **406**, 423 (1993).

[405] R. Barbieri, P. Creminelli, A. Strumia, and N. Tetradis, *Baryogenesis through leptogenesis*, Nucl. Phys. B **575**, 61 (2000), arXiv:hep-ph/9911315.

[406] M. Beneke, B. Garbrecht, C. Fidler, M. Herranen, and P. Schwaller, *Flavoured Leptogenesis in the CTP Formalism*, Nucl. Phys. B **843**, 177 (2011), arXiv:1007.4783 [hep-ph].

[407] B. Garbrecht, F. Glowna, and P. Schwaller, *Scattering Rates For Leptogenesis: Damping of Lepton Flavour Coherence and Production of Singlet Neutrinos*, Nucl. Phys. B **877**, 1 (2013), arXiv:1303.5498 [hep-ph].

[408] S. Lavignac and B. Schmauch, *Flavour always matters in scalar triplet leptogenesis*, JHEP **05** (2015), 124, arXiv:1503.00629 [hep-ph].

[409] C. S. Fong, *Cosmic evolution of lepton flavor charges*, Phys. Rev. D **105**, 043004 (2022), arXiv:2109.04478 [hep-ph].

[410] N. Haba, K. Hamaguchi, and T. Suzuki, *Cosmological constraint on the Zee model*, Phys. Lett. B **519**, 243 (2001), arXiv:hep-ph/0108013.

[411] R. K. Ellis *et al.*, *Physics Briefing Book: Input for the European Strategy for Particle Physics Update 2020* (2019), arXiv:1910.11775 [hep-ex].

[412] G. Aad *et al.* (ATLAS), *Search for a heavy charged Higgs boson decaying into a W boson and a Higgs boson in final states with leptons and b-jets in* $\sqrt{s} = 13$ *TeV pp collisions with the ATLAS detector* (2024), arXiv:2411.03969 [hep-ex].

[413] G. Aad *et al.* (ATLAS), *Search for charged Higgs bosons produced in top-quark decays or in association with top quarks and decaying via* $H^{\pm} \to \tau^{\pm}\nu_{\tau}$ *in 13 TeV pp collisions with the ATLAS detector* (2024), arXiv:2412.17584 [hep-ex].

[414] P. W. Angel, Y. Cai, N. L. Rodd, M. A. Schmidt, and R. R. Volkas, *Testable two-loop radiative neutrino mass model based on an* $LLQd^cQd^c$ *effective operator*, JHEP **10** (2013), 118, [Erratum: JHEP 11, 092 (2014)], arXiv:1308.0463 [hep-ph].

[415] S. Pascoli, S. T. Petcov, and W. Rodejohann, *On the connection of leptogenesis with low-energy CP violation and LFV charged lepton decays*, Phys. Rev. D **68**, 093007 (2003), arXiv:hep-ph/0302054.

[416] S. Pascoli, S. T. Petcov, and A. Riotto, *Leptogenesis and Low Energy CP Violation in Neutrino Physics*, Nucl. Phys. B **774**, 1 (2007), arXiv:hep-ph/0611338.

[417] S. Pascoli, S. T. Petcov, and A. Riotto, *Connecting low energy leptonic CP-violation to leptogenesis*, Phys. Rev. D **75**, 083511 (2007), arXiv:hep-ph/0609125.

[418] E. Molinaro and S. T. Petcov, *The Interplay Between the 'Low' and 'High' Energy CP-Violation in Leptogenesis*, Eur. Phys. J. C **61**, 93 (2009), arXiv:0803.4120 [hep-ph].

[419] C. Hagedorn, R. N. Mohapatra, E. Molinaro, C. C. Nishi, and S. T. Petcov, *CP Violation in the Lepton Sector and Implications for Leptogenesis*, Int. J. Mod. Phys. A **33**, 1842006 (2018), arXiv:1711.02866 [hep-ph].

[420] E. J. Chun *et al.*, *Probing Leptogenesis*, Int. J. Mod. Phys. A **33**, 1842005 (2018), arXiv:1711.02865 [hep-ph].

[421] H. H. Patel, *Package-X 2.0: A Mathematica package for the analytic calculation of one-loop integrals*, Comput. Phys. Commun. **218**, 66 (2017), arXiv:1612.00009 [hep-ph].

[422] V. Ilisie, *Concepts in Quantum Field Theory. A Practitioner's Toolkit*, UNITEXT for Physics (Springer, 2016), ISBN: 978-3-319-22965-2, 978-3-319-38723-9, 978-3-319-22966-9.

[423] H. Haber, *Massless 2-body and 3-body phase space integrals*, `http://scipp.ucsc.edu/~haber/ph222/PhaseSpaceIntegrals.pdf` (2020), accessed 2024/03/04.

[424] D. Prange, *Epstein-Glaser renormalization and differential renormalization*, J. Phys. A **32**, 2225 (1999), arXiv:hep-th/9710225.

[425] M. Flory, R. C. Helling, and C. Sluka, *How I Learned to Stop Worrying and Love QFT* (2012), arXiv:1201.2714 [math-ph].

[426] R. J. Eden, P. V. Landshoff, D. I. Olive, and J. C. Polkinghorne, *The analytic S-matrix* (Cambridge Univ. Press, Cambridge, 1966), ISBN: 978-0-521-04869-9.

[427] H. Hannesdottir and M. D. Schwartz, *A Finite S-Matrix*, Phys. Rev. D **107**, L021701 (2023), arXiv:1906.03271 [hep-th].

[428] H. Hannesdottir and M. D. Schwartz, *S-Matrix for massless particles*, Phys. Rev. D **101**, 105001 (2020), arXiv:1911.06821 [hep-th].

[429] J. Racker, *Unitarity and CP violation in leptogenesis at NLO: general considerations and top Yukawa contributions*, JHEP **02** (2019), 042, arXiv:1811.00280 [hep-ph].

[430] T. Blažek and P. Maták, *Cutting rules on a cylinder: a simplified diagrammatic approach to quantum kinetic theory*, Eur. Phys. J. C **81**, 1050 (2021), arXiv:2104.06395 [hep-ph].

[431] H. Murayama, *Notes on Phase Space*, `http://hitoshi.berkeley.edu/233B/phasespace.pdf` (2007), accessed 2023/10/11.

[432] A. Abada, S. Davidson, F.-X. Josse-Michaux, M. Losada, and A. Riotto, *Flavor issues in leptogenesis*, JCAP **04** (2006), 004, arXiv:hep-ph/0601083.

[433] P. Fileviez Perez, C. Murgui, and A. D. Plascencia, *Baryogenesis via leptogenesis: Spontaneous B and L violation*, Phys. Rev. D **104**, 055007 (2021), arXiv:2103.13397 [hep-ph].